Uncovering novel host factors driving pathological neuroinflammation in a mouse model of cerebral malaria

Sabrina Torre

Department of Human Genetics

McGill University

Montreal, QC, Canada

December 13, 2016

A thesis submitted to McGill University in partial fulfillment of the requirements of the degree of Doctor of Philosophy

Abstract

Cerebral malaria (CM) is a neurological encephalitis caused by *Plasmodium falciparum* infection in humans and is the leading cause of death in children from sub-Saharan Africa. Here, we describe a genome-wide N-ethyl-N-nitrosourea (ENU) mutagenesis screen in mice that has identified genes that, when inactivated, cause experimental cerebral malaria (ECM)-resistance in *Plasmodium berghei* ANKA (PbA)-infected mice. Such ECM-protective mutations affect genes and pathways required for pathological neuroinflammation, and the corresponding proteins and associated pathways might represent valuable novel targets for drug discovery. Genome scans and/or whole exome sequencing approaches have identified disruptive recessive ENU-induced mutations in the genes that encode THEMIS and USP15 which protect mice from lethal neuroinflammation. We found that *Themis*^{I23N} homozygous mutants exhibited a profound decrease in T cell numbers, and thus impaired T cell-dependent pro-inflammatory responses, which was protective in the mouse model of ECM but detrimental for *M. tuberculosis* infection. Unlike THEMIS mutants, ECM-resistance in *Usp15*^{L749R} homozygous mutants was not caused by a cellular immunodeficiency, but rather, resistance was linked to dampened type I interferon responses in the brain protecting mice from neuroinflammation in both ECM and experimental autoimmune encephalitis (EAE). Using biochemical, genetic and RNA-sequencing approaches, we found that USP15, together with its binding partner, E3 ubiquitin ligase TRIM25, positively regulated type I interferon responses to drive pathogenesis during neuroinflammation. Since *THEMIS* and *USP15* have also been detected as genetic risk factors for a number of common human inflammatory diseases, our mouse studies validate the critical role that these genes play in common pathogenic mechanisms of human inflammatory diseases. Lastly, in a second ENU mutagenesis screen, we found that susceptibility to ECM was regulated by epistatic interaction between chromosome 4 (*Berr8*) and chromosome 1 (*Berr7*) loci in mice derived from B6 and 129S1 parental crosses. Our study raises the possibility that this two-locus system may also be relevant to other unrelated inflammatory conditions in humans. Overall, these findings not only contribute to our understanding of infectious and inflammatory disease mechanisms, but have also proposed novel targets of pharmacological interest. The neuroinflammatory-

protective genetic alteration could be mimicked by pharmacological inhibition of the corresponding target to alleviate CM and possibly other chronic human inflammation conditions as well.

Résumé

Le neuropaludisme est une encéphalite neurologique causée par le parasite *Plasmodium falciparum* chez l'humain; c'est la première cause de décès chez les enfants en Afrique subsaharienne. Nous décrivons ici une mutagenèse aléatoire du génome entier de souris par N-éthyl-N-nitrosourée (ENU) qui nous a permis d'identifier des gènes qui, lorsque désactivés, entraînent une résistance au neuropaludisme expérimental chez des souris infectées par *Plasmodium berghei* ANKA (PbA). Ces mutations protectrices touchent les gènes et les voies responsables des pathologies neuroinflammatoires, et les protéines correspondantes et voies associées pourraient constituer des cibles novatrices précieuses pour la recherche pharmacologique. Les méthodes de séquençage de l'ensemble du génome et/ou de l'ensemble de l'exome ont permis d'identifier des mutations disruptives récessives induites par ENU dans les gènes qui codent pour THEMIS et USP15 qui protègent les souris d'une neuroinflammation létale. Nous avons constaté chez les mutants homozygotes *Themis*^{I23N} une importante diminution du nombre de lymphocytes T, et donc une diminution de la réponse pro-inflammatoire liée aux lymphocytes T, ce qui a un effet protecteur pour le modèle murin de neuropaludisme expérimental, mais un effet préjudiciable pour l'infection à *M. tuberculosis.* Contrairement au cas des mutants THEMIS, la résistance au neuropaludisme expérimental des mutants homozygotes *Usp15*^{L749R} n'était pas due à une immunodéficience cellulaire, mais plutôt à une atténuation de la production d'interférons de type 1 dans le cerveau, ce qui protégeait les souris de la neuroinflammation à la fois pour le neuropaludisme expérimental et pour l'encéphalite auto-immune expérimentale (EAE). À l'aide de méthodes biochimiques, génétiques et de séquençage de l'ARN, nous avons découvert que USP15, avec son partenaire de liaison l'ubiquitine ligase E3 TRIM25, régulait positivement la production d'interférons de type 1 pour favoriser la neuroinflammation. Comme *THEMIS* et *USP15* ont aussi été identifiés comme facteurs de risque génétiques pour un certain nombre de maladies inflammatoires chez l'humain, nos études sur la souris confirment le rôle essentiel des gènes dans les mécanismes pathogènes communs des maladies inflammatoires chez l'humain. Enfin, dans une deuxième mutagenèse par ENU, nous avons découvert que la susceptibilité au

neuropaludisme expérimental était régulée par une interaction épistatique entre les locus *Berr8* du chromosome 4 et *Berr7* du chromosome 1 chez des souris issues d'un croisement entre les souches B6 et 129S1. Notre étude soulève la possibilité que ce système à deux locus puisse être aussi impliqué dans d'autres maladies inflammatoires non reliées, chez l'humain. Dans l'ensemble, non seulement ces résultats contribuent-ils à la compréhension des mécanismes des maladies infectieuses et inflammatoires, mais ils proposent aussi de nouvelles cibles pour la recherche pharmacologique. L'effet protecteur de l'altération génétique contre la neuroinflammation pourrait être reproduit par l'inhibition pharmacologique de la cible correspondante pour soigner le neuropaludisme et potentiellement d'autres maladies inflammatoires chroniques chez l'humain.

Preface

The work described in Chapters 2 through 4 of this thesis is published as follows:

Chapter 2: Torre, S., Faucher, S. P., Fodil-Cornu, N., Bongfen, S. E., Berghout, J., Schwartzentruber, J. A., et al. (2014). THEMIS is Required for Pathogenesis of Cerebral Malaria and for Protection Against Pulmonary Tuberculosis. *Infection and Immunity*. http://doi.org/10.1128/IAI.02586-14

Chapter 3: Torre, S., Polyak, M. J., Langlais, D., Fodil, N., Kennedy, J. M., Radovanovic, I., et al. (2016). USP15 regulates type I interferon response and is required for pathogenesis of neuroinflammation. *Nature Immunology*. http://doi.org/10.1038/ni.3581

Chapter 4: Torre, S.*, van Bruggen, R.*, Kennedy, J. M., Berghout, J., Bongfen, S. E., Langat, P., et al. (2013). Susceptibility to lethal cerebral malaria is regulated by epistatic interaction between chromosome 4 (*Berr6*) and chromosome 1 (*Berr7*) loci in mice. *Genes and Immunity*. http://doi.org/10.1038/gene.2013.16

* Equal contribution

Erratum: Since the publication of this article, we have corrected the nomenclature of the *Berr6* locus to *Berr8*. The authors apologize for any inconvenience caused.

Contribution of Authors

***Chapter 2*:** The studies in Chapter 2 were performed in collaboration with colleagues and collaborators as follows: Silayuv Bongfen, Joanne Berghout and Sandra Salem provided valuable guidance throughout the work presented in this chapter. ENU mouse mutants were generated and intravenously infected by mouse technicians (Genevieve Perreault and Patricia D'Arcy). I bred, genotyped, and phenotyped all mice within the mutant pedigree *Melvin*. Genome-wide linkage analysis and whole exome sequencing were analyzed by myself, Joanne Berghout and Jeremy Schwartzentruber. I preformed all molecular cloning and biochemical assays - with excellent guidance from my peer, Sandra Salem. I performed immunological experiments with James Kennedy. I performed all experiments relating to phosphorylation of THEMIS by LCK in a co-transfection assay. Dr. Andrea Cooper performed all experiments related to *Mycobacterium tuberculosis*. I wrote the first draft of the manuscript with Dr. Philippe Gros, and prepared all figures. All authors edited and provided helpful comments on the manuscript.

***Chapter 3*:** The studies in Chapter 3 were performed in collaboration with colleagues and collaborators as follows: I identified the mutation in *Usp15* by whole exome sequencing analysis with the aid of Joanne Berghout, Jeremy Schwartzentruber and Dr. Mark Lathrop. Genevieve Perreault, Susan Gauthier and I, bred all mice related to this project. I performed biochemical work related to protein expression in mouse tissues and protein stability. Irena Radovanovic, James Kennedy and I performed the immunological experiments (FACS, ELISAs). Dr. David Langlais performed all RNA sequencing-related bioinformatic analyses, and I performed all RNA sequencing validation experiments by qRT-PCR. Dr. Maria Polyak performed all experiments related to Experimental Autoimmune Encephalitis (EAE), and biochemical assays such as protein-protein interactions and deubiquitination. We received mouse knockouts and mutants from collaborators: Dr. Subburaj Ilangumaran, Dr. Karen Mossman, Dr. Chen Liang, and Dr. Klaus-Peter Knobeloch. Primary cells from brain were provided and characterized by Dr. Jack Antel, Dr. Nathalie Arbour, Dr. Alexandre Prat, Dr. Maria Polyak and Dr. Luke M. Healy, with additional contribution from Gabriel A. Leiva-Torres.

I performed *Listeria* experiments with guidance from Dr. Connie Krawczyk. I wrote the first draft of the manuscript with Dr. Philippe Gros, Dr. David Langlais and Dr. Maria Polyak. I prepared all figures for the manuscript. All authors edited and provided helpful comments on the manuscript.

***Chapter 4*:** The studies in Chapter 4 were performed by both Rebekah van Bruggen and I. Silayuv Bongfen and Joanne Berghout provided valuable guidance throughout the work presented in this chapter. Genevieve Perreault, Patricia D'Arcy, and I bred all mice related to this project. I performed all PbA infection experiments, DNA extractions, and genetic analyses by linkage mapping on all pedigree *Carmelo*-related animals, with help from Adam Li. Rebekah van Bruggen validated the chromosome 4 effect on resistance to ECM in 10 independent B6 x 129S1 mouse pedigrees that segregated resistance to ECM. I wrote the first draft of the manuscript with Dr. Philippe Gros and Rebekah van Bruggen. All authors edited and provided helpful comments on the manuscript.

Table of Contents

List of Figures

Chapter 1

Chapter 2

Chapter 3

Chapter 4

List of Tables

Chapter 1

Chapter 3

List of Appendices

List of Abbreviations

ACT	Artemisinin-combination therapy
BBB	Blood-brain barrier
Berr	Berghei-resistance
bp	Base pair
CABIT	Cysteine-containing, all-β in Themis domains
CFU	Colony-forming units
Chr.	Chromosome
CM	Cerebral malaria
CNS	Central nervous system
CSA	Chondroitin sulphate A
CSP	Circumsporozoite protein
DC	Dendritic cell
DN	Double negative
DNA	Deoxyribonucleic acid
DP	Double positive
DUB	Deubiquitinase
DUSP	Domain present in ubiquitin-specific proteases
EAE	Experimental autoimmune encephalitis
ECM	Experimental cerebral malaria
ENU	*N*-ethyl-*N*-nitrosourea
FDR	False discovery rate
G6PD	Glucose-6-phosphate dehydrogenase
GPI	Glycophosphatidylinositol
H&E	Hematoxylin and eosin
HLA	Human leukocyte antigen
i.p.	Intraperitoneal
i.v.	Intravenous
ICAM-1	Intercellular adhesion molecule-1
IFN	Interferon
IFN-α	Interferon alpha
IFN-β	Interferon beta
IFN-γ	Interferon gamma
IRF	Interferon regulatory factor
ISG	Interferon-stimulated gene

kDa	Kilodalton
LCK	Lymphocyte-specific protein tyrosine kinase
LOD	Logarithm of the odds
ng	Nanogram
µg	Microgram
mM	Millimolar
M	Molar
MA	Metabolic acidosis
Mb	Megabase
MHC	Major histocompatibility complex
Mtb	*Mycobacterium tuberculosis*
p.i.	Post-infection
PAM	Pregnancy-associated malaria
PbA	*Plasmodium berghei* ANKA
PBS	Phosphate buffered saline
PCR	Polymerase chain reaction
*Pf*EMP1	*Plasmodium falciparum* erythrocyte membrane protein 1
pRBC	Parasitized red blood cell
qPCR	Quantitative polymerase chain reaction
RBC	Red blood cell
RNA	Ribonucleic acid
SMA	Severe malarial anemia
SNP	Single-nucleotide polymorphism
TCR	T cell receptor
THEMIS	Thymus-Expressed Molecule Involved in Selection
TLR	Toll-like receptor
TNF	Tumor-necrosis factor
TRIM25	Tripartite-motif containing protein 25
TSP	Thrombospondin
Ub	Ubiquitin
UBL	Ubiquitin-like
UCH	Ubiquitin carboxyl hydrolase
USP15	Ubiquitin specific protease 15
VCAM-1	Vascular cell adhesion molecule-1
WES	Whole exome sequencing

Acknowledgements

I would like to take this opportunity to acknowledge my supervisor, Dr. Philippe Gros - without his expertise and guidance this dissertation would not have been possible. The wealth of scientific and general knowledge that I have acquired under his supervision will always positively impact my life. I am eternally grateful, thank you!

My studies would not have been possible without the support of various lab mates and collaborators. I am grateful for the advice from my supervisory committee members, Dr. Danielle Malo and Dr. Silvia Vidal. I would like to acknowledge Silayuv Bongfen and Joanne Berghout who took me under their wings as I began my studies. I would like to express my deepest appreciation to David Langlais for all of the guidance that he provided for all of my projects, and whose enthusiasm for science has had a lasting impact on me. A big thank you to Sandra Salem who was not only a great lab mate, but a best friend. I am grateful to my friends, Jimmy Kennedy and Vicki Leung, both of which have made my time at the lab extremely enjoyable. I am grateful to Susan Gauthier and Normand Groulx, the backbone of the Gros laboratory. I am very grateful to all of the animal technicians that have contributed significantly to all of my projects; namely Genevieve Perreault and Patricia D'Arcy. I would like to thank all past and present Gros lab members, as well as the Complex Traits Group for a wonderful working environment; for all of the laughs, cries, and memories that we have experienced together along the way!

I would like to thank all of my family and friends; their moral support has been invaluable. I am very grateful to my parents who have supported me in every single way throughout the course of my education. They have shaped me into the woman that I am today, and I will never be able to thank them enough. Finally, I would like to thank my partner, Shant, for being my everything; my rock through the most difficult moments of both my personal life and graduate school, and for his endless encouragement and support.

Last but not least, I would like to express my gratitude for the generous financial support provided by CIHR and Amorchem that have made my studies possible.

Objectives and Rationale

Despite the profound progress that has been made recently toward decreasing the burden of malaria, novel drugs and an effective vaccine remain essential. Strategies to combat the disease are limited by substantial gaps in understanding of the host, parasite, and the complex interaction between them. A better understanding of pathways that regulate host immune responses to *Plasmodium* are critical for the development of treatments against the most lethal form of the disease, cerebral malaria (CM).

Mouse models of malaria have provided an invaluable opportunity to investigate disease in experimentally controlled conditions. Previous studies have shown that laboratory mice with single-gene defects in host inflammatory molecules or receptors (e.g. *Cd4*, *Cd8*, *Cxcr3*, *Ifng*, *Ifnar1, Gzmb*) are protected against CM-associated lethal neuroinflammation. As susceptibility to CM is multigenic and complex, we hypothesize that there are additional unidentified host factors that mediate disease pathogenesis. Therefore, the main objective of this thesis centers on uncovering and characterizing novel host genetic determinants of pathological neuroinflammation during experimental cerebral malaria (ECM). To achieve our objective, we used a forward genetic N-ethyl-N-nitrosourea (ENU) mutagenesis approach in mice to uncover novel host ECM-protective mutations in an unbiased, genome-wide fashion. Following successful identification of an ECM-resistant mutant pedigree, we carried out genetic, biochemical and immunological characterization within each family, which make up the content of Chapters 2 through 4 of this thesis. The overall goal of these studies is to identify proteins and associated pathways that could be targeted with therapeutic drugs to alleviate progression, severity, and/or death by CM in humans, but also to provide parallels or strategies to combat other neuroinflammatory diseases (i.e. multiple sclerosis (MS)), or pathological inflammatory diseases (i.e. systemic lupus erythematosus (SLE), rheumatoid arthritis (RA), inflammatory bowel disease (IBD).

Chapter 1:

Introduction & Literature Review

1.1 Malaria overview

Malaria is the most ancient and devastating parasitic disease known to humans. It was first described centuries ago in writings describing disease of enlarged spleens and recurrent fevers [1]. Ancient Romans believed that malaria was transmitted by breathing “mal aria” – the Italian translation for “bad air” – from the foul decay wafting from unsanitary swamps and marshes [2,3]. It was not until the year 1880 that the French scientist, Alphonse Laveran, discovered that the *Plasmodium* parasite was the true cause of malaria [2,3].

Today, the World Health Organization (WHO) estimates that roughly 3.2 billion people – about half of the world’s population – are at risk for malaria. The disease claimed the lives of 438,000 people in 2015 alone [4]. It has been estimated that more than 100 countries are endemic for malaria, a dominating number of cases (85%) arising in Sub-Saharan Africa [5]. Children living in sub-Saharan Africa under the age of five that have little to no immunity against the pathogen carry the highest risk. Pregnant women and their fetuses are also more vulnerable to malaria due to their reduced immune-status, which contributes to miscarriage, low birth rate, and neonatal mortality in endemic areas of disease [6].

Between the years 2000 and 2015, the number of new malaria cases has declined by roughly 18% and the mortality rate by 60% [4]. Moreover, 57 of the 106 countries endemic for malaria have decreased disease incidence by more than 75% [4]. This outstanding progress was achieved through the implementation of effective malaria prevention strategies that include: sleeping under insecticide-treated mosquito nets, prompt diagnostic testing, and easier access to antimalarial drugs. Though significant progress has been made toward decreasing disease burden, malaria remains the leading cause of death in children in sub-Saharan Africa claiming the life of a child every two minutes [4].

Although artemisinin-combination therapies (ACTs) are currently highly effective against infection with *Plasmodium*, resistance to artemisinin has started to appear, highlighting the need for new treatment strategies. In fact, the *Plasmodium* parasite has

achieved resistance to almost every drug used against it [7]. Moreover, the complex life cycle of *Plasmodium* parasites, the large antigenic diversity exhibited by each of its life cycle stages, along with its immune evasion strategies have all contributed to significant challenges in developing effective vaccines that are still lacking [8]. A greater understanding of malaria pathophysiology and host-pathogen interactions will pave the way for new avenues of treatment and prevention to combat the parasitic disease.

1.2 *Plasmodium*, a highly successful phylum of obligate intracellular parasites

The protozoan parasite that causes malaria, *Plasmodium*, is transmitted to humans through blood-feeding by the infected female *Anopheles* mosquitoes. Less frequently, infections can occur through exposure of infected blood products (blood transfusions) and by transmission during pregnancy [9]. There are five species of the genus *Plasmodium* that are known to infect humans; *Plasmodium ovale*, *Plasmodium malariae*, *Plasmodium knowlesi*, *Plasmodium falciparum* and *Plasmodium vivax* - the latter two species cause the majority of infections [5]. Species of *Plasmodium* can co-exist in various combinations in endemic regions [10]. In particular, infection with *P. falciparum* poses the most significant threat to human life accounting for almost all malaria-associated deaths, while *P. vivax* infections occasionally cause fatal disease as well [5]. *P. falciparum* parasites are more virulent than other strains of *Plasmodium* because they can invade all red blood cells (RBCs) precursors and cells, leading to high levels of blood parasitemia, and they can express knob-like protrusions on infected RBC surface allowing for cytoadherence and sequestration of infected cells within the microvasculature, including the brain, lungs and placenta [11,12]. On the other hand, *P. vivax* parasites are more selective and preferentially invade a younger subpopulation of RBCs (reticulocytes), particularly those that are positive for the Duffy blood group [11].

The *Plasmodium* parasite is a highly successful intracellular pathogen. *Plasmodium* has evolved to reside within cells of its human host and to evade detection and elimination by the immune response. Residing within erythrocytes is advantageous for the parasite because they have access to a rich source of nutrients for feeding, and because they are protected from host immune defences since RBCs cannot present cell-surface MHC-based antigens to initiate an immune response [13,14].

1.2.1 Plasmodium life cycle

Plasmodium parasites have a complex life cycle that requires both a human and an insect host. When a person is bit by a *Plasmodium*-infected *Anopheles* mosquito (**Figure 1-1**), sporozoites are released into the bloodstream and travel to the liver where they proceed to multiply within hepatocytes. Over the course of one to two weeks, each sporozoite multiplies into up to 30,000 daughter merozoites forming what is known as a liver schizont [5,15]. Alternatively, *P. vivax* or *P. ovale* sporozoites may remain dormant in the liver (asymptomatic hypozoites), and reactivation into symptomatic blood-stage malaria can occur months or years following the initial infection [16]. Thousands of liver-stage merozoites burst free from the schizonts and enter the bloodstream where they can bind to and penetrate erythrocytes with the use of specialized surface proteins [14]. Within erythrocytes, merozoites mature into trophozoites, feeding off of a rich niche of nutrients (e.g. hemoglobin), and ultimately destroying the red blood cell, allowing propagation of infection to neighboring erythrocytes [14]. Repetitive rounds of invasion and multiplication within erythrocytes can result in more than 10^{12}-parasitized erythrocytes in the bloodstream [5,15]. The impact of erythrocyte rupture at this magnitude is a significant decline in red blood cell mass, as well as a large release of host cellular debris and cytokines which lead to the development of acute clinical symptoms, like fever and myalgias [17]. The life cycle of the parasite is fulfilled when a fraction of intraerythrocytic parasites develop into gametocytes (sexual stage) and circulate in the blood such that they can be ingested by another feeding *Anopheles* mosquito to perpetuate transmission to another host (**Figure 1-1**).

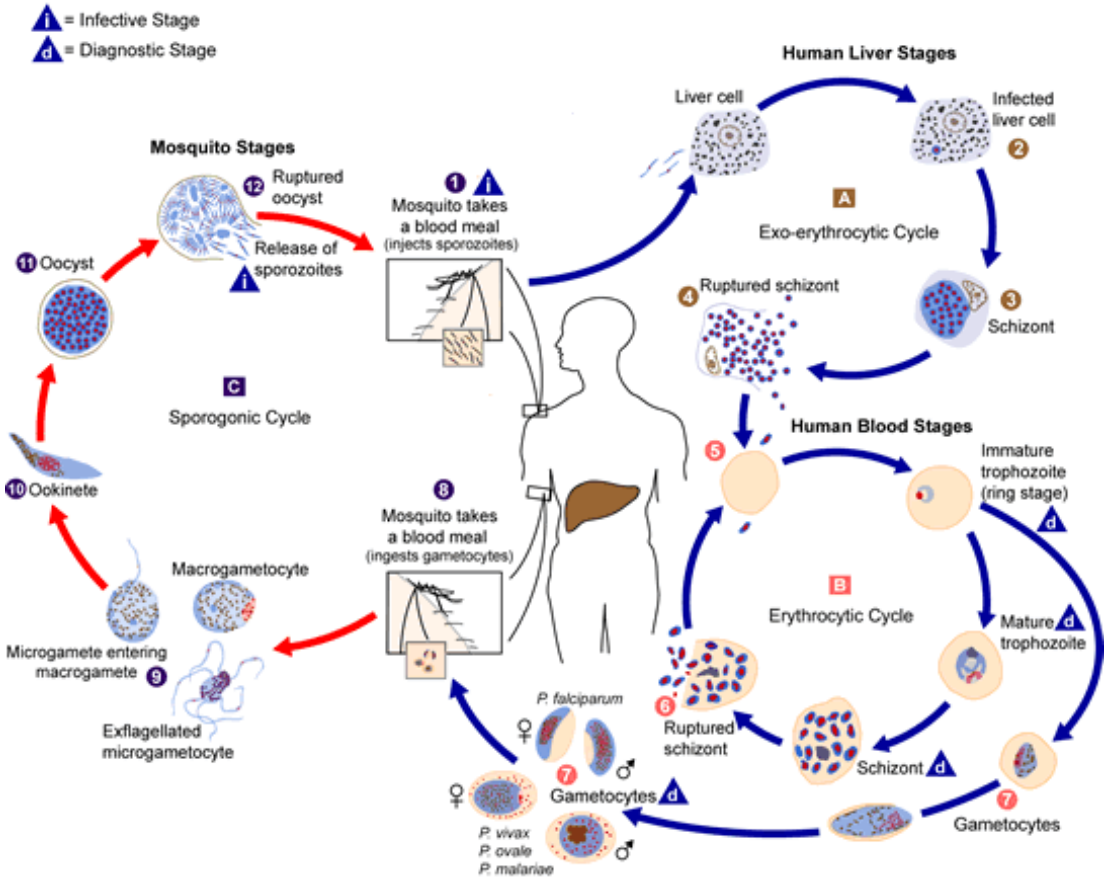

Figure 1-1. *Plasmodium* life cycle in humans and in the *Anopheles* mosquito vector

During a blood meal, a malaria-infected female *Anopheles* mosquito injects sporozoites into the human host. (**A**) Sporozoites infect hepatocytes of the liver where they multiply into thousands of daughter merozoites to form a liver schizont. The schizont ruptures to release thousands of merozoites into the bloodstream (**B**), where they can invade and mature within erythrocytes, and ultimately destroy them. Repetitive rounds of invasion and multiplication within erythrocytes perpetuate the cycle. Some parasites differentiate into male (microgametocyte) and female (macrogametocyte) gametocytes, which can be ingested by another feeding *Anopheles* mosquito. (**C**) Within the mosquito, the gametocytes penetrate to generate a motile ookinete. The ookinetes invade the midgut wall of the mosquito where they develop into oocysts. The oocysts mature, rupture and release sporozoites that travel to and reside in the mosquito salivary gland. Inoculation of the sporozoites into a new human host perpetuates the malaria life cycle.

Figure is reproduced from the Centers for Disease Control and Prevention <http://www.cdc.gov/malaria/about/biology/>

1.3 Human Malarial Disease

1.3.1 Life-threatening complications of malaria in humans

The initial clinical symptoms of malaria infection in humans are non-specific and can be easily confused with other illnesses or common infections, leading to a delay in diagnosis. An infected individual will most commonly experience clinical symptoms which include: fever (>92% of cases), chills (79%), headaches (70%) and diaphoresis (64%) [5,9]. Less frequently, they will also experience nausea, vomiting, mild diarrhea, jaundice, pallor, hepatomegaly and splenomegaly [9]. Symptoms typically appear 10 to 16 days after the infectious mosquito bite [9]. A definitive malarial diagnosis can be specified when the presence of *P. falciparum* is observed on a blood smear by microscopy (a 'gold standard' for diagnosing malaria) and/or by rapid diagnostic testing, after all other causes of encephalopathy have been excluded (viral encephalitis, bacterial meningitis) [18].

The clinical outcome of a malaria infection experienced by an individual can range from uncomplicated (asymptomatic) to very severe (death); the outcome is influenced by complex interactions between the parasite, host (discussed in **Section 1.3.3**), and geographic and social factors, as illustrated in **Figure 1-2**. The majority of *P. falciparum*-infected individuals experience an uncomplicated, mild, febrile disease which is controlled and terminated by the host immune response, and/or by treatment with antimalarials [19]. In endemic regions of malaria, it is common for individuals to be positive for blood parasitemia in absence of clinical symptoms; these individuals remain untreated and function as asymptomatic parasite reservoirs that contribute to malaria transmission [17]. However, in roughly 1% of individuals, *P. falciparum* infection can progress to life-threatening complications that involve the nervous, respiratory, renal, and/or the hematopoietic systems. These complications encompass three overlapping syndromes of severe malaria: cerebral malaria (CM), severe malaria-associated anemia (SMA), and metabolic acidosis (MA) [20]. In pregnant women, complications in both mother and fetus can arise (pregnancy-associated malaria (PAM)). Briefly, these syndromes (summarized in **Table 1-1**) are caused by a combination of organ-specific parasitized erythrocyte sequestration, host inflammatory response, and consequent

dysfunction of vital organs [5]. Both *P. falciparum* and *P. vivax* can cause severe anemia, but it is strictly the *P. falciparum* parasite that is responsible for causing the life-threatening syndromes [11]. Furthermore, the manifestations of severe *P. falciparum* malaria depend greatly on the age of the infected individual; SMA is more common in children, whereas acute pulmonary oedema, acute kidney injury and jaundice are more common in adults; CM and MA affect individuals within all age groups [21].

1.3.1.1 Treatment options for clinical malaria

Early diagnosis and treatment of malaria reduces disease incidence and prevents death. The primary treatment against clinical malaria is artemisinin-combination therapy (ACT). ACT includes delivery of potent artemisinin-derivatives (artesunate, artemether and arteether) in combination with a partner drug such as mefloquine, lumefantrine, amodiaquine, piperaquine and sulfadoxine/pyrimethamine [22]. The use of artemisinin monotherapy is strongly discouraged in order to avoid appearance and spread of artemisinin-resistant *P. falciparum* parasites. Resistance to artemisinins has now been detected in five countries: Cambodia, Lao People's Democratic Republic, Myanmar, Thailand and Viet Nam [4], and widespread resistance is a major concern and a public health threat. In addition, in regions of Cambodia and Thailand, *P. falciparum* has developed multi-drug resistance to both artemisinin and partner drugs [4,11], further emphasizing that novel drugs and/or an effective antimalarial vaccine are urgently needed.

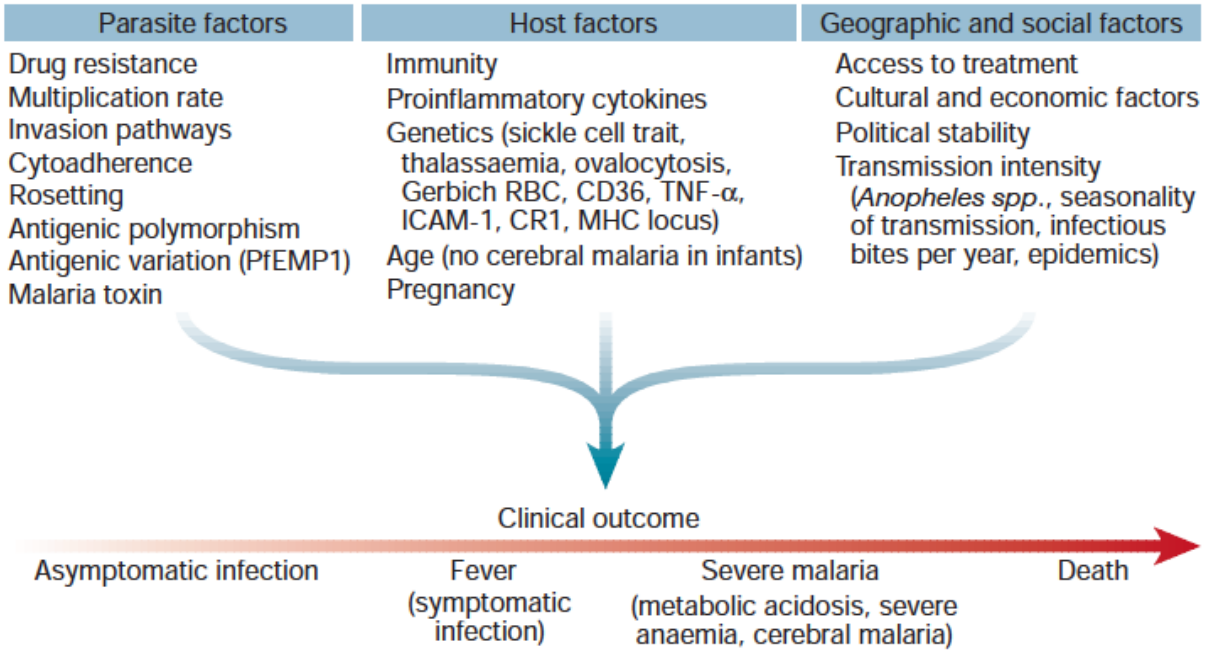

Figure 1-2. The clinical outcome of malaria infection

The clinical outcome of a malaria infection can range from an uncomplicated, asymptomatic infection to severe, sometimes followed by death. The range of clinical outcomes is influenced by complex interactions between the parasite (e.g. ability to cytoadhere), host (e.g. genetics) and geographical and social factors (e.g. access to treatment).

Figure is reproduced with permission from [11].

Syndrome	Clinical features	Mechanism	Refs
Severe anemia	• Low hemoglobin levels • Low red blood cell counts • Paleness/Jaundice	• Rupture of parasitized red blood cells • Accelerated removal of erythrocytes • Worsened by impaired erythropoiesis in the bone marrow	[5,20,23]
Metabolic acidosis "respiratory distress"	• Hyperventilation • Impaired consciousness • Hypoglycemia • Elevated levels of lactate in plasma and cerebrospinal fluid	Accumulation of lactic acid in the blood arising from increased anaerobic glycolysis in host blood vessels due to obstruction by sequestered parasitized erythrocytes (tissue hypoxia)	[24-26]
Cerebral malaria	• Unarousable coma • Impaired consciousness • Seizures • Lethargy • Neurological deficits	• Activation of the immune system and vascular endothelial cells by parasite components • Disruption of blood brain barrier and vascular leakage • Obstruction of brain capillaries and venules by sequestration of parasites and host immune cells (obstructed blood flow, hypoxia of brain parenchyma)	[27]
Placental malaria	• Miscarriage/Stillbirth • Premature delivery • Low birth weight • Fetal growth retardation • Fetal anemia • Neonatal and maternal mortality	• Parasite expresses proteins that bind to chondroitin sulphate A (CSA) present in the placental intervillous space • Placental cell infiltrates and inflammation	[5,28]

Table 1-1. *P. falciparum* malaria-associated syndromes and probable mechanisms of disease

Adapted from table published in [27].

1.3.2 Human cerebral malaria

Human CM is an acute, neurological encephalitis arising from infection with *P. falciparum*, and is the most lethal form of disease that primarily affects young children and pregnant women [29]. Clinical manifestations of cerebral disease include: headache, delirium, seizures, impaired consciousness and coma, and in up to 15 to 20% of cases, death [18]. The onset of symptoms may be sudden with convulsions, or can be gradual with increasing drowsiness and confusion, followed by coma that can last several hours to several days [9]. In some instances coma can be reversible, but survivors will typically suffer from persistent neurocognitive sequelae (cognitive and behavioral impairment, blindness, hearing or speech impairments, and epilepsy) [18,30], and has been estimated to occur in nearly 4000 survivors each year in sub-Saharan Africa alone [30].

In 1892, malariologist, Ettore Marchiafava, and pathologist, Amico Bignami, autopsied a deceased CM-patient and were the first to document histopathological findings describing sequestration of pRBCs within the brain microvasculature accompanied by brain capillary occlusion, rise in intracranial tension and intense hyperemia [31,32]. These fundamental observations were the first to shed light onto the key pathophysiological mechanisms that caused death in CM. Since then, others have described severe manifestations of the disease which include: (a) distinct malarial retinopathy with hemorrhages in both children and adults, (b) increased blood lactate-pyruvate ratios, (c) prominent presence of leukocytes in the cerebral vessels of children, (d) disruption of endothelial intercellular tight junctions of the blood brain barrier occurring predominantly in children, and (e) cerebral oedema often present in children [5]. All of these findings suggest that both extensive microvascular obstruction and the host immune response contribute to disease pathogenesis in CM.

1.3.3 Host genetic determinants of malaria infection

The genetic component of susceptibility to human malaria is both complex and multigenic. Host genetics can influence susceptibility to severe malaria disease by affecting the number of clinical episodes, level of blood parasitemia, rate of transmission, and disease severity [33]. Linkage and genome-wide association approaches have identified loci that control malaria susceptibility in humans; although genetic associations have been reported in certain malaria-endemic populations, several of them remain difficult to replicate in large studies across different populations [34]. Limitations of genetic studies in humans include factors such as host and pathogen genetic variability, individual variables (e.g. age), environmental influences (e.g. co-infection), as well as their potential interactive, joint effects [34,35]. To counter these limitations, the experimental mouse models of malaria have been critical to identify and to validate host genetic contributions to disease, and will be discussed in greater detail in **Chapter 1.4**.

The co-evolution of the *Plasmodium* parasite and human host over 10,000 years has substantially impacted the human genome [36]. In fact, no infectious disease has shaped the human genome more than has malaria [5]. Malaria has had a profound mortality toll in endemic regions, posing a major force of evolutionary selection. The selective pressure of malaria is reflected by retention of deleterious allelic variants in genes related to both the erythrocyte and the host immune response. Epidemiological studies have identified protective variants against severe malaria (CM, SMA and MA), and they are summarized in **Tables 1-2** and **1-3.** A greater understanding of natural host defense mechanisms provides insight not only to pathogenesis, but may put forward novel host-based targets for pharmacological intervention.

1.3.3.1 Erythrocyte disorders associated with protection from malaria

The *Plasmodium* parasite life cycle depends on host erythrocytes for growth. Structural or enzymatic perturbations of the red blood cell impede the parasite's survival or ability to replicate. In fact, several hematological disorders have been strongly associated with reduced malaria susceptibility, and have risen to high frequency in

malaria-endemic areas due to their protective effect (**Table 1-2**). The most common and best-characterized polymorphisms are the hemoglobinopathies (HbS, HbC, HbE, and α and β-thalassemias) and deficiency for glucose-6-phosphase dehydrogenase (G6PD) [37]. Evidence for natural selection and retention of such deleterious alleles comes from observations that deleterious mutations affecting the erythrocyte have increased in frequency in malaria-endemic regions, an hypothesis first proposed over 60 years ago by J.B.S Haldane [38]. The mechanistic basis for malaria protection is understood for some of these erythrocyte disorders and they usually affect parasite invasion or intraerythrocytic replication and development [37].

Hemoglobin is a red blood cell protein involved in the binding and transport of oxygen. It comprises two alpha (α) and two beta (β) globin chains encoded by *HBA* and *HBB* genes respectively. Hundreds of *HBB* gene variants exist at low prevalence worldwide, though only three hemoglobin variants are observed at polymorphic frequencies: HbS (sickle trait) (β6Glu→Val), HbC (β6Glu→Lys), and HbE (β26Glu→Lys) [39]. Despite individuals homozygous for HbS (HbSS) experiencing life-threatening sickle cell disease, heterozygotes (HbAS) are healthy and have up to a ten-fold protection against severe malaria (CM and/or severe anemia) [35,40]. HbAS is widespread in Africa, the Middle East, and India. High frequencies of HbAS in different endemic populations of the world have presumably resulted from independent processes of natural selection – validating the large selective pressure that malaria has posed on the human genome [41]. Conversely, the HbC variant causes mild anemia in homozygotes, but both homozygotes (HbCC) and heterozygotes (HbAC) have demonstrated protection against severe malaria disease (CM, MA and/or SMA) [42,43]. The most common hemoglobin variant, HbE, is most prevalent in South East Asia, attaining carrier frequencies between 55 to 70%, and has also been shown to offer protection to severe malaria disease, though evidence of protection within different populations have been conflicting [39,41,42].

Another division of hemoglobinopathies with well-known protective effects against severe malaria are the thalassemias (α and β-Thalassemia). Thalassemia is a blood disorder caused by deletions or point mutations in the non-coding portions of *HBA*

or HBB genes, which cause inadequate synthesis of either the α or β-globin chains [44]. More than 200 thalassemia-causing mutations have been discovered within different malaria-endemic populations, supporting positive selection of these alleles during human evolution [44]. The molecular basis of malaria protection remains elusive, though there are suggestions that the blood disorder limits disease manifestation (reduced oxidative tissue damage and reduced pro-inflammatory cytokines), rather than limit parasite replication [39].

Erythrocyte disorders are not limited to the hemoglobinopathies; in fact, enzymatic and structural red blood cell defects have also been associated with protection from malaria. The most common enzymatic erythrocyte defect is a deficiency for glucose-6-phosphate dehydrogenase (G6PD) [41]. The G6PD enzyme is necessary for maintenance of a reducing environment within red blood cells. The frequency of G6PD deficiency is high in some malaria-endemic regions, attaining allele frequencies between 5 to 25% [42]. Heterozygotes of G6PD have up to 50% protection against severe malaria [42].

Another red blood cell defect with high frequency in malaria-endemic regions conferring significant protection from disease involves the Duffy antigen. *P. vivax* uses the Duffy cell-surface receptor for attachment to the erythrocyte. A mutation in the GATA-1 binding site of the DARC/*FY* chemokine receptor gene causes a reduction in receptor expression (the Duffy-negative blood group), and thereby impairing the parasite's entry into the cell [44,45]. Other polymorphisms affecting erythrocyte membrane proteins, such as a 27 base pair deletion in Band 3 (*SLC4A1Δ27*) has been shown to protect against CM in the heterozygous state [46]. This deletion causes South-East Asian (or Melanasian) ovalocytosis, a condition that is lethal in homozygotes, but advantageous in heterozygotes [44,46]. The *ABO* gene encodes the glycosyltransferase enzyme that determines the ABO blood groups. Individuals who are homozygous for a single nucleotide deletion (rs8176719) in *ABO* have an inactive form of the glycosyltransferase and are classified as blood group O [47]. Strong epidemiological evidence has found that blood group O individuals are more protected against *P. falciparum* malaria, while A, B and AB blood group individuals are more susceptible

[48]. Lastly, over 100 mutations in the *PKLR* gene in humans have been described to cause pyruvate kinase (PK) deficiency, the most common cause of non-spherocytic hemolytic anemia [49]. PK is an essential enzyme required for glucose metabolism in the erythrocyte, a process which provides energy to the red blood cell [44]. *Ex vivo* studies have shown that PK deficient human erythrocytes are resistant to invasion by *P. falciparum* and are more readily cleared by macrophages [50,51]. Very recently, studies in a Thai population have found that heterozygosity for an R41Q variant in PKLR affects the frequency and the intensity of malaria episodes induced by different *Plasmodium* parasites in endemic populations [33].

Red blood cell disorder	Human malaria susceptibility
Hemoglobin C (*HbC*)	HbAC: ↓ HbCC: ↓
Hemoglobin E (*HbE*)	HbAE: ↓ HbEE: unclear
Hemoglobin S (*HbS*)	HbAS: ↓ HbSS: ↓
α-Thalassemia	↓
β-Thalassemia	Unclear
Glucose-6-phosphate dehydrogenase deficiency (*G6PD*)	↓
Pyruvate kinase deficiency (*PKLR*)	Unknown
Ovalocytosis (*SLC4A1*)	↓
Glycophorins (*GYP ABC*)	Unclear
Blood group (*ABO*)	O-type ↓, A and AB-type ↑
Haptoglobin (*HP*)	↓
Duffy negative (*FY*)	↓ (in *P.vivax* infections)
Haem oxygenase 1 (*HO-1*)	↓

Table 1-2. Genetic polymorphisms of the erythrocyte system involved in resistance/susceptibility to *P. falciparum* malaria

"Human malaria susceptibility" refers to evidence for an association with reduced or increased risk of severe malaria (i.e. CM, SMA, and MA).

↓ decreased or ↑ increased susceptibility

Adapted from tables published in [36,37,39,52].

1.3.3.2 Immunological and cytoadherence gene polymorphisms associated with differential response to P. falciparum malaria

Many human case-control and genome-wide linkage studies have associated polymorphisms in or near host inflammatory genes (*TNF*, *IFNAR1*, *IFNG*, *IL12*, *CD40L* and *NOS2*), antigen recognition and presentation genes (*HLA*), and cytoadherence-mediating genes (*ICAM1*, *CD36*, *CR1*) (selected listing in **Table 1-3**) with differential susceptibility to severe malaria. Although these associations have been reported in certain populations where the disease is endemic, many have not be replicated either in larger studies or in different populations [34]. The reasons underlying the difficulties in reproducing positive associations are not simple, but could involve differences in: (1) sample size, (2) population substructure and/or admixture, (3) sampling methodology, (4) sensitivity of methods, and (5) role of co-infection [34]. For an extensive detailed list of genetic polymorphisms reported to be significantly associated with the host phenotype of susceptibility or resistance of *P. falciparum* malaria, please see 'Additional table 1' published in [34], as well as excellent reviews by [36,39,52].

Only a few of these associations have been confirmed in independent studies with different populations. In fact, erythrocyte genetic variants (**Table 1-2**) have provided the most solid epidemiological evidence for malaria protection. The strength of associations with malaria phenotypes for genes coding for proteins involved in cytoadherence and in immune responses is not as robust; however, polymorphisms within the promoter region of *TNF* constitute an exception. *TNF*-promoter polymorphisms causing and increase in *TNF* RNA production have been independently associated with increased risk of severe malaria [36,42]. Gambian children homozygous for the *TNF*-308A allele have increased susceptibility to CM; in Gabon, this allele is associated with increased risk to develop symptomatic re-infections with *P. falciparum*; while in Kenya, carriers displayed higher malaria morbidity [36]. These independent studies confirm the importance of TNF as an important mediator of CM pathogenesis in humans.

Function	Gene (Symbol)
Antigen presentation	Major histocompatibility complex (*HLA*)
Cytoadherence	Complement receptor 1 (*CR1*) Intracellular adhesion molecule-1 (*ICAM-1*) Platelet-endothelial cell-adhesion molecule (*PECAM1*) Thrombospondin receptor (*CD36*)
Immune response	CD40 ligand (*CD40L*) Fcγ receptor IIb (*FCGR2B*) Interferon alpha/beta receptor (*IFNAR1*) Interferon gamma (*IFNG*) Interferon regulatory factor 1 (*IRF1*) Interleukin-12 beta subunit (*IL12B*) Interleukin-13 (*IL13*) Nitric oxide synthase 2 (*NOS*2) Thrombospondin receptor (*CD36*) Toll-like receptor 4 (*TLR4*) Tumor necrosis factor (*TNF*)

Table 1-3. Loci reported at least once as impacting susceptibility to *P. falciparum* malaria

Table adapted from [36,52]. For an extensive detailed list, please see 'Additional file 1' published in [34].

1.4 Experimental Mouse Models of Cerebral Malaria

Studying CM disease in humans is made difficult for several reasons. Ethical, cultural or religious boundaries pose a difficult challenge for research with human subjects or samples. Data obtained from post-mortem human studies reflect the end stage of the disease, thereby limiting our ability to study the sequence of events associated with pathogenesis [53]. Genetic studies of malaria are also very difficult to accomplish in humans due to complex gene-environment interactions, genetic heterogeneity within human populations and parasite strains, and individual variables such as age, diet and co-infection. To counter these limitations, mouse models of malaria have provided an invaluable opportunity to investigate disease in experimentally controlled conditions.

1.4.1 Mice, the foundation of in vivo *experimentation*

In many ways, mice mirror human biology remarkably well [54]. Parallels between mice and humans are reflected by the similarity of both genomes, with 99% of the genome conserved between the two [55]. Experimentation in mice is advantageous due to: (1) the ability to control environmental factors (parasite dose, strain, route of infection, nutritional intake), (2) their great reproductive capacity (short gestation period, large litter sizes), (3) the availability of genome-sequences of many inbred strains, and (4) recent technological advancements that have made manipulation of the mouse genome feasible [55,56]. Mouse models of malaria have contributed significantly to the development and testing of drugs and vaccines, and to study disease pathogenesis, including host immune regulation and genetics of susceptibility/resistance to infection. However, there exist some differences between the human disease and the mouse models of experimental malaria, which must be taken into account in extrapolating data from the mouse to human [57].

1.4.2 Plasmodium berghei *ANKA*

There are four species of *Plasmodium* that can cause malaria in rodents: *P. berghei*, *P. yoelli*, *P. chabaudi*, and *P. vinckei* [1]. Models of CM have been established in susceptible mouse strains infected with erythrocytes parasitized with either *P. berghei*

ANKA (PbA), *P. berghei* K173, or with *P. yoelli* 17XL [58]. The most widely used and best available experimental model of CM (ECM) is the *P. berghei* ANKA (PbA) model. While *P. berghei* K173 and *P. yoelli* 17XL infections can induce CM-like symptoms in mice, they also produce phenotypes that differ greatly from the human syndrome (e.g. peripheral parasitemia can reach up to 80-100%), therefore these models are less frequently used [59].

CM-susceptible mice infected with *Plasmodium berghei* ANKA develop rapidly fatal neurological symptoms (tremors, ataxia, fitting, coma) typically occurring within 5 to 10 days post-infection (cerebral phase). These symptoms are followed by lethality in about 60 to 100% of the mice (dependent on the strain of mouse and dose of parasite inoculum) with relatively low blood parasitemia levels [60]. Infected mice that do not develop neurological symptoms during the cerebral phase will survive until about day 21 (CM-resistant), where they ultimately succumb to symptoms of malaria-induced anemia due to rupture of pRBCs caused by extensive hyperparasitiemia [1].

Although the PbA murine model does not reproduce all features of the complex human disease, there are numerous common aspects of pathogenesis and immune response in this rodent model, which makes it the accepted experimental model of CM. A comparison of the specific features of the human and mouse CM are summarized in **Table 1-4**.

1.4.2.1 Benefits of the PbA-induced ECM model

Briefly, features shared between human CM and its mouse counterpart include appearance of neurological symptoms such as convulsions, paralysis and seizures [58]. Histopathological features such as vascular obstruction, parenchymal haemorrhage, leukocyte adhesion, cerebral oedema and focal demyelination are similar between the syndromes as well [61]. Furthermore, sequestration of pRBCs within various organs, primarily the lung, brain and spleen, is observed in affected humans and in the mouse model [61]. Investigation of inflammatory cytokines in human blood and serum indicate that the host immune response contributes to pathogenesis of CM [62], an observation that parallels what is observed in the ECM model. Key immune cells and immunological

pathways involved in disease pathogenesis are similar, particularly, the involvement of monocytes, T cells and platelets [61]. Other shared features include astroglial activation, changes in blood-brain barrier integrity [63], and upregulation of antigen presentation molecules (e.g. MHC-I and MHC-II) and of host endothelial adhesion molecules (e.g. ICAM-1) on cerebral vessels [61,64]. Overall, there are clear overlaps in features of these syndromes, yet the relevance of the experimental model has been a topic of heated debate [65,66], described in more detail below.

1.4.2.2 Limitations of the PbA-induced ECM model

A major difference between the human disease and the PbA mouse model is the degree of parasite sequestration in the brain microvasculature. A principal feature of human CM is the packing of sequestered pRBCs and leukocytes in brain tissue [63]; In mice however, leukocyte sequestration in the brain is much more prevalent than the sequestration of pRBCs [67,68]. Nonetheless, there is a large body of experimental evidence to support that pRBCs are present in the brain microvasculature of mice displaying CM neurological symptoms [66,67,69-72]. Concerns over the experimental murine model are worsened by the lack of the mouse PbA parasite equivalent of *P. falciparum* erythrocyte membrane protein 1 (PfEMP1), a molecule that mediates pRBC sequestration in tissues by binding to host cell receptors in human CM [73]. It has been argued that binding of pRBCs to host endothelial cells in the murine model is not mediated by host-parasite interactions, but instead reflects the accumulation or trapping of pRBCs in capillaries of the brain [73].

Another major weakness of the CM mouse model is the artificial delivery of parasites to the blood through intravenous infection, which evades the parasite's natural anatomic target site, the skin. In human infections, mosquito-transmitted sporozoites travel from the skin to the liver where they initiate an immune response [74,75]. In mice however, blood-forms of the parasite are typically delivered to the blood by intravenous or intraperitoneal infection for ease of experimentation, which is a highly artificial route of infection [76]. This experimental setup bypasses the liver-stage infection altogether, and rather, initiates an immune response in the spleen instead [60]. Evidently, there

may be differences in the immunological host response initiated in the liver (human) and spleen (mouse), which may have great implications. One study has suggested that, although more cumbersome and laborious, subcutaneous injection of isolated parasites, as well as mice subjected to bites from an infectious mosquito, could represent alternative approaches to address the issue [76]. They conclude that parasite challenge to its natural anatomic target, the skin, would therefore not be as prone to artifacts of the intravenous challenge and may represent an alternative compromise, but also acknowledge that these alternative approaches have their limitations as well [76].

All in all, the limitations of the PbA-induced ECM mouse model are important to acknowledge, but they are overshadowed by many benefits of utilizing the model to understand pathogenesis of CM disease.

Parameter	Human CM	PbA mouse model
PHYSICAL & BEHAVIORAL		
Convulsions, paralysis, seizures	+	+
Fever	+	-
Hypothermia	-	+
BRAIN HISTOPATHOLOGY		
Astrocyte & microglial changes	+	+
Sequestration of pRBCs	+	+
Sequestration of leukocytes	+	+
Sequestration of platelets	+*	+
Knob-like protrusions on pRBCs	+	-
Parenchymal hemorrhage	+	+
Neuronal damage	+	+
Oedema	+	+
IMMUNOLOGICAL		
Expression of proinflammatory cytokines	+	+
Overexpression of MHC Class I & II	+	+
Cell-adhesion molecule upregulation	ICAM-1, VCAM-1, E-selectin, TSP, CSA, hyaluronic acid	ICAM-1, VCAM-1
BIOCHEMICAL		
Increased lactate	+	+
Increased kynurenine pathway metabolites	+	+

Table 1-4. Feature comparisons of human versus mouse CM disease

*Present in children with CM from sub-Saharan Africa, but not reported in adult CM

Adapted from tables published in [68], [58], [77], [78] and [79].

1.4.3 Pathogenesis of CM

CM is a complex syndrome that involves the sequestration of parasitized red blood cells (pRBCs), extensive host inflammation, and perturbed hemostasis in the brain microvasculature [1]. Studies in human clinical samples have been complemented by studies in mouse models to identify the host pathways and responses that are associated with CM. The major steps of pathogenesis in the mouse model of ECM are illustrated in **Figure 1-3**.

1.4.3.1 Priming of the immune response

In human CM, malaria infection is initiated in the liver by the sporozoite form of the parasite. However, in mice blood-forms of the PbA parasite are typically delivered to the blood by intravenous or intraperitoneal infection for ease of experimentation. In this model, infected cells (pRBCs) travel through the spleen where the presence of parasite-derived products primes the host immune response. Splenic dendritic cells (DCs) phagocytose and cross-present parasite antigens, priming and activating parasite-specific $CD4^+$ and $CD8^+$ T cells [60]. NK cells are also required to enhance the capacity of DCs to prime $CD8^+$ T cells [80]. The subsequent release of IFN-γ from these inflammatory cells contributes to the activation of more DCs and macrophages, favoring Th1 polarization and secretion of additional cytokines, such as TNF [80]. The proinflammatory host immune response is required for early control of blood-stage malaria infection, but persistent activation of this response is a central event in ECM pathogenesis.

1.4.3.2 Sequestration, endothelial cell activation and blood brain barrier disruption

The blood brain barrier is a highly selective permeability barrier that serves to separate the brain and the cerebrospinal fluid from the rest of the body. Its proper function is vital for maintaining homeostasis and protecting the central nervous system from dangerous pathogens, chemical insults, or exposure to undesired catabolic products present in the blood, and that could disturb brain function [12]. The integrity of

the BBB is compromised during human and mouse CM, and is thought to be initiated by local sequestration of pRBCs and further amplified by host inflammatory reactions [12].

Sequestration of pRBCs in the brain microvasculature has a central role in the pathogenesis of cerebral disease in both mice and humans. In human infections, cytoadherence of parasitized red blood cells is attributable to specialized parasite proteins, *P. falciparum* erythrocyte membrane protein 1 (*Pf*EMP1) [11]. Within the RBC, *P. falciparum* exports hundreds of parasitic proteins to the cytoplasm and membrane, remodeling the cell for its own growth and survival advantage [12,81]. Consequently, the infected RBCs will develop knob-like protrusions on their cell surface which express *Pf*EMP1, mediating binding to a variety of host receptors displayed on the surface of brain endothelium, particularly ICAM-1, VCAM-1, CD36, P-selectin and E-selectin [11,12]. In mice, sequestration of PbA-infected RBCs in the brain has also been observed, though some argue that this binding is not mediated by interactions between parasite ligands and endothelial receptors, but rather, the consequence of cell accumulation and trapping in the blood capillaries [73].

Parasitized red blood cells also release inflammatory ligands such as glycosylphosphatidylinositol (GPI) anchors, hemozoin crystals and parasitic DNA that result in brain endothelial cell activation [27,60]. Activated endothelial cells secrete chemokines and cytokines that will consequently upregulate the expression of endothelial cell surface adhesion receptors (e.g ICAM-I) and antigen-presentation molecules (e.g. MHC-I), and further exasperate the recruitment of leukocytes, platelets and additional pRBCs, forming a detrimental positive feedback loop.

The recruitment and sequestration of inflammatory leukocytes, particularly T cells, play a critical pathological role during ECM. While $CD4^+$ T cells mediate the early induction phase of cerebral malaria disease, $CD8^+$ T cells are required for late-stage immunopathology where they directly contribute to BBB damage [82,83]. T cells activated in the spleen will upregulate the expression of cell-surface chemokine receptors (e.g. CXCR3) mediating leukocyte trafficking toward a gradient of chemokines (e.g. CXCL10) that have been released as a ‘danger signal’ by activated brain

endothelial cells in response to *Plasmodium*. Recruitment of $CD8^+$ T cells, and the release of granzyme b and perforin molecules from these cells, directly contributes to cytolysis of brain endothelial cells and damage to the BBB [60].

The extensive microvascular obstruction and extensive host inflammation contribute to the breakdown of the BBB, causing impairment of the blood flow in the brain (hypoxia), buildup of toxic waste products, and ensuing irreversible tissue damage [12,59,84,85].

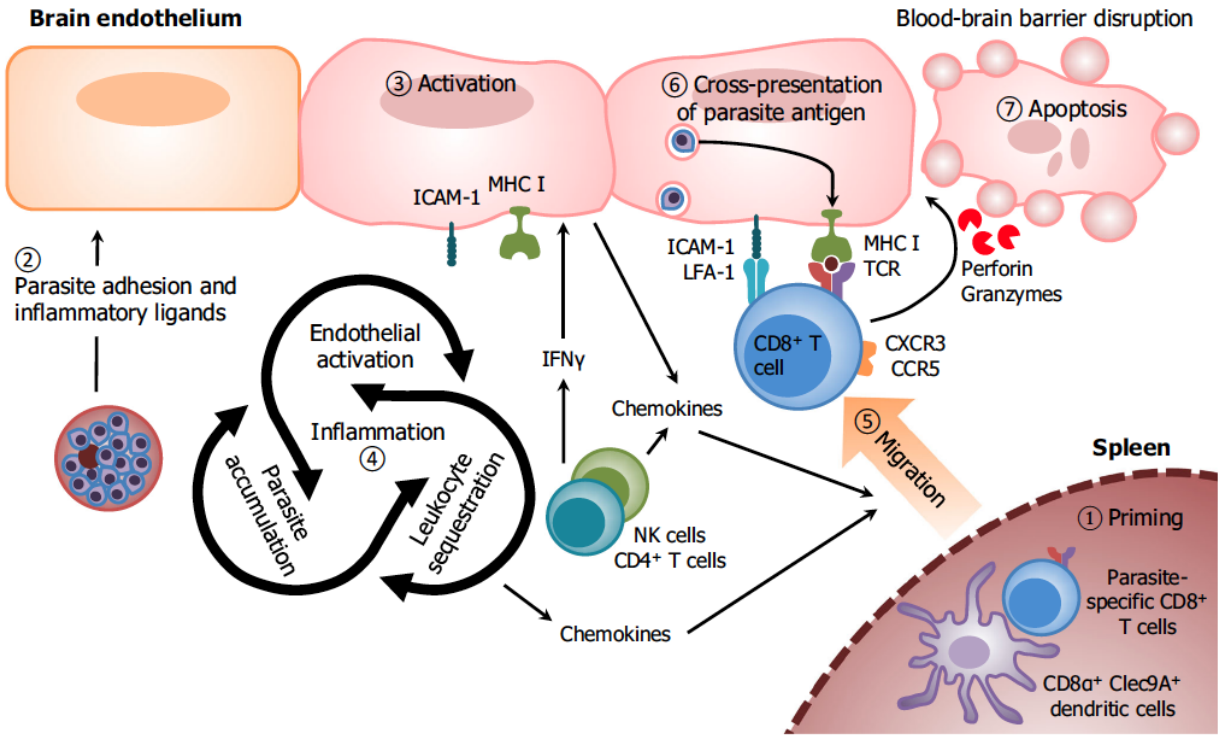

Figure 1-3. Proposed model of ECM pathogenesis

(**1**) Upon infection with PbA merozoites, splenic dendritic cells phagocytose and present parasite antigens, priming parasite-specific $CD4^+$ and $CD8^+$ T cells. (**2**) Parasitized RBCs cytoadhere to brain endothelial cells and also release parasitic inflammatory products. (**3**) In response to these stimuli, brain endothelial cells become activated, secreting chemokines and cytokines and upregulating adhesion receptors (ICAM-1) and molecules associated with antigen presentation (MHC-I). (**4**) A proinflammatory cycle ensues *in situ* with endothelial activation, leukocyte, platelet and parasite recruitment and sequestration forming positive feedback loops. (**5**) Activated $CD8^+$ T cells express CXCR3 and CCR5 receptors and migrate up the chemokine gradient to the brain, where LFA-1 promotes their adhesion to endothelial ICAM-1. (**6**) Brain endothelial cells become activated by IFN-γ secreted by NK cells and $CD4^+$ T cells, and acquire the ability to phagocytose and cross-present parasite antigen. (**7**) Upon TCR-MHC class I engagement, $CD8^+$ T cells secrete perforin and granzymes, inducing endothelial cell apoptosis and ensuing breakdown of the blood-brain barrier.

Figure is reproduced with permission from [60].

1.4.4 Murine genetic determinants of malaria infection

The contribution of host genetics to malaria susceptibility have been dissected in experimental mouse models, starting with the observation that genetically well-defined inbred mouse strains greatly vary in their susceptibility to ECM with strains such as C57BL/6J, CBA/J, 129S1/SvImJ being susceptible and strains such as BALB/c, A/J, DBA/2, C3H/HeJ, being resistant [86].

1.4.4.1 Berghei resistance loci in mice

Several chromosomal loci regulating susceptibility to PbA-induced ECM have been mapped. Briefly, two inbred mouse strains with differential susceptibility are mated for two generations, producing an F2 progeny that segregates different fractions of each parental genome. The resulting F2 progeny are phenotyped for resistance or susceptibility, and genetic loci affecting malaria phenotypes, like parasitemia or survival, are mapped by quantitative trait locus (QTL) mapping and whole-genome scan. Several mouse *Berr* loci (*Ber*ghei *r*esistance) that regulate susceptibility to PbA infection (survival time and/or parasitemia kinetics) have been mapped in informative crosses (**Table 1-5**). Candidate genes within those loci have been suggested, but identification of the underlying gene has not been achieved for many of these loci due to the large size of the QTL region, and the large number of positional candidates to be considered. Large-scale mouse mutagenesis projects (**Section 1.5**) are the subject of this thesis and this approach has proven more amenable for the unambiguous identification of genes affecting ECM pathogenesis.

Mouse cross	Locus	Chr.	Candidate genes	Ref.
C57BL/6J x DBA/2J	Unnamed	18	*Csf1r, Cd14*	[87]
CBA x DBA/2J	*cmsc*	17	*Tnf, Lta*	[88]
C57BL/6J x WLA	*Berr1*	1	*Tgfb2*	[89]
C57BL/6J x WLA	*Berr2*	11	--	[89]
C57BL/6J x WLA	*Berr3*	9	*Ccr5, Rbp*	[86]
C57BL/6J x WLA	*Berr4*	4	*Tlr4, C8b*	[86]
C57BL/6J x BALB/c	*Berr5*	19	*Ifti1-3 cluster*	[90]
32 inbred strain survey	*Berr6*	6	*Ppar-γ, Tsen2*	[91]
C57BL/6J x 129S1	*Berr7*	1	--	[92]
C57BL/6J x 129S1	*Berr8*	4	--	[92]
FVB/NJ x DBA/2J	*Berr9*	9	*Rora, Irak1bp1, Ibtk*	[93]

Table 1-5. Genetic loci affecting susceptibility to PbA in mice

1.4.4.2 Single-gene defects associated with resistance to ECM

Major advances in genomic technologies have increased our capacity to decipher and study genetic effects in susceptibility to ECM, including the production and characterization of mouse strains bearing targeted loss-of-function alleles at set genes (reverse genetics) (**Table 1-6**).

It has been well established that there is a strong neuroinflammatory component to ECM, and inactivation of many immune-related genes confers resistance to PbA-induced ECM presumably by abrogating the host inflammatory response that drives pathogenesis in this model. Mice with knockout mutations in proinflammatory cytokines and chemokines (e.g. *Ifng*$^{-/-}$, *Cxcl9*$^{-/-}$, *Cxcl10*$^{-/-}$, *Il12*$^{-/-}$, *Il2*$^{-/-}$, *Lta*$^{-/-}$), receptors (e.g. *Ifngr1*$^{-/-}$, *Ifnar1*$^{-/-}$, *Ccr5*$^{-/-}$, *Cxcr3*$^{-/-}$, *Il12rb2*$^{-/-}$) and certain transcription factors that regulate expression of these genes in immune cells (e.g. *Irf1*$^{-/-}$, *Irf3*$^{-/-}$, *Irf7*$^{-/-}$, *Irf8*$^{-/-}$, *Stat1*$^{-/-}$, *Socs1*$^{-/-}$) are highly resistant to ECM. The ECM model has also been used to demonstrate the critical role of immune cells such as T cells (e.g. *Cd4*$^{-/-}$, *Cd8*$^{-/-}$, *Rag2*$^{-/-}$, *Gzmb*$^{-/-}$, *Jak3*$^{-/-}$, *Lck*$^{-/-}$), natural killer (NK) cells (e.g. *Prf1*$^{-/-}$, *Cd1*$^{-/-}$), and platelets (e.g. *Pfx*$^{-/-}$) in pathogenesis. The ECM model has also shown that inactivation of cytoadherence-related genes in mice like *Icam1*, *Itgal*, and *Selp*, also provide protection to disease; suggesting that host proteins involved in pRBC cytoadherence to host endothelium are also required for pathogenesis. Together, these observations support a central role for immune-mediated pathology during ECM, with Th1-proinflammatory responses being primarily implicated.

Novel drugs directed against host-based targets could mimic the protective effect of inactivation mutations in these genes, and may have novel therapeutic value in CM. Such an approach may additionally circumvent the problem of parasite resistance to anti-microbial drugs [55].

Table 1-6. Single-gene defects associated with response to PbA

Gene symbol	Gene name	Knockout effect on PbA infection	References
Abca1	ATP-binding cassette, sub-family A, member 1	Increased survival	[94]
Alox5	Arachidonate 5-lipoxygenase	Susceptible	[95]
Apoa1	Apolipoprotein A-I	Susceptible	[96]
Apoe	Apolipoprotein E	Increased survival	[96]
Arhgef2	Rho/Rac Guanine Nucleotide Exchange Factor 2	Susceptible	Unpublished
B2m	Beta-2 microglobulin	Increased survival	[97]
Bpgm	2,3-bisphosphoglycerate mutase (ENU-induced loss-of-function mutation)	Increased survival	Unpublished
C3	Complement component 3	Increased survival	[98]
C4	Complement component 4	Susceptible	[98]
C5ar	Complement component 5a receptor	Controversial	[99-101]
C5ar2	Complement component 5a receptor 2 (or C5L2)	Susceptible	[100]
Casp1	Caspase 1	Susceptible	[102,103]
Casp12	Caspase 12	Susceptible	[104]
Ccdc88b	Coiled-coil domain-containing 88B (ENU-induced loss-of-function mutation)	Increased survival	[105]
Ccr2	Chemokine (C-C motif) receptor 2	Susceptible	[106]
Ccr5	Chemokine (C-C motif) receptor 5	Increased survival	[107]
Cd1	CD1 antigen, NK T cells	Controversial	[108,109]
Cd14	CD14 antigen	Increased survival	[110]
Cd36	CD36 antigen	Susceptible	[111,112]
Cd4	CD4 antigen	Increased survival	[113]
Cd40	CD40 antigen	Increased survival	[114]
Cd40lg	CD40 ligand	Increased survival	[114]
Cd8	CD8 antigen	Increased survival	[82,113,115]
Cfb	Complement factor b	Susceptible	[98]
Clec4a2	C-type lectin domain family 4, member a2 (or DCIR)	Increased survival	[116]
Cnr2	Cannabinoid receptor 2	Increased survival	[117]
Cpn	Carboxypeptidase N	Susceptible	[118]
Cr3	Complement receptor 3	Susceptible	[119]
Cr4	Complement receptor 4	Susceptible	[119]
Crp	C-reactive protein	Increased survival	[120]
Cxcl10	Chemokine (C-X-C motif) ligand 10 (or IP-10)	Increased survival	[121,122]
Cxcl9	Chemokine (C-X-C motif) ligand 9 (or MIG)	Increased survival	[121]
Cxcr3	Chemokine (C-X-C motif) receptor 3	Increased survival	[121,123]
Cybb	Cytochrome b-245, beta polypeptide (or $gp91^{phox}$)	Susceptible	[124]

Dock8	Dedicator of cytokinesis 8	Increased survival	Unpublished
Fas	Fas/TNF receptor superfamily member 6 (hypomorph)	Increased survival	[125-128]
Fcer1a	Fc receptor, IgE, high affinity I, alpha polypeptide	Increased survival	[129]
Fcgr2	Low affinity immunoglobulin gamma Fc region receptor II	Increased survival	[130]
Gpx1	Glutathione peroxidase 1	Susceptible	[124]
Gzmb	Granzyme b	Increased survival	[83]
Hc	Hemolytic complement (or C5)	Increased survival	[101]
Hdc	Histidine decarboxylase	Increased survival	[131]
Hrh3	Histamine H3 receptor	Susceptible	[132]
Hp	Haptoglobin	Susceptible	[133]
Icam1	Intercellular adhesion molecule 1	Increased survival	[134-137]
Ido1	Indoleamine 2,3-dioxygenase 1	Susceptible	[138]
Ifit1	Interferon-induced protein with tetratricopeptide repeats 1	Susceptible	[139]
Ifitm3	Interferon-induced transmembrane protein 3	Susceptible	[140]
Ifnar1	Interferon (alpha and beta) receptor 1	Increased survival	[141,142]
Ifng	Interferon gamma	Increased survival	[97]
Ifngr1	Interferon gamma receptor 1	Increased survival	[142-145]
Ighe	Immunoglobulin heavy constant epsilon	Increased survival	[129]
Igtp	Interferon gamma induced GTPase (or Irgm3)	Increased survival	[146]
Il10	Interleukin 10	Susceptible	[97]
Il12	Interleukin 12	Increased survival	[147]
Il12rb2	Interleukin 12 receptor subunit, Beta 2	Increased survival	[148]
Il17	Interleukin 17	Susceptible	[149]
Il17r	Interleukin 17 receptor	Susceptible	[150]
Il18	Interleukin 18	Susceptible	[103]
Il1b	Interleukin 1 beta	Susceptible	[103]
Il1r	Interleukin 1 receptor, type I	Susceptible	[102]
Il1rl1	Interleukin 1 receptor-like 1 (or ST2)	Increased survival	[151]
Il2	Interleukin 2	Increased survival	[97]
Il22	Interleukin 22	Susceptible	[152]
Irak4	Interleukin-1 receptor-associated kinase 4	Increased survival	[121,122,153]
Irf1	Interferon regulatory factor 1	Increased survival	[121,139,154]
Irf3	Interferon regulatory factor 3	Increased survival	[155]
Irf7	Interferon regulatory factor 7	Increased survival	[121,123,156]
Irf8	Interferon regulatory factor 8 (hypomorph)	Increased survival	[124,139]
Irgm1	Immunity-related GTPase family M member 1	Increased survival	[125-128,139,146]
Isg15	ISG15 ubiquitin-like modifier	Susceptible	[129,139]
Itgal	Integrin-alpha L (or LFA-1)	Increased survival	[119,130]

Jak3	Janus kinase 3	Increased survival	[124,157]
Lck	Lymphocyte-specific protein tyrosine kinase	Increased survival	[83,158]
Ldlr	Low density lipoprotein receptor	Susceptible	[96]
Lgals3	Galectin 3	Increased survival	[101,110]
Lrp1	Low density lipoprotein receptor-related protein 1	Susceptible	[96]
Lta	Lymphotoxin alpha	Increased survival	[71,131,159,160]
Ltbr	Lymphotoxin beta receptor	Increased survival	[132,160]
Mapk9	Mitogen-activated protein kinase 9 (or JNK2)	Increased survival	[133,161]
Mavs	Mitochondrial Antiviral Signaling Protein	Susceptible	[155]
Mmp9	Matrix metallopeptidase 9 (or Gelatinase B)	Susceptible	[134-137,162]
Msr1	Macrophage scavenger receptor 1	Susceptible	[138,163]
Myd88	Myeloid differentiation primary response gene 88	Controversial	[103,139,159,164,165]
Nlrc4	NLR family, CARD domain containing 4	Susceptible	[139,140]
Nlrp3	NLR family, pyrin domain containing 3	Controversial	[102,141,142,166]
Nos2	Nitric oxide synthase 2, inducible	Susceptible	[97,167]
Nos3	Nitric oxide synthase 3, endothelial cell	Susceptible	[142-145,167]
P2rx7	Purinergic receptor P2X	Susceptible	[102,129]
Pfx	Platelet factor 4 (or Cxcl4)	Increased survival	[146,168]
Pik3cg	Phosphatidylinositol-3-kinase gamma	Increased survival	[97,169]
Plau	Plasminogen activator, urokinase	Increased survival	[147,170]
Plaur	Plasminogen activator, urokinase receptor	Increased survival	[148,170]
Prf1	Perforin 1	Increased survival	[115,125,126,149,171]
Prkcq	Protein kinase C-theta	Increased survival	[150,172,173]
Pycard	Apoptosis-associated speck-like protein containing a CARD	Susceptible	[102]
Rag2	Recombination activating gene 2	Increased survival	[103,126]
Rasal3	Ras protein activator like 3	Increased survival	Unpublished
Selp	P-selectin	Increased survival	[102,136,174]
Socs1	Suppressor of cytokine signaling 1	Increased survival	[151,175]
Socs2	Suppressor of cytokine signaling 2	Controversial	[97,175,176]
Smurf2	SMAD specific E3 ubiquitin protein ligase 2	Susceptible	[155]
Stat1	Signal transducer and activator of transcription 1	Increased survival	[139,152]
Tap1	Transporter 1, ATP-binding cassette, sub-family B	Increased survival	[82]
Tbk1	Tank-binding kinase 1 (hypomorph allele)	Increased survival	[177]
Tbx21	T-box 21 (or T bet)	Increased survival	[178]
Themis	Thymus-expressed molecule involved in selection (ENU-induced loss-of-function mutation)	Increased survival	[158]
Ticam1	Toll-like receptor adaptor molecule 1 (or Trif)	Susceptible	[159,179]
Tirap	Toll-interleukin 1 receptor (TIR) domain-containing adaptor protein	Susceptible	[159]

Tlr1	Toll-like receptor 1	Susceptible	[159]
Tlr2	Toll-like receptor 2	Controversial	[159,164,179]
Tlr3	Toll-like receptor 3	Susceptible	[159]
Tlr4	Toll-like receptor 4	Susceptible	[159,179]
Tlr5	Toll-like receptor 5	Susceptible	[179]
Tlr6	Toll-like receptor 6	Susceptible	[159]
Tlr7	Toll-like receptor 7	Controversial	[159,165,179]
Tlr9	Toll-like receptor 9	Controversial	[159,164,165,179]
Tnf	Tumor necrosis factor	Susceptible	[71,160]
Tnfr2	Tumor necrosis factor receptor superfamily, member 1b	Increased survival	[180,181]
Tnfrsf1a	Tumor necrosis factor receptor superfamily, member 1a	Susceptible	[160,181]
Trim21	Tripartite motif-containing 21	Susceptible	Unpublished
Trim25	Tripartite motif-containing 25	Increased survival	[155]
Ttpa	Tocopherol (alpha) transfer protein	Increased survival	[182]
Usp15	Ubiquitin-specific protease 15	Increased survival	[155]
Vldlr	Very low density lipoprotein receptor	Susceptible	[96]
Zbtb7b	Zinc finger and BTB domain containing 7B (ENU-induced loss-of-function mutation)	Increased survival	Unpublished

1.5 ENU Mutagenesis, a forward genetics tool

1.5.1 Genetic approaches to determine gene function

There are 2 major approaches that are relevant to the genetic analysis of susceptibility to ECM as described in my thesis, “reverse genetics” (gene-to-phenotype) and “forward genetics” (phenotype-to-gene). In the reverse genetics approach, a gene of interest is inactivated and the effect of this inactivation on a given phenotype is analyzed in corresponding transgenic mice, knockouts, knock-ins, CRISPR/Cas9 and so on. The “forward genetics” approach is phenotype-driven, and aims to study the genetic basis of differential response to stimuli, for instance, ECM induced by PbA. This approach is most powerful when coupled to chemical mutagenesis with ENU, and where mutations causing a unique phenotype can be quickly identified by novel genomic methods (whole exome and whole genome sequencing) [183]. Random mutagenesis can be achieved by treatment of animals with several DNA-damaging agents such as ionizing radiation, chlorambucil, ethyl methane sulphonate, acrylamide, or N-ethyl-N-nitrosourea (ENU) [183]. Depending on which agent is utilized, mutagenesis can result in either single base-pair mutations, rearrangements or deletions [183]. Introduction of germ-line mutations by ENU mutagenesis has become the most favored mutagenic agent due to its potency, preferential activity in spermatogonial stem cells, and a propensity to introduce random point mutations [56].

1.5.2 Mutagenizing the mouse genome by ENU

In the early 1980s, W. L. Russell and his colleagues first described ENU as the most potent chemical mutagen of mice [184]. ENU is an alkylating agent that introduces random, genome-wide single base pair mutations [185]. The mutagen transfers its ethyl group onto oxygen or nitrogen radicals in DNA of spermatogonial cells, creating DNA adducts that provoke mispairing and heritable base-pair substitutions if unrepaired by host cell machinery during replication [56]. Sequence-based approaches have estimated that ENU has an average point mutation rate of 1.5 per Mb of genomic DNA [186], with preferential bias toward AT to GC transitions (45%) and AT to TA transversions (25%) [56,187]. Analysis of the largest ENU mutant repertoire

(Mutagenetix), containing 185 mutant stocks, revealed that the majority of substitutions result in missense mutations (61%), and less frequently by nonsense alleles (19%), splicing defects (18%), and frame-shift mutations (2%) [56].

Since ENU primarily induces point mutations, it can generate an array of possible mutant forms of a gene (i.e. allelic series); animals that carry missense mutations, loss-of-function mutations, gain-of-function mutations, hypomorphs, hypermorphs, and antimorphs [188]. In contrast to knock-out animals (i.e. complete absence of a protein), these allelic variants are valuable because they provide a range of phenotypes in which a gene's function can be affected [188]. The full range of alleles generated by ENU model genetic variation found in the human genome better than a knockout would [189]. In fact, many human diseases are caused by mutations that influence protein structure or function, or binding affinity rather than complete inactivation [190]. This approach offers a unique opportunity to uncover or dissect molecular pathways involved in host response to infection in the mouse to better understand mechanisms of human disease.

1.5.3 Breeding strategies

Typically, adult male mice are administered 1 intraperitoneal injection of the ENU mutagen (80 to 100 mg/kg dose) weekly for 3 weeks, followed by a 12-week rest period to allow recovery of fertility [187]. The breeding schemes used to propagate the induced-mutations depend upon whether the study aims to screen for recessive or dominant mutations. Briefly, ENU-treated generation 0 males (G0) are bred to wild type females to produce the first generation of mutagenized offspring (G1), which carry ENU-induced mutations in the heterozygous state. It is estimated that each G1 male carries in the order of 30 to 50 potential functional mutations throughout its genome [187]. For dominant mutation screens, G1 offspring can be phenotyped directly. If one chooses to study recessive mutations, third-generation (G3) mice are required for phenotyping. G3 offspring can be produced by intercrossing second-generation (G2) mutant littermates, or by backcrossing G2 females to their G1 fathers (**Figure 1-4**) [187]. On average, 4 to 5 loss-of-function homozygous mutations are present in the homozygous state in G3 mice [56].

1.5.4 Applications

Point mutations introduced within the mouse genome by ENU can translate into disruptive alterations of a protein and associated pathways, and could express itself as a novel phenotype in the mouse, or phenodeviance (i.e. resistance to ECM in a mouse that would otherwise be susceptible). In our screen, animals were considered phenodeviant (resistant to ECM) if they survived the cerebral phase (days 5 to 12 post-PbA infection) of the disease. A recessive homozygote variant segregating within a pedigree that produces a phenodeviant phenotype at a frequency of about 25% in G3 animals can be identified using a labor-intensive positional cloning approach or by whole-exome sequencing (WES). Emergence of a reference genome alongside recent advances and affordability of next-generation sequencing technology have propelled ENU mutation discovery from a laborious exercise to an efficient form of causal mutation discovery [189]. In the WES approach, the sequence of all exons and exon-intron boundaries in a subset of resistant G3 animals from the same pedigree are determined and aligned to the annotated reference C57BL/6J genome. SNP lists generated for each sequenced mouse are compared to identify homozygous variants common between them. These ENU-induced variants are validated by genotype-phenotype correlations of additional G3 mice from the pedigree (i.e. ECM-resistant animals should be homozygous for the mutant variant, while ECM-susceptible animals should be homozygous for WT alleles).

Results from one of our several ENU screens is summarized in **Figure 1-5**, where over 2000 G3 mice were tested for survival to ECM in 91 mutant pedigrees (unpublished data). A total of 6 phenodeviant pedigrees displaying robust ECM resistance were identified in this screen, and a subset of them were characterized further in the work of this thesis.

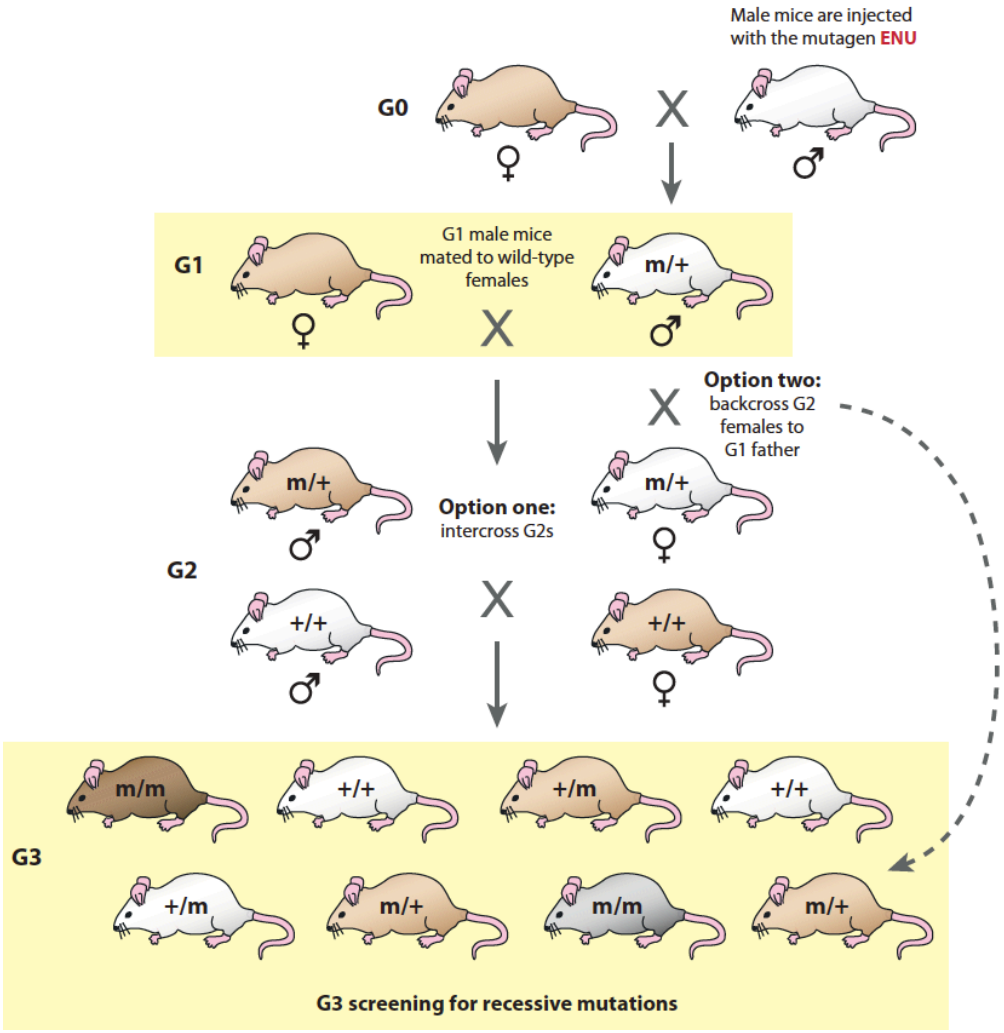

Figure 1-4. Breeding mice to screen for ENU-induced recessive mutations

Treatment with ENU introduces point mutations in the germ-line of generation 0 male (♂) (G0) mice. The mutagenized male is outcrossed to a wild-type female (♀) to produce first generation offspring (G1), which are heterozygous for ENU-induced mutations (m/+). Second generation (G2) mutants are produced by outcrossing the G1 male to additional wild-type females. For screening of recessive mutations, third-generation (G3) mice are required. Breeding of G3 mice can be produced two ways; the first strategy involves intercrossing second-generation (G2) mutant littermates, and the second strategy involves backcrossing G2 females to their G1 fathers. G3 mice are expected to carry homozygous ENU-induced mutations (m/m) in 25% of the offspring.

Figure is reproduced with permission from [187].

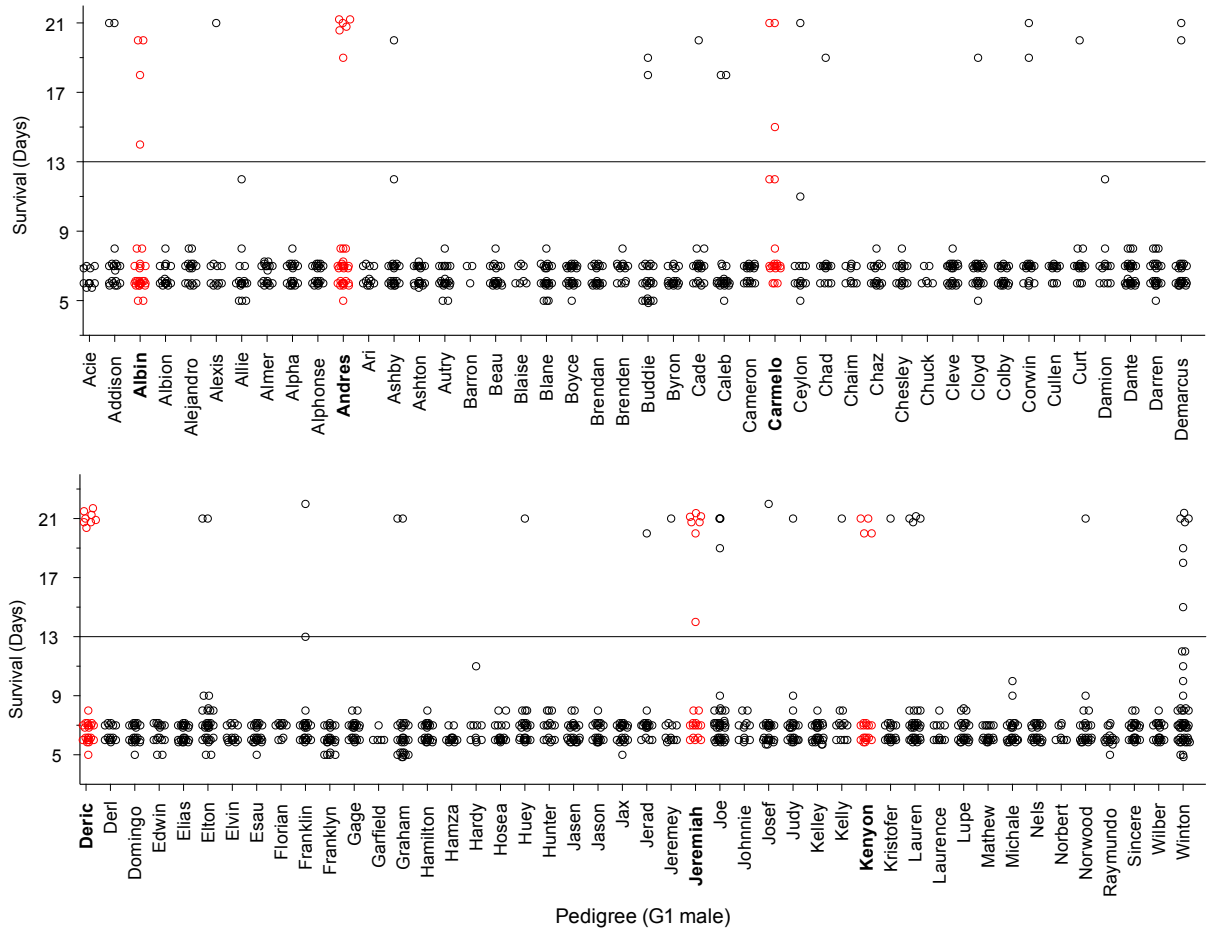

Figure 1-5. Overall survival of G3 mice from the B6-B10 2009 ENU screen

Over 2000 G3 mice (represented by individual dots) in 91 independent pedigrees were phenotyped for survival to PbA-induced ECM in the B6-B10 screen. PbA-infected animals that developed neurological symptoms of disease between days 5 to 12 post-infection were deemed ECM-susceptible, while those that did not develop symptoms and survived beyond day 13 were considered ECM-resistant. A total of 6 ECM-resistant pedigrees were discovered (indicated in red) on the basis of consistently producing resistant offspring in multiple infection experiments, and at the expected frequency of about 25% for carriers of recessive homozygous ENU mutations.

Chapter 2:

THEMIS is required for pathogenesis of Cerebral Malaria and for protection against pulmonary Tuberculosis

2.1 Abstract

We identify an N-ethyl-N-nitrosourea (ENU)-induced I23N mutation in the THEMIS protein that causes protection against experimental cerebral malaria (ECM) caused by infection with *Plasmodium berghei* ANKA (PbA). *Themis*^{I23N} homozygote mice show reduced CD4^{+} and CD8^{+} T lymphocyte numbers. ECM-resistance in PbA-infected *Themis*^{I23N} mice is associated with decreased cerebral cellular infiltration, retention of blood-brain barrier integrity, and reduced pro-inflammatory cytokine production. THEMIS^{I23N} protein expression is absent in mutant mice, concurrent with decreased THEMIS^{I23N} stability observed *in vitro*. Biochemical studies *in vitro*, and functional complementation *in vivo* in *Themis*$^{I23N/+}$*:Lck*$^{-/+}$ double-heterozygotes demonstrate that functional coupling of THEMIS to LCK tyrosine kinase is required for ECM pathogenesis. Dampening of pro-inflammatory responses in *Themis*^{I23N} mice causes susceptibility to pulmonary tuberculosis. Thus, THEMIS is required for development, and ultimately function of pro-inflammatory T cells. *Themis*^{I23N} mice can be used to study the newly discovered association of *THEMIS* (6p22.33) with inflammatory bowel disease, and multiple sclerosis.

2.2 Introduction

The inflammatory response to microbial stimuli is a multi-step process that involves sensing of a danger signal, recruitment of myeloid (neutrophils, basophils, monocytes, macrophages) and lymphoid ($CD4^+$ and $CD8^+$ T lymphocytes, NK cells) cells, production of pro-inflammatory cytokines (TNF-α, IFN-γ, IL-1), and chemokines (IL-8, MCP1, KC), elimination of the microbial threat, and tissue destruction and repair [191,192]. In the presence of persistent tissue injury, or of an unusual infectious or environmental insult, overexpression of pro-inflammatory mediators or insufficient production of anti-inflammatory signals (PGE2, IL-10, TGF-b, IL-1Ra) causes acute or chronic states of pathological inflammation. Population studies of chronic inflammatory diseases such as inflammatory bowel disease, multiple sclerosis, rheumatoid arthritis and others have identified a complex genetic architecture to disease susceptibility, with additional effects of microbial triggers that initiate and sustain pathological inflammation [193-195]. Many of the mapped disease loci and genes are common to two or more such diseases, suggesting that some critical features of pathogenesis are shared between these conditions.

Cerebral malaria (CM) is an acute life-threatening encephalitis that is a complication of *Plasmodium falciparum* infection in children and pregnant women [29]. CM-associated neuroinflammation has been studied in a mouse model of experimental cerebral malaria (ECM) induced by infection with *Plasmodium berghei* ANKA (PbA) [80]. In this model, brain endothelial cells activated by trapped parasitized red blood cells (pRBCs) produce cytokines and chemotactic factors that recruit neutrophils and activated $CD8^+$ and $CD4^+$ T cells. Release of cytotoxic molecules by inflammatory leukocytes leads to loss of integrity of the blood-brain barrier (BBB), microthrombosis, hypoxia of the brain parenchyma, leading to neurological symptoms including seizures and coma, and ultimately death [67,196]. Recent findings show that elevated levels of inflammatory molecules (TNF-α, IFN-γ, IL-1β, MIP-1α, MIP-1β, CXCL10, C5a) are associated with increased risk of CM, supporting a neuroinflammatory component to human CM [100,197,198]. Antibody-mediated cell ablation experiments have demonstrated a strong pathological role for $CD8^+$ T cells, and $CD4^+$ T cells, NK cells

and neutrophils in ECM [80]. Conversely, we and others have demonstrated an ECM protective effect of mutations in major pro-inflammatory genes such as interferon γ (*Ifng*) and its receptor (*Ifngr1*), lymphotoxin (*Lta*/*Ltb*), complement component 5a (*Hc*) (reviewed in [55]), and certain transcription factors that regulate expression of these genes in myeloid and lymphoid cells, including interferon regulatory factor 1 (IRF1) [154] , IRF8 and STAT1 [139]. Whole brain transcript profiling along with chromatin immunoprecipitation and sequencing (ChIP-seq) data comparing ECM-susceptible to resistant (*Irf8*^{myls} BXH2 strain) mice identified a core transcriptome activated during ECM [139]. This transcriptome contains several genes, including IRF1, IRF8 and STAT1, which have been identified as risk factors for acute and chronic human inflammatory conditions. Thus, studies in the mouse model of ECM may identify critical regulatory genes and pathways that underlie shared etiology and pathogenesis of acute and chronic human inflammatory diseases.

To uncover novel host factors that, when inactivated, protect against the development of ECM, we employed an N-ethyl-N-nitrosourea (ENU) mutagenesis screen in mice. We report a recessive mutation in the gene *Themis* ('THymus-Expressed Molecule Involved in Selection') (MGI accession: 2443552) that protects mice from lethal neuroinflammation upon infection with PbA. The effect of this mutation on immune cell function has been characterized at the cellular and molecular levels.

2.3 Materials and Methods

Ethics statement

This study was performed in accordance and compliance with the strict guidelines of the Canadian Council on Animal Care (CCAC). Protocols were approved by the ethics committee of McGill University (Protocol Number 5287), and the institutional care and use committee of Trudeau Institute, USA (Protocol number IACUC 02-191 (Cooper)). Mice were euthanized by carbon dioxide inhalation, and every effort was made to minimize animal suffering.

Mice

Inbred C57BL/6J (B6) and C57BL/10J (B10) mice were purchased from the Jackson laboratories (Bar Harbor, Maine, USA). *Lck* mutant mice (*Lck*^{tm1Mak} referred to as *Lck*$^{-/-}$) were provided by Dr. André Veillette (IRCM, Montreal). Eight week-old B6 males were administered 3 weekly doses of ENU (N-ethyl-N-nitrosourea; 90 mg/kg) by intraperitoneal (ip) injections. Mutagenized G0 males were bred to wild-type (WT) B10 to generate a G1 offspring, which were backcrossed again to B10 females (G2 offspring). Two G2 females per pedigree were backcrossed to their G1 father to generate G3 mice for phenotyping. Homozygote *Themis*^{I23N} G3 mice were intercrossed to produce a stable mouse line.

Parasites and Infections

Plasmodium berghei ANKA (PbA) parasites from the Malaria Reference and Research Reagent Resource Center (MR4) were maintained as frozen stocks at -80°C. Blood parasitemia was determined on thin blood smears stained with Diff-Quick reagents. Seven week-old G3 mice were intravenously (iv) infected with 10^6 parasitized red blood cells (pRBCs). Mice were monitored for appearance of neurological symptoms 3 times daily. In other experiments, mice were infected (iv) with $5x10^5$ *Plasmodium chabaudi* AS pRBCs, and blood parasitemia was monitored over time. *Plasmodium* strains were provided by Dr. Mary M. Stevenson (McGill University Health Center Research Institute, Montreal).

Genomic Analyses

Melvin G3 mice were genotyped using a panel of 193 single nucleotide polymorphic (SNP) markers informative for parental B6 vs. B10 strains [199]. Linkage analysis was performed with the R/qtl software package using the binary model, where survival past day 13 (ECM-resistance vs. susceptibility) was used as a phenotype to detect linkage. Whole-exome sequencing was carried out on two ECM-resistant *Melvin* G3 mice. Exome capture was performed using a SureSelect Mouse All Exon kit (Agilent Technologies, USA) and parallel sequencing on an Illumina HiSeq 2000 (100 bp paired-end reads). Reads were aligned to mouse genome assembly July 2007 (NCBI37/mm9) with Burrows-Wheeler Alignment (BWA) tool [200] and coverage was assessed with BEDTools [201]. Variants were called using Samtools pileup and varFilter [200], and were annotated using Annovar [202]. The *Themis* mutation was genotyped by PCR (Primers: 5'-CCACCCCCATGTGTTTCTAC-3', 5'-CACTTTGTTTGCTGGGTGTG-3') followed by sequencing of the PCR product.

Reverse transcriptase quantitative polymerase chain reaction

RT-qPCR was performed using the following primers; 5'-TGAAATCCAAGGTGTGCTGA-3' and 5'-CGTCCGTAGACAGCAACTGA-3'. Themis mRNA was expressed relative to the HPRT reference control.

Protein Expression in Transfected Cells

A full-length wild-type *Themis* cDNA was PCR amplified from a B6 thymus mRNA template, using the following primer sequences: 5'-ACTGGAATTCCCACCATGGCTTTATCTCTGGAAG-3', and 5'-CAGTCTCGAGTCACAGTGGTGCTTGCGG-3'. Restriction sites for EcoRI (GAATTC) and XhoI (CTCGAG) were introduced into the primers to facilitate cloning into pcDNA3 expression plasmid. A full-length $Themis^{I23N}$ mutant was generated by site-directed mutagenesis using primers 5'-CCTGACTGGTTTTCTAGGA-3' and 5'-TCCTAGAAAACCAGTCAGG-3'. HEK293 cells (ATCC-CRL-1573) were transfected with Lipofectamine 2000 reagent (Life Technologies) followed by selection in Geneticin (G418, 500 μg/ml) (Invitrogen, CA, USA). Protein expression was monitored by

immunoblotting using an anti-THEMIS antibody (3D4) (R.H. Schwartz, NIH). For protein stability studies, stably transfected cells were incubated with cycloheximide (20 µg/ml). Cells were lysed in 50 mM Tris pH 7.5, 150 mM NaCl, 1% TritonX-100, and 0.1% sodium dodecyl sulfate (SDS), supplemented with protease/phosphatase inhibitors.

THEMIS Tyrosine Phosphorylation

HEK293T cells (ATCC- CRL-3216) ($3x10^6$) were co-transfected with WT or *Themis*^{I23N} constructs, and either WT or a hyperactive F505 *Lck* variants (Dr. André Veillette, IRCM, Montreal), and 24 hours later, cells were lysed in 50 mM Tris pH 7.5, 150 mM NaCl, 1% TritonX-100, and 0.1% SDS. THEMIS was immunoprecipitated (IP) with anti-THEMIS antibody (16 hours, 4°C), followed by capture with Protein G agarose beads. IP products were separated on gel, followed by immunoblotting with a mouse anti-phosphotyrosine antibody (P-Tyr-100) (Cell Signaling Technology, MA, USA) and anti-mouse TrueBlot ULTRA IgG HRP secondary antibody (eBioscience). Blots were re-probed with anti-THEMIS antibody and blots from whole cell lysate were probed with anti-LCK antibody (Dr. André Veillette) to validate immunoprecipitation and transfection efficiency, respectively.

Evans Blue Dye Extravasation

PbA-infected mice (day 6 post-infection) were injected (iv) with 0.2 ml 1% Evans blue dye (Sigma-Aldrich, Oakville, Canada). One hour later, mice were exsanguinated and perfused with PBS. Brains were excised and incubated with 1 ml of dimethyl formamide for 48 hours to extract Evan's blue dye from the tissues. Optical density was measured at 610 nm, and measurements were converted into µg of dye extravasated per gram of tissue.

Immunophenotyping

Thymus and spleen cells ($1\text{-}2x10^8$) were stained with anti-CD4-PECy7 and anti-CD8-PE, and double negative (DN; $CD4^-CD8^-$), double positive (DP; $CD4^+CD8^+$), CD4 single positive ($CD4^+$; $CD4^+CD8^-$) and CD8 single positive ($CD8^+$, $CD4^-CD8^+$) T cells were isolated by FACS sorting. Leukocytes infiltrating the brain of infected animals were isolated as previously described [203]. Thymus and spleen cells from control and PbA-

infected mice were analyzed by FACS using markers of lymphoid cells (anti-CD45-APC-efluor780, anti-CD8-Bv421, anti-CD4-PE, anti-TCRβ-FITC), and myeloid cells (anti-CD45-APC-efluor780, anti-CD11b-APC, anti-Ly6G-FITC). All antibodies purchased from BioLegend. Viable leukocytes were gated as $CD45^{+}$ in the spleen and thymus, and as $CD45^{hi}$ cells in the brain. Spleen cells were stimulated with either CD3/CD28 (eBioscience), or with IL12p70/IL-18 (BioLegend) for 48 hours, followed by measurement of TNF-α and IFN-γ by ELISA (BioLegend). Cytokines were also measured in sera of naïve and PbA-infected mice.

Infection with Mycobacterium tuberculosis (Mtb)

Eight-week-old mice were infected via the aerosol route with ~ 200 colony-forming units (CFUs) of *Mycobacterium tuberculosis* H37Rv. Bacterial replication was determined by colony counts on organ homogenates. Histology was performed on the lung caudal lobe with formalin-fixed sections stained with hematoxylin and eosin (H&E), or stained for acid-fast bacilli by Ziehl-Neelsen.

2.4 Results

We used ENU mutagenesis in mice to identify genes that, when inactivated, protect against lethal experimental cerebral malaria (ECM) induced by *P. berghei* (PbA) infection [92,157]. In this screen, G3 offspring were generated (**Figure 2-1A**) and infected with PbA. ECM-susceptible C57BL/6J (B6) and C57BL/10J (B10) controls develop fatal neurological symptoms (paralysis, tremors, and seizures) between days 5-8 post-infection. Conversely, PbA-infected G3 mice that do not develop cerebral symptoms and survive beyond day 13 are considered ECM-resistant. Mating of G1 male *Melvin* to two G2 females produced G3s where 19% of them were ECM-resistant (8/34 pups; **Figure 2-1B**). Linkage analysis revealed a linkage peak on Chr 10 (LOD~8.63, position 27.6 Mb) (**Figure 2-1C**). Haplotype analysis of ECM-resistant mice showed enrichment for homozygosity of B6-derived alleles (A; from ENU-treated G0) on proximal Chr 10, while ECM-susceptible mice displayed enrichment for homozygosity for WT B10 alleles (B) (**Figure 2-1D**). This suggests that ECM-resistance in the *Melvin* pedigree is caused by homozygosity for an ENU-mutation on proximal Chr 10.

Whole exome sequencing of 2 ECM-resistant G3 mice identified an ENU-associated homozygous mutation under the linkage peak on Chr 10. The T-to-A transversion in exon 1 of *Themis* ('THymus-Expressed Molecule Involved in Selection') causes a substitution of isoleucine (I) to asparagine (N) at position 23 (I23N) of the 'cysteine-containing, all-β in Themis-1' (CABIT-1) domain of THEMIS (**Figure 2-2A**). I23 is invariant in the THEMIS family and the I23N substitution is non-conservative, suggesting that it is likely to be pathological (**Figure 2-2A**). Genotype-phenotype correlations in additional *Melvin*-derived mice validated that homozygosity for I23N (*Themis*^{I23N}) is fully protective against ECM, while heterozygosity is mildly protective, and all WT mice are ECM-susceptible (Figure 2B). The ECM-resistance phenotype in *Themis*^{I23N} mice is independent of PbA blood parasitemia between days 1-6 (**Figure 2-2C**). In addition, challenging mice with *Plasmodium chabaudi* AS, a malarial parasite whose pathogenesis is limited to blood stage replication without cerebral disease, indicates that *Themis*^{I23N} has no effect on the ability of mice to control replication (days 4-9) and eradicate (days 9-12; days 14-18) blood stage parasites (**Figure 2-2D**).

THEMIS is a 73 kDa protein expressed in the thymus, spleen and lymph nodes [204-206]. We found that expression of THEMIS was very low in the thymus of homozygous *Themis*^{I23N} mutant mice, while heterozygote mutants showed expression levels similar to B6 or 129S1/SvImJ WT (**Figure 2-3A**). Expression of the THEMIS^{I23N} variant was extremely low in sorted CD4$^+$CD8$^+$ double positive (DP) thymic lymphocytes, and was undetectable in all other sorted T cell populations from thymus or spleen (Figure 3B). We found that the mutation had no effect on messenger RNA expression in sorted T cells (Figure 3C). To investigate a possible effect of the mutation on protein stability, HEK293 cells stably expressing WT or *Themis*^{I23N} variants were treated with cycloheximide (CHX) and analyzed by immunoblotting (**Figure 2-3D**,**E**). The THEMIS^{I23N} variant shows a drastic reduction in half-life (estimated ~6 hours), when compared to WT (>12 hours), strongly suggesting that the I23N mutation impairs protein stability resulting in low levels of THEMIS^{I23N} expression *in vivo*.

We investigated the effect of the *Themis*^{I23N} mutation on the number and function of T cells, both at steady state and during infection. FACS analysis indicated a significant depletion of single positive CD4$^+$ (**, p=0.0026) and CD8$^+$ (*, p=0.0335) T cell compartments in the thymus of *Themis*^{I23N} mice compared to WT (**Figure 2-4A**,**C**). Depletion of singly positive T cells was also evident in splenic CD4$^+$ (**, p=0.0069) and CD8$^+$ (*, p=0.0152) cells (**Figure 2-4B**,**D**). Such depletion of CD4$^+$ and CD8$^+$ T cells has been reported for null mutant alleles at *Themis* [204-208], suggesting that I23N is a complete loss-of-function allele. The effect of the *Themis*^{I23N} mutation on number and function of T cells was investigated at day 5 post PbA infection, a time at which peripheral T cells become activated [80]. PbA infection caused a significant increase in the number of CD4$^+$ splenic T cells in both mutant and WT; however, the total number and relative frequency of CD4$^+$ T cells was much greater in the control than the mutant (**, p=0.0079) (**Figure 2-5A**,**B**). We observed reduced IFN-γ production *in vitro* by *Themis*^{I23N} mutant splenocytes from PbA-infected mice upon T cell receptor activation via anti-CD3/CD28 stimulation (**, p=0.0012), or following incubation with IL-12/IL-18 (**, p=0.0022) (Figure 5C). Decreased IFN-γ production by mutant splenocytes *in vitro*

was paralleled *in vivo* by lower levels of serum IFN-γ in infected mutant mice (*, p=0.0147) (**Figure 2-5E**). Similarly, splenocytes from *Themis*^{I23N} mutants produced significantly less TNF-α in response to stimulation with anti-CD3/CD28 (*, p=0.0154). Neuroinflammation in ECM is associated with breakdown of the blood-brain barrier (BBB) [84,209]. Evans Blue dye extravasation assay was used to assess BBB integrity of PbA-infected mice. As opposed to the brains of PbA-infected B6 controls that cannot exclude the blue dye, brains from *Themis*^{I23N} mutants remained unstained, indicative of intact BBB (**Figure 2-5G**). By flow cytometry analysis, we observed a reduced cellular infiltration of CD45^{hi} leukocytes, and CD45^{hi}Ly6G^{+}/CD11b^{+} neutrophils and of CD45^{hi}CD4^{+} and CD8^{+} T cells in the brain of *Themis*^{I23N}-infected mice compared to controls (**Figure 2-5H**). Hence, ECM-resistance in *Themis*^{I23N} mice is concomitant to reduced numbers of CD4^{+} and CD8^{+} T cells, reduced pro-inflammatory cytokine production during infection, and preservation of BBB integrity.

THEMIS participates in T cell receptor signaling, and its activity is regulated by the CD4 and CD8 glycoprotein-associated tyrosine kinase LCK [210-213]. We examined the coupling of THEMIS and LCK in pathogenesis of ECM. We first examined LCK-mediated tyrosine phosphorylation of the WT and THEMIS^{I23N} variants *in vitro* (**Figure 2-6A**). The hyperactive LCK^{F505Y} tyrosine-phosphorylated WT and THEMIS^{I23N} with similar efficiency. Furthermore, we examined the requirement of LCK for neuroinflammation in the ECM model. *Lck*$^{-/-}$ mice challenged with PbA were resistant to ECM (**Figure 2-6B**), ultimately succumbing from hyperparasitemia later in infection (days 18-21), similarly to ECM-resistant *Themis*^{I23N} homozygotes. We also conducted genetic complementation studies in mice that are doubly heterozygote for loss-of-function mutations at *Themis* and *Lck* (*Themis*$^{I23N/+}$:*Lck*$^{-/+}$). PbA-infected *Themis*$^{I23N/+}$:*Lck*$^{-/+}$ double heterozygotes showed increased ECM-resistance (43% survival) compared to mice heterozygote for *Themis*$^{I23N/+}$ alone (16% survival), although this difference did not reach statistical significance (Log-Rank statistical test; p=0.088). (**Figure 2-6B**). However, PbA-infected *Themis*$^{I23N/+}$:*Lck*$^{-/+}$ double heterozygotes are ECM-resistant when compared to B6 WT controls (p=0.006). Taken together, these results show that LCK and THEMIS are individually required for pathological inflammation during ECM, with possible functional coupling between the two proteins.

Pro-inflammatory Th1 cytokines produced by T cells are required for protection against intracellular infections [139]. We evaluated the response of *Themis*^{I23N} mice to infection with *Mycobacterium tuberculosis* (Mtb). Mice were infected with low dose aerosol Mtb, and bacterial replication was assessed in lungs, spleen and liver at day 35, 60, and 90 post-infection (**Figure 2-7A**). *Themis*^{I23N} mutants displayed a 5-to-10 fold increase in Mtb replication when compared to controls. Histological analysis of Mtb-infected B6 lungs identified typical small mononuclear accumulations on the background of normal lung alveolar network, while large segments of *Themis*^{I23N} mutant lungs were consolidated with extensive infiltration of leukocytes, and with areas of necrosis (**Figure 2-7B**). Increased microbial burden in these inflammatory lesions in the *Themis*^{I23N} mutants was also evident upon staining for acid-fast bacilli (**Figure 2-7B**). Together, these results indicate that *Themis* is required for protection against mycobacterial infections.

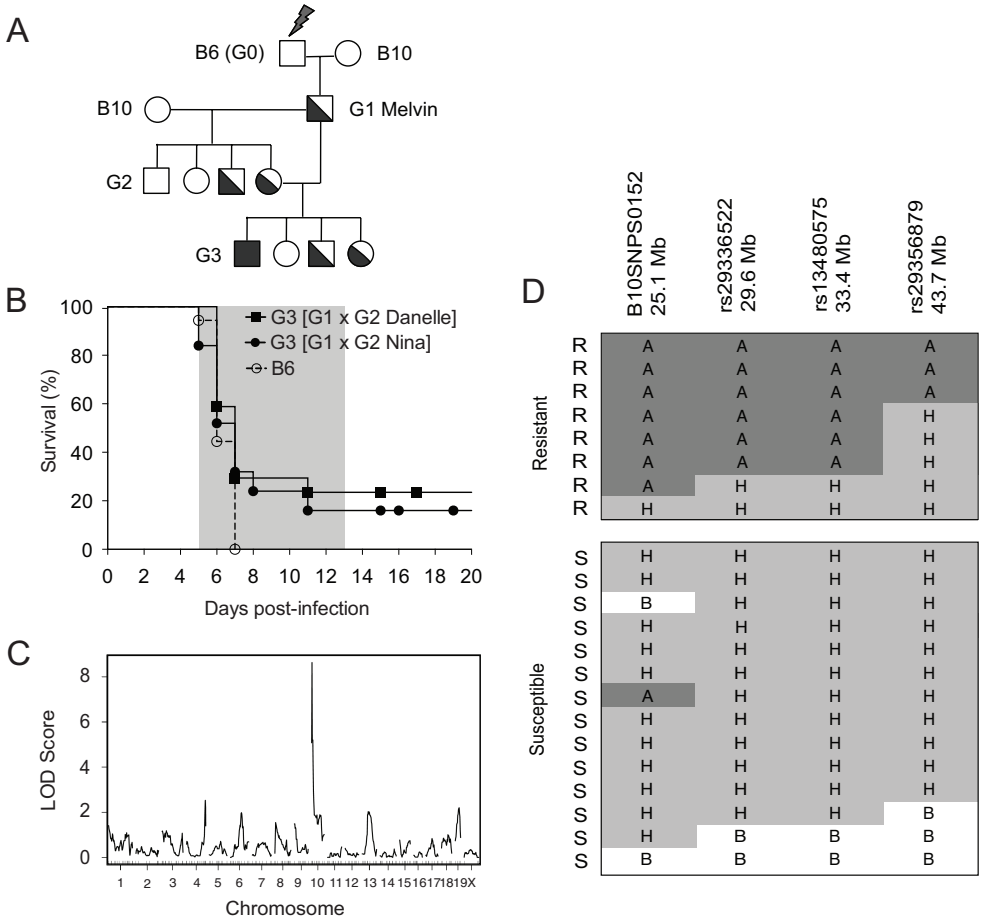

Figure 2-1. Resistance to *P. berghei* ANKA-induced cerebral malaria in the *Melvin* pedigree

(**A**) Breeding scheme for the production of ENU-induced mutant mice [see Materials and Methods for details]. (**B**) G2 females, Danelle and Nina, were backcrossed to their G1 father *Melvin*, and their offspring infected with 106 PbA-parasitized red blood cells (pRBCs) and monitored for neurological symptoms and survival. Mice that survive beyond day 13 are considered ECM-resistant. G3 [G1xG2 Danelle] (n=17), G3 [G1xG2 Nina] (n=25), B6 (n=18). (**C**) Genome-wide linkage analysis was performed on 22 G3 DNA samples from pedigree *Melvin* (8 resistant, R, and 14 susceptible, S) using a panel of 193 informative markers that distinguish B6 vs B10. The LOD score trace detects significant linkage to proximal Chr 10 (LOD~8.63, position 27.6 Mb, p=0.05). (**D**) Compiled haplotype data from pedigree *Melvin* animals show enrichment for homozygous B6 (A) alleles between position 25.1 and 33.4 Mb on Chr 10 in resistant mice, indicating that an ENU-induced mutation generated on the B6 background of these mice is conferring ECM-resistance. Susceptible mice genotype as either heterozygous (H) or homozygous B10 (B).

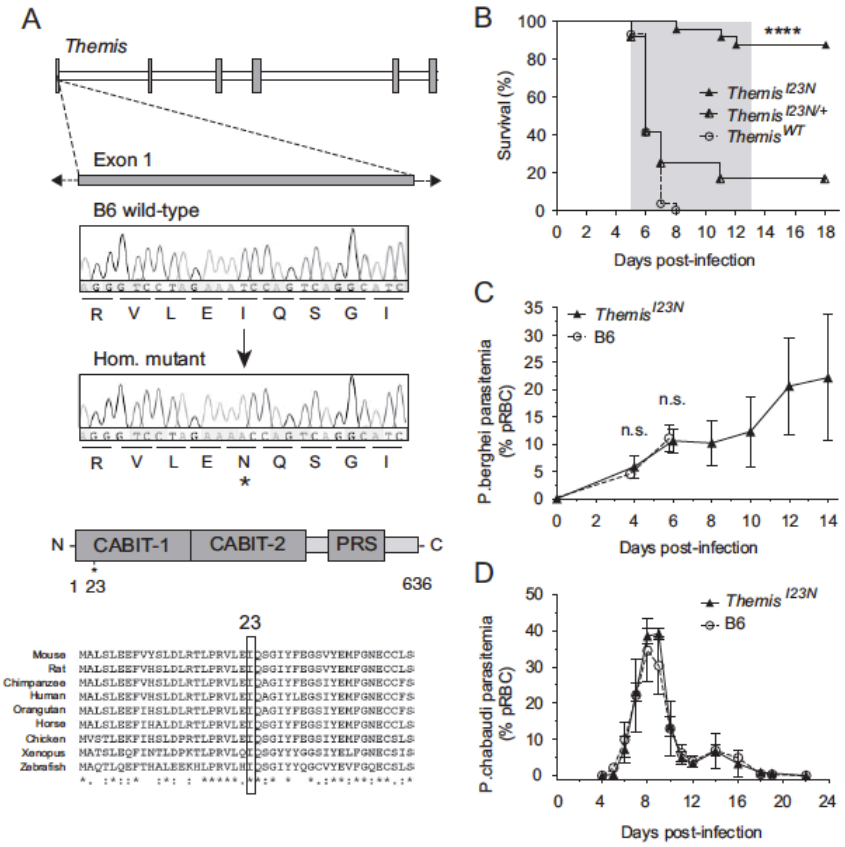

Figure 2-2. An ENU-induced mutation in the CABIT-1 domain of protein THEMIS protects against experimental cerebral malaria

(**A**) Whole-exome sequencing identifies a T-to-A transversion in exon 1 of the *Themis* gene, causing an isoleucine (I) to asparagine (N) amino acid substitution at position 23 in the 'cysteine-containing, all-β in Themis 1' (CABIT-1) domain. Isoleucine at position 23 of the protein is highly conserved across species. (**B**) Survival plots of PbA-infected *Themis* homozygote mutants (*Themis*^{I23N}) (n=24), heterozygotes (*Themis*$^{I23N/+}$) (n=12), and *Themis* wild-type (WT) or C57BL6/J (B6) (n=29) mice. Statistical significance between homozygote mutant and WT mice was determined using the Log-rank test (****, p<0.0001). Data is compiled from 13 independent infections. (**C**) The course of *P. berghei* ANKA blood parasitemia is similar in wildtype B6 controls and in *Themis*^{I23N} homozygotes (n=5/group). (**D**) *Themis*^{I23N} homozygote mutants (n=3) challenged with *Plasmodium chabaudi* parasites are resistant to blood-stage malaria and display blood parasitemia similar to that of B6 controls (n=5). Data is compiled from two independent experiments. (**C-D**) Data are expressed as mean ± SD for each group. Statistical analysis was performed using the two-tailed unpaired student t-test. (n.s., non-significant).

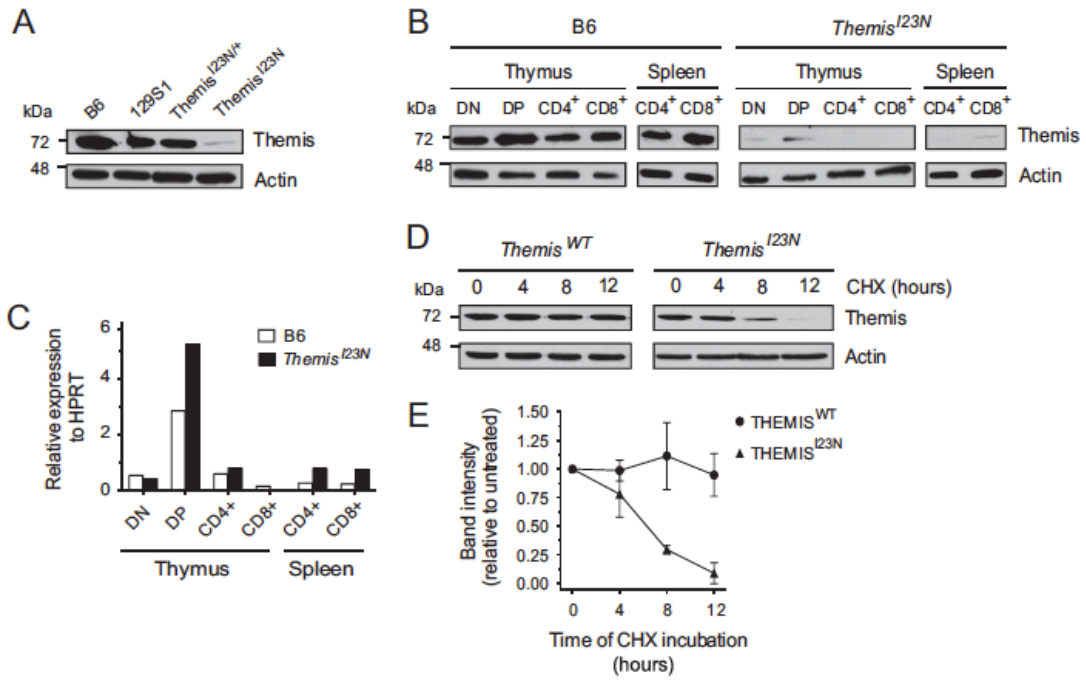

Figure 2-3. Reduced protein expression, and reduced stability of the THEMIS^{I23N} variant in vivo and in vitro

(**A**) Cell extracts from the thymus of wild-type control C57BL/6J (B6) and 129S1/SvImJ (129S1), and Themis heterozygote (*Themis*$^{I23N/+}$) and homozygote (*Themis*^{I23N}) mice were analyzed for THEMIS protein expression by immunoblotting. (**B**) Cell extracts from sorted spleen and thymic T cells; CD4$^-$CD8$^-$ (DN), CD4$^+$CD8$^+$ (DP), CD4$^+$CD8$^-$ (CD4$^+$), and CD4$^-$CD8$^+$ (CD8$^+$) were analyzed for expression of WT and THEMIS^{I23N} protein variant by immunoblotting. (**C**) Reverse transcriptase quantitative polymerase chain reaction (RT-qPCR) was performed on RNA isolated from sorted T cell populations from thymus and spleen. *Themis* mRNA is expressed relative to the HPRT reference control. The data is from a representative experiment, with RNA isolated from two mice per group. (**D**) Transfected HEK293 cells stably expressing WT or THEMIS^{I23N} protein variant were treated with cycloheximide (CHX, 20 µg/ml) for 4, 8, and 12 hours, and equal amounts of protein (50 µg) were analyzed by immunoblotting. Data is a representation of three independent experiments, assessing two different clones per construct. (**E**) Data from Figure 3D was quantified by ImageJ; THEMIS band intensities were normalized to actin loading controls, and expressed as the fraction of protein expression present at T0 (untreated) for each construct. Data is expressed as a mean ± SD.

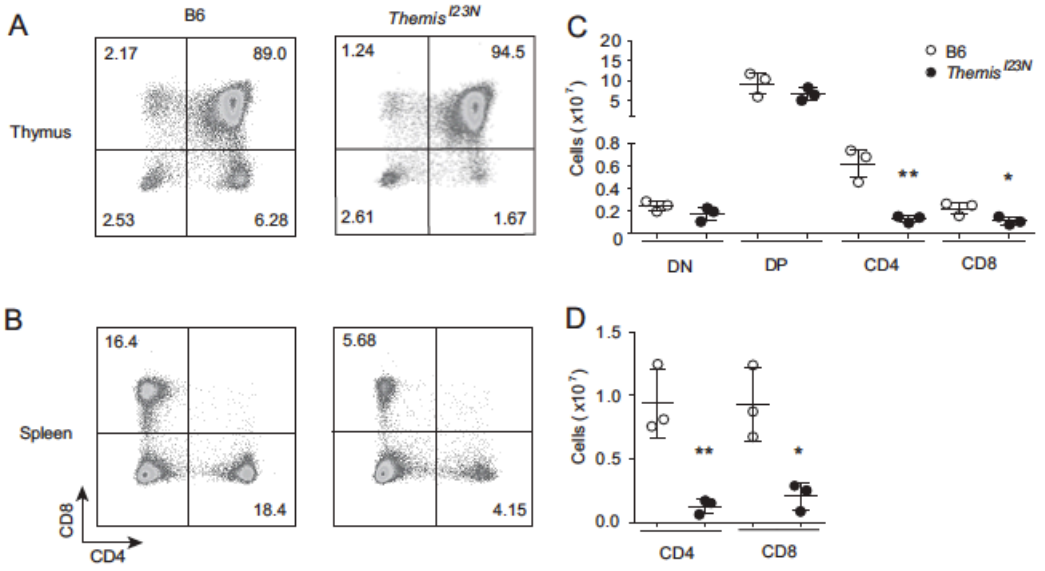

Figure 2-4. Themis^{I23N} mutants show a defect in thymocyte development

Thymocytes and splenocytes from WT and from *Themis*^{I23N} mutants (n=3/group) were stained with anti-CD45-APC efluor780, anti-CD4-PE, and anti-CD8-Bv421, and analyzed by flow cytometry. (**A-B**) Representative FACS plots showing CD4 vs CD8 profiles expressed as a percentage of viable CD45$^+$ thymic (A) and splenic cells (B). (**C**) Total numbers of T cell populations from thymus. *Themis*^{I23N} mice have significantly decreased numbers of CD4$^+$ T cells (**, p=0.0026), and of CD8$^+$ T cells in the thymus (*, p=0.0335) compared to wild-type. (**D**) Total numbers of T cells from spleen. *Themis*^{I23N} mice have a significantly decreased number of peripheral CD4$^+$ T cell (**, p=0.0069) and CD8$^+$ T cells (*, p=0.0152) compared to wild-type. Data are expressed as mean ± SD for each group, and represents data from two independent experiments. Statistical analysis was performed by two-tailed unpaired student t-test.

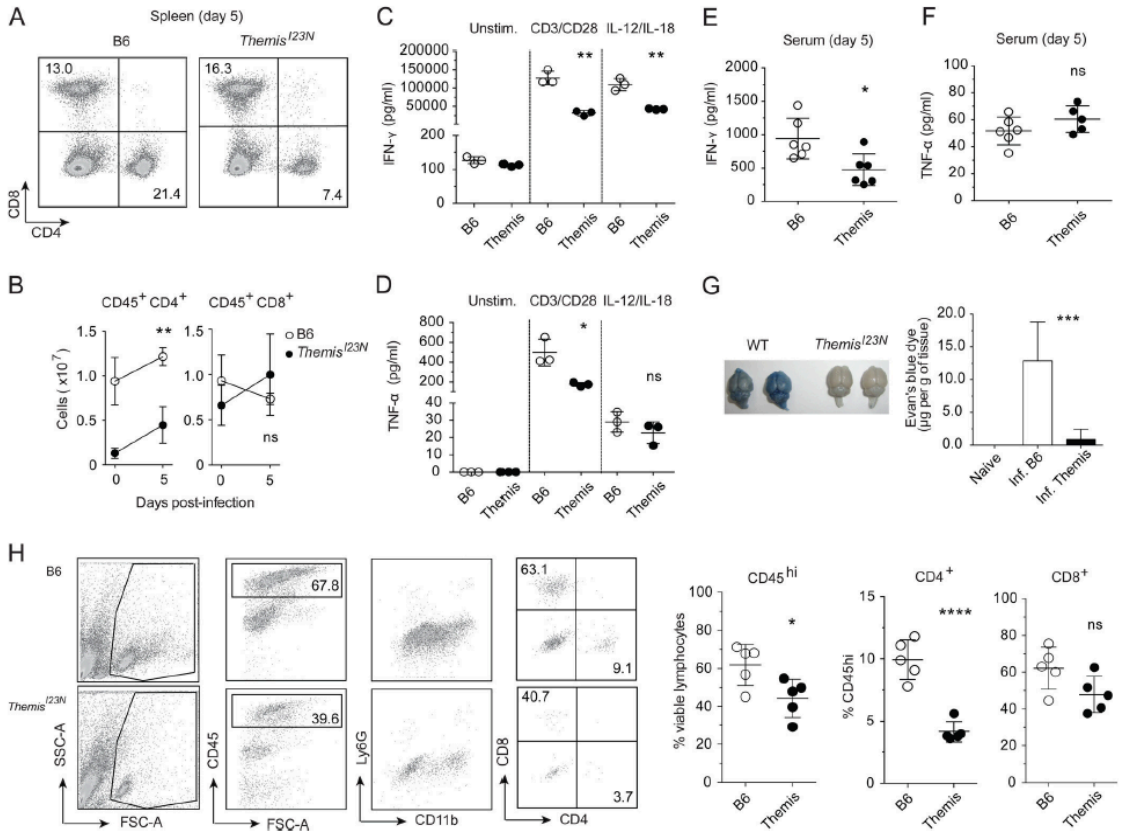

Figure 2-5. Immunophenotyping of Themis^{I23N} mutants following PbA infection

Control B6 and *Themis*^{I23N} mutants were infected with PbA, and 5 days later the function of peripheral T cells (spleen) was examined. FACS analysis indicates a reduced proportion (**A**) and absolute number (**B**) of CD45^{+}CD4^{+} T cells in PbA-infected *Themis*^{I23N} mutants compared to B6 WT controls (**, p=0.0079; n=3). (**C**) Splenocytes from PbA-infected *Themis*^{I23N} mice produce significantly less IFN-γ *ex vivo* in response to stimulation with anti-CD3/anti-CD8 or with IL-12/IL-18 (**, p=0.0012, and **, p=0.0022, respectively) than WT B6 controls. (**D**) Same as in (C) but TNF-α was measured in culture supernatant. (**E, F**) Serum cytokines were measured by ELISA and show decrease of circulating IFN-γ (*, p=0.0147) in *Themis*^{I23N} mutants compared to B6 controls. Data are expressed as mean ± SD for each group, and represents data from two independent experiments. Statistical analysis was performed using the two-tailed unpaired student t-test. (**G**) Evans blue extravasation assay to assess integrity of the blood-brain barrier (BBB) of PbA-infected WT (C57BL6/J, or 129S1/SvImJ) and *Themis*^{I23N} mutants. Six days following infection, mice were injected with Evans blue dye. Evan's blue dye was extracted from the brain tissues, and optical density was measured at 610 nm. Measurements were converted into µg of dye extravasated per gram of tissue. Brains from *Themis*^{I23N} mutants remain unstained by Evan's blue (***,

p=0.0003). Naïve WT (n=3), PbA-infected B6 (n=3), PbA-infected *Themis*^{I23N} (n=8). Data are expressed as mean ± SD for each group, and represents data from two independent experiments. Statistical analysis was performed using the two-tailed unpaired student t-test. (**H**) Five days following PbA infection, infiltrating leukocytes were isolated by Percoll gradient from brain homogenates and were analyzed by FACS. Representative FACS plots of cellular infiltration in the brain indicate reduced infiltration of $CD45^{hi}$ leukocytes, $CD45^{+}CD11b^{+}Ly6G^{+}$ neutrophils, $CD45^{+}CD4^{+}$ T cells, and $CD45^{+}CD8^{+}$ T cells in brains of *Themis*^{I23N} mutants. Data are expressed as a percentage of viable $CD45^{hi}$ cells in the brain, expressed as mean ± SD for each group, and is a representation of two independent experiments. Statistical analysis was performed by two-tailed unpaired student t-test.

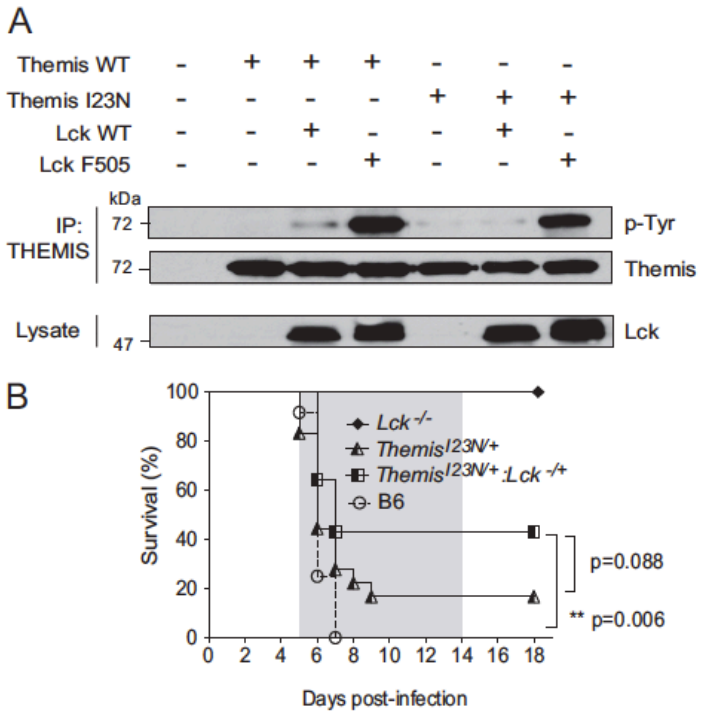

Figure 2-6. LCK protein tyrosine kinase mutants are resistant to ECM

(**A**) Plasmids encoding either WT or *Themis*^{I23N} variant were co-transfected with either *Lck*^{WT} or with the hyperactive *Lck*^{F505Y} plasmid in HEK293T cells. THEMIS protein was immunoprecipitated (IP) from total cell lysate and assessed for tyrosine phosphorylation by immunoblotting with an anti-phosphotyrosine (p-Tyr) antibody. LCK (56 kDa) was assessed in total cell lysate to ensure successful co-transfection. In the presence of hyperactive Lck^{F505}, both WT and mutant THEMIS protein are subjected to tyrosine phosphorylation. (**B**) Survival of *Lck* knockout (*Lck*$^{-/-}$, n=12), *Themis* heterozygotes (*Themis*$^{I23N/+}$, n=18), *Themis-Lck* double heterozygote mutants (*Themis*$^{I23N/+}$:*Lck*$^{-/+}$, n=14) and B6 WT controls (n=12) following infection with PbA. The Log-Rank statistical test indicated a significant increase in CM-resistance of the *Themis-Lck* double heterozygotes compared to WT B6 (**, p=0.006), and suggests increased resistance compared to the *Themis*$^{I23N/+}$ mice, although this difference did not reach statistical significance, p=0.088).

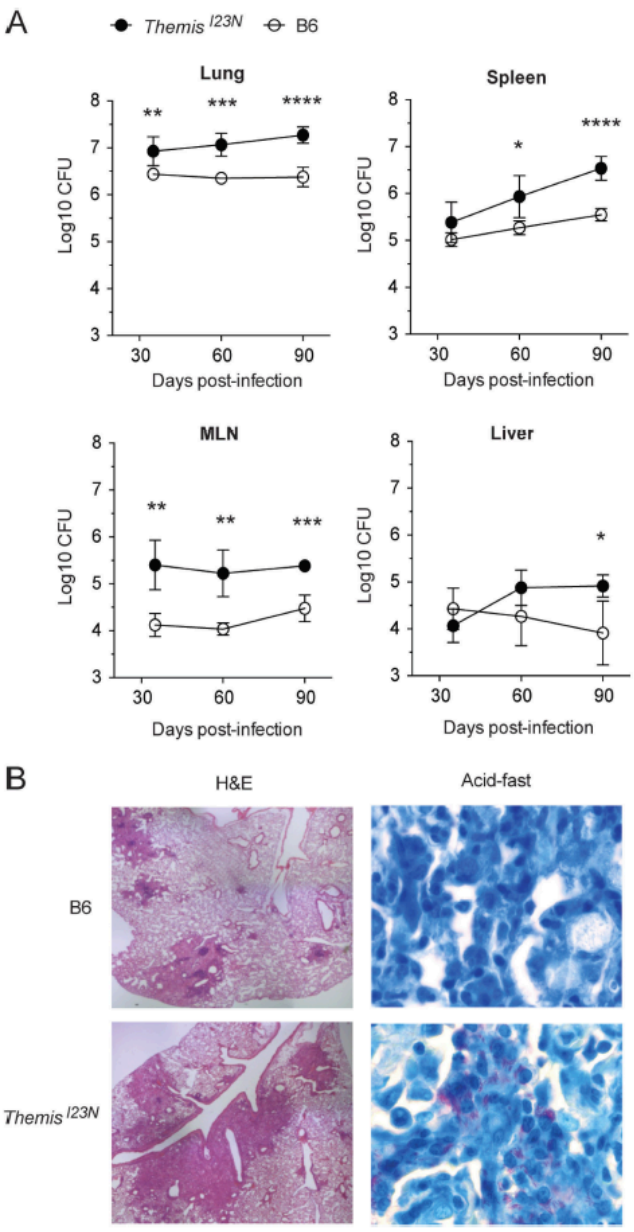

Figure 2-7. Loss of THEMIS function causes susceptibility to tuberculosis

(A) Control B6 and *Themis*^{I23N} mutants were infected with 200 colony forming units (CFU) of *Mycobacterium tuberculosis* H37Rv by the aerosol route, and 35, 60 and 90 days post-infection organs were harvested and microbial replication was determined by CFU counts. Each group contained 5 mice, and statistical significance was estimated by the two-tailed unpaired student t-test (*, $p<0.05$; **, $p<0.01$; ***, $p<0.001$). **(B)** Histological analysis of *M. tuberculosis*-infected lungs from B6 controls and from *Themis*^{I23N} mutants at day 90 post-infection with hematoxylin & eosin (H&E) staining and for visualization of acid-fast bacilli by Ziehl-Neelsen.

2.5 Discussion

We have identified a I23N mutation in THEMIS that causes resistance against cerebral malaria. In summary, the I23N mutation is phenotypically expressed as a) decreased protein stability, b) reduced $CD4^+$ and $CD8^+$ T cell numbers in the thymus and spleen, c) decreased pro-inflammatory cytokine (IFN-γ, TNF-α) production by T cells at steady state and during infection, d) retention of BBB integrity, and e) emergence of susceptibility to pulmonary tuberculosis. THEMIS acts a regulator of positive selection of thymic lymphocytes from $CD4^+CD8^+$ double positive cells to mature singly positive $CD4^+$ and $CD8^+$ cells [204-208]. Mice lacking $CD8^+$ T cells or their secreted products (TCRαβ [113], TAP-1 [82], β2-microglobulin [97], perforin [126]), or mice deficient in $CD4^+$ T cells [82,113,214] are ECM-resistant. The effect of the *Themis*^{I23N} mutation on thymic T cell maturation and peripheral T cell activity is similar to those described for null mutations in *Themis* [204-208]. Hence, studies in models of infectious diseases with our *Themis*^{I23N} mutant provide insight and are generally reflective of loss of THEMIS function.

The CM-protective effect of *Themis*^{I23N} may reflect the essential role of TCR signaling in the intra-thymic development of functional T cell repertoires. Indeed, studies in mice lacking TCR structural components [82,113] or downstream signaling molecules such as LCK [210], LAT [215], GRB2 [216], TESPA1 [217], and ITK [218] cause severe defects in T cell development with significant immunodeficiency (reviewed in [219]). LCK acts immediately downstream TCR, and upon its activation, it phosphorylates THEMIS [211-213]. Phosphorylated THEMIS has been proposed to interact with additional members of the TCR signalosome to propagate TCR proximal signaling [220]. In this study, we show that *Lck*$^{-/-}$ mutant mice are, like *Themis*^{I23N}, resistant to development of ECM. In addition, genetic complementation studies in mice doubly heterozygote for loss-of-function mutations in *Themis* and *Lck* (*Themis*$^{I23N/+}$:*Lck*$^{-/+}$) also display increased resistance to ECM, unlike singly heterozygote control mice. These data establish that THEMIS and LCK are both required for neuroinflammation.

THEMIS has two amino-terminal globular cysteine-containing, all-β in Themis domains (CABIT-1, CABIT-2), that are predicted to form an extended β-sandwich-like

fold or a dyad of six-stranded β-barrel units [204,205,220]. Though the CABIT structural motifs that have been identified by sequence conservation, their structure-function relationships have yet to be clearly defined. Recent studies have shown that deletion of a part of the CABIT-1 domain (D150-174) in mouse THEMIS causes a defect in T cell development [221]. We show that the I23N mutation in the CABIT-1 domain causes protein instability in primary thymic cells, and in transfected cells, suggesting that I23N may cause misfolding of the protein, and consequently, is targeted for degradation. Hence, integrity of the CABIT-1 domain is required for THEMIS protein stability.

Finally, genome-wide association studies have recently identified *THEMIS* (6p22.33) as a candidate gene for the Chr 6 locus associated with celiac disease in humans (Chr 6;127.99-128.38 Mb, CRCh37/hg19) [222-224]. Duodenal mucosa from active celiac patients showed higher *THEMIS* gene expression compared to patients undergoing effective treatment or to healthy controls [192,225]. *THEMIS* was also recently identified as a risk factor for multiple sclerosis [226]. The demonstration herein that *Themis* elimination protects against neuroinflammation in mice validates the proposed role of *THEMIS* in pathological inflammation in humans. Furthermore, the association of *THEMIS* with different inflammatory diseases that affect different anatomical sites, and that follow different pathogeneses, places *THEMIS* as one of the core “inflammatory” genes that regulate common aspects of pathological inflammation *in vivo*, and that participate in etiology of these different inflammatory diseases.

2.6 Acknowledgements

This work was supported by a Team Grant to PG and SV from the Canadian Institutes of Health Research (CIHR Team in ENU Mutagenesis and Infectious Diseases [CTP-87520]), and by a grant to PG from the National Institutes of Health USA [R01AI035237]. PG is supported by a James McGill Professorship award. SMV is supported by the Canada Chairs Research Program.

The authors are indebted to Patricia D'Arcy, Geneviève Perreault, Leigh Piercey-Brunet, Mifong Tam and Susan Gauthier for expert technical assistance, and to Sandra Salem and Vicki Leung for help with protein work and imaging, respectively.

Chapter 3:

USP15 regulates type I interferon response *in vivo* and is required for pathogenesis of neuroinflammation

Preface to Chapter 3

A slightly modified version of Chapter 3 is published in Nature Immunology, http://doi.org/10.1038/ni.3581.

3.1 Abstract

Genes and pathways in which inactivation dampens tissue inflammation present new opportunities for understanding the pathogenesis of common human inflammatory diseases, including inflammatory bowel disease, rheumatoid arthritis and multiple sclerosis. We identified a mutation in the gene encoding the deubiquitination enzyme USP15 (*Usp15*^{L749R}) that protected mice against both experimental cerebral malaria (ECM) induced by *Plasmodium berghei* and experimental autoimmune encephalomyelitis (EAE). Combining immunophenotyping and RNA sequencing in brain (ECM) and spinal cord (EAE) revealed that *Usp15*^{L749R}-associated resistance to neuroinflammation was linked to dampened type I interferon responses *in situ*. In hematopoietic cells and in resident brain cells, USP15 was coexpressed with, and functionally acted together with the E3 ubiquitin ligase TRIM25 to positively regulate type I interferon responses and to promote pathogenesis during neuroinflammation. The USP15-TRIM25 dyad might be a potential target for intervention in acute or chronic states of neuroinflammation.

3.2 Introduction

Cerebral malaria (CM) is a severe complication of *Plasmodium falciparum* infection in humans. In CM, rapid progressing encephalitis causes high mortality and morbidity in affected children and pregnant women [58]. The pathogenesis of CM involves both microthrombosis and neuroinflammation *in situ* associated with trapping of *Plasmodium* infected erythrocytes in the microvasculature. The neuroinflammatory component of CM can be studied in the mouse model of *Plasmodium berghei* ANKA (PbA) infection, known as experimental cerebral malaria (ECM) [80]. In this model, activation of blood brain barrier (BBB) endothelial cells in response to trapped parasitized red blood cells (pRBCs) causes early release of chemo-attractants, recruitment of activated myeloid and lymphoid cells *in situ*, loss of integrity of the BBB, microthrombosis, and hypoxia of the brain tissue, appearance of neurological symptoms, and death [67,196]. ECM has been used to demonstrate the critical role of $CD8^+$ and $CD4^+$ T cells, natural killer (NK) cells, and neutrophils in pathogenesis, as well as to establish the contribution of pro-inflammatory molecules such as TNF, interferon-γ (IFN-γ), interleukin 1β (IL-1β), macrophage inflammatory protein 1α (MIP-1α), MIP-1β, CXCL9, CXCL10, and complement component 5a (C5a) in pathogenesis of CM [80,100,197,198]. Parallel findings show that elevated circulating concentrations of these inflammatory molecules are associated with increased risk of malaria progression to CM in humans [100,197,198]. Furthermore, gene mutations that affect the numbers of $CD4^+$ T cells, $CD8^+$ T cells and myeloid cells, production of critical pro-inflammatory molecules by these cells (*Lta*, *Ltb, Hc*) including type I (*Ifnar*) and type II interferons (*Ifng, Ifngr1*), as well as the induction of transcription factors (*Irf1*, *Stat1*, *Irf8*) that regulate the development and function of these cells and production of pro-inflammatory mediators, all result in ECM-protection [55,139,154].

We have implemented a genome-wide screen in chemically mutagenized mice (N-ethyl-N-nitrosourea, ENU) to identify genes that, when inactivated, cause ECM-resistance in PbA infected mice [56]. Such ECM-protective mutations affect genes and pathways that are required for pathological neuroinflammation, and the corresponding proteins may represent valuable entry points to better understand the disease process

and to suggest novel targets for drug discovery. The robustness of this screen was validated through the identification of mutations in genes that are known (e.g, *Jak3*, *FoxN1*, *Lyst, Themis*) to play a role in inflammatory and immune functions [157,158]. This screen has also identified novel proteins (CCDC88B) which role in the immune system was previously unknown [105]. In addition, several of the genes which inactivation cause ECM-resistance have been detected as genetic risk factors for common human inflammatory diseases, including *THEMIS*, *CCDC88B*, *JAK3*, *IRF8*, *IRF1*, *STAT1* [193,195,222,226-228] and several others (reviewed in [229]).Thus, studies in the ECM model may identify critical regulatory genes and pathways that underlie the shared etiology and pathogenesis of acute and chronic human inflammatory diseases.

In the present study, we have identified an ENU-induced mutation in the deubiquitinase enzyme USP15 (*Usp15*^{L749R}) that conveys ECM-resistance, but also causes resistance to experimental autoimmune encephalomyelitis (EAE). We show that USP15-dependent protection against neuroinflammation is linked to dampened induction of type I interferon response *in situ* in mutant mice. The E3 ubiquitin ligase TRIM25 is a target of USP15 [230,231]. Using biochemical, genetic, and RNA-sequencing approaches, we demonstrate that USP15 acts in concert with TRIM25 as a positive regulatory loop to activate type I interferon response and drive pathogenesis during neuroinflammation.

3.3 Materials and Methods

Ethics statement

This study was performed in accordance and compliance with the guidelines and regulations of the Canadian Council on Animal Care (CCAC). All protocols were approved by the Animal Care Committee of McGill University (protocol number 5287). Mice were anesthetized, and euthanized by carbon dioxide inhalation, and every effort was made to minimize animal suffering. For isolation of microglia from non-malignant cases of temporal lobe epilepsy, informed consent was obtained from all donors and approved by the governing ethics committee (McGill University Health Centre Ethics board; #ANTJ1988/3 and #ANTJ2001/1). Astrocytes were obtained from the human fetal tissue repository of the Albert Einstein College of Medicine, with informed consent obtained from all donors and approved by the institutional review board (IRB #1993-042).

Mice

Inbred C57BL/6J (B6) and 129S1/SvImJ (129S1) mice were purchased from the Jackson laboratories. ENU mutagenesis was performed as we have previously described [105,158]. Briefly, mutagenized G0 B6 males were bred to wild-type (WT) 129S1 to generate a G1 offspring, which were backcrossed to 129S1 females to generate G2 offspring. Two G2 females per pedigree were backcrossed to their G1 father, *Corbin*, to generate G3 mice for phenotyping. The *Usp15*^{L749R} mutation was backcrossed to B6 for 4 generations, where ultimately, *Usp15*^{L749R} homozygotes were intercrossed to generate a pure line. Genotyping with informative markers indicated that the genome of these mice was >90% of B6 origin. *Trim25* knockout mice (*Trim25*$^{-/-}$) were originally reported and were obtained from RIKEN (Japan; mutant stock RBRC 02844) [232,233]. *Socs1*$^{fl/fl}$ mice obtained from A. Yoshimura (Tokyo) were crossed with *Socs3*$^{fl/fl}$ and T-cell specific *Lck-Cre* mice (both from the Jackson Laboratories) to simultaneously ablate *Socs1* and *Socs3* in T cells [234]. All mutants were maintained on C57BL/6J genetic background.

Parasites and Infections

Plasmodium berghei ANKA (PbA) parasites were obtained from the Malaria Reference and Research Reagent Resource Center (MR4). Parasites were maintained as frozen stocks at -80°C and passaged weekly in B6 mice. Blood parasitemia was determined on thin blood smears stained with Diff-Quick reagents. Seven to eight week-old mice were infected intravenously with 10^6 parasitized red blood cells (pRBCs). Mice were monitored for appearance of neurological symptoms 3 times daily. Mice displaying severe cerebral symptoms were euthanized. Animals that survived the experimental cerebral phase (ECM; days 5-13) were considered ECM-resistant, and were euthanized on day 18 post-infection (experimental endpoint).

Whole-exome sequencing

Whole-exome sequencing was carried out on three ECM-resistant *Corbin* G3 mice. Exome capture was performed using a SureSelect Mouse All Exon kit (Agilent Technologies) and parallel sequencing on an Illumina HiSeq 2000 (100 bp paired-end reads). Reads were aligned to the reference mouse genome assembly (NCBI37/mm9) with Burrows-Wheeler Alignment (BWA) tool[200] and coverage was assessed with BEDTools [201]. Variants were called using Samtools pileup and varFilter and were annotated using Annovar, as we have previously described [105,158]. The analysis identified one common *de novo* homozygote variant, a T-to-G transversion, at position 122,562,078 bp on Chr. 10 (NCBI37/mm9) in exon 17 of the *Ubiquitin-specific protease 15* (*Usp15*) gene. The *Usp15*^{L749R} mutation was genotyped by PCR amplification from genomic DNA (5′-AATGAATGCCTTCAACAGTGG-3′, 5′-ACAATGCCAACTTTCAGAAGC-5′) followed by DNA sequencing.

Plasmids

A full-length mouse *Usp15* cDNA (pFLCIII-*Usp15*-WT; Riken Fantom Clones) was modified to include a C-terminal hemagglutinin (HA) epitope tag, and restriction enzyme sites for HindIII (CCACC) and XhoI (CTCGAG) to allow cloning into pcDNA3 expression plasmid. The resulting WT plasmid, pcDNA3-m*Usp15*-WT-HA, was used as a template for the generation of mutants by site-directed mutagenesis, including *Usp15*^{L749R}. Plasmid encoding the full-length human WT *USP15*, pcDNA3-Xpress-His-

USP15, was obtained from commercial sources (Addgene, plasmid ID: p5953), and was used as a template to produce mutants L720R, C269A, S923L, and C783A by site-directed mutagenesis. The pEF-*TRIM25*-FLAG plasmid was kindly provided by J. U. Jung (Harvard Medical School, University of Southern California Keck School of Medicine). The integrity of all plasmid constructs were verified by complete nucleotide sequencing of the corresponding cDNA inserts.

Antibodies

Endogenous USP15 protein expression was monitored by immunoblotting using a rabbit polyclonal anti-USP15 antibody (Abcam, ab97533), while epitope tagged USP15 variants were detected using a mouse anti-HA (Covance, HA.11), or mouse anti-Xpress (LifeTechnologies, R910-25) monoclonal antibodies (mAb). Native TRIM25 was detected using a rabbit polyclonal anti-TRIM25 antiserum (Proteintech, 12573-1-AP), while epitope-tagged TRIM25 was detected using a mouse anti-FLAG (Sigma Aldrich, Clone M2) mAb. Ubiquitinated TRIM25 was detected by immunoblotting with a mouse anti-Ubiquitin mAb (Santa Cruz, P4D1; SC8017).

USP15 protein expression and stability

Mouse tissues were homogenized in 50 mM Tris pH 7.5, 150 mM NaCl, 1% TritonX-100, and 0.1% sodium dodecyl sulfate (SDS), supplemented with protease and phosphatase inhibitors. Discrete immune cell populations were isolated from spleen and thymus by flow cytometry and cell sorting (BD FACSAriaII) following staining with combinations of cell surface markers to obtain $CD4^+$ T cells ($CD4^+CD8^-$), $CD8^+$ T cells ($CD4^-CD8^+$), NK cells ($TCR\beta^-CD49b^+$), B cells ($TCR\beta^-CD19^+$), and thymic double-negative T cells ($CD4^-CD8^-$), and thymic double-positive T cells ($CD4^+CD8^+$). For protein stability studies, HEK293 cells (ATCC-CRL-1573) were stably transfected with HA-tagged mouse *Usp15* constructs using Lipofectamine 2000 reagent (Life Technologies) followed by clonal selection and expansion in Geneticin (G418, 500 μg/ml) (Invitrogen). Stably transfected cells were treated with cycloheximide (20 μg/ml) for 10, 15, 20, and 25h, followed by cell lysis in 50 mM Tris pH 7.5, 150 mM NaCl, 1% TritonX-100, and

0.1% sodium dodecyl sulfate. Equal amounts of protein (25 μg) were analyzed by immunoblotting.

Co-immunoprecipitation Experiments

HEK293T cells were transiently transfected with plasmids using Lipofectamine 2000. Cells were lysed 24 to 48h post-transfection in either 1% NP40 lysis buffer (1% NP-40, 50 mM Tris-HCl (pH 7.4), 150 mM NaCl; for examining physical association) or 1% NP-40 RIPA buffer (for functional studies) plus protease inhibitors. Lysates were incubated with antibody directed against the indicated epitope tags followed by incubation with Protein G Sepharose beads. Beads were washed extensively and protein eluted using Laemmli buffer. Pre-immunoprecipitate lysates and immunoprecipitate samples were analysed by SDS-PAGE and immunoblot.

Experimental Autoimmune Encephalomyelitis

Experimental Autoimmune Encephalomyelitis (EAE) was induced according to published experimental protocols[235]. Briefly, 8-12 weeks female mice were treated with myelin oligodendrocyte glycoprotein (MOG; peptide sequence 35-55) emulsified in Complete Freund Adjuvent (CFA) (50 μg/mouse, s.c., at day 0) and pertussis toxin (PTX; 300 ng/mouse, i.p., at days 0 and 2). The mice were weighed and monitored daily for clinical signs of EAE, which were scored as follows: Tail (0, no symptoms; 1, weak; 2, hooked or paralyzed tail); hind limb (0, no symptoms; 1, weak; 2, full paresis; 3, no movement); front limbs (0, no symptoms; 1, weak; 2, full paresis; 3, no movement). Each limb was scored individually and total scores were tabulated for each animal. For ethical reasons, severely impaired animals were euthanized. At pre-determined time intervals, spinal cords were dissected for histology and for extraction of RNA.

Cellular Immunophenotyping

Five days post-PbA infection, mice were ex-sanguinated and perfused with 20 ml PBS-containing 2mM EDTA. Brains were harvested and homogenized in RPMI media-containing 0.5 mg/ml collagenase (Gibco LifeTechnologies), 0.01 mg/ml DNase I (Roche) and 2 mM EDTA. Infiltrating cells were separated on a 33.3 % Percoll solution. Cells were stained for flow cytometry analyses (BD FACS Canto II, BD FACS Diva

software, FlowJo v10 software by Treestar) with the following antibodies; anti-CD45-APC-eFluor780 (clone 30-F11, eBioscience), anti-CD4-PerCP Cyanine5.5 (clone RM4-5, eBioscience), anti-CD8alpha-PE (clone 53-6.7, eBioscience), anti-TCRbeta-FITC (clone H57-597, eBioscience), anti-CD11b-APC (clone M1/70, eBioscience), anti-Ly6C-PE (clone HK1.4, eBioscience), and anti-Ly6G-FITC (clone 1A8, BioLegend). Leukocytes were gated as $CD45^{hi}$ cells. Live cells were identified using Zombie Aqua Dye-V500 (BioLegend). Splenocytes from naïve and PbA-infected mice were analyzed by flow cytometry using markers of lymphoid cells (anti-CD45-APC-efluor780, anti-CD8-Bv421, anti-CD4-PE, anti-TCR-β-FITC), and myeloid cells (anti-CD45-APC-efluor780, anti-CD11b-APC, anti-Ly6G-FITC). In stimulation experiments, 4×10^6 splenocytes per well were cultured with either anti-CD3 (5 μg/ml, eBioscience)/anti-CD28 (2 μg/ml, eBioscience), or with PMA (50 ng/ml) and ionomycin (500 ng/ml) for 4h, followed by assessment of intracellular staining for IFN-γ by flow cytometry. Serum cytokines were measured using a cytokine/chemokine 32-multiplex Luminex array (Eve Technologies).

RNA sequencing & validation by qPCR

Brains from perfused naïve and PbA-infected B6 and *Usp15*^{L749R} mice (at day 3 and 5) and from spinal cords of mice undergoing EAE (at day 7) were harvested and frozen in liquid nitrogen; a comparative RNA-seq study was also performed as indicated on brains of day 5 PbA-infected B6 and *Trim25*$^{-/-}$ mice. Total RNA was isolated using Trizol-chloroform (Life Technologies), followed by DNase-digestion and purification on RNeasy columns (Qiagen). RNA integrity was assessed on a Bioanalyzer RNA pico chip, followed by rRNA depletion and library preparation using Illumina TruSeq Stranded Total RNA Library preparation kit. The RNA-seq libraries were sequenced on an Illumina HiSeq 2500 sequencer in paired-end 50 bp configuration. Resulting sequence reads were mapped to the mm9 reference genome using TopHat 2.0.9 and Bowtie 1.0.0 algorithm combination [236,237]. Gene expression was quantified by counting the number of uniquely mapped reads with the featureCounts tool using default parameters [238]. Normalization and differential gene expression analysis was conducted independently for PbA and EAE datasets using the edgeR Bioconductor package [239]. We retained genes that had a minimum expression level of 5 counts per

million reads (CPM) in at least 3 of the samples for PbA, and at least 2 out of 4 for EAE datasets. Genes with differential expression in *Usp15*^{L749R} were considered significant if fold change ≥1.5 and adjusted *P* value <0.05. For Figure 5b and 6i, RNA-seq sequence density profiles were normalized per 10 million reads using a succession of genomeCoverageBed and wigToBigWig tools and visualized in IGV genome browser [240]. We proceeded to unbiased clustering of the 316 genes with significant dysregulation in PbA and/or EAE (**Appendix Table 1**) using Pearson uncentered correlation with average distance metric within MeV software [241].

Differences of expression between samples were validated by quantitative polymerase chain reaction (qPCR) on independent biological samples at multiple time points in PbA-infected brains. Briefly, complimentary DNA (cDNA) was synthesized with M-MLV reverse transcriptase (Thermo Fisher Scientific). qPCR was performed on an Applied Biosystems instrument (Life Technologies) using PerfeCTa SYBR green Super Mix + ROX reagent (Quanta Biosciences), and primer pairs listed in **Table 3-1**. Comparative quantification was calculated using the $2^{-\Delta Ct}$ method and target genes were expressed relative to the hypoxanthine phosphoribosyltransferase (*Hprt*) reference gene, unless otherwise indicated. Fold changes in gene expression in infected mice was expressed relative to naïve mice.

Identification of USP15-regulated pathways and cellular responses

Genes differentially expressed in a USP15-dependent fashion were identified in the RNA-sequencing datasets (fold change ≥1.5, adjusted *P* value <0.05) from brain and spinal cords obtained from control (B6), and from *Usp15*^{L749R} mutant mice. Gene ontology enrichment analysis was performed using DAVID bioinformatics resources [242]. The USP15 differential gene expression profiles (brain, spinal cord) was also subjected to gene set enrichment analysis using GSEA [243] and using MSigDB v5.0 public immunologic gene signatures (cell specific, response to stimuli). Following identification of enriched immunological signatures in GSEA (FDR <0.01) (representative examples are shown in **Figure 3-4d**), the leading-edge genes were identified for each of these signatures (genes that appear in the ranked list at or before the point at which the running sum reaches its maximum deviation from zero); the

leading-edge genes are driving the enrichment signals during the statistical analysis. For PbA, 1347 genes were driving the enrichment of 235 immunological signatures, whereas in EAE, there were 849 genes for 102 signatures. In order to identify cellular responses and pathways regulated *in situ* by USP15 in both brain (in response to PbA infection) and in spinal cord (during EAE induction), we performed unbiased clustering (using Kendall's Tau distance metric with complete linkage) of the leading edge genes in the PbA and EAE datasets. For the clustering analyses, only genes implicated in at least 2% of the signatures were considered (PbA: 530 genes, EAE: 353 genes). Since the clustering analysis of individual datasets revealed the enrichment of common immunological functions, we have combined both leading datasets, kept genes associated in the enrichment of at least 5 signatures (627 genes for 264 signatures) and performed clustering. Results of the combined clustering analysis is shown in **Figure 3-9a**, and a detailed matrix of this dendogram is provided in **Appendix Table 2**.

Isolation and activation of neural cells

Human fetal CNS tissues from 14 to 20 week embryos were acquired from the Albert Einstein College of Medicine human fetal tissue bank (Bronx, NY) [IRB 1993-042]. Purified astrocytes were isolated and cultured as previously described [244]. Cells were activated for 48h with IFN-γ (200U/ml, ThermoScientific) in combination with either TNF (2000U/ml, Invitrogen) or IL-1β (10 ng/ml, Invitrogen). Cell samples were collected in RIPA lysis buffer (1% NP-40, 0.5% sodium deoxycholate, 0.1% SDS, 50 mM TRIS-HCl, 150 mM NaCl) plus inhibitors and analysed by immunoblot analysis.

Adult microglia was isolated from the biopsy samples. Briefly, normal appearing cortical tissue was resected from pharmacologically intractable non-malignant cases of temporal lobe epilepsy. Informed consent was obtained from all donors according to the local ethics committee (McGill University Health Centre Ethics board; #ANTJ1988/3 and #ANTJ2001/1). Tissue was processed as described previously [245]. Briefly, tissue was mechanically dissociated, digested using trypsin and DNAase followed by separation through a nylon mesh filter. Single cell suspension underwent a fickle ultracentrifugation step to remove myelin. Dissociated cells were centrifuged, counted, and plated at 2×10^6 cells/ml in MEM supplemented with 5% FBS, 0.1% P/S and 0.1% glutamine.

Microglia were grown for 3 days, collected and plated at 1 × 10^5 cells/ml and maintained in culture for 6 days during which time cells were left untreated or polarized to M1. To generate M1 microglia, cells were treated cells with GM-CSF (5 ng/ml) for 48h, GMCSF was then replenished for an additional 48–72h. M1 cells were activated with IFN-γ (20 ng/ml) for 1h followed by a 48h treatment with LPS (serotype 0127:B8, 100 ng/ml). At day 7, M0 and M1 cells were lysed in RIPA lysis buffer plus inhibitors and subsequently used for immunoblot analysis.

Bone Marrow transfer

Mice were lethally irradiated with 2 times 450 rads within 3h intervals on an X-Ray RS-2000 Biological irradiator. After 3h, mice were injected intravenously with 10^7 red blood cell-depleted bone marrow from indicated sex-matched donors. The engraftment was verified after 6 weeks by flow cytometry with anti-CD45 and anti-B220 antibodies. At 7 weeks post engraftment, mice were infected intravenously with 10^6 PbA parasites and monitored for neurological symptoms and for survival.

***In vitro* cell stimulations for induction of interferon stimulated genes**

For splenocyte stimulations experiments, ten million splenocytes (n=5/group) per 24-well were cultured with either media alone or with 5 μg/ml Polyinosinic:polycytidylic acid (Poly(I:C)) in complete RPMI media (containing 10% FBS, 1 mM sodium pyruvate, 1x non-essential amino acids, 1x Penicillin Streptomycin, 1x β-mercaptoethanol). Splenocytes were collected after 4h of stimulation followed by RNA isolation, cDNA synthesis and qPCR. For primary bone marrow-derived macrophage (BMDM) stimulation experiments, BMDMs were isolated from animals and cultured in 10% FBS/DMEM/1% Penicillin-Streptomycin/20% L cell conditioned medium (LCCM; BMDM media). An additional 10% LCCM was added at day 5 of culture. At day 7, cells were lifted from plates using PBS-citrate and seeded at 4 × 10^5 cells/ml into 6-well plates. Transfections with 5′-ppp-RNA control (200 ng/ml; Invivogen) or 5′-ppp-RNA (25 ng to 200 ng/ml; Invivogen) were performed using Lipofectamine 2000 (Invitrogen) according to manufacturer's instructions. Cells were collected 24h post-transfection followed by RNA isolation, cDNA synthesis and qPCR.

Statistics and Reproducibility

Statistical analyses were performed using Graphpad Prism software, version 6. Statistical significance was calculated using an unpaired, two-tailed Student's t-test for comparison between groups, or by the Log-rank test for survival comparisons, as detailed in the figure legends.

3.4 Results

A mutation in Usp15 protects mice against cerebral malaria

We used N-ethyl-N-nitrosourea (ENU) genome-wide mutagenesis in mice to identify genes and pathways, whose inactivation leads to protection against lethal encephalitis in the ECM model of *Plasmodium berghei* ANKA (PbA) infection [92,105,157,158]. In this screen for recessively inherited ECM-protective mutations (**Figure 3-1a**), G3 offspring derived from mutagenized G0 males are infected with 10^6 PbA-parasitized red blood cells (pRBCs). By day 5 post-infection, ECM-susceptible mice develop rapidly fatal encephalitis (coma, paralysis, tremors and seizures), while animals that survive beyond day 9 post-infection without development of cerebral symptoms, are deemed ECM-resistant.

In pedigree *Corbin*, 28 of 70 G3 offsprings produced by mating of *Corbin* (G1) to G2 females *Doshia* and *Kala* displayed ECM-resistance (**Figure 3-1a,b**). Exome sequencing of three ECM-resistant G3 offspring identified a single *de novo* homozygote sequence variant common to the three mice, a T-to-G transversion (Chr. 10: 122,562,078 bp, genome build NCBI37/mm9) in exon 17 of the *Ubiquitin-specific protease 15* (*Usp15*) gene (**Figure 3-1c**) which causes a non-conservative leucine (L) to arginine (R) amino acid substitution at position 749 (L749R) in the carboxy terminal moiety of USP15. Genotype-phenotype correlations in additional *Corbin* G3 mice validated that homozygosity for the mutation ($Usp15^{L749R}$) is ECM-protective (>80% survival); heterozygosity ($Usp15^{L749R/+}$) conferred low but significant ECM-protection (~30% survival), compared to $Usp15^{+/+}$ and B6 controls that were ECM-susceptible (**Figure 3-1d**). Continuous backcrossing of the $Usp15^{L749R}$ mutation to a pure C57BL/6J genetic background confirmed that $Usp15^{L749R}$ was ECM-protective (data not shown). A null *Usp15* knockout ($Usp15^{-/-}$) mutant was also found to be ECM-resistant (85% survival), validating the role of USP15 in neuroinflammation. Also, $Usp15^{L749R/-}$ double heterozygotes ($Usp15^{L749R}$ homozygote x $Usp15^{-/-}$) were ECM-resistant (~95% survival; **Figure 4-1d**), suggesting that $Usp15^{L749R}$-associated protection is linked to a loss of function inherited in an incompletely recessive fashion. Finally, we observed that the protective effect of $Usp15^{L749R}$ against neuroinflammation was independent of blood-

stage replication of the PbA parasite, as kinetics of blood parasitemia were similar in both controls and *Usp15* mutants (**Figure 3-1e**). Our findings suggest that USP15 is required for pathological neuroinflammation.

Reduced stability of USP15^{L749R} protein

USP15 is a member of the USP family of cysteine protease deubiquitination enzymes. It contains several structural motifs which include an N-terminal regulatory DUSP domain (Domain in Ubiquitin Specific Protease) [246], two ubiquitin-like folds (UBL), a long C-terminal catalytic domain (UCH) that includes a catalytic triad (C269, H862, D879) and Zn-coordinating cysteine residues (C419, C422, C780, C783) [247]. Although the role of L749 in USP15 is unknown, L749 is invariant across vertebrates, hence its substitution to the large positively charged arginine is likely to be detrimental to protein structure and function (**Figure 3-2a**). We first investigated USP15 protein and mRNA expression in tissues and cell types possibly associated with ECM pathogenesis. *In situ* hybridization with embryonic and adult mouse sections revealed low ubiquitous *Usp15* mRNA expression in most tissues (**Figure 3-3**). USP15 protein was detected as a 112-kilodalton species in spleen and thymus (**Figure 3-2b**), where it was ubiquitously expressed in lymphoid and myeloid cells including all $CD3^+$ T cell subsets ($CD4^+$, $CD8^+$, $CD4^+CD8^+$, $CD4^-CD8^-$), NK cells, B cells, and in macrophages, dendritic cells, and in primary embryo fibroblasts (**Figure 3-2c**). The observed ubiquitous expression of *Usp15* RNA and protein suggests that it may play a complex role during neuroinflammation, possibly implicating multiple organs, cell types and associated responses. USP15 protein could not be detected in spleen and thymus of *Usp15*^{L749R} mutants (**Figure 3-2b**), similar to *Usp15*$^{-/-}$ mice used as controls, suggesting reduced expression or reduced stability of the L749R variant. Consequently, cells expressing HA-tagged USP15 (WT) or USP15^{L749R} variants were treated with cycloheximide (CHX), and protein abundance was monitored over time (**Figure 3-2d**). The USP15^{L749R} variant showed a reduced half-life (~10h) compared to WT (>25h), with no L749R variant protein detected after 20h of CHX incubation. The corresponding human USP15 (L720R) variant also showed reduced protein stability in the same assay (**Figure 3-4**).

These results strongly suggest that the L749R mutation behaves as a loss of function in USP15, phenotypically expressed as reduced protein stability.

Usp15^{L749R} protects against autoimmune neuroinflammation

We investigated the effect of the *Usp15*^{L749R} mutation on recruitment and activity of immune cells in the brain at day 5 post-PbA infection. We observed reduced infiltration of CD45^{hi} leukocytes, including T cells, F4/80^{+}CD11b^{+} macrophages, and Ly6G^{+}CD11b^{+} neutrophils in the brains of ECM-resistant *Usp15*^{L749R}-infected mice compared to ECM-susceptible B6 controls (**Figure 3-5a**). Analysis of major serum cytokines and chemokines showed significantly reduced concentrations of the pro-inflammatory chemoattractant MIP-1b/CCL4 in mutant animals, while concentrations of major myeloid (IL-12p40) and lymphoid (IFN-γ, TNF) Th1 cytokines were similar in both groups (**Figure 3-5b**). Additional immunophenotyping at steady state and during PbA infection failed to reveal major immune defects in the *Usp15*^{L749R} mutant animals, with respect to a) the frequency of T cells, B cells, NK cells, neutrophils and monocytes, b) the intracellular cytokine production and secretion (IL-2, IFN-γ, TNF), c) the maturation (CD62L^{-}CD44^{+}), and activation of T cells (CD69^{+}) upon TCR engagement (anti-CD3/anti-CD28) or PMA/ionomycin stimulation (**Figure 3-6**), and d) ROS production by neutrophils (data not shown). These results suggest that, in contrast to other mutants identified in our ENU screen (*Jak3*, *Ccdc88b*, *Themis*, *Irf1*, *Irf8*) [105,157,158], ECM-resistance in the *Usp15*^{L749R} mutant is not caused by a dampened Th1 immune response.

We also investigated the *Usp15*^{L749R} mutation in a non-microbial model of neuroinflammation, experimental autoimmune encephalomyelitis (EAE) (**Figure 3-5c–g**). In EAE, neuroinflammation and axonal damage is induced by autoimmune response to myelin oligodendrocyte glycoprotein (MOG) co-administered with pertussis toxin (PTX). *Usp15*^{L749R} mutant mice were protected against EAE, compared to B6 (susceptible) and to *Jak3*$^{-/-}$ mutant (resistant) controls, displaying reduced body weight loss (**Figure 3-5c**), lower clinical scores (**Figure 3-5d**), and reduced lethality (**Figure 3-5e**). Clinical scores for individual mice (**Figure 3-5f**) indicated that while B6 controls

progress rapidly to fatal paralysis associated with infiltration of inflammatory cells in the spinal cord (data not shown), *Usp15*^{L749R} mutants display a much milder phenotype that resembles relapsing-remitting disease, with significant recovery and survival in 21 of 27 animals. Measurements of serum cytokines indicated reduced concentrations of circulating CCL3 and CCL4 in *Usp15*^{L749R} mutants very early (day 2) following induction of EAE (**Figure 3-5g**). These results confirm the importance of USP15 in neuroinflammation and suggest a role for USP15 in early production of chemokines and cytokines required for leukocyte recruitment to the site of injury [248].

Usp15 regulated pathways during neuroinflammation

We used global RNA sequencing (RNA-seq) to identify cells and pathways regulated *in situ* by USP15, and whose inactivation leads to protection against lethal neuroinflammation. These would be detected as differentially expressed (WT vs. *Usp15*^{L749R} mutant) in brain during ECM (at day 5 post-infection), and in spinal cord during EAE (at day 7 post-initiation) at early time points that precede appearance of clinical symptoms in either groups. Dimension reduction analysis shows clear clustering of the datasets for each group with at least three principal components: tissue origin, disease type and progression, and genotype (**Figure 3-7a**). Analysis of differentially expressed genes (1.5 fold cut-off; adjusted *P* value of <0.05) identified 173 genes down-regulated in the brain of PbA infected *Usp15*^{L749R} mutant mice and 112 down-regulated in the spinal cord of *Usp15*^{L749R} mutants undergoing EAE (**Figure 3-7b**), including an overlapping set of 39 genes down-regulated in a USP15-specific fashion in both ECM and EAE (complete listing in **Appendix Table 1**); together these down-regulated transcripts define the USP15-regulated transcripts. Gene ontology annotations (GO term) of these genes (**Figure 3-7c**) showed significant enrichment for immune response functions ($\log_{10} P<10^{-3}$ to $\log_{10} P<10^{-23}$), including “response to virus”.

We next performed gene set enrichment analyses (GSEA analysis [243]), a pair-wise analysis of detected gene sets (i.e. B6 vs. *Usp15*^{L749R}) using >1900 cell-specific and pathway-specific immune signatures. GSEA also provides a normalized enrichment score (NES) and a false-discovery rate (FDR) to evaluate the significance of

associations. GSEA analysis identified enrichment (FDR <0.01) for signatures associated with responses of different cells to viral infections, response to virus vaccines in PBMCs, and response to IFN-a (complete listing in **Appendix Table 2**, illustrative examples in **Figure 3-7d**). In GSEA, “leaders” are the genes that drive enrichment of a particular signature, (beyond maximal cumulative enrichment scores; past green line in **Figure 3-7d**). In leading edge analysis (LEA) [243], these genes and intersecting signatures can be clustered to examine the involvement of specific responses and associated cell types in the affected tissue. LEA of the ECM (**Figure 3-8a**), EAE (**Figure 3-8b**), and of the combined ECM/EAE datasets (**Figure 3-9a, b**) clearly identified the principal USP15-regulated “leaders” and associated signatures corresponding to the type I interferon response (*Oasl1/2*, *Isg15*, *Ifi41*, *Ifit1/3*, *Irf7/9*, *Usp18*, *Mt1/2*, *Mx1*) (see list in **Appendix Table 2**; illustrative examples in **Figure 3-9b**) as defined in the Interferome database [249]. This was evidenced by strength of USP15 effect on expression of drivers, number of differentially expressed drivers, and number of intersecting signatures. Several poorly annotated genes whose function in the immune system is unknown (e.g. *Plin4*) were also detected in this analysis. Cell-specific lymphoid and myeloid signatures were also detected, albeit less strongly, possibly reflecting tissue infiltration by these cells (**Figure 3-9a**; also **Figure 3-5a)**.

Additional RNA expression studies (qPCR) in brains at days 1, 3 and 5 post-PbA infection (**Figure 3-9c-f**) confirmed the major effect of USP15 on genes associated with type I interferon responses (*Oasl2*, *Ifit3*, *Usp18*, *Irf7*, *Irf9*, *Ifi35*; **Figure 3-9c**), lymphoid cells (*Gmzb*, *Cd3g*, *Lat*; **Figure 3-9d**), myeloid cells (*Cebpd*, *C4b*, *Cd11b*; **Figure 3-9e**), and genes of unknown function (*Plin4*; **Figure 3-9f**), and further suggested that the USP15 effect was rapid and detectable as early as day 3 post-infection. Early responses were further investigated by RNA-seq (**Figure 3-9g,h**). Juxtaposition of GSEA normalized enrichment scores (NES) for signatures depleted by the *Usp15* mutation at day 3 vs. day 5 show enrichment of type I interferon signatures at both day 3 and day 5, while myeloid and lymphoid signatures are more evident at day 5 (**Figure 3-9g**). Temporal analysis of leading edge genes clearly shows that genes driving IFN signatures are already present at day 3 in both B6 (2.5X) and *Usp15*^{L749R} infected mutants, while lymphoid-specific (1.31X) and myeloid-specific (1.09X) signatures

become most evident only by day 5 post-infection (**Figure 3-9g,h**). In all cases, the absolute expression levels of leading edge genes defining these signatures is reduced in *Usp15*^{L749R} mutant mice (**Figure 3-9g**). These results demonstrate that USP15 may act early (day 3) to regulate type I IFN response *in situ* during neuroinflammation. Finally, the relevance of USP15-regulated type I interferon response on susceptibility to ECM was investigated. We determined that a mouse mutant for the key LEA leader *Irf3* is ECM-resistant (**Figure 3-10)**. On the other hand, mice deficient for the adaptor protein *Mavs*, display high susceptibility to ECM (**Figure 3-10**), indicating that type I interferon signaling pathways dependent on *Mavs* are not required for ECM pathogenesis, whereas IRF3 protein is necessary.

These results suggest that impaired USP15-dependent engagement of type I interferon responses is a key contributor to ECM and EAE resistance in the *Usp15*^{L749R} mutant.

USP15 and TRIM25 co-regulated responses during ECM

USP15 can deubiquitinate the E3-ubiquitin ligase, TRIM25, that plays a role in RIG-I signaling [230,231]. A potential role for the USP15:TRIM25 dyad in response to neuroinflammation was investigated. In transfected HEK293T cells, USP15 and TRIM25 physically interact (**Figure 3-11a**), and the L720R mutation (in human USP15 backbone) does not impair interaction with TRIM25. As previously reported [230], TRIM25 was deubiquitinated by USP15 (**Figure 3-11b**; lanes 1-3), and we detected reduced activity of the human L720R and the mouse L749R variants, when compared to WT and to inactive catalytic mutants (C269A and C783A) used as positive and negative controls, respectively (**Figure 3-11b**). We further determined that *Trim25*$^{-/-}$ mutant mice display ECM-resistance (**Figure 3-11c**), and as is the case for *Usp15*^{L749R}, this is unrelated to blood parasitemia levels (**Figure 3-11d**). Finally, we detected genetic interaction between *Usp15* and *Trim25* and observed that introducing one null *Trim25* allele in *Usp15*$^{L749R/+}$ heterozygotes (*Trim25*$^{-/+}$:*Usp15*$^{L749R/+}$ double heterozygotes) causes an increase in ECM-resistance (60%) when compared to single heterozygote mice used as controls (**Figure 3-11e**). These results demonstrate functional interaction

between USP15 and TRIM25 during neuroinflammation, and establish that inactivation of the USP15:TRIM25 dyad is sufficient for ECM-protection. To investigate the pathways regulated by USP15:TRIM25 during neuroinflammation, we conducted RNA-seq in brains of *Usp15*^{L749R} and *Trim25*$^{-/-}$ mutants at day 5 post-PbA infection, and compared their gene expression profiles to naïve and infected B6 controls (**Figure 3-11f-i**). Global GSEA signature analysis (**Figure 3-11f,g**) identified TRIM25-specific signatures (LPS-treated macrophages, PBMC response to vaccine), and USP15-specific signatures (response to interferon, response to virus) as well as genes commonly dys-regulated between the two mutants (**Figure 3-11f**). This group contains 22 genes, including 14 members of the ISG family (**Figure 3-11h**). Illustrative RNA sequence tracks for *Zfp36, Mt2, Cebpd, Cdkn1a, Gzmb,* and *Socs3* are shown in **Figure 3-11i**. This analysis clearly points to ISG expression as a main component of differential gene expression common to *Trim25* and *Usp15* mutants in the brain *in situ* during PbA infection.

The cellular compartment responsible for USP15-dependent effects in neuroinflammation and in type I interferon response was investigated. Studies in bone marrow (BM) chimeras showed that transfer of *Usp15*^{L749R} mutant BM (CD45.2) into irradiated B6 (CD45.1) confers significant ECM resistance, and at a level similar to that seen in *Usp15*^{L749R} mutant animals receiving *Usp15*^{L749R} mutant BM (**Figure 3-12a**), while transfer of B6 (CD45.1) BM into irradiated *Usp15*^{L749R} mice (CD45.2) conveys ECM sensitivity (**Figure 3-12a**). In addition, we observed that spleen cells from *Usp15*^{L749R} and from *Trim25*$^{-/-}$ mutants display reduced ISG activation (*Irf7*, *Usp18*) compared to WT B6, when stimulated with poly(I:C) *in vitro* (**Figure 3-12b**). Also, RIG-I dependent, and double-stranded RNA (3PRNA)-induced ISG gene activation (*Ifit3*, *Irf7*) in transfected primary bone marrow-derived macrophages (BMDMs) is significantly decreased in *Usp15*^{L749R} mutants compared to WT B6 controls (**Figure 3-12c**). These results identify a major hematopoietic contribution to ECM resistance in *Usp15*^{L749R} mice.

USP15 protein expression was investigated in primary human brain cells (informed consent was provided by donors; see Methods). In microglia, USP15 is

expressed at steady state and is further induced upon stimulation with IFN-γ and LPS (**Figure 3-12d**). USP15 is expressed in primary astrocytes at steady state and further induced after their activation with IFN-γ+IL-1β and IFN-γ+TNF (**Figure 3-12e**). TRIM25 protein is co-expressed with USP15 in primary microglia and astrocytes at steady state (**Figure 3-12d,e**). In astrocytes, TRIM25 protein expression is further increased following activation with IFN-γ+IL-1β and IFN-γ+TNF (**Figure 3-12e**). These data suggest that USP15 and TRIM25 may play a functional role in microglia and astrocytes; however the contribution of these cells to USP15-dependent neuroinflammation phenotypes remain to be established.

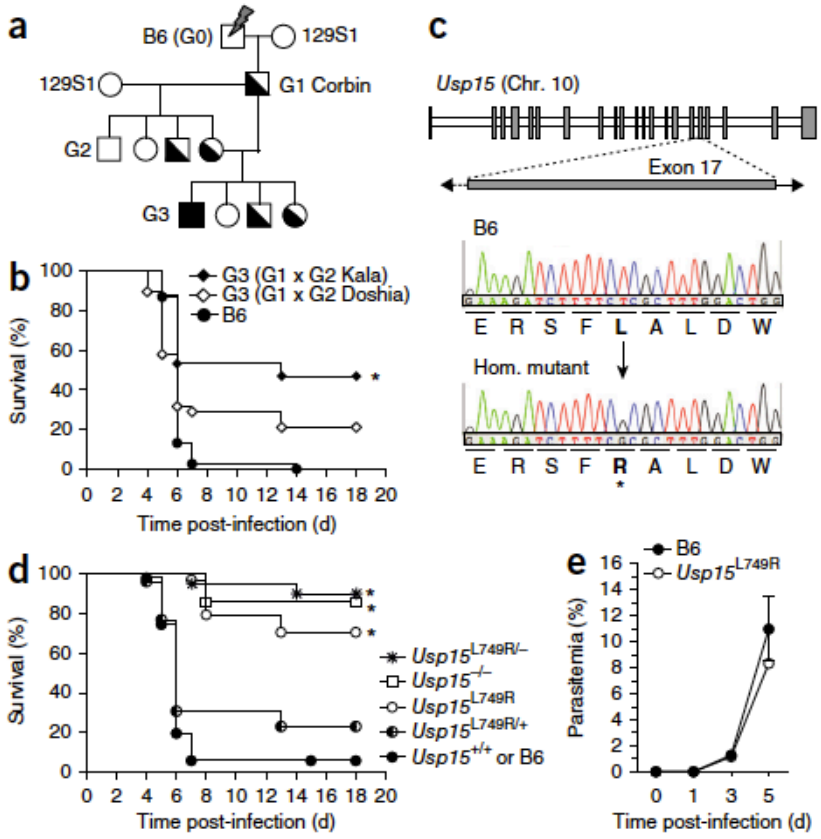

Figure 3-1. An ENU-induced mutation in *Usp15* protects mice against development of experimental cerebral malaria

(a) Breeding scheme for the production of ENU-induced mutant mice. **(b)** Survival of *Corbin* derived mice following infection with *P.berghei* (PbA). G2 females, *Doshia* and *Kala,* were backcrossed to their G1 father *Corbin*, and their G3 offspring [G1 x G2 Doshia, n=38; G1 x G2 Kala, n=32] were infected with PbA and monitored for appearance of neurological symptoms and for survival. Statistical significance was assessed using a Log-rank statistical test (**** P<0.0001) **(c)** Whole-exome sequencing identified a T-to-G transversion in exon 17 of the *Usp15* gene in pedigree *Corbin*, causing a leucine (L) to arginine (R) amino acid substitution at position 749 of the protein. **(d)** Survival plots of PbA-infected *Usp15* homozygote mutants (*Usp15*^{L749R}, n=34), heterozygotes (*Usp15*$^{L749R/+}$, n=26), *Usp15* knockout (*Usp15*$^{-/-}$, n=7), double heterozygotes (*Usp15*$^{L749R/-}$, n=20) and wild type *Usp15* (*Usp15*$^{+/+}$) or B6 controls (n=51). Data is a combination of 8 independent experiments. Statistical significance for survival between *Usp15*-related mutants and B6 controls was determined by the Log-rank test (**** P<0.0001). **(e)** Blood stage parasitemia during PbA infection (n=5/group). Data is a representation of two independent experiments and is expressed as a mean ± SD.

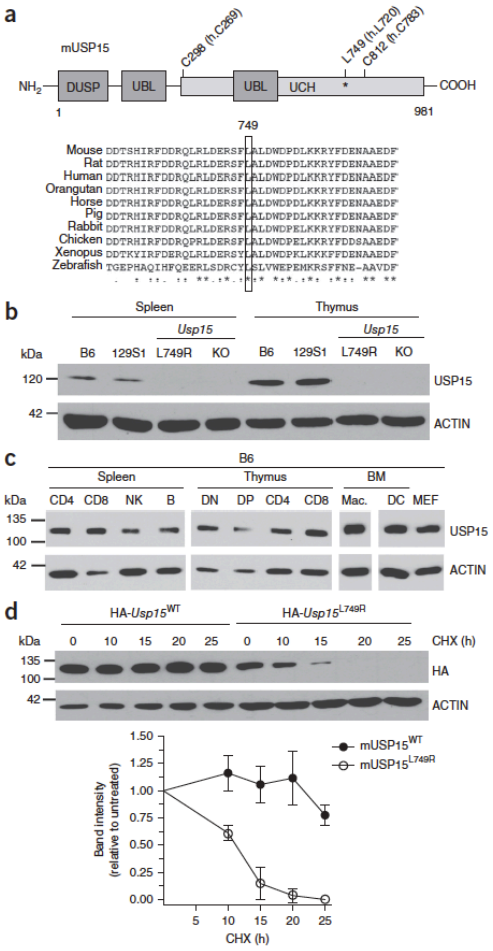

Figure 3-2. Reduced protein expression and reduced stability of the USP15^{L749} variant in vivo and in vitro

(a) Schematic representation of the structural features of USP15, including the deubiquitinase-specific domain in USP (DUSP), the ubiquitin-like (UBL) domain, and the position of the L749 residue, and the known catalytic Cysteines (C298,C812); L749 in the catalytic domain of USP15 is highly conserved across species. **(b)** Immunoblotting analysis of USP15 expression in spleen and thymus from control B6, 129S1, and *Usp15*^{L749R} homozygote mutants and *Usp15*$^{-/-}$ (KO) mice. Data is representative of two independent experiments. **(c)** Immunoblotting analysis of USP15 protein expression in lymphoid and myeloid cells isolated from spleen and thymus by cell sorting, from *in vitro* derived bone marrow macrophages (mac) and dendritic cells (DC), and from mouse embryonic fibroblasts (MEF). Splenic CD4 T cells (CD4$^+$CD8$^-$), CD8 T cells (CD4$^-$ CD8$^+$), NK cells (TCRβ^-CD49b$^+$) and B cells (TCRβ^-CD19$^+$); Thymic double negative T cells (DN: CD4$^-$CD8$^-$), double positive T cells (DP: CD4$^+$CD8$^+$), single positive CD4 T cells (CD4$^+$CD8$^-$) and single positive CD8 T cells (CD4$^-$CD8$^+$). Data is representative of two independent experiments. **(d)** HEK293 cells expressing HA-tagged WT or USP15^{L749R} proteins were treated with cycloheximide (CHX, 20 μg/ml) for 10, 15, 20, and 25h, and analyzed by immunoblotting. Data is a representation of two independent experiments (2 clones per construct), and expressed as a mean ± SD.

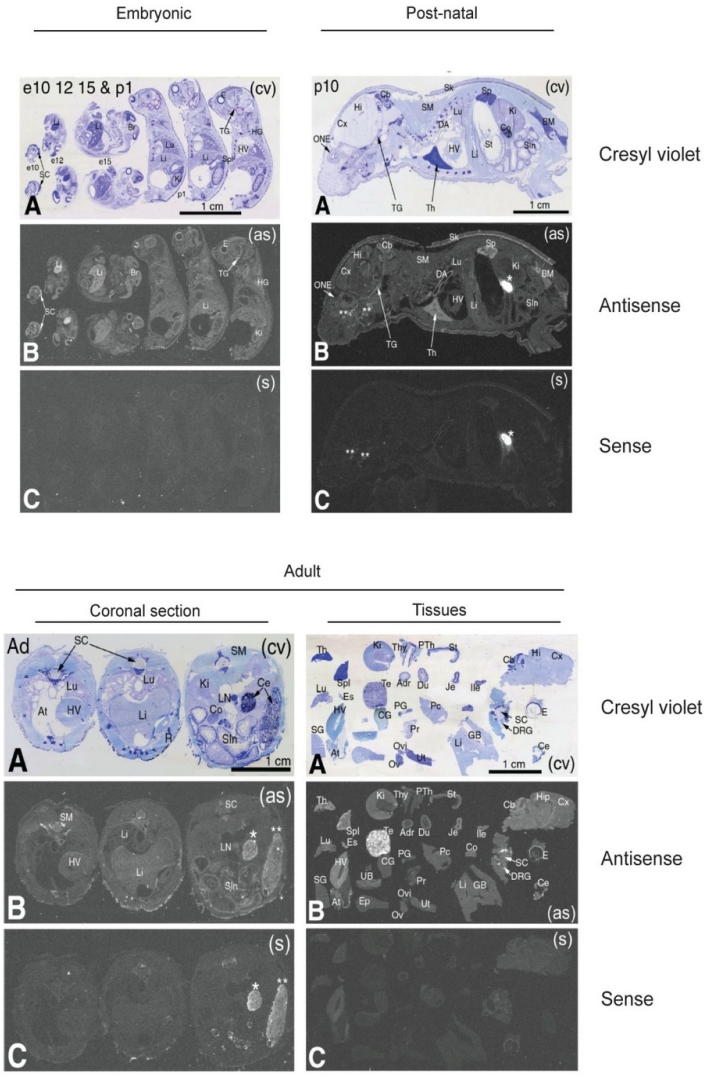

Figure 3-3 (Supplementary Figure). Ubiquitous pattern of *Usp15* mRNA expression in embryonic, post-natal and adult mice

Mouse sections were stained with cresyl violet to localize *Usp15* RNA to specific organs and structures. *In situ* hybridization was carried out using radiolabelled antisense (as) and sense (s) probes. The results shown are from X-ray film autoradiography obtained following 5-days exposure. Non-specific localized signals (visible with sense and anti-sense probes) are indicated with an asterisk (*); in the teeth (p10) and the large intestine lumen (p10 and adult). (Magnification: Embryonic x2.4, Post-natal x3, Adult x2.4). Abbreviations: Adr–adrenal gland; At–heart atrium; Br–brain; Bro–bronchcus; Car– cartilage; Cb–cerebellum; Co–colon; Cx–cerebral cortex; Du – duodenum; E – eye; Ep – epididymis; Es – esophagus; GB – gallbladder; HV–heart ventricle; Il–ileum; Je–jejunum; Ki–kidney; Li–liver; LI–large intestine; Lu–lung; OL–olfactory lobe; Ov–ovary; Ovi–oviducts; PB–pelvis bone; Pc–pancreas; PG–pituitary gland; Pr–prostate; PTh–parathyroid gland; R–ribs; Sk–skin; Spl–spleen; St–stomach; SV–seminal vesicle; Te–testis; Th–thyroid gland; UB–urinary bladder; Ut-uterus; CA–central artery; GC-germinal center; LN–lymphatic nodule; RP–red pulp; Tr–trabeculum; V-vein; LF–lymphoid follicle; Me–medulla; MG–mammary glands; Cx–cortex.

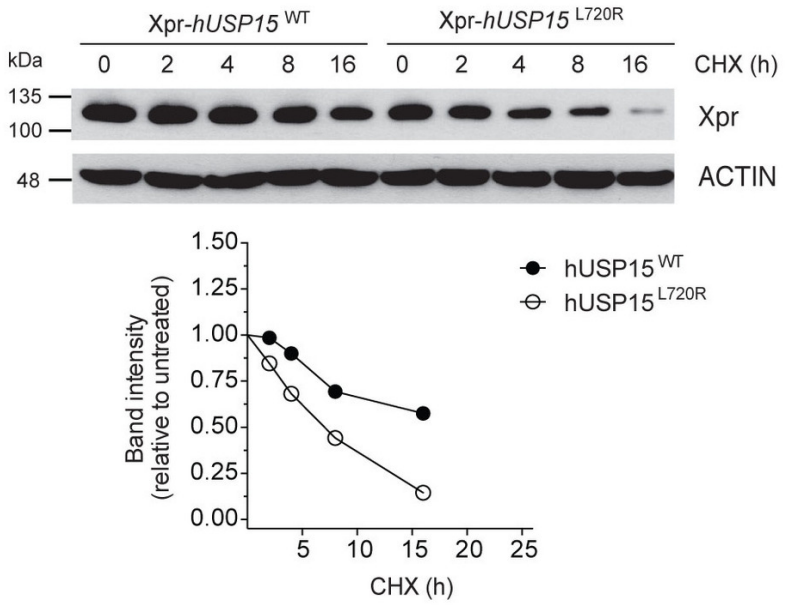

Figure 3-4 (Supplementary Figure). Reduced protein stability of the USP15 L720R human variant *in vitro*

HEK293 cells stably expressing HA-tagged WT or USP15^{L720R} proteins were treated with cycloheximide (CHX, 20 μg/ml) for 2, 4, 8, and 16h, and equal amounts of protein were analyzed by immunoblotting. Data is from a single experiment.

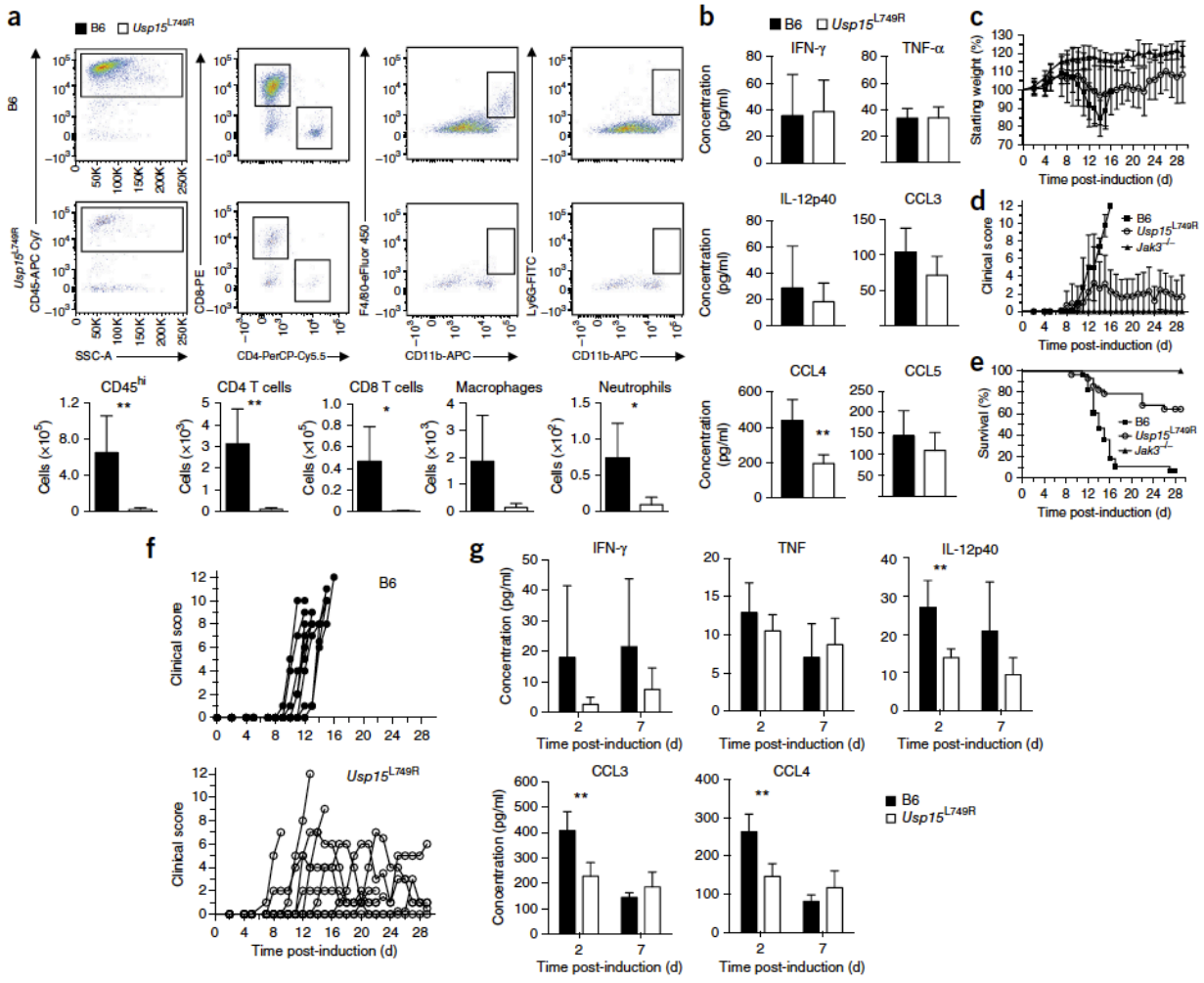

Figure 3-5. Reduced ECM and EAE cerebral pathogenesis in Usp15^{L749R} homozygotes

(a) Representative flow cytometry plots of brain cellular infiltrates in PbA-infected control B6 and *Usp15*^{L749R} mice at day 5 post-infection (n=5/group). Data are expressed as the total number of viable cells in the brain. Data is a representation of two independent experiments. **(b)** Serum cytokines from PbA-infected mice at day 5 post-infection were analyzed by Luminex (n=5/group). Data is from a single representative experiment. **(c)** EAE was induced in control B6 (n=8), *Usp15*^{L749R} (n=10), and *Jak3*$^{-/-}$ (n=5) mutants with MOG_{35-55} (d0) and pertussis toxin (d0, d2). Animals were monitored daily for **(c)** weight, **(d)** clinical score, and **(e)** survival. **(f)** Clinical scores for individual B6 and *Usp15*^{L749R} animals. Data is representative of three independent experiments. **(g)** Serum cytokines were analyzed at day 2 and day 7 post-EAE induction by Luminex (n=5/group). **(a-g)** All data are expressed as a mean ± SD for each group, and all statistical analyses were performed using the two-tailed unpaired Student's t-test; * P<0.05, ** P<0.01.

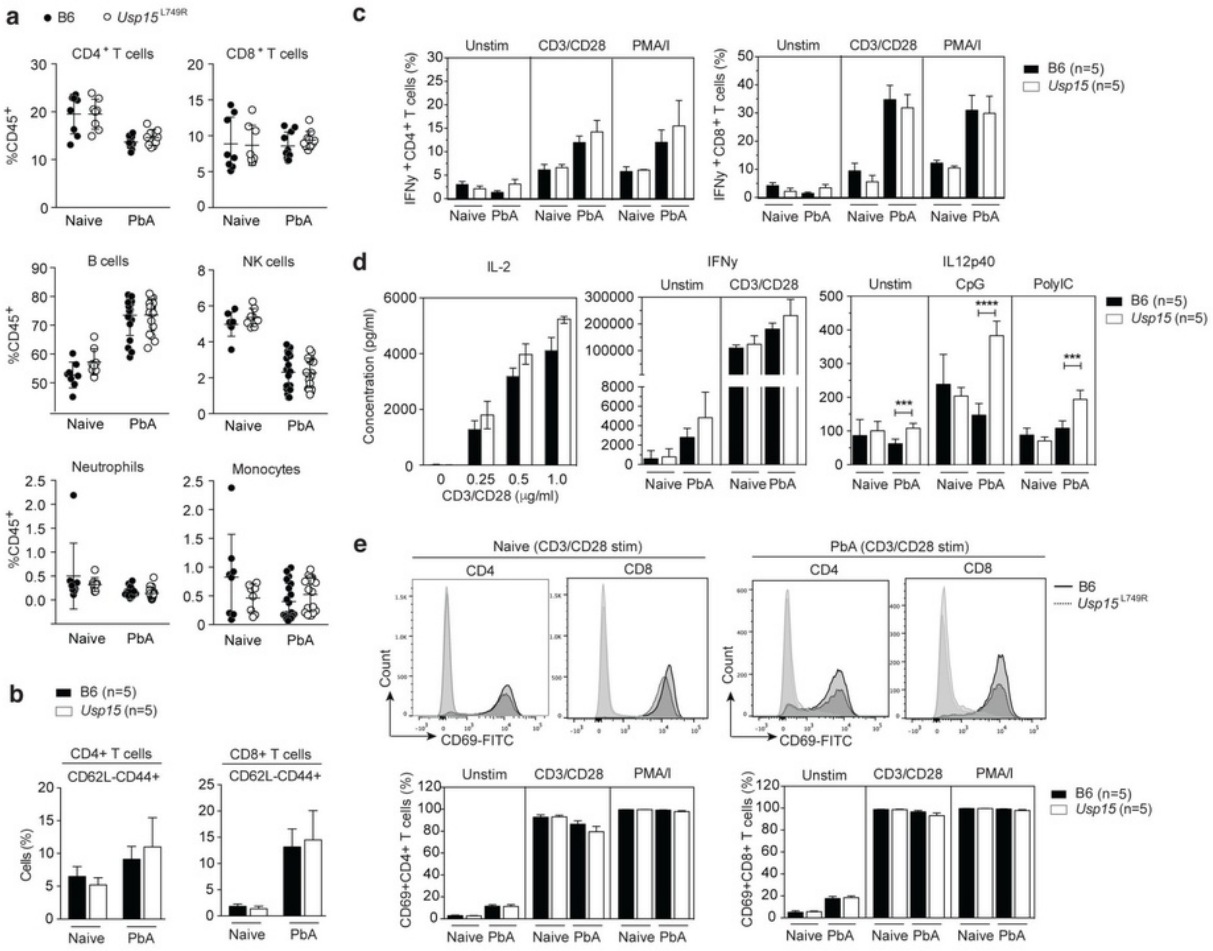

Figure 3-6 (Supplementary Figure). Immunophenotyping of *Usp15*^{L749R} mutants at steady-state and following *P. berghei* ANKA infection

(a) The number and proportions of different spleen cell types from naïve and from day 5-PbA infected animals, were established by flow cytometry with markers for T cells (CD4, CD8), B cells (B220), NK cells (NK1.1), monocytes and neutrophils (CD11b, Ly6G). Results are pooled from 5 independent experiments. (**b**) The percentage of splenic CD4$^+$ and CD8$^+$ effector T cells (CD62L$^-$CD44$^+$) were also assessed. Data represents a single experiment with 5 mice per group, and are expressed as a mean ± SD. **(c-d)** Cells were re-stimulated *in vitro* with either media alone (unstimulated, US), with anti-CD3 and anti-CD28 (TCR engagement), with PMA/Ionomycin, with CpG, or with Poly:IC and cytokine production was assessed by flow cytometry (C, intracellular staining), or by ELISA (D, culture supernatants). Data is a representation of two independent experiments with 5 mice per group, and is expressed as a mean ± SD. (**e**) The activation state of CD4$^+$ and CD8$^+$ T cells were assessed by analysis of CD69 cell surface expression in response to TCR engagement (anti-CD3/anti-CD28). Data represents a single experiment with 5 mice per group, and is expressed as a mean ± SD.

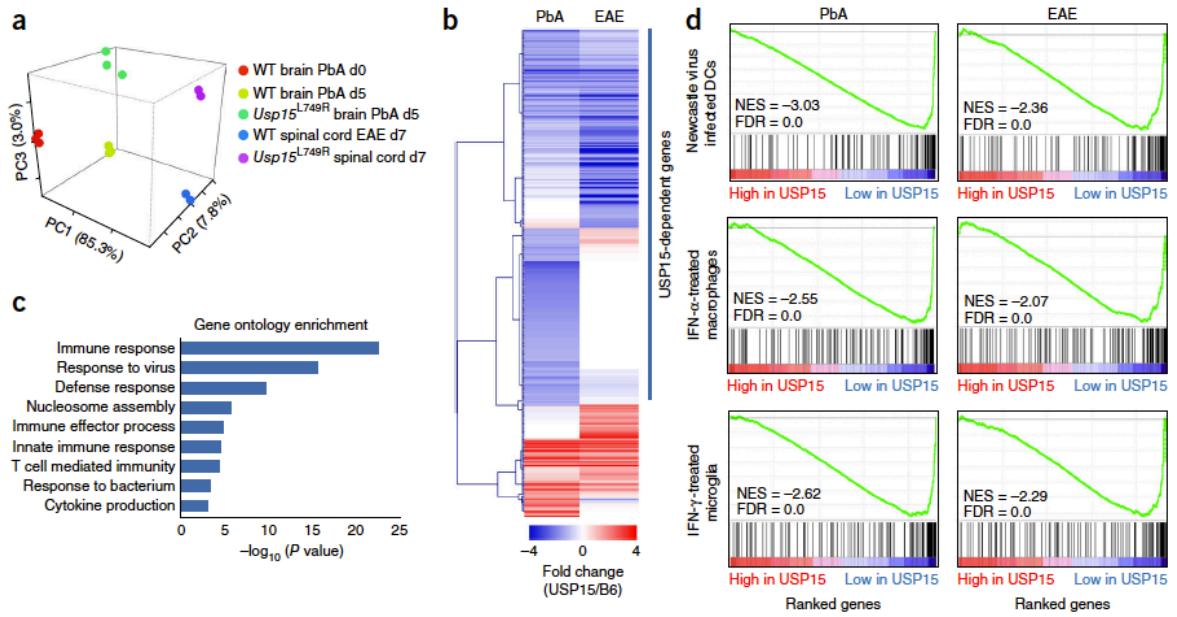

Figure 3-7. Effect of USP15 on global gene expression during neuroinflammation of the brain, and of the spinal cord

RNA-seq of whole brain RNA from controls and from PbA-infected (day 5) WT and *Usp15*^{L749R} mutants, and from spinal cord of WT and *Usp15*^{L749R} undergoing EAE (day 7) (n=3/group). **(a)** Dimension reduction analysis using partial least square method performed on normalized gene expression values for all RNA-seq datasets. The first three principal components are shown in a three-dimensional graph. **(b)** Dendogram presenting unbiased clustering of genes significantly dys-regulated (≥1.5 fold change and adjusted *P* value <0.05) in *Usp15*^{L749R} mutants during ECM and/or EAE. The 244 genes with reduced expression in *Usp15*^{L749R} mice (USP15-dependent genes) are identified. **(c)** Histogram showing gene ontology enrichment analysis of the USP15-dependent genes (-log10 *P* values are shown). **(d)** GSEA analysis of genes differentially expressed in *Usp15*^{L749R} mutant mice (compared to B6 controls) in either the PbA or the EAE neuroinflammation models. GSEA graphs illustrate the cumulative enrichment score for the three most highly enriched immunological signatures in the PbA and EAE conditions; the occurrence of the signature genes is shown as individual black lines over the distribution of brain or spinal cord gene profiles. Normalized enrichment scores (NES) and false-discovery rate (FDR) are shown for each displayed analysis.

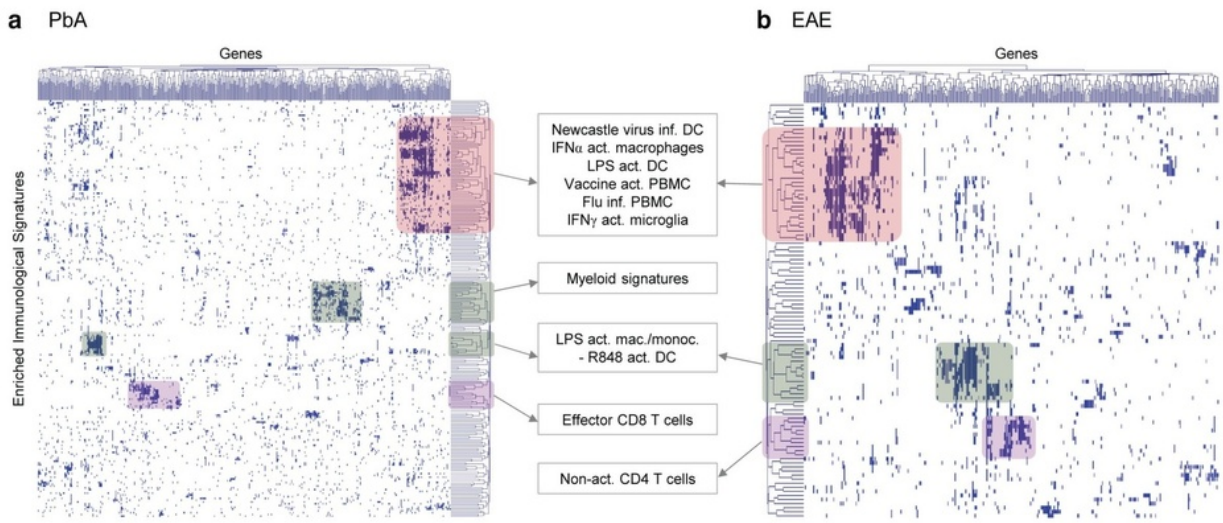

Figure 3-8 (Supplementary Figure). Cell populations and associated molecular pathways differentially regulated in a USP15-dependent fashion

(a) LEA dendogram for genes with reduced expression in *Usp15*^{L749R} mutant mice compared to B6 (day 5 post-PbA infection) and that drive significant enrichment (FDR<0.01) of immunological expression signatures (GSEA). Enriched immunological signatures and functions are highlighted by color boxes: red = signatures of IFN activation, green = myeloid signatures and responses, and purple = T cell signatures. Refer to Online Methods for details on LEA analysis. **(b)** LEA clustering analysis as described in (A) for immunological signatures depleted in *Usp15*^{L749R} mutant mice during EAE neuroinflammation progression.

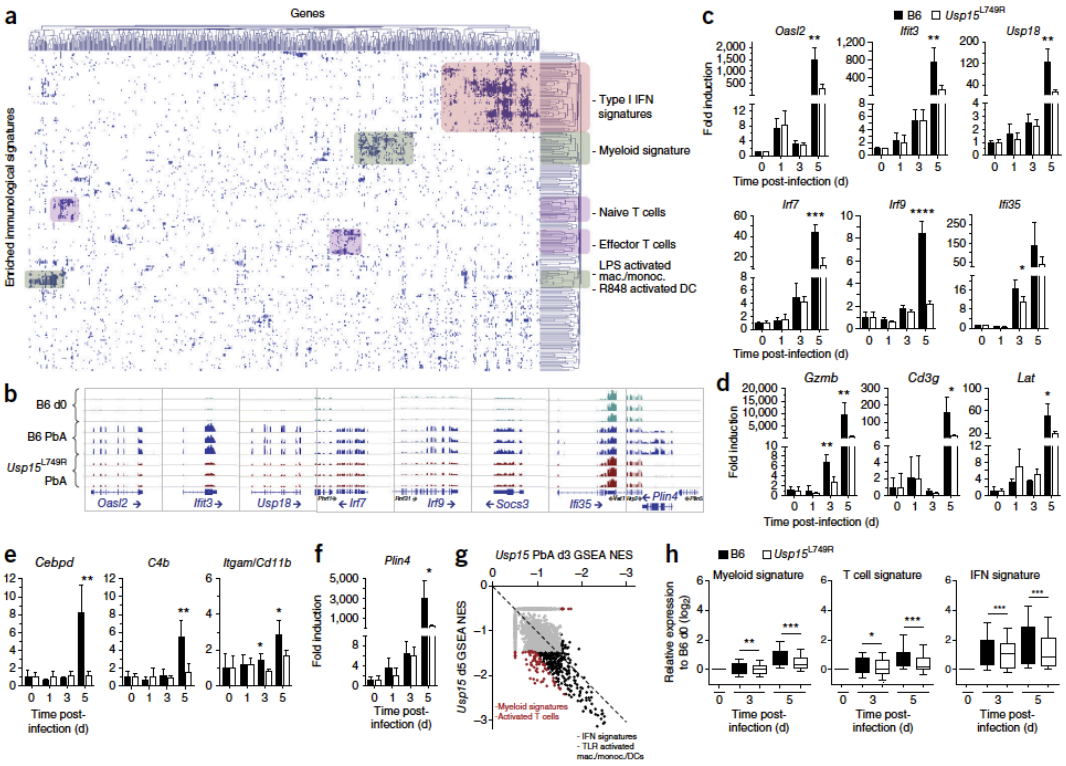

Figure 3-9. Cell populations and associated molecular pathways differentially regulated in a USP15-dependent fashion

(a) Dendogram showing clustering of genes driving enrichment of GSEA immunological signatures corresponding to IFN activation (pink): myeloid cells (green) and T cells signature (purple). **(b)** RNA-seq (normalized sequence read profiles over exon structure; biological triplicates) of representative type I IFN response genes; naïve B6 (B6 d0), and B6 (B6 PbA) and *Usp15*^{L749R} (USP15 PbA) at day 5 post-infection. **(c)** RT-qPCR analysis of type I IFN stimulated genes prior to (d0) and during PbA infection (d1, 3, and 5) in brains of B6 and *Usp15*^{L749R} mutants (n=5/group). Gene expression was normalized relative to *Hprt* expression and expressed as fold induction relative to day 0 (mean ± SD); *P* values (*Usp15*^{L749R} vs. B6) were determined using unpaired Student's t-test (* $P<0.05$, ** $P<0.01$, *** $P<0.001$). Gene expression was assessed for **(d)** lymphoid-specific markers, **(e)** myeloid-specific markers**,** and for **(f)** *Plin4*. **(g)** Comparative analysis of dys-regulated genes (B6 vs. *Usp15*^{L749R} mutants; n=3/group) and associated GSEA analysis at day 3 and day 5 post-PbA infection. Normalized enrichment scores (NES) for GSEA signatures were compared (day 3 vs. day 5), and identify signatures that are not affected (grey signatures; FDR > 0.05), signatures that show a >1.5 fold change in NES from day 3 to day 5 (red), and signatures that increase similarly from day 3 to day 5 (black). (**h**) Box plot showing relative gene expression (log2; ratio of PbA-infected/B6 non-infected) for LEA drivers of myeloid cells, T cells and IFN signatures. *P* values were calculated using a two-tailed paired Student's t-test comparing B6 vs. *Usp15* mutants at day 3 vs. day 5 (* $P<0.05$, ** $P<0.01$, *** $P<0.001$).

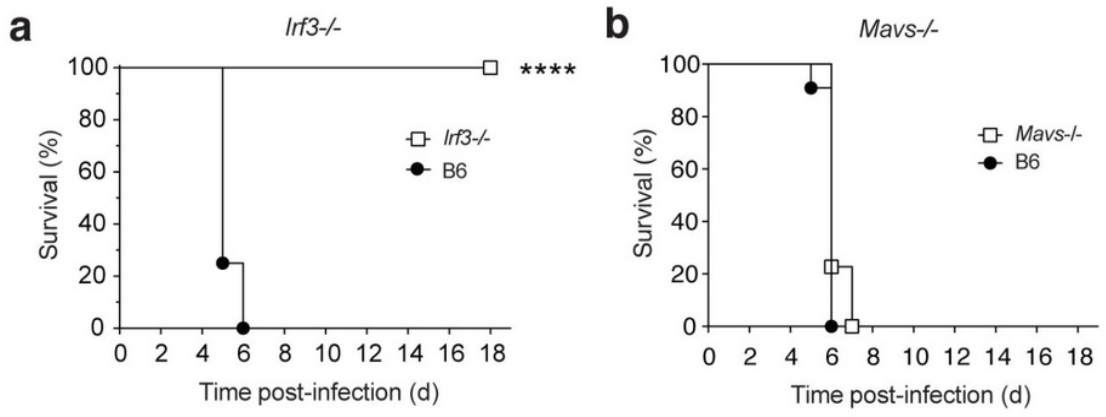

Figure 3-10 (Supplementary Figure). Mouse mutants bearing a loss of function mutation in *Irf3* are protected against neuroinflammation

Survival plots for PbA-infected (**a**) *Irf3* mutants (*Irf3*$^{-/-}$) (n=13) and B6 controls (n=8), and (**b**) *Mavs* mutants (*Mavs*$^{-/-}$) (n=22) and B6 (n=11). Statistical significance for survival between groups of mice was determined by the Log-rank test (* P<0.05, **** P<0.0001).

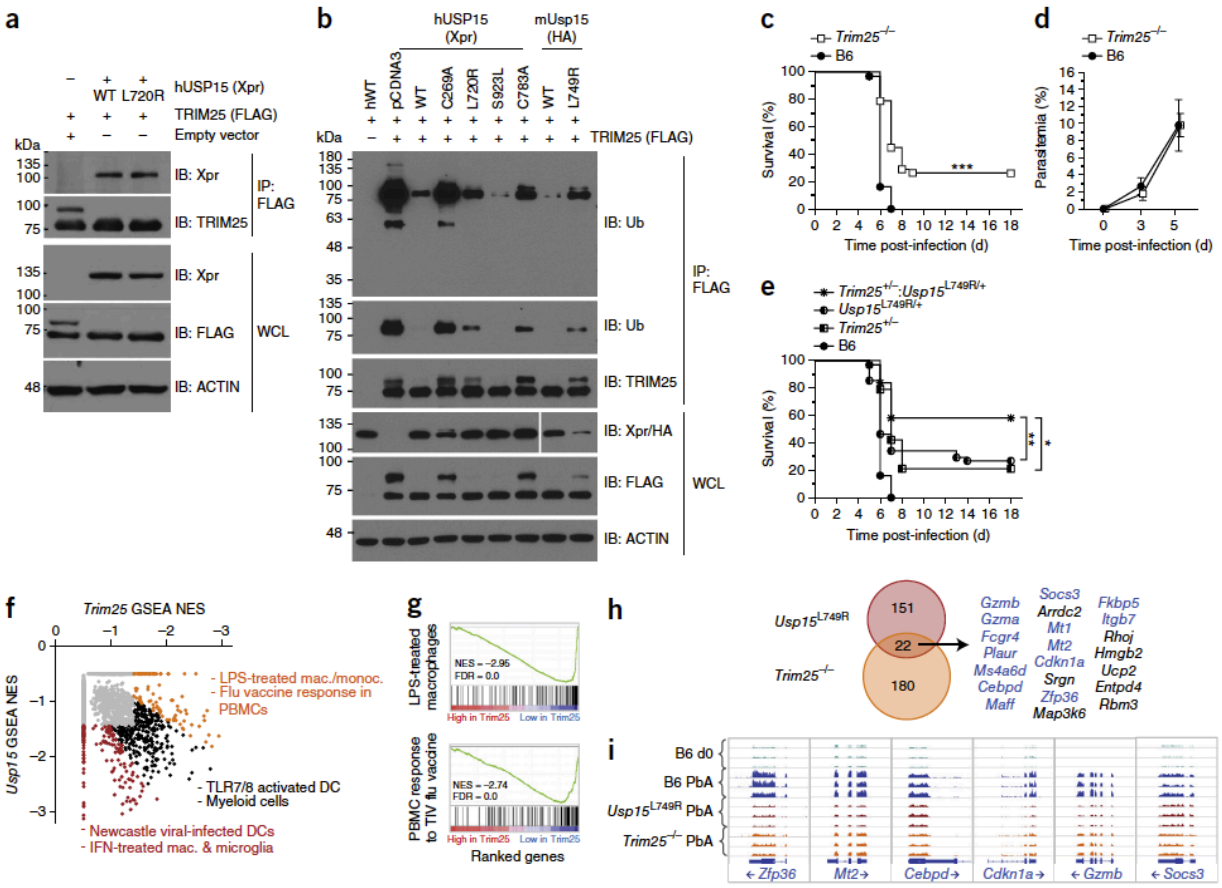

Figure 3-11. USP15 modulates the type I IFN response through interaction with TRIM25

(a,b) Cells expressing either Xpress (Xpr)-tagged human USP15, wild type (WT) or mutant USP15 variants, and co-transfected with FLAG-tagged TRIM25, were immunoprecipitated with either anti-Xpr or anti-FLAG antibodies, and whole cell lysates (WCL) and immunoprecipitated samples (IP) were analyzed by immunoblotting (IB) using the indicated antibodies. Data is representative of two independent experiments. **(b)** Top 2 panels in **(b)** are two exposures of the same blot. Data is representative of 4 independent experiments. (**c**,**e**) Survival plots of PbA-infected *Trim25* mutants (*Trim25*$^{-/-}$) (n=36), *Trim25* heterozygotes (*Trim25*$^{+/-}$) (n=19), *Usp15*^{L749R} heterozygotes (*Usp15*$^{L749R/+}$) (n=41), *Usp15*$^{L749R/+}$:*Trim25*$^{+/-}$ double heterozygotes (n=31) and B6 controls (n=31). Data are a combination of 3 independent PbA-infections. Statistical significance was determined by the Log-rank test (* P<0.05, ** P<0.01, **** P<0.0001). (**d**) Blood stage parasitemia levels in PbA-infected *Trim25*$^{-/-}$ animals (n=5/group). Data represents a single experiment (mean ± SD). (**f-i**) Comparative analysis of dys-regulated leading genes and associated GSEA signatures in brain of *Usp15*^{L749R} and *Trim25*$^{-/-}$ mutants (n=3/group). **(f)** Comparisons of normalized enrichment scores, identifying GSEA signatures specifically enriched in *Trim25*$^{-/-}$ (orange) or in *Usp15*^{L749R}

(red) or in both (black) (see legend in Figure 5g). Signatures most affected in each group are indicated. (**g**) Representative GSEA graphs for signatures most significantly affected in *Trim25*$^{-/-}$ mice. (**h**) Venn diagram showing intersection between genes differentially expressed at day 5 post-PbA infection (≥1.5 fold change, adjusted *P* value <0.05) in *Trim25*$^{-/-}$ vs. *Usp15*^{L749R} mutants, including 14 members of the IFN-stimulated gene family (ISG, blue). (**i**) Representative examples of RNA-seq profiles for some of these ISGs are shown.

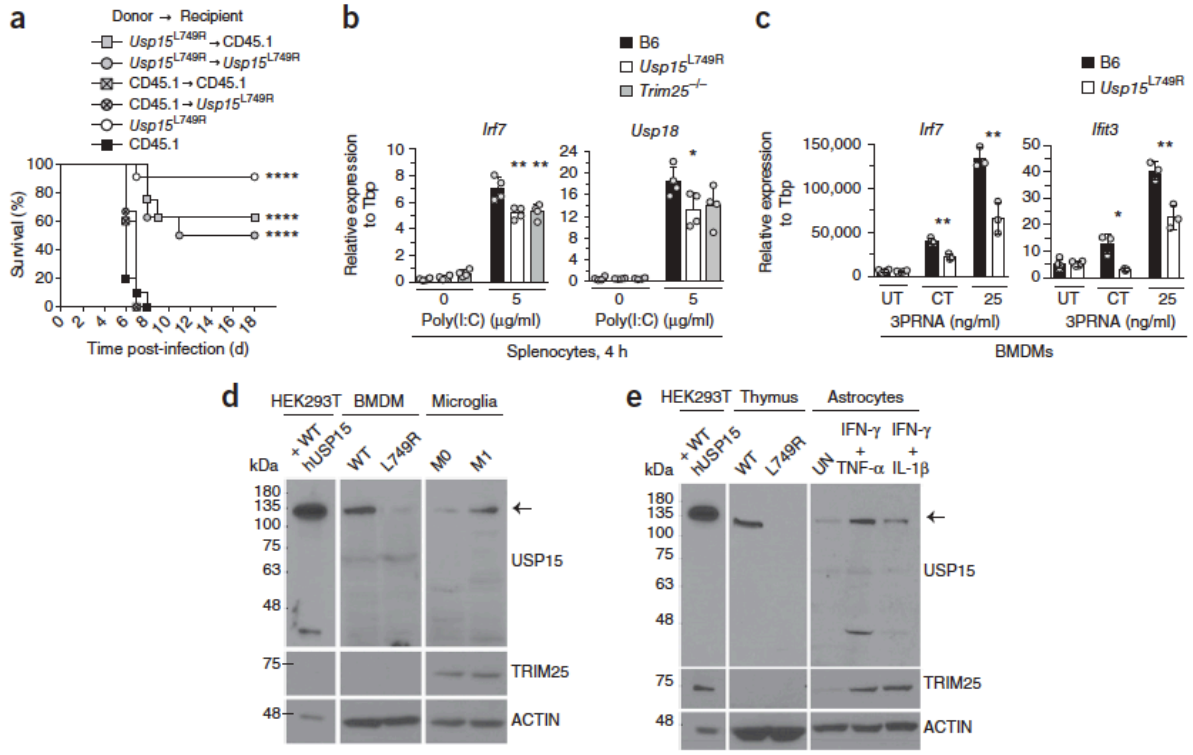

Figure 3-12. Cellular compartments expressing USP15-dependent effects in neuroinflammation and in type-I interferon response

(**a**) Lethally irradiated mice (recipients) were reconstituted with bone marrow from the indicated sex-matched donors, and later infected with 10^6 PbA parasites. Survival plots of PbA-infected CD45.1 (n=10), *Usp15* homozygous mutants (*Usp15*^{L749R}) (n=11), CD45.1→ *Usp15*^{L749R} (n=9), CD45.1→ CD45.1 (n=10), *Usp15*^{L749}→ *Usp15*^{L749R} (n=8) and *Usp15*^{L749}→ CD45.1 (n=8). Data is a representation of two independent experiments. Statistical significance in survival between experimental groups vs. CD45.1 control was determined by the Log-rank test (**** P<0.0001). (**b-c**) Interferon-stimulated genes mRNA expression (*Irf7*, *Usp18*, *Ifit3*) was assessed by RT-PCR (relative to control *Tbp* gene expression) in Poly(I:C)-stimulated splenocytes (2 independent experiments; n=4 mice/group) **(b)**, or in bone marrow-derived macrophages (BMDMs) transfected with double-stranded RNA, 3PRNA, to activate RIG-I dependent signaling (one experiment; n=3 mice/group) **(c)**. Data is shown as mean ± SD; P values were calculated for comparison of B6 vs. mutant using unpaired Student's t-test (* P<0.05, ** P<0.01, *** P<0.001). (**d**) Human microglia either untreated (MO) or activated by exposure to IFN-γ + LPS (M1) and **(e)** human astrocytes either untreated (UN) or activated with IFN-γ + TNF or IFN-γ + IL-1β were lysed and protein expression analyzed by immunoblotting. (**d-e**) Cells expressing human USP15 (hUSP15 WT), as well as bone marrow-derived macrophage or thymus cells from control and from *Usp15*^{L749R} mutants were used as positive and negative controls. Data is representative of two independent experiments, using two biological samples per cell type.

Gene	Orientation	Sequence (5'-----3')
C4b	sense	GATGAGGTTCGCCTGCTATT
C4b	antisensee	GACTTGGGTGATCTTGGACTC
Cd3g	sense	TCTTCCTTGCTCTTGGTGTATATC
Cd3g	antisensee	GAGATGGCTGTACTGGTCATATT
Cebpd	sense	TCGACTTCAGCGCCTACATTGA
Cebpd	antisensee	CCGCTTTGTGGTTGCTGTTGAA
Gmzb	sense	CGGGAGTGTGAGTCCTACTTTA
Gmzb	antisensee	GTGGAGGTGAACCATCCTTATATC
HPRT	sense	TCAGTCAACGGGGGACATAAA
HPRT	antisensee	GGGGCTGTACTGCTTAACCAG
Ifi35	sense	GATCCAGAAAGCCGAGATCAA
Ifi35	antisensee	CTGGAAGTGGATCTCAAGGATG
Ifit3	sense	CTGAACTGCTCAGCCCACAC
Ifit3	antisensee	TGGACATACTTCCTTCCCTGA
Irf7	sense	CGACTTCAGCACTTTCTTCCGAGA
Irf7	antisensee	AGATGGTGTAGTGTGGTGACCCTT
Irf9	sense	AAATGGGAGGACCAATGGCGTT
Irf9	antisensee	ATAGATGAAGGTGAGCAGCAGCGA
Itgam (CD11b)	sense	GAAAGTAGCAAGGAGTGTGTTTG
Itgam (CD11b)	antisensee	GGGTCTAAAGCCAGGTCATAAG
Lat	sense	GGATGAAGACGACTATCCCAAC
Lat	antisensee	CCTCACTCTCAGGAACATTCAC
Oasl2	sense	GGACCCGTTCCCCGACCTGT
Oasl2	antisensee	CGACCTCCCGGTTTCTCGCC
Plin4	sense	CATCATGTCAGCTTCAGGAGAT
Plin4	antisensee	GGGTCTGTTGCTGTTTGTAAG
Trim25	sense	AACTGAAGGCAGAGGTTGAG
Trim25	antisensee	CCCTTGGTAGATTCCCATTATCA
Usp18	sense	CGTGCTTGAGAGGGTCATTTG
Usp18	antisensee	GGTCGGGAGTCCACAACTTC

Table 3-1. (Supplementary Table). qPCR validation primers

3.5 Discussion

What are the cellular and molecular pathways controlled by USP15 that play a role in pathogenesis of acute neuroinflammation? Recent studies in cell-based model systems have implicated USP15 in multiple unrelated biochemical pathways and cellular responses. USP15 deubiquitinase activity alone, or in combination with other proteins, has been associated with regulation of IkBa and activation of NF-kB [250], parkin-mediated mitochondrial ubiquitination and mitophagy [251], MAPK activity through stabilization of the E3 ligase BRAP/IMP [252], the Nrf2 pathway in anti-oxidant response [253], and histone (ubH2B) deubiquitination [254]. USP15 has also been shown to regulate TGF-b signaling and associated transcriptional activation, with SMAD3, the E3 ubiquitin ligase SMURF2 and the type I TGF-b receptor being direct targets for USP15-dependent deubiquitination [255-257]. Recently, USP15 has been implicated in regulation of certain aspects of the immune system *in vivo*. USP15 can negatively regulate Th1 responses in $CD4^+$ T cells (anti-*Listeria* and anti-tumor activities) through active stabilization of the E3 ubiquitin ligase MDM2, and with concomitant degradation of NFATc2 [258]. Finally, recent studies have suggested that USP15 may contribute to regulation of type I interferon response. However, the role of USP15 in type I interferon response remains controversial, having been alternatively demonstrated to act as a strong activator (through deubiquitination of TRIM25) [230], or a potent inhibitor of this response (through deubiquitination of RIG-I) [259].

Cellular immunophenotyping of our *Usp15*^{L749R} mutant mice following *L. monocytogenes* infection supports published results and suggests that in this model USP15 can act as a negative regulator of Th1 response [258]. Indeed, *L. monocytogenes*-infected *Usp15*^{L749R} mutants show increased maturation (fraction of $CD4^+/CD44^+$), and increased activation (IFN-γ production) of $CD4^+$ T cells in response to listeriolysin (LLO) (**Figure 3-13**). However, parallel studies of PbA-infected mice failed to demonstrate an effect of USP15 on the fraction of effector T cells ($CD44^+$), activation of T cells ($CD69^+$), and Th1 cytokine production (IFN-γ, TNF, IL-2) by $CD4^+$ and by $CD8^+$ T cells in response to TCR engagement or to non-specific stimuli (**Figure 3-6)**. Therefore, ECM-resistance in *Usp15*^{L749R} mutants does not appear to be linked to

increased Th1 responses associated with loss of USP15 function. On the contrary, ECM protection has been previously associated with a dampening or inactivation of Th1 response in mouse strains bearing null alleles at loci such as *Ifng*, *Ifngr*, *Stat1*, *Irf1*, *Irf8*, *Lck*, *Themis*, and *Jak3* [55,105,139,157,158].

On the other hand, RNA sequencing datasets from brain (ECM model) and spinal cord (EAE model) showed a striking effect of the *Usp15*^{L749R} mutation on induction of the type I interferon response. This differential induction was a) highly significant, b) detected as the dominant pathways both by GO and GSEA/LEA analysis (response to virus, response to type I IFN, response to vaccine), and c) validated by RT-qPCR. These results establish for the first time that USP15 acts as an *in vivo* activator of type I interferon response during acute neuroinflammation and encephalitis. The E3 ubiquitin ligase TRIM25 ubiquitinates the pattern recognition receptor RIG-I (for double-stranded viral RNAs) and positively regulates RIG-I mediated production of IFN-α and IFN-β [231]; ubiquitination of TRIM25 by LUBAC (HOIL-1L, HOIP) stimulates degradation of TRIM25 and suppresses RIG-I signaling [260]. Here, we observe that USP15 physically interacts and deubiquitinates TRIM25, as previously reported [230]. Importantly, we show that loss of TRIM25 function causes enhanced ECM resistance, and we further demonstrate genetic interaction between USP15 and TRIM25 expressed as robust ECM resistance in *Usp15*$^{L749R/+}$*:Trim25*$^{-/+}$ double heterozygotes. We also observed reduced deubiquitinase activity of the USP15^{L749R} mutant towards another known USP15 target, SMURF2 [257] (**Figure 3-14**). However, in contrast to TRIM25, loss of SMURF2 function in *Smurf2*$^{-/-}$ null mutants does not protect against ECM (data not shown). These results confirm that USP15 acts as an activator of type I IFN response *in vivo* during neuroinflammation, and further demonstrate a critical and specific role for the USP15:TRIM25 regulatory dyad in this activation.

In the context of recently published studies, our results suggest a critical dual but opposite role of type I IFN in the pathogenesis of cerebral malaria [27,74]. Studies of the early liver stage disease in primary hepatocytes and in liver cell lines infected with *P. berghei* sporozoites (insect form) have demonstrated strong induction of type I IFN within 36 to 48h of infection. This liver stage response to PbA infection is defective in

mice bearing null mutations at the type I IFN receptor (*Ifnar1*$^{-/-}$) or in proteins associated with nucleic acid sensing (*Rig-I*$^{-/-}$), induction (*Mavs*$^{-/-}$, *Mda5*$^{-/-}$) and amplification (*Irf3*$^{-/-}$) of IFN-α/IFN-β production. This initial liver stage type I IFN response is protective, as *Ifnar1*$^{-/-}$ mutant mice show increased liver infection load and increased blood stage parasitemia [74,75]. Conversely, we demonstrate that engagement of type I IFN response in later stages of *P. berghei* infection (in response to blood-stage merozoites) is detrimental to the host, and drives pathogenesis of cerebral disease in the brain *in situ*. Indeed, we show that the dampening of type I IFN response in *Usp15*^{L749R} and in *Trim25*$^{-/-}$ mutant, and in markers of this pathway such as *Irf3*$^{-/-}$ and T cell-specific *Socs1/Socs3* mutants protect against lethal ECM (data not shown), in agreement with the previously reported ECM-resistance of *Irf7*$^{-/-}$ and *Ifnar1*$^{-/-}$ mutants [141,142,177]. On the other hand, we show that type I IFN signaling pathways dependent on MAVS are not required for ECM pathogenesis, indicating that USP15 mediates the induction of type I interferon pathway by MAVS-independent pathway(s). Amongst the known components of type I IFN signaling pathways tested in the ECM model, *Trif*$^{-/-}$ mice were shown to be susceptible, while *Tbk1* hypomorphs showed resistance [159,177,179]. Altogether, this leads us to speculate that the USP15:TRIM25 dyad may be implicated in the regulation of a type I IFN pathway activated by an unidentified receptor, signaling possibly through STING and to activate TBK1 and IRF3:IRF7 [177]. Phenotyping of additional knockouts in type I interferon induction pathway components will allow us to dissect the precise mechanism of action for USP15 in type I interferon signaling. These results demonstrate a critical dual role of type I IFN in malaria progression, being protective early (liver stage) and detrimental in late stages (cerebral malaria) of disease.

Finally, recent genetic studies in large cohorts of human patients have identified an association between genomic variants near *USP15* and asthma [261]. These findings in humans, together with the current report in animal models of neuroinflammation, suggest that USP15 may be a valuable target for drug discovery in inflammatory diseases.

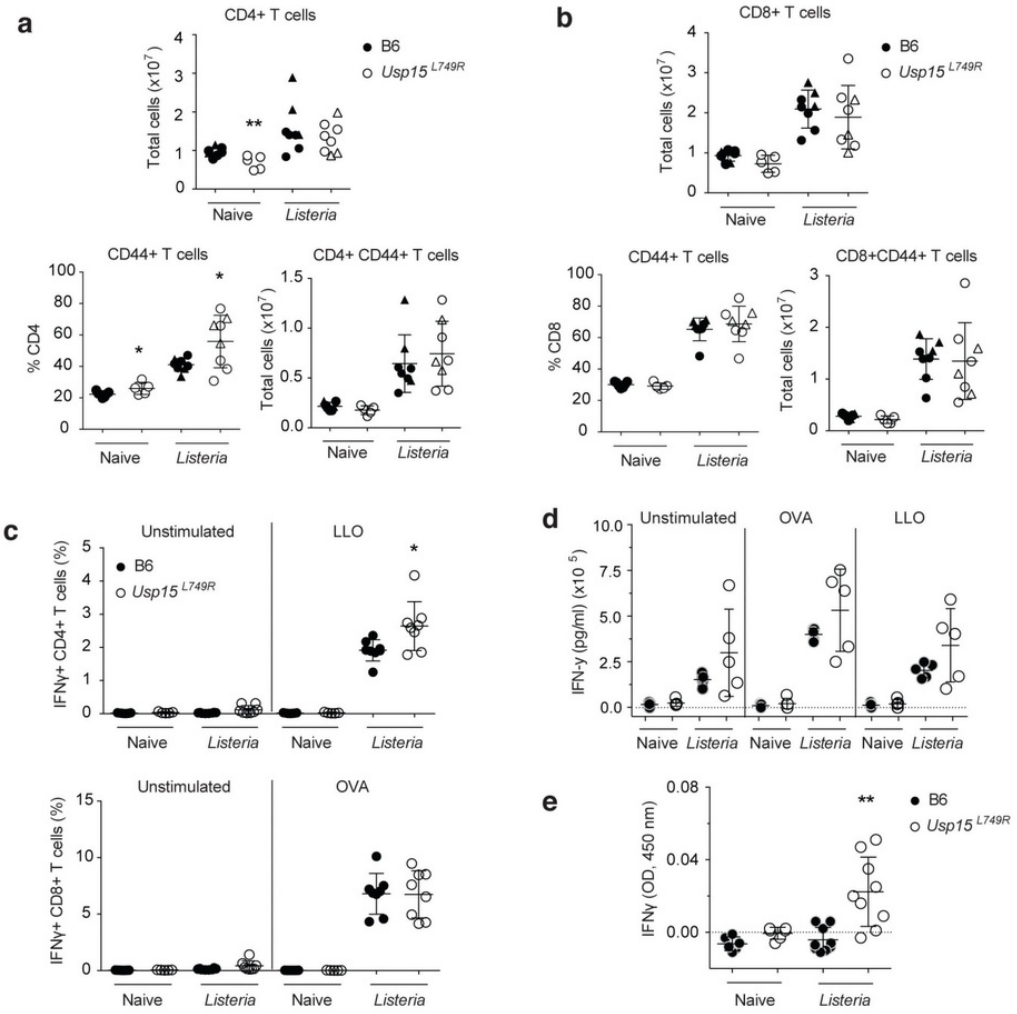

Figure 3-13 (Supplementary Figure). USP15 negatively regulates CD4$^+$ T cell activation during *Listeria monocytogenes* infection

Wild type B6 mice and *Usp15*^{L749R} mutants infected with 1x10^4 CFU of *Listeria monocytogenes* (strain 10403s) expressing ovalbumin (OVA) were sacrificed on day 7 post-infection, and phenotyped for the activation of the T cell response in spleen cell populations. **(a, b)** CD44 expression (T cell activation) on CD4$^+$ T cells (A), or CD8$^+$ T cells (B), expressed as percentage and total cell numbers. **(c, d)** Cells were re-stimulated *in vitro* with *Listeria*-specific antigens, LLO or OVA, and IFN-γ production was assessed by flow cytometry (C, intracellular staining), or by ELISA (D, culture supernatants) for CD4$^+$ and CD8$^+$ T cells. **(e)** Serum IFN-γ levels were measured by ELISA, and plotted as optical density absorbance (OD) at 450 nm. **(a-e)** Data is a combination of two independent experiments. All data are expressed as a mean ± SD for each group, and all statistical analyses were performed using the two-tailed unpaired Student's t-test.

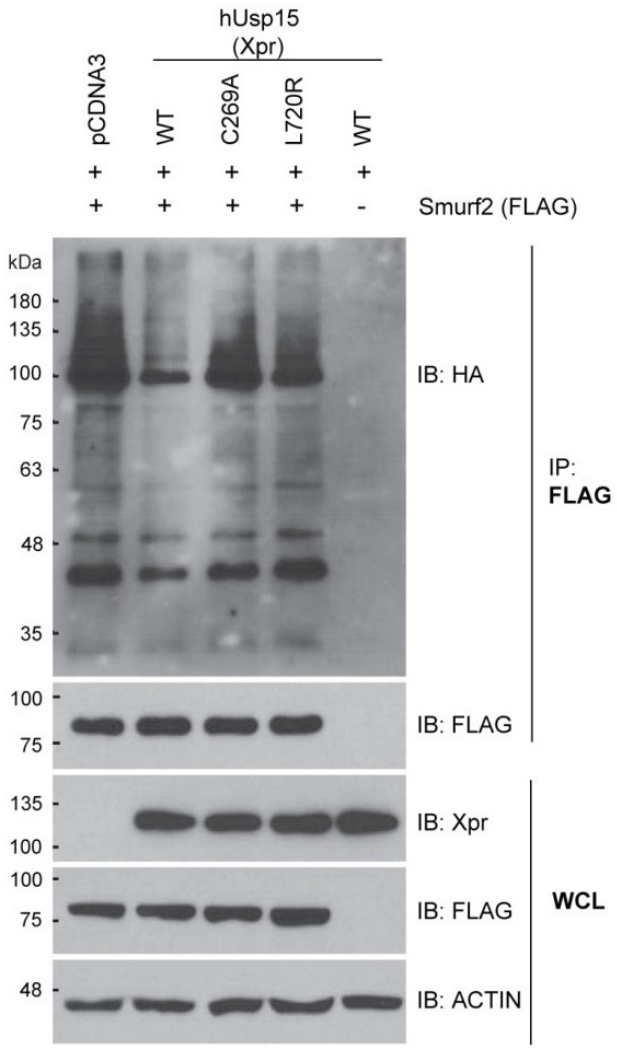

Figure 3-14 (Supplementary Figure). The L720R mutation affects the ability of USP15 to deubiquitinate SMURF2

HEK293T cells transiently expressing *Smurf2*-FLAG with or without *Usp15*-Xpress construct plus HA-tagged ubiquitin (Ub) were lysed 48h post-transfection, SMURF2 was immunoprecipitated using anti-FLAG antibody and immunoblotting analysis was performed as indicated. Construct expression in whole cell lysates (WCL) was confirmed by western blot.

3.6 Acknowledgements

This work was supported in part by research grants to P. Gros, and S. Vidal from the Canadian Institutes of Health Research [MOP119342; MOP133487], and from Amorchem [PT63088]. The authors are indebted to R. Van Bruggen, S. Gauthier, P. D'Arcy and G. Perreault for assistance in the ENU project, and to C. Meunier for technical assistance.

Chapter 4:

Susceptibility to lethal cerebral malaria is regulated by epistatic interaction between chromosome 4 (*Berr6*) and chromosome 1 (*Berr7*) loci in mice

Preface to Chapter 4

Since the publication of “Genes and Immunity (2013) 14, 249–257; doi:10.1038/gene.2013.16,”18 April 2013, we have corrected the nomenclature of the *Berr6* locus. The *Berr6* designation has been changed to *Berr8*. The authors apologize for any inconvenience caused.

4.1 Abstract

In humans, cerebral malaria (CM) is a rare but often lethal complication of infection with *Plasmodium* parasites, the occurrence of which is influenced by complex genetic factors of the host. We used a mouse model of experimental cerebral malaria (ECM) with *P. berghei* ANKA to study genetic factors regulating appearance of neurological symptoms and associated lethality. In a genome wide screen of ENU mutagenized mice derived from C57BL/6J (B6) and 129S1/SvImJ (129) mouse strains, we detected a strong interaction between the genetic backgrounds of these strains, which modulates ECM-resistance. We have mapped a major gene locus to central chromosome 4 (LOD 6.7; 79.6-97.3 Mb), that we designate *Berr6*. B6 alleles at *Berr6* are associated with resistance, and are inherited in a co-dominant fashion. In mice heterozygous for *Berr6* B6/129 alleles, resistance to ECM is strongly modulated by a second locus, *Berr7*, that maps to the proximal portion of chromosome 1 (LOD 4.03; 41.4 Mb). 129 alleles at *Berr7* are associated with ECM resistance in a dosage dependent fashion. Results are discussed in view of the possible role of this two-locus system in susceptibility to unrelated inflammatory conditions in mice and humans.

4.2 Introduction

Malaria is one of the clearest examples of an infectious pathogen exerting selective pressure on the genome of its host, with obvious signs of co-evolution [36,55]. For example, the widespread retention of heterozygosity for deleterious hemoglobinopathy-causing alleles brings about resistance to malaria in regions of endemic disease: These include sickle cell anemia [50,262], α- and β-thalassemia [50,263,264], ovalocytosis [46,265,266], and glucose-6-phosphate dehydrogenase deficiency [267,268]. Genetic variants in other host genes have been associated with presence, intensity and outcome of malaria, including cell-adhesion molecules [269,270], proteins involved in erythrocyte metabolism [51] as well as elements of the host immune response, including HLA [271] and TNF-α [272]. Several excellent reviews detail these host genetic factors [36,39,42]. Despite these clear examples, the genetic component influencing the human response to malarial parasites is complex, multigenic, and influenced by environmental factors including virulence determinants of the parasite [11,29,273].

Cerebral malaria (CM) is the most severe and lethal complication of *Plasmodium falciparum* infection in humans [274,275]. CM is most prevalent in immunologically naïve children and is characterized by high fever, progressing rapidly to severe cerebral symptoms including impaired consciousness, seizures, and coma [196,275], and ultimately leading to lethality in about 20% of all cases [18,55]. During CM, parasitized erythrocytes (pRBCs) become trapped within the brain microvasculature [11], thereby triggering a strong pro-inflammatory response [274,275] leading to activation of the vascular endothelium [196], and the recruitment of immune cells and activated platelets [68,276,277]. This host-directed immune response results in disruption of blood brain barrier integrity [29], suggesting that CM pathogenesis is at least partially caused by over-activation of the inflammatory response [18,55,196]. Although a genetic component to CM susceptibility has been established in humans, the identity of the genes involved have remained elusive. The discovery of genetic determinants that predispose or protect against CM may reveal valuable novel targets for intervention against this lethal disease.

Major gene effects modulating response to CM can be identified by genetic analysis in the mouse model of *Plasmodium berghei* ANKA (PbA) induced experimental cerebral malaria (ECM). Susceptible mice infected with PbA develop neurological symptoms of CM by days 5-8 post-infection, including ataxia, hind limb paralysis, coma and death by days 7-9 [67]. Histological features of ECM include sequestration of parasitized erythrocytes within brain microvasculature as well as infiltration of T cells, myeloid cells and activated platelets [276-278]. On the other hand, intrinsically resistant inbred mouse strains, or mutants bearing loss of function mutations in certain pro-inflammatory cytokines and pathways, survive the CM phase but subsequently succumb to hyperparasitemia and severe anemia within 3 weeks post infection [55]. Forward genetic analyses have been used to map several *Berr* loci (***Ber****ghei* ***r****esistance*) that regulate intrinsic differences in susceptibility to ECM amongst different inbred mouse strains. Studies in informative crosses derived from C57BL/6J (susceptible) and DBA/2J (resistant) identified an unnamed locus with linkage to two markers on central Chr. 18 (*D18Mit123*, *D18Mit202*) influencing survival time [87]. Dominantly inherited resistance with polygenetic control was observed in a cross between the susceptible C57BL/6J and resistant wild-derived WLA/Pas mice [89]. This inheritance was mapped to two loci that regulated penetrance of the WLA-associated resistance phenotype (prolonged survival time): *Berr1* on Chr. 1 (*D1Mit221*, near *Tgfb2)* and *Berr2* on Chr. 11 (*D11Mit338*) [89]. A third locus on distal Chr. 9 (*Berr3*; *D9Mit18*) also interacts with *Berr1* to control survival time in PbA-infected mice from the same C57BL/6J and WLA crosses [86], while a fourth locus on Chr. 4 (*Berr4*; *D4Mit27*) controls onset and intensity of blood stage parasitemia in mice surviving the cerebral phase of PbA infection [86]. Independently, Ohno and Nishimura mapped a locus (designated *Cmsc*) near the MHC on Chr. 17 that regulates differential susceptibility to ECM in mouse strains CBA (susceptible) and DBA/2 (resistant) [88]. Finally, *Berr5* was identified as a major locus regulating survival following PbA infection in crosses derived from parental C57BL/6J (susceptible) and BALB/c (resistant) mice. *Berr5* was found to co-localize with three other immune-related loci, *Trl-4* (resistance to tuberculosis), *Tsiq2* (T cell secretion of IL-4), and *Eae19* (experimental allergic encephalitis 19), and was found to contain within its boundary a strong positional candidate, the *Ifit1-3* gene cluster whose

expression is modulated in response to infection in a mouse strain-dependent fashion [90]. ECM pathogenesis is driven by acute neuroinflammation; mutations in pro-inflammatory cytokine genes, the transcription factors that regulate their expression, or elimination of cell populations secreting such cytokines, all result in significant protection against cerebral malaria [55].

In this study, we report the chromosomal mapping of a new two-locus system that shows epistatic interaction in controlling resistance to ECM in offspring from multiple crosses involving the C57BL/6J (B6) and 129S1/SvImJ (129) strain combination. The first locus, *Berr6*, maps to Chr. 4 and was discovered as a strong modulator of ECM-resistance in multiple independent pedigrees during a genome-wide N-ethyl-N-nitrosourea (ENU) mutagenesis screen. At this locus, B6 alleles are associated with ECM-resistance and inherited in a co-dominant fashion, while homozygosity for 129 alleles is strictly associated with ECM-susceptibility. A second locus, *Berr7,* maps to Chr. 1 and controls survival in mice heterozygous for B6/129 *Berr6* alleles, where inheritance of 129-derived *Berr7* alleles is associated with increased resistance.

4.3 Materials and Methods

Mice

Inbred C57BL/6J (B6), C57BL/10J (B10), and 129S1/SvImJ (129) mice were purchased from the Jackson laboratories (Bar Harbor, Maine, USA). Mice were bred and maintained under pathogen-free conditions in the animal facility of the Goodman Cancer Center, McGill University. Mice were handled according to the guidelines of the Canadian Council of Animal Care, and all experiments were performed in compliance with the ethics committee of McGill University.

ENU mutagenesis and breeding

N-ethyl-N-nitrosourea (ENU) mutagenesis and breeding of informative pedigrees were performed as we have previously described [157]. Twenty male B6 mice were given a total of 3 consecutive intraperitoneal injections of ENU chemical mutagen (90 mg/kg/week) at 8 weeks of age. Mutagenized mice (G0) were bred to wild type 129 females to establish heterozygous B6/129 G1 offspring. In some earlier studies, the G0 males were also bred to B10 females. G1 males were outcrossed a second time to 129 females to generate the G2 generation and then two G2 females per pedigree were backcrossed to the paternal G1 in order to produce G3 offspring. G3 mice were infected with *P. berghei* ANKA and phenotyped for resistance to ECM, using neurological symptoms and survival time as phenotypic markers of resistance to ECM. In parallel, pairs of G2 animals were intercrossed to produce F2S progeny, which were also phenotyped for resistance to ECM. For pedigree *Carmelo*, eleven G2 couples were randomly intercrossed to produce F2S mice. In either configuration, 25% of G3 and F2S animals are expected to inherit a portion of the mutations carried by the G1 male in a homozygous state. Appearance of ECM-resistant animals in individual pedigrees suggested the presence of a segregating protective mutation, which was validated by phenotyping additional animals from the same cross.

Parasites and Infections

Plasmodium berghei ANKA (PbA) parasites were originally obtained from MR4 and kindly provided by Dr. Mary M. Stevenson (McGill University, Montreal, Canada).

Parasites were maintained as frozen stocks at -80°C, and infectious stock was produced by up to three sequential weekly passages in B6 mice. Infected blood from passage mice was collected by cardiac puncture when parasitemia levels reached 4 to 8%. Parasitemia was determined by examination of thin blood smears fixed and stained by Diff-Quik reagents (Dade, Behring, Newark, DE, USA). Eight-week old experimental G3 or F2S mice were infected intravenously with $1x10^6$ parasitized red blood cells suspended in phosphate buffered saline (PBS). Mice were monitored up to 3 times daily. Susceptibility to cerebral malaria was diagnosed by appearance of clinical symptoms (paralysis, tremors, ataxia, seizures and coma) starting between days 5 and 8 post-infection [67]. Mice that did not exhibit clinical symptoms and survived beyond day 13 post-infection were considered ECM-resistant.

DNA preparation and Genetic analysis

Genomic DNA was prepared from mouse tails by standard proteinase K digestion and phenol-chloroform extraction. F2S mice (24 CM-resistant, 42 CM-susceptible) from the *Carmelo* pedigree were genotyped at The Center for Applied Genomics (The Hospital for Sick Children, Toronto, Canada) using a low-density Illumina mouse panel that contained 245 polymorphic markers informative for the B6/B10 vs. 129 strains. Linkage analysis was performed with the R/qtl software package using the binary model, where survival post day 13 (ECM resistance vs. susceptibility) was used as a phenotype to detect linkage. In the *Carmelo* pedigree, associations were considered significant for LOD scores above 3.91 (1000 permutations, α=0.05). In order to determine if other additive or interactive contributing loci were also present, we performed a two-dimensional scan while controlling for the genotype at the peak marker on Chr. 4. For finer mapping of the interval, additional primers were designed to amplify single nucleotide polymorphisms (SNPs) described in the Mouse Genome Informatics Database (www.informatics.jax.org). PCR-products were subjected to automated sequencing (McGill University and Genome Quebec Innovation Center; Montreal, Canada), and corresponding genotypes were used for linkage mapping and haplotype analysis.

4.4 Results

Resistance to P. berghei-*induced cerebral malaria in pedigree* Carmelo

We have implemented a genetic screen in ENU-mutagenized mice to identify genes, proteins and pathways whose inactivation protects mice against lethal experimental cerebral malaria (ECM) caused by infection with P. berghei ANKA (PbA) [157]. The breeding scheme to screen for recessive mutations (**Figure 4-1A**) involves crossing mutagenized C57BL/6J (G0) male to 129S1/SvlmJ (129) or C57BL/10J (B10) (data not shown) females. The G1 males are crossed to 129 and the ensuing G2s are then backcrossed to G1 males generating G3 progeny where several G0 mutations are fixed to homozygosity. In parallel, G1 males were occasionally crossed to 129 and the resulting G2 mice intercrossed to produce F2S. In our phenotyping protocol, infection with PbA (10^6 parasitized erythrocytes, i.v.) is lethal for inbred mouse strains such as B6, B10 and 129 by day 8 post-infection, and for the F1 and F2 animals derived from them. Therefore, appearance of PbA-resistant animals in successive F2S and G3 pedigrees derived from the same G1 male suggests transmission of a novel ECM-protective mutation. One such pedigree was issued from G1 male *Carmelo* (**Figure 4-1B**). This G1 male was initially flagged as transmitting resistance on the basis of having produced 3 ECM-resistant G3 mice out of 17 offspring (generated in a B6/B10 configuration; data not shown). In parallel, *Carmelo* G1 was also crossed to 129 females. Several F2S pedigrees issued from independent G2 *Carmelo* daughters featured resistant animals surviving >d13 post-infection, as opposed to B6 controls which all succumbed by day 7 (**Figure 4-1C**). These animals were detected in a proportion varying between 20 to 35% (**Figure 4-1C**). These results are consistent with the presence of a single ECM-protective mutation segregating in *Carmelo* pedigrees, which appears to be inherited in a recessive fashion.

*Localization of major locus (*Berr6*) on Chr. 4 regulating susceptibility to PbA-induced CM*

To determine complexity, pattern of inheritance and chromosomal location of the protective locus segregating in *Carmelo*, 24 ECM-resistant and 42 ECM-susceptible mice derived from a subset of *Carmelo*-derived F2S pedigrees showing segregation of

resistant animals were genotyped for 245 informative SNPs capable of distinguishing the B6-129 parental strains. Analysis of genotyping data by R/qtl indicated highly significant linkage on the distal portion of Chr. 4 (**Figure 4-2A**, **4-2B**), with a peak LOD score of 6.7 (95% Bayesian interval 58-114 Mb). The effect of genotype at the peak marker rs3708061 (Chr. 4, 79.6 Mb) on survival to PbA infection in *Carmelo*-derived F2S mice was examined (**Figure 4-2C**). Mice homozygous for the 129 allele (BB) were uniformly susceptible, 80% of mice homozygous for the B6 allele (AA) were resistant, while AB heterozygotes were present in both the susceptible and resistant groups (60:40 ratio). These results suggest that ECM-resistance in *Carmelo*-derived pedigrees is determined by a major locus on distal Chr. 4, with B6-associated resistance alleles being inherited in a co-dominant fashion.

Parallel linkage mapping, genotyping and exome sequencing in 27 additional phenodeviant pedigrees derived from independent G1 males unrelated to *Carmelo*, identified an enrichment for B6-derived haplotypes at Chr. 4 in ECM-resistant animals from 10 additional unrelated pedigrees, suggesting the possibility that a strain background effect may be influencing the phenotype, rather than multiple ENU-derived de novo mutations. Genotyping analysis for Chr. 4 markers rs27905346 (62 Mb), rs13468783 (63 Mb), rs27122718 (90 Mb), rs28156957 (93 Mb), rs27518264 (120 Mb), and rs3682864 (123 Mb) in 276 mice from all ten pedigrees clearly identified an enrichment for B6-derived haplotypes in resistant animals (50%; 56/111) compared to susceptible animals (12%; 19/165), while 129 haplotypes were almost entirely excluded from the CM-resistant group (5%; 5/111) compared to the susceptible group (35%; 58/165); Heterozygotes were almost evenly distributed in resistant (45%; 50/111) and susceptible animals (53%; 88/165) (**Figure 4-3A**). These differences are statistically significant (Fisher's Exact test, $p=4.6x10^{-16}$), confirming the effect of a Chr. 4 locus in multiple pedigrees derived from B6 and 129 crosses. A similar picture emerged from analyzing the effect of homozygosity and/or heterozygosity for B6 vs. 129-derived Chr. 4 haplotypes on survival fraction and survival time following PbA infection (**Figure 4-3B**). Using Pearson's chi-squared test, the genotype segregation patterns across Chr. 4 in each pedigree was shown to be within Hardy-Weinberg equilibrium ($\chi^2 = 1.0435$, $p=0.5934$). It is important to note that these numbers are approximate values, as some

of the genotypes were imputed, and recombinant haplotypes cannot be formally assigned to resistant or susceptible groups without knowledge of the precise position of the underlying gene.

The above-mentioned results suggest that a common Chr. 4 effect is contributing to the differential response to PbA infection in multiple phenodeviant pedigrees derived from different G1 progeny. We would like to give this locus the temporary designation of *Berr6*, for **Ber**ghei **r**esistance locus 6. Further genotyping of F2S mice derived from the *Carmelo* pedigree, and using additional Chr. 4 markers allowed us to narrow down the minimal physical interval for the *Berr6* genetic effect on ECM resistance (**Figure 4-4**). Haplotype mapping studies showed complete exclusion of homozygosity for 129 alleles in ECM-resistant F2S mice for the 79.6-97.3 Mb region (**Figure 4-4**). In addition, recombinant haplotypes detected in mice F2S-52.42R and F2S-55.29R from the resistant F2S cohort, further suggested a minimum physical interval of 18 Mb for *Berr6*, which is defined by markers rs3708061 (79.6 Mb) on the proximal side, and rs3705454 (97.3 Mb) on the distal side (**Figure 4-4**).

*Identification of a two-locus system on Chr. 4 (*Berr6*) and Chr. 1 (*Berr7*) that regulate susceptibility to PbA-induced CM*

The observation that *Carmelo* F2S mice heterozygous for *Berr6* alleles on Chr. 4 are found in both CM-resistant and CM-susceptible groups, suggests co-dominance or incomplete penetrance of B6 protective alleles at *Berr6* (**Figure 4-4**). A similar situation was detected when multiple independent pedigrees showing a Chr. 4 effect were pooled and analyzed (**Figure 4-3A**). Hence, we tested the possibility that additional genetic effects may further modulate penetrance and expressivity of the *Berr6* genetic effect. This was investigated by a two-dimensional genome scan, aimed to assess the genome-wide contribution of any additional loci on survival in the three allelic classes when controlled for *Berr6* (AA, BB, AB) as defined by the marker rs3708061 (79.6 Mb). This analysis revealed a single significant linkage peak on the proximal portion of Chr. 1 at 41.4 Mb (peak LOD 4.03; marker gnf01.037.906) (**Figure 4-5A**, **4-5B**). We would like to propose the temporary designation of *Berr7* for this locus. Combined haplotype analysis in *Carmelo* F2S demonstrated a strong genetic interaction between the Chr. 1

locus (*Berr7*) and the *Berr6* locus, and revealed an epistatic interaction regulating survival of PbA-infected mice (**Figure 4-5C**). In this system, homozygosity for 129 alleles (BB) at *Berr6* causes uniform susceptibility to CM, with no effect of Chr. 1 *Berr7* alleles, while homozygosity for B6 alleles at *Berr6* (AA) is associated with resistance. However, in *Berr6* AB heterozygotes, presence of 129 (B) alleles at *Berr7* increases resistance in a dosage-dependent fashion, with homozygosity for 129 alleles at *Berr7* (BB) linked to resistance and homozygosity for B6 alleles (AA) linked to susceptibility (Chi-square statistic; (AB) p=0.0253* and (BB) p=0.0006***). Although very few *Carmelo* mice were available for analysis, a similar trend for the effect of *Berr7* was also observed in mice homozygous for B6 alleles at *Berr6* (**Figure 4-5C**). The *Berr7* genetic effect detected in the *Carmelo* pedigree was validated in additional unrelated G3 pedigrees (n=10) that showed linkage of CM-resistance to Chr. 4 (**Figure 4-6**). In these mice, the *Berr7* effect was most noticeable in *Berr6* AB heterozygotes, where presence of one (AB) or two (BB) 129-derived *Berr7* alleles was associated with increased CM resistance compared to AA *Berr7* homozygotes (Chi-square statistic; (AB) p=0.0457*, and (BB) p=0.0249*) (**Figure 4-6**).

Therefore, our studies define an epistatic interaction between loci on Chr. 4 (*Berr6*) and Chr. 1 (*Berr7*) that regulates lethality associated with PbA-induced ECM. For the *Berr6* locus, B6 alleles are associated with resistance, while 129 alleles are associated with susceptibility. The parental effect is reversed for the *Berr7* locus, with B6 alleles being linked to susceptibility, while 129 alleles are linked to resistance.

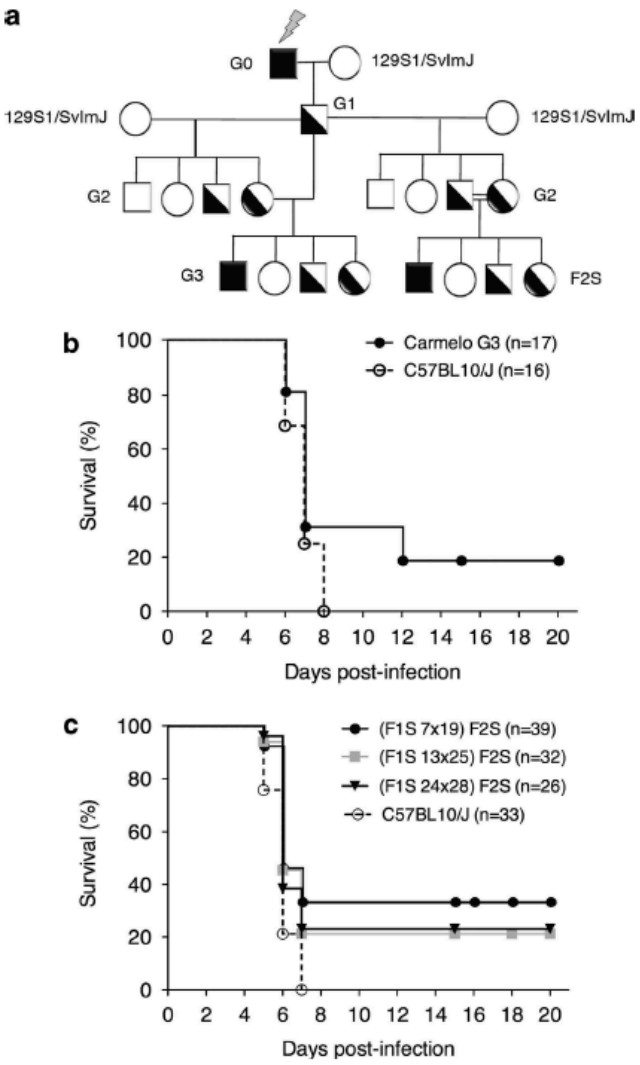

Figure 4-1. Segregation of resistance to *P. berghei* ANKA-induced cerebral malaria in the *Carmelo* pedigree

(A) Breeding scheme for the production and identification of ENU-induced recessive mutations protective against experimental cerebral malaria; See text of Materials and Methods for breeding scheme details. **(B)** The *Carmelo* G1 male (derived from mutagenized B6) was initially backcrossed to B10, to produce G3 animals that were assessed for response to *P. berghei* ANKA infection. **(C)** Subsequently, *Carmelo* was crossed to 129, and independent F2S intercrossed pedigrees were phenotyped. Mice were infected with *P. berghei* ANKA (10^6 *P. berghei* ANKA-parasitized red blood cells, i.v.) and the appearance of cerebral symptoms and accompanying morbidity was recorded for up to three weeks. Mice surviving past day 13 post infection were considered ECM-resistant, and no mice developed neurological symptoms after that point. Between 20-30% of G3 and F2S animals derived from *Carmelo* were found to be resistant to *P. berghei* ANKA-induced cerebral malaria.

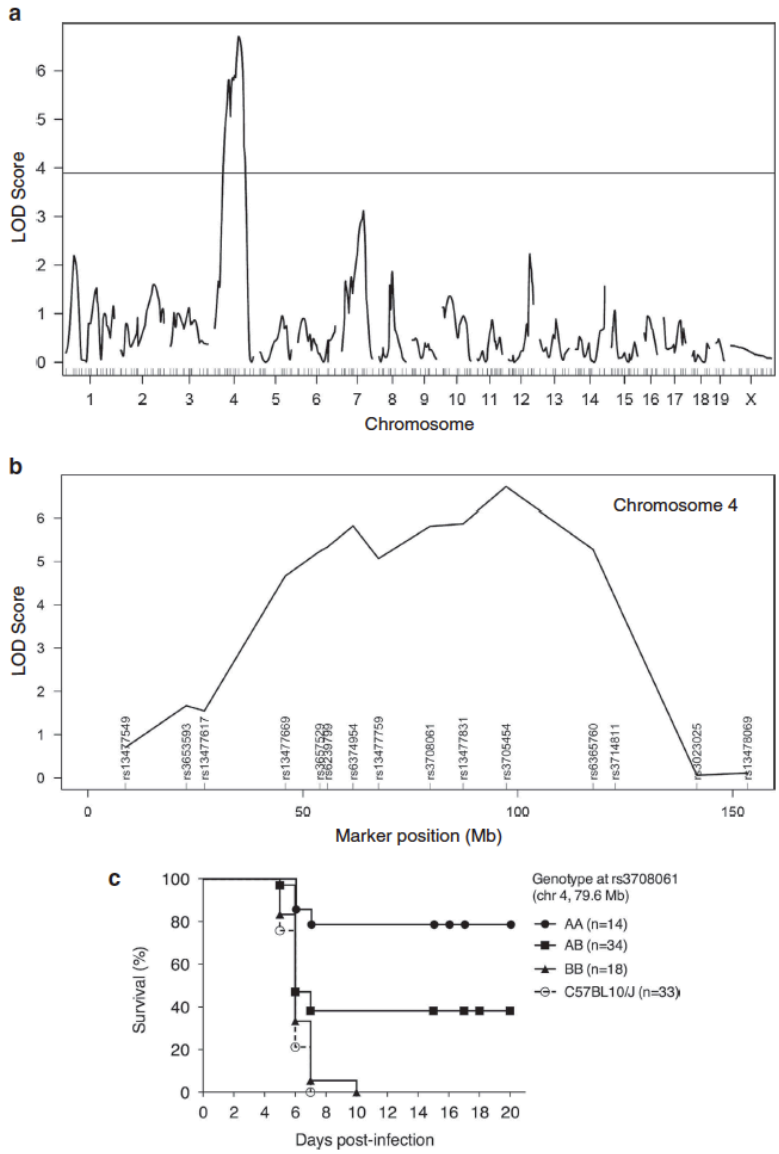

Figure 4-2. Resistance to *P. berghei* ANKA-induced cerebral malaria maps to central chromosome 4

(A) Genome-wide linkage analysis in a total of 24 resistant and 42 susceptible F2S mice derived from pedigree *Carmelo*. LOD score trace identifying significant linkage to Chr. 4 (LOD 6.7). **(B)** LOD score trace identifying linkage to central portion of Chr. 4 (95% Bayesian interval 58-114 Mb). **(C)** Effect of allele combination at rs3708061 (79.6 Mb) on survival of *Carmelo*-derived F2S mice following infection with *P. berghei* ANKA is shown. Mice were infected and monitored as described in the legend of Figure 1.

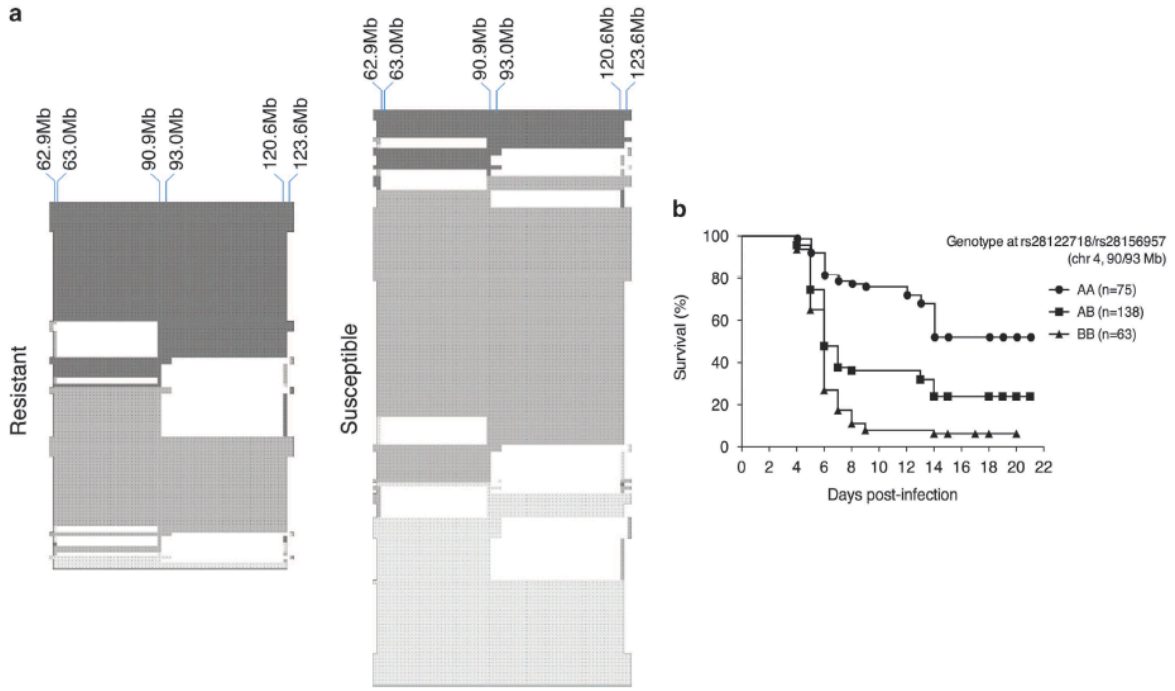

Figure 4-3. Validation of Chromosome 4 effect on resistance to experimental cerebral malaria

(**A**) A total of 276 animals from 10 independent B6 X 129 pedigrees segregating resistance to P. berghei-induced cerebral malaria were genotyped and showed evidence of linkage to Chr. 4 (Fisher's Exact test, 2x3 contingency table) as established by genotyping with Chr. 4 SNPs at positions: 62937051 bp (rs27905346), 63007346 bp (rs13468783), 90930807 bp (rs28122715), 93020907 bp (rs28156957), 120648008 bp (rs27518264), and 123623913 bp (rs3682864). Compiled haplotype map data across Chr. 4 for tag SNPs spanning the 62-123 Mb segment, with the color code, dark gray (B6 homozygote; A), light gray (129 homozygote; B), gray (B6/129 heterozygote; H). Haplotype analysis shows the Chr. 4 effect. Resistant animals (n=111): 50% B6 (56/111), 45% Het (50/111), 5% 129 (5/111) Susceptible animals (n=165): 12% B6 (19/165), 53% Het (88/165), 35% 129 (58/165). Differences between the two groups are statistically significant, Fisher's exact test, $p<0.0005$. (**B**) Effect of allelic combination at rs28122718 (90 Mb) and rs28156957 (93 Mb) on survival of 276 animals from 10 independent B6 X 129 pedigrees.

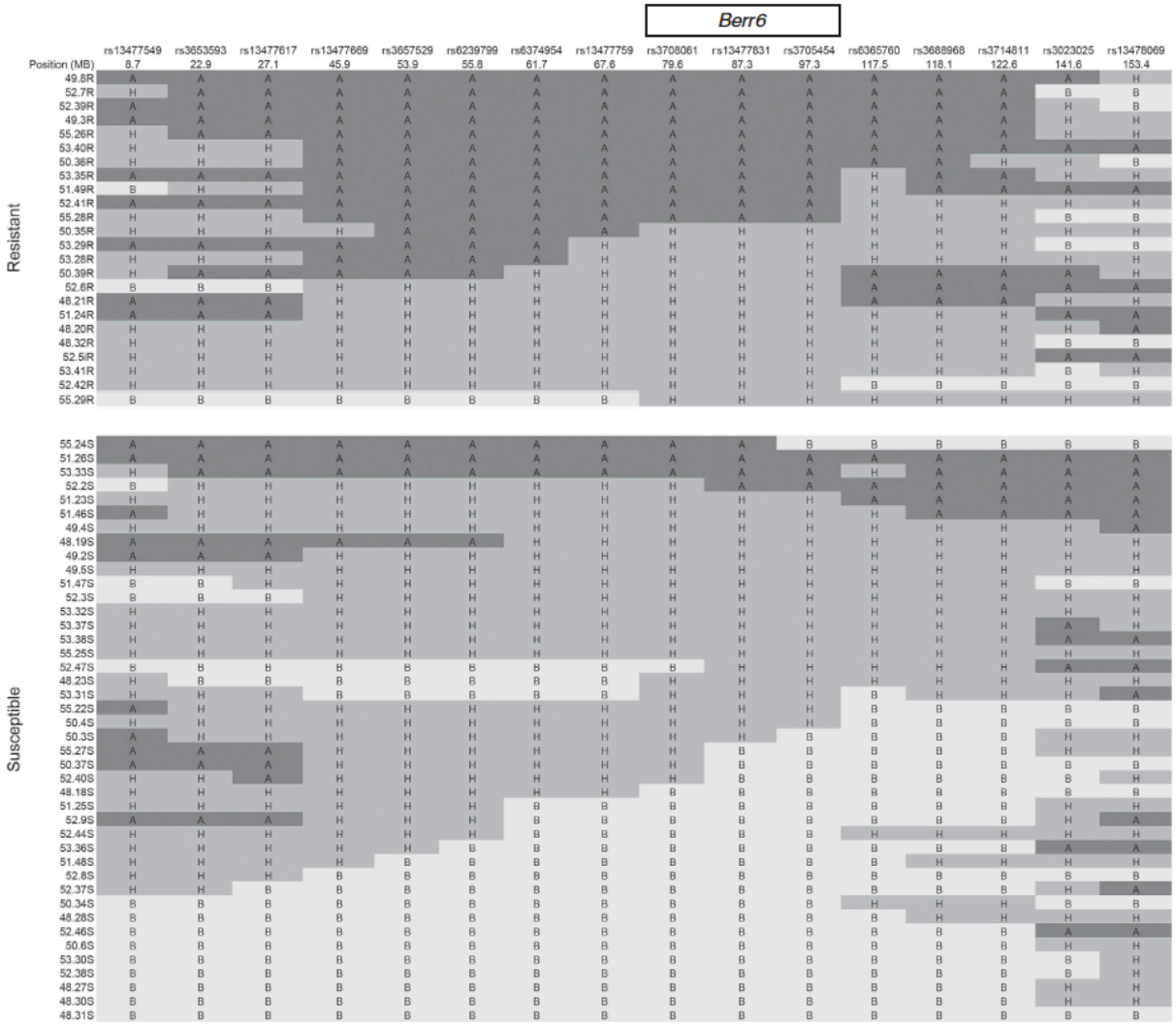

Figure 4-4. Haplotype map of *Carmelo* F2S mice delineates the *Berr6* locus

A total of 24 resistant and 42 susceptible F2S mice derived from pedigree *Carmelo* were genotyped with sixteen Chr. 4 SNPs, and the allelic combinations are shown as B6 homozygote (A, dark gray), 129 homozygote (B, light gray), and B6/129 heterozygotes (H, gray). The data show exclusion of 129 homozygosity for the central Chr. 4 region in ECM-resistant animals. In addition, recombinant haplotypes detected in two ECM-resistant mice (F2S-52.42R and F2S-55.29R), further suggest a minimum physical interval of 18 Mb for *Berr6* and defined by markers rs3708061 (79.6 Mb) on the proximal side, and rs3705454 (97.3 Mb) on the distal side.

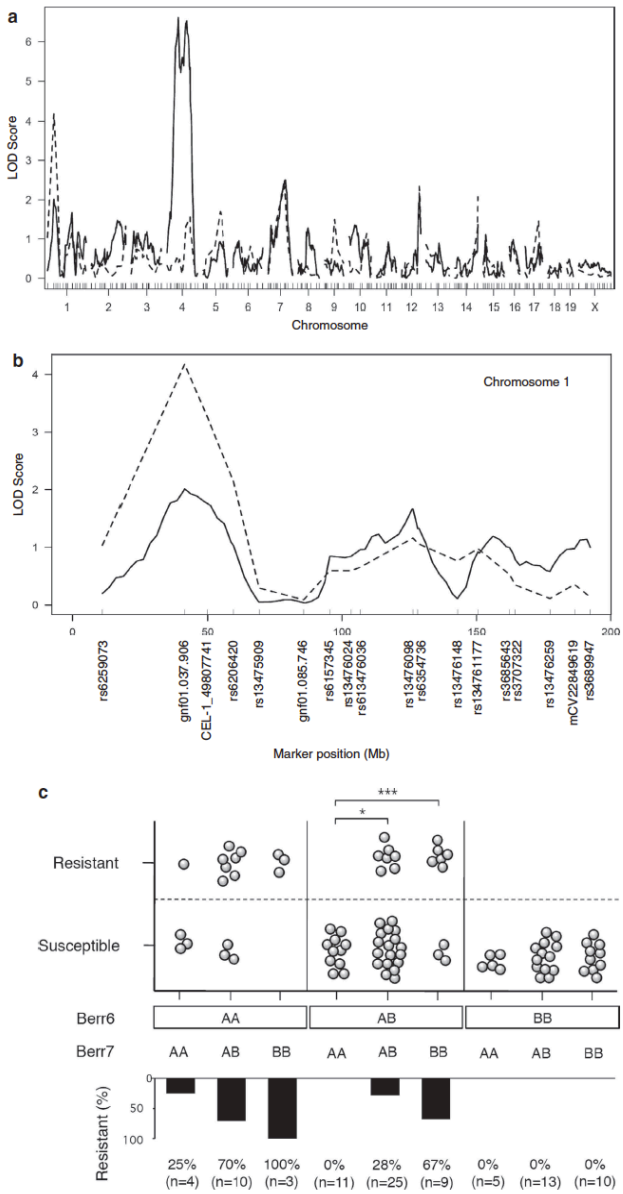

Figure 4-5. Genetic interaction between Chr 4 (*Berr6*) and Chr 1 (*Berr7*) in regulating resistance to *P. berghei* ANKA-induced CM in the *Carmelo* pedigree

(A) Two-dimensional genome scan to detect genome wide effects modulating survival of *Carmelo*-derived animals fixed for *Berr6* alleles (defined by marker rs3708061, 79.6 Mb). Genome-wide analysis identified a single significant hit on Chr. 1 (dash-line trace). The solid-line trace corresponds to the LOD score trace from the genome-wide single marker analysis. **(B)** Maximal linkage is at the proximal portion of Chr. 1 at 41.4 Mb (peak LOD 4.03; marker gnf01.037.906). **(C)** The effect of each allelic combination at the *Berr6* and the Chr. 1 locus (*Berr7*; gnf01.037.906) on resistance (survival) and susceptibility to *P. berghei* ANKA induced ECM in *Carmelo*-derived F2S mice is shown (A, B6-derived allele; B, 129-derived allele). Dots represent individual mice. The results show a strong protective effect of the 129 allele at the Chr. 1 locus (*Berr7*) on survival of mice heterozygous (AB) at *Berr6* (Chi square statistic; *Berr6*(AB)/*Berr7*(AA) vs *Berr6*(AB)/*Berr7*(AB) P=0.0253*, *Berr6*(AB)/*Berr7*(AA) vs *Berr6*(AB)/*Berr7*(BB) P=0.0006***).

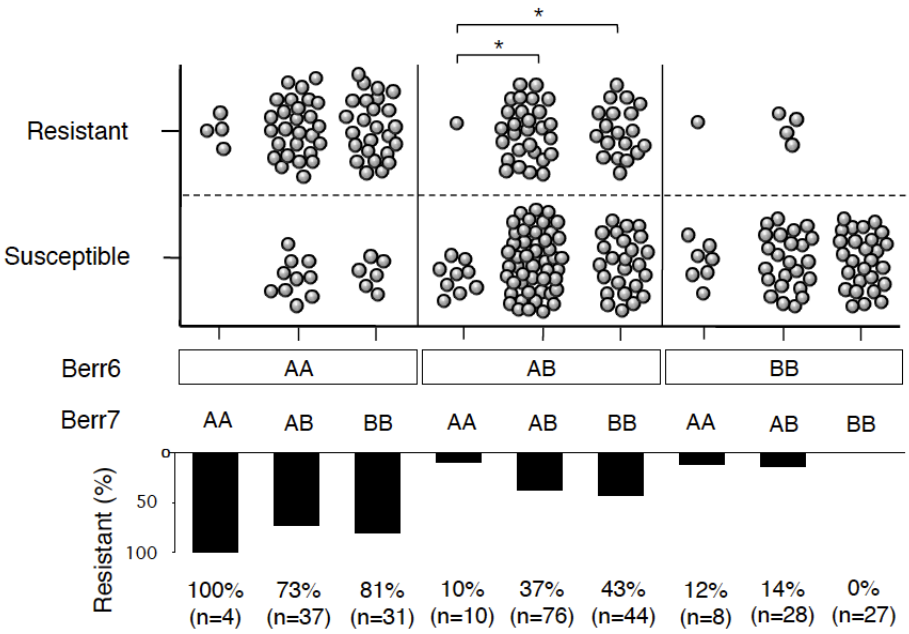

Figure 4-6 (Supplementary Figure). Genetic interaction between Chromosome 4 (*Berr6*) and Chromosome 1 (*Berr7*) alleles in regulating resistance to *P. berghei* ANKA-induced cerebral malaria in multiple unrelated B6 X 129 pedigrees

Showing the effect of all possible allelic combination at *Berr6* (Chr. 4) and *Berr7* (Chr. 1; gnf01.037.906) on resistance (survival) and susceptibility to *P. berghei* ANKA induced ECM in 10 G3 pedigrees demonstrating a *Berr6* effect (A, B6-derived allele; B, 129-derived allele). Dots represent individual mice. The results show a strong protective effect of the 129 allele at the Chr. 1 locus on survival of mice heterozygous (AB) at *Berr6* (Chi square statistic; *Berr6*(AB)/*Berr7*(AA) vs *Berr6*(AB)/*Berr7*(AB) P=0.0457*, *Berr6*(AB)/*Berr7*(AA) vs *Berr6*(AB)/*Berr7*(BB) P=0.0249*).

4.5 Discussion

During an ENU mutagenesis campaign aimed at identifying genetic mutations that protect mice against experimental cerebral malaria (ECM), we opted to cross ENU-mutagenized B6 mice (G0) to the 129 strain. The purpose of this was to increase litter size in ensuing crosses, and to introduce a distinct genetic background that would facilitate mapping of resistance associated ENU mutations in B6 X 129 backcross and intercrosses. Genetic linkage studies and exome sequencing revealed an effect of Chr. 4 alleles in an unexpected proportion of phenodeviant pedigrees, expressed as a strong enrichment for B6-derived alleles in ECM-resistant animals, concomitant with a complete exclusion of 129-derived homozygous alleles in ECM-resistant animals. The frequency of observed resistance was greater than expected for two ECM susceptible progenitor strains. Likewise, the rate of Chr. 4-linked pedigrees was much higher than expected, suggesting that this phenomenon was unrelated to the ENU mutagenesis process, but rather reflecting a unique re-assortment of genetic background effects within phenodeviant pedigrees, despite the fact that 129 and B6 parental strains are themselves susceptible to ECM. We have mapped a major Chr. 4 locus and have given it the provisional appellation, *Berr6*. In some of the Chr. 4 associated pedigrees (n=10), we also detected epistatic interaction with another locus located on Chr. 1, *Berr7*, which modulates ECM resistance and susceptibility in mice heterozygous for 129/B6 alleles at *Berr6.*

The chromosomal location of *Berr6* appears to overlap with that of *Berr4*, a locus previously described as contributing weakly (LOD 3.42) to host response during PbA infection [86]. The *Berr4* locus was detected along with *Berr1* and *Berr3*, in crosses derived from inbred C57BL/6J and wild-derived *Mus musculus* WLA mouse strains. However, several lines of evidence suggest that *Berr4* and the Chr. 4 locus (*Berr6*) detected herein are distinct. First, *Berr4* and *Berr6* affect different aspects of *P. berghei* infection. *Berr4* was detected in a group of [B6 X WLA]F2 mice who do not develop cerebral malaria, where it regulates the timing and intensity of late blood stage parasitemia (4-6 weeks post-infection). Meanwhile, *Berr6* regulates the immediate appearance of cerebral symptoms and associated lethality within 8-10 days post-

infection, a markedly different pathology. Secondly, B6 alleles at the *Berr4* locus are associated with susceptibility to PbA infection in [B6 X WLA]F2 mice (early onset of high blood parasitemia), whereas B6 alleles at *Berr6* are associated with resistance to cerebral disease. Thus, although formal demonstration that *Berr4* and *Berr6* are distinct awaits the identification of the genes and proteins involved, current results suggest that the underlying factors are likely to be different.

In the mouse model of cerebral malaria induced by PbA infection, acute and ultimately lethal pathological neuroinflammation is mediated in part by recruitment and production of pro-inflammatory cytokines by myeloid cells (e.g. IL12, IL17, Type I IFN) and T lymphocytes (IFNγ) [58,154,279]. A number of quantitative trait loci (QTLs) influencing the inflammatory response have been regionally assigned to the *Berr6* region (35-50 cM interval on central Chr. 4) in mouse crosses involving C57BL/6J [280-282]. Of note is the *Sle2* locus (*D4Mit9*, pst. 39.4 cM; LOD 6.7), one of several loci mapped in [NZB X B6] X NZB backcross mice as regulating appearance of severe glomerulonephritis in a spontaneous model of systemic lupus erythematosus (SLE) characteristic of the NZB 2410/Aeg strain [283]. In addition, Loh et al (2011) detected interaction between SLE susceptibility loci on Chr. 4 (32.2-150 Mb; possibly *Sle2*) and Chr. 1 (126.6-183.0 Mb) in B6 congenic mice [284]. Independently, it was shown that Irf2 deficiency (*Irf2*$^{-/-}$) causes a psoriasis-like skin disease in mice. A locus (*Psds1*) regulating expressivity of this trait was mapped in *Irf2*$^{-/-}$ mutant mice crossed to either BALB/c or B6 [285]. The *Psds1* locus (LOD 8.5) maps at position 42.5 cM on Chr. 4, and regulates presence and severity of skin lesions. It is tempting to speculate that the *Sle2*, *Psds1*, and *Berr6* may reflect the activity of the same gene in different models of pathological inflammation.

We note the co-localization of the *Berr7* locus with the *Psrs4* QTL (psoriasis susceptibility 4; pst. 23.7 cM), which regulates susceptibility to psoriasis in certain mouse strains. The strain PL/J carries a hypomorphic allele (*CD18*^{hypo}) at the common chain of β2 integrins (*Itgb2*), which causes a skin disease closely resembling human psoriasis [286]. Transferring the hypomorph CD18 allele onto a B6 background suppresses the inflammatory psoriasis phenotype [287]. Studies in [PL/J X B6] X PL/J

backcross mice indicate that modulation of the psoriasis trait is under polygenic control regulated, in part, by the *Psrs4* locus on Chr. 1 (*D1Mit236*; 25 cM/46 Mb; LOD 2.6), and the *Psrs6* locus that maps in the general vicinity of *Berr6* on the central part of Chr. 4 (*D4Mit170,* 66 cM). It is tempting to speculate that the epistatic system (*Berr6, Berr7*) regulating susceptibility to acute neuroinflammation in ECM mapped herein is related or identical to the two locus system (*Psrs4*, *Psrs6*) that impacts a chronic inflammatory condition, psoriasis.

The *Berr6* region (Chr. 4, 79.6-97.3 Mb interval) appears to be orthologous to human chromosome 1p31.3, while the peak marker position for the *Berr7* locus (gnf01.037.906; Chr. 1, 41.4 Mb) appears to correspond to human chromosome 6p12. A literature search for possible two-loci systems in humans involving 1p31 and 6p, and association with either autoimmune or inflammatory disorders revealed a possible association with autoimmune vitiligo. Linkage analysis in a large family with vitiligo and Hashimoto thyroiditis showed oligogenic control, including a major locus on 1p31.3-p32.2, which was designated *AIS1*, and an additional interacting locus on 6p [288]. The 1p31 linkage was validated by further studies of 70 families with generalized vitiligo [289].

Taken together, our results raise the possibility that the *Berr6/Berr7* epistatic system regulating inter-strain differences in susceptibility to acute neuroinflammation in the ECM model may be relevant to other chronic inflammation conditions in humans.

4.6 Acknowledgements

This work was supported by a Team Grant to PG and SV from the Canadian Institutes of Health Research (CIHR Team in ENU mutagenesis and infectious diseases). PG is supported by a James McGill Professorship award. SMV is supported by the Canada Chairs Research Program. RVB is supported by a Neuroinflammation CIHR Strategic Training Program. The authors are indebted to Patricia D'Arcy, Geneviève Perreault, Nadia Prud'homme, Adam Li, Jean-Daniel Castonguay, and Susan Gauthier for expert technical assistance.

Chapter 5:

Summary and General Discussions

5.1 Summary

Despite decades of research, malaria remains a global health problem. Cerebral malaria, the most lethal form of the disease, is driven in part by host inflammatory responses in the brain. Inflammation is a complex physiological host response critical for the elimination of invading pathogens and maintenance of tissue homeostasis, however, dysregulated or sustained inflammatory responses have severe pathological consequences [290]. A better understanding of the mechanisms of neuroinflammation at play during CM are critical to the development of novel therapeutic strategies to combat the disease. To do this, we set up an unbiased, genome-wide chemical mutagenesis screen in mice using the PbA experimental mouse model of CM as a phenotypic screen.

This thesis describes novel proteins and their associated pathways discovered by this approach and that are shown to be critical to the pathogenesis of ECM, namely THEMIS, and USP15. These findings have improved our understanding of immunity and susceptibility to *Plasmodium* infection, and have also proposed novel targets of pharmacological interest. Interestingly, these genes have also been detected as genetic risk factors for common human inflammatory diseases like multiple sclerosis (MS), systemic lupus erythematosus (SLE), and inflammatory bowel disease (IBD); therefore these proteins may represent valuable entry points to better understand inflammatory processes commonly engaged in these diseases.

In **Chapter 2**, we identified and characterized a disruptive ENU-induced mutation in THEMIS, a molecule involved in T cell development, which conferred resistance to ECM. *Themis*^{I23N} homozygous mice had a reduced number of circulating T cells, and thereby exhibited an impairment in T-cell mediated neuroinflammation. These results are consistent with the current understanding of the role of T cells in CM pathogenesis. While the lack of a pro-inflammatory Th1 response in *Themis*^{I23N} homozygous mutants is protective in the ECM model, we demonstrated its detrimental role to mice infected with *Mycobacterium tuberculosis* due to their inability to contain bacterial replication. Furthermore, we showed that mice deficient for LCK tyrosine kinase (*Lck*$^{-/-}$), a kinase downstream of the T cell receptor, were also highly resistant to ECM, and demonstrated

the functional coupling of both proteins during ECM pathogenesis through genetic complementation studies. Interestingly, *THEMIS* has been identified as a candidate gene for the chromosome 6 locus associated with susceptibility to celiac disease in humans, as well as a risk factor for multiple sclerosis. The findings in Chapter 2, along with the association of *THEMIS* to several proinflammatory disease in human association studies, places THEMIS as a core inflammatory gene that regulates common aspects of pathological inflammation in different inflammatory diseases.

In **Chapter 3**, we identified and characterized a disruptive ENU-induced mutation in USP15, a ubiquitously expressed deubiquitinase with multiple unrelated functions, which conferred protection to neuroinflammation in both ECM and EAE. Unlike findings in Chapter 2 (THEMIS) or other mutants found in screens from our lab (JAK3, CCDC88B and ZBTB7B), USP15 does not directly impact T-cell mediated immune responses, but rather, implicates the type-I IFN pathway in neuroinflammation. We established that *Usp15*^{L749R}-associated resistance to neuroinflammation was linked to dampened type I interferon responses in the brain (during PbA-infection) and in the spinal cord (after induction of EAE disease). The importance of the type-I IFN pathway in ECM pathogenesis was also demonstrated by observations of ECM-resistance in mice deficient for other type-I IFN pathway members, TRIM25 and IRF3. These findings are consistent with previously published type-I IFN pathway members, IRF7, IFNAR, TBK1, which also display resistance to ECM when deficient in mice. We demonstrated that during blood-stage PbA infection, USP15 functionally cooperates with the E3 ligase, TRIM25, to activate a type-I interferon response in the brain and promotes lethal neuroinflammation. Although the precise mechanistic role for the USP15-TRIM25 dyad in the type-I IFN pathway requires phenotyping of additional pathway members, we speculate that they function by way of an unidentified receptor, possibly signaling through STING to activate TBK1 and IRF3/IRF7. Furthermore, in large human genetic studies, genomic variants near the *USP15* locus have been associated with asthma. The findings in Chapter 3, as well as the potential association of USP15 to another inflammatory-driven disease in humans, suggests that USP15 may be a potential target for intervention not only for neuroinflammatory conditions, but also for other unrelated inflammatory-driven diseases.

While Chapters 2 and 3 described successful identification of ECM-protective mutations within single genes, **Chapter 4** instead describes the ECM-protective effect conferred by the gene-gene (i.e. epistatic) interaction between mixed host genetic backgrounds. We observed a considerably high percentage of resistance in offspring containing B6 and 129S1 mixed genetic backgrounds (overall CM-resistance of ~8% in the B6-129S1 screen vs. <5% in our initial B6-B10 screen [56]). The observation that resistance was associated with B6 alleles on same distal chromosome 4 locus in a third of phenodeviant pedigrees led us to hypothesize that ENU mutagenesis was not causing the resistance phenotype, but rather, caused by random segregation of B6 and 129S1 parental alleles in informative mouse crosses. We mapped a two-locus system regulating resistance to PbA-induced ECM involving mouse chromosome 4 (*Berr8*) and mouse chromosome 1 (*Berr7*) in G3 animals from independent pedigrees. Our study raises the possibility that this two-locus system may also be relevant to other unrelated inflammatory conditions in both mice and humans. A literature search for possible two-loci systems in humans involving human orthologous Chr 1p31 (mouse Chr 4 79-97 Mb) and Chr 6p12 (mouse Chr 1 41.6 Mb) revealed a possible association with inflammatory conditions like, autoimmune vitiligo and Hashimoto thyroiditis.

5.2 Lessons from a forward genetic screen in mice

In this thesis, I have described the first *Plasmodium berghei* ANKA infectious challenge screen of ENU-mutagenized mice and how it has offered an opportunity to study proteins and associated pathways involved in the host response to infection. Although our program has been largely successful for identifying phenodeviant pedigrees and their associated protective mutations, it is important to discuss limitations of the approaches that were used in our study.

5.2.1 Limitations of ENU mutagenesis

ENU mutagenesis in the mouse is a valuable tool (**Chapter 1.5**), but it also has drawbacks. Firstly, although ENU typically introduces mutations randomly within DNA of spermatogonial cells, there are preferential “hot spots” within the genome. ENU preferentially alters AT base pairs, therefore genes that are GC-rich would be mutated far less often than those of lower GC content [291]. Larger genes would also be targeted more often than smaller ones by virtue of their superior size [187]. Secondly, recovery of mutated host genes that result in embryonic lethality would not be possible. Lastly, Identification of X-linked mutations would not be possible in our screen because of the breeding strategy we used to generate mutants. We used G1 males to propagate our mutant lines, and they carry X chromosomes from their non-mutagenized mothers [187,292]. This constitutes a limitation because the X chromosome is known to carry many key immune-related genes, namely Toll-like receptor 7 (*Tlr7*), CD40 ligand (*Cd40l*) and forkhead box P3 (*Foxp3*) [293].

Due to the laborious, time-consuming nature of the screen, failure of mice to maintain strong reproductive capacity was also a challenge we faced. Several months were required to generate and phenotype multiple litters with many animals to ensure that we had enough statistical power for mutation identification and robust validation. Furthermore, the amount of time required to identify the causative mutation lead to difficulties in generating homozygous mutant mouse lines for subsequent applications, i.e. G1 males and G2 females had aged considerably and were less likely to reproduce. This was particularly true in situations where positional cloning was used to locate the

causal variant, prior to the availability of whole-exome sequencing (WES). A potential solution to this issue could involve the cryopreservation of sperm or ovaries such that interesting mouse pedigrees could be revisited at a later date.

5.2.2 Limitations of whole-exome sequencing

Recent advances and availability of next-generation sequencing technology have driven ENU mutation discovery from a time-consuming exercise (positional cloning) to a rapid form of mutation discovery [189]. Whole exome sequencing is a technology that involves sequencing every annotated protein-coding exon within the genome (about 1.5% of the genome), relying on resources such as the Consensus Coding Sequence (CCDS) database and the RefSeq database [189]. This implies that ENU-induced point mutations that occur within introns, unannotated genes or regulatory sequences (enhancers or promoters) would be undetected by the WES approach. Mutations within promoter or regulatory regions have been gaining importance in human disease, and thus the inability to identify such mutations constitutes a drawback to WES [189]. It is tempting to speculate that we have overlooked mutations induced within these regions in phenodeviant pedigrees where the causal mutations were not identified.

5.2.3 Confounding epistatic interactions

Inbred mouse strain choice is an important feature in the design of a phenotypic screen in ENU mutagenized mice like the one described in this thesis. The work in Chapter 4 highlights that while the presence of two genetic backgrounds in mouse crosses is valuable for linkage studies, it can also be confounding to the experimental goal of a phenotypic screen due to potential genetic background interactions. In fact, the influence of genetic background on mouse phenotypes has been recognized for years. There are many examples of the same mutation exhibiting different phenotypes on different mouse genetic backgrounds suggesting that genes, unrelated to the targeted one, can influence a phenotype [294]. One such example is the effect of the obese (ob) and diabetes (db) mutations (affecting the leptin and leptin-receptor genes, respectively) causing hyperglycemia and obesity on the B6 genetic background but causing overt diabetes when on the C57BLKS/J genetic background [295].

As mentioned previously, we chose to carry out mutagenesis on the well-characterized B6 inbred strain and propagate mutations by outcrossing to 129S1 females in one of our three ENU mutagenesis screen efforts. B6 and 129S1 strains were chosen on the basis that they were similar phenotypically (i.e. ECM-susceptible), while differing genetically enough to possess a significant amount of SNPs for chromosomal mapping. We observed a considerably high percentage of resistance in mice from the B6-129S1 mixed genetic background screen. We anticipated recovery of single point mutations caused by ENU mutagenesis in resistant pedigrees, but instead we unravelled an intricate gene-gene interaction formed by reassortment of B6 and 129S1 parental alleles in informative mouse F2 crosses. The detected epistatic interaction behaved phenotypically like a strong loss-of-function mutation in an immune gene, highlighting the complex genetic nature of CM.

Epistasis, or interaction between genes or loci, is a complex but important concept. It is generally defined as an interaction between genotypes at two or more loci to influence a trait [296]. Epistasis is thought to contribute greatly to the genetic architecture of human diseases [297,298], particularly contributing to the variable disease susceptibility observed amongst individuals despite carrying the same allele that determines a phenotype [299]. Not surprisingly, it is believed that epistasis can greatly impair genetic mapping studies of complex traits and diseases like malaria, possibly responsible for failure to identify and replicate significant individual genetic effects typically observed in human mapping studies [300]. Epistatic interactions are challenging to map in humans because of the large number of possible combinations of genetic factors to be evaluated (i.e phenotypic variation may be controlled by several genes or loci, each of which has a modest or weak effect), as well as their interactive effects with environmental factors [301,302]. It is also experimentally challenging to acquire human samples in large enough numbers to detect and map these interactions.

Powerful genetic tools are available for mouse studies which enable the mapping of such interactive loci [295]. These studies are facilitated in mice because of the availability of many inbred strains to generate desired experimental crosses within a short generation time, the availability of dense genetic maps, the ease of genetic

manipulation, and the strict maintenance of environmental factors [295]. Understanding the complex genetic architecture of disease in animal models will help us to identify candidate loci in humans which will ultimately help us to predict, prevent and treat complex human diseases [296,303].

To avoid uncovering potentially confounding epistatic interactions not foreseen in the design of a phenotypic screen, and that can phenotypically mimick the effect of a sought after strong single gene mutation, a single genetic background (mutagenized B6 crossed to B6) should be used in future ENU mutagenesis screens. A screen carried out on a pure genetic background will eliminate the potential for confounding epistatic interactions, and instead would lead to identification of *de novo* single base pair mutations underlying a phenodeviant trait induced by ENU. The advent of next generation sequencing technology, by-passing the need to genetically map the mutation, has made a screen on a uniform genetic background feasible.

5.3 USP15, an emerging therapeutic target for pathological inflammation

The overall goal of my thesis work was to identify novel host proteins and associated pathways that could serve as novel targets for drug discovery against inflammatory-driven diseases in the mouse model of CM. A host protein with great therapeutic potential identified in this thesis is USP15. The following section will discuss why the USP15 deubiquitinating enzyme is an attractive target for drug development.

5.3.1 Deubiquitinases are good therapeutic drug targets

Ubiquitin-specific proteases (USPs) comprise the largest family of deubiquitinating enzymes (DUBs) with over 55 members in humans [304]. They deconjugate ubiquitin from target proteins, which in turn is essential for regulating cell homeostasis, protein stability and a variety of signaling pathways [305].

Recently, USPs have drawn attention as potential targets for cancer therapy, as more than 30 USPs, including USP15, have been differentially expressed or activated in tumors or their microenvironments [304]. USPs have also been implicated in the control of immune pathways and their dysregulation is commonly observed in pathological inflammatory-driven diseases [306]. Given the apparent contribution of DUBs to a variety of human diseases, the search for small compounds to selectively block the function of these enzymes has become an active area of research for pharmaceutical companies [307]. Unfortunately, there are no DUB inhibitors currently approved for clinical use in either the cancer or inflammatory context [306].

The therapeutic potential of USP15 is highlighted not only by its involvement in several pathologies, but by its unique biochemical structure and enzymatic activity. In particular, the enzymatic activity of a deubiquitinase is what makes them very attractive targets for drug discovery [308]. However, development of a selective inhibitor targeted solely against USP15 is particularly challenging due to high structural conservation at the active site across USP family members [308]. In parallel, development of drugs targeted to a regulatory domain or protein-protein interaction domain unique to USP15 would be valuable, as it alleviates concerns about cross-reactivity at the active site [308].

In instances where a USP is not pharmacologically accessible (i.e. “druggable”), signal transduction pathway members may also serve as therapeutic targets. For example, inhibition of E3 ubiquitin ligase TRIM25, the binding partner or USP15 in type I IFN signaling, may also emerge as a valid therapeutic strategy. Other proposed strategies include blocking gene transcription of the deubiquitinase by targeting extracellular factors or nuclear factors that activate expression of these genes [305]. Additional targets of pharmacological interest include genes that are commonly regulated by both USP15 and TRIM25. By RNA sequencing, we identified a list of 22 genes commonly downregulated by aberrant USP15 and TRIM25 signaling during ECM in our mutant animals (e.g. *Maff*, *Socs3*, additional genes listed in **Figure 3-11h**), and they may serve as additional targets of pharmacological interest.

5.3.2 USP15 as a novel therapeutic target for cancer

As it relates to cancer, USP15 has been implicated in the aberrant activation or silencing of pathways like the transforming growth factor β (TGF-β) pathway, the NF-kB pathway [250] and the Wnt signaling pathway [309], to name a few. One clear example of this is the amplification of the *USP15* gene in human breast and ovarian tumors, and in glioblastoma, and its association with poor patient prognosis [304]. In these tumors, the amplification of *USP15* is detrimental because it leads to aberrant TGF-β signaling, a pathway that when overactivated promotes tumor growth [256,257]. Therefore, inhibiting or modulating the function of USP15 with a small molecule inhibitor, alone or in combination with other drugs, could provide an improved treatment for cancer patients.

5.3.3 USP15 as a novel therapeutic target for inflammatory pathologies

In the central nervous system, glial cells (microglia, astrocytes and oligodendocytes) not only serve supportive and nutritional roles in the brain, but they also become engaged in protective roles against tissue injury or invading pathogens [310]. These cells can become activated and contribute to ensuing inflammatory processes depending on the nature, intensity, and duration of the insult [310]. Sustained inflammatory responses in the brain have severe pathological consequences. To date,

neuroinflammation has been documented in individuals with CM, as well as patients suffering from MS, Parkinson's disease, and Alzheimer's disease, to name a few [311]. Since USPs play a role in the control of immune pathways, modulation of their activity by small molecule inhibitors may be beneficial in the treatment of neuroinflammatory-driven pathologies [306]. The work in this thesis highlights the value of targeting the USP15-TRIM25 dyad as a novel strategy to dampen neuroinflammation.

Furthermore, in human genetic studies, genomic variants near the *USP15* locus have been associated with asthma [261], suggesting that USP15 may be a potential target for intervention not only for neuroinflammatory conditions, but also for unrelated inflammatory-driven diseases.

5.4 Final conclusions

Cerebral malaria, a neurological encephalitis caused by *P. falciparum* infection, is the most lethal form of malaria. As demonstrated in this thesis, a forward genetic ENU mutagenesis screen in mice is an effective platform to identify genes, proteins and associated pathways that are involved in neuroinflammation during ECM. This work successfully identified and characterized host proteins, THEMIS and USP15, as critical mediators of ECM-pathogenesis. Mutations that affect the function of these proteins have proven to be protective against cerebral disease, and thus, suggest novel targets for drug discovery. This work also allowed us to successfully map a complex two locus-system (*Berr7* and *Berr8*) regulating susceptibility to ECM in animals of mixed genetic background. Altogether, the genetic alterations conferring the neuroinflammatory protective effect identified herein could be mimicked by pharmacological inhibition of the corresponding target to alleviate CM and possibly other human inflammatory conditions as well.

Original contributions to knowledge

1. Production of two ENU-induced mouse pedigrees segregating resistance to PbA-induced ECM; one pedigree carries a mutation within THEMIS (I23N), and the other within USP15 (L749R). These mouse mutant stocks can used to study a variety of other phenotypes and diseases, potentially contributing to important scientific discoveries in the future.

2. Established an important role for THEMIS in infectious disease and neuroinflammation. ECM-resistance and TB-susceptibility observed in *Themis*^{I23N} homozygous mutant mice are due to impaired T-cell mediated pro-inflammatory responses caused by reduced number of T cells. `Demonstrated that LCK tyrosine kinase, as well as the functional coupling of THEMIS and LCK, are necessary for ECM pathogenesis.

3. Described a novel role for the USP15 in the type-I interferon pathway; how it functionally cooperates with TRIM25 to drive neuroinflammation during ECM and EAE. Dampened type-I IFN gene signatures *in situ* cause ECM-resistance observed in *Usp15*^{L749R} homozygous mutant mice.

4. Identified of a novel two-locus system in mice that regulates lethality to ECM. We mapped a major gene locus to central Chr 4 (LOD 6.7, 79.6-97.3 Mb) designated *Berr8*, and a second gene locus to proximal Chr 1 (LOD 4.03, 41.4 Mb) designated *Berr7* that strongly modulates resistance to ECM in a dose dependent fashion.

References

1. Engwerda C, Belnoue E, Grüner AC, Rénia L. Experimental models of cerebral malaria. Curr Top Microbiol Immunol. 2005;297: 103–143.

2. Cox FE. History of the discovery of the malaria parasites and their vectors. Parasites Vectors. 2010;3: 5. doi:10.1186/1756-3305-3-5

3. Power HJ. History of Malaria. Chichester, UK: John Wiley & Sons, Ltd; 2001. doi:10.1038/npg.els.0003575

4. World Health Organization. World Malaria Report 2015. World Health Organization; p. 280.

5. White NJ, Pukrittayakamee S, Hien TT, Faiz MA, Mokuolu OA, Dondorp AM. Malaria. Lancet. 2013. doi:10.1016/S0140-6736(13)60024-0

6. Desai M, Kuile ter FO, Nosten F, McGready R, Asamoa K, Brabin B, et al. Epidemiology and burden of malaria in pregnancy. The Lancet Infectious Diseases. 2007;7: 93–104. doi:10.1016/S1473-3099(07)70021-X

7. Goldberg DE, Siliciano RF, Jacobs WR. Outwitting evolution: fighting drug-resistant TB, malaria, and HIV. Cell. 2012;148: 1271–1283. doi:10.1016/j.cell.2012.02.021

8. Hoffman SL, Vekemans J, Richie TL, Duffy PE. The march toward malaria vaccines. Vaccine. 2015;33 Suppl 4: D13–23. doi:10.1016/j.vaccine.2015.07.091

9. Trampuz A, Jereb M, Muzlovic I, Prabhu RM. Clinical review: Severe malaria. Crit Care. 2003;7: 315–323. doi:10.1186/cc2183

10. McQueen PG, McKenzie FE. Competition for red blood cells can enhance Plasmodium vivax parasitemia in mixed-species malaria infections. Am J Trop Med Hyg. The American journal of tropical medicine and …; 2006;75: 112–125.

11. Miller LH, Baruch DI, Marsh K, Doumbo OK. The pathogenic basis of malaria. Nature. 2002;415: 673–679. doi:10.1038/415673a

12. Hora R, Kapoor P, Thind KK, Mishra PC. Cerebral malaria--clinical manifestations and pathogenesis. Metab Brain Dis. 2016;31: 225–237. doi:10.1007/s11011-015-9787-5

13. Silvie O, Mota MM, Matuschewski K, Prudêncio M. Interactions of the malaria parasite and its mammalian host. Curr Opin Microbiol. 2008;11: 352–359. doi:10.1016/j.mib.2008.06.005

14. Cowman AF, Crabb BS. Invasion of red blood cells by malaria parasites. Cell. 2006;124: 755–766. doi:10.1016/j.cell.2006.02.006

15. Su X, Hayton K, Wellems TE. Genetic linkage and association analyses for trait mapping in Plasmodium falciparum. Nat Rev Genet. 2007;8: 497–506. doi:10.1038/nrg2126

16. Hulden L, Hulden L. Activation of the hypnozoite: a part of Plasmodium vivax life cycle and survival. Malar J. 2011;10: 90. doi:10.1186/1475-2875-10-90

17. Lindblade KA, Steinhardt L, Samuels A, Kachur SP, Slutsker L. The silent threat: asymptomatic parasitemia and malaria transmission. Expert Rev Anti Infect Ther. 2013;11: 623–639. doi:10.1586/eri.13.45

18. Mishra SK, Newton CRJC. Diagnosis and management of the neurological complications of falciparum malaria. Nat Rev Neurol. 2009;5: 189–198. doi:10.1038/nrneurol.2009.23

19. Miller LH, Ackerman HC, Su X-Z, Wellems TE. Malaria biology and disease pathogenesis: insights for new treatments. Nat Med. 2013;19: 156–167. doi:10.1038/nm.3073

20. Mackintosh CL, Beeson JG, Marsh K. Clinical features and pathogenesis of severe malaria. Trends in Parasitology. 2004;20: 597–603. doi:10.1016/j.pt.2004.09.006

21. Dondorp AM, Lee SJ, Faiz MA, Mishra S, Price R, Tjitra E, et al. The relationship between age and the manifestations of and mortality associated with severe malaria. Clin Infect Dis. 2008;47: 151–157. doi:10.1086/589287

22. Moradin N, Torre S, Gauthier S, Tam M, Hawari J, Vandercruyssen K, et al. Cysteamine broadly improves the anti-plasmodial activity of artemisinins against murine blood stage and cerebral malaria. Malar J. 2016;15: 260. doi:10.1186/s12936-016-1317-3

23. Price RN, Simpson JA, Nosten F, Luxemburger C, Hkirjaroen L, Kuile ter F, et al. Factors contributing to anemia after uncomplicated falciparum malaria. Am J Trop Med Hyg. 2001;65: 614–622.

24. Maitland K. Severe malaria: lessons learned from the management of critical illness in children. Trends in Parasitology. 2006;22: 457–462. doi:10.1016/j.pt.2006.07.006

25. Maitland K, Newton CRJC. Acidosis of severe falciparum malaria: heading for a shock? Trends in Parasitology. 2005;21: 11–16. doi:10.1016/j.pt.2004.10.010

26. Taylor TE, Borgstein A, Molyneux ME. Acid-base status in paediatric Plasmodium falciparum malaria. Q J Med. 1993;86: 99–109.

27. Gazzinelli RT, Kalantari P, Fitzgerald KA, Golenbock DT. Innate sensing of malaria parasites. Nat Rev Immunol. 2014;14: 744–757. doi:10.1038/nri3742

28. Moya-Alvarez V, Abellana R, Cot M. Pregnancy-associated malaria and malaria in infants: an old problem with present consequences. Malar J. 2014;13: 271. doi:10.1186/1475-2875-13-271

29. Hunt NH, Golenser J, Chan-Ling T, Parekh S, Rae C, Potter S, et al. Immunopathogenesis of cerebral malaria. International Journal for Parasitology. 2006;36: 569–582. doi:10.1016/j.ijpara.2006.02.016

30. Jamison DT. Disease and mortality in sub-Saharan Africa. 2006.

31. White NJ, Turner GDH, Day NPJ, Dondorp AM. Lethal malaria: Marchiafava and Bignami were right. J Infect Dis. 2013;208: 192–198. doi:10.1093/infdis/jit116

32. Marchiafava E, Mannaberg J, Thompson JH, Felkin RW. Two monographs on malaria and the parasites of malarial fevers. 1894.

33. van Bruggen R, Gualtieri C, Iliescu A, Louicharoen Cheepsunthorn C, Mungkalasut P, Trape J-F, et al. Modulation of Malaria Phenotypes by Pyruvate Kinase (PKLR) Variants in a Thai Population. PLoS ONE. 2015;10: e0144555. doi:10.1371/journal.pone.0144555

34. Driss A, Hibbert JM, Wilson NO, Iqbal SA, Adamkiewicz TV, Stiles JK. Genetic polymorphisms linked to susceptibility to malaria. Malar J. 2011;10: 271. doi:10.1186/1475-2875-10-271

35. Chapman SJ, Hill AVS. Human genetic susceptibility to infectious disease. Nat Rev Genet. 2012. doi:10.1038/nrg3114

36. Kwiatkowski DP. How malaria has affected the human genome and what human genetics can teach us about malaria. Am J Hum Genet. 2005;77: 171–192. doi:10.1086/432519

37. Lelliott PM, McMorran BJ, Foote SJ, Burgio G. The influence of host genetics on erythrocytes and malaria infection: is there therapeutic potential? Malar J. 2015;14: 289. doi:10.1186/s12936-015-0809-x

38. Clegg JB, Weatherall DJ. Thalassemia and Malaria: New Insights into an Old Problem. Proceedings of the Association of American Physicians. Blackwell Science Inc; 1999;111: 278–282. doi:10.1046/j.1525-1381.1999.99235.x

39. Verra F, Mangano VD, Modiano D. Genetics of susceptibility to Plasmodium falciparum: from classical malaria resistance genes towards genome-wide association studies. Parasite Immunology. 2009;31: 234–253. doi:10.1111/j.1365-3024.2009.01106.x

40. Ackerman H, Usen S, Jallow M, Sisay-Joof F, Pinder M, Kwiatkowski DP. A comparison of case-control and family-based association methods: the example of sickle-cell and malaria. Ann Hum Genet. 2005;69: 559–565. doi:10.1111/j.1529-8817.2005.00180.x

41. Allison AC. Genetic control of resistance to human malaria. Current Opinion in Immunology. 2009;21: 499–505. doi:10.1016/j.coi.2009.04.001

42. Bongfen SE, Laroque A, Berghout J, Gros P. Genetic and genomic analyses of host-pathogen interactions in malaria. Trends in Parasitology. 2009;25: 417–422. doi:10.1016/j.pt.2009.05.012

43. Modiano D, Luoni G, Sirima BS, Simporé J, Verra F, Konaté A, et al. Haemoglobin C protects against clinical Plasmodium falciparum malaria. Nature. 2001;414: 305–308. doi:10.1038/35104556

44. Min-Oo G, Gros P. Erythrocyte variants and the nature of their malaria protective effect. Cell Microbiol. 2005;7: 753–763. doi:10.1111/j.1462-5822.2005.00524.x

45. Miller LH, Mason SJ, Clyde DF, McGinniss MH. The resistance factor to Plasmodium vivax in blacks. The Duffy-blood-group genotype, FyFy. N Engl J Med. 1976;295: 302–304. doi:10.1056/NEJM197608052950602

46. Genton B, Al-Yaman F, Mgone CS, Alexander N, Paniu MM, Alpers MP, et al. Ovalocytosis and cerebral malaria. Nature. 1995;378: 564–565. doi:10.1038/378564a0

47. Malaria Genomic Epidemiology Network, Malaria Genomic Epidemiology Network. Reappraisal of known malaria resistance loci in a large multicenter study. Nat Genet. 2014;46: 1197–1204. doi:10.1038/ng.3107

48. Weatherall DJ. Genetic variation and susceptibility to infection: the red cell and malaria. British Journal of Haematology. Blackwell Publishing Ltd; 2008;141: 276–286. doi:10.1111/j.1365-2141.2008.07085.x

49. McMullin MF. The molecular basis of disorders of red cell enzymes. J Clin Pathol. 1999;52: 241–244.

50. Ayi K, Turrini F, Piga A, Arese P. Enhanced phagocytosis of ring-parasitized mutant erythrocytes: a common mechanism that may explain protection against falciparum malaria in sickle trait and beta-thalassemia trait. Blood. 2004;104: 3364–3371. doi:10.1182/blood-2003-11-3820

51. Ayi K, Min-Oo G, Serghides L, Crockett M, Kirby-Allen M, Quirt I, et al. Pyruvate kinase deficiency and malaria. N Engl J Med. 2008;358: 1805–1810. doi:10.1056/NEJMoa072464

52. Hernandez-Valladares M, Rihet P, Iraqi FA. Host susceptibility to malaria in human and mice: compatible approaches to identify potential resistant genes. Physiological Genomics. American Physiological Society; 2014;46: 1–16. doi:10.1152/physiolgenomics.00044.2013

53. Zuzarte-Luís V, Mota MM, Vigario AM. Malaria infections: what and how can mice teach us. J Immunol Methods. 2014;410: 113–122. doi:10.1016/j.jim.2014.05.001

54. Mestas J, Hughes CCW. Of Mice and Not Men: Differences between Mouse and Human Immunology. The Journal of Immunology. 2004;172: 2731–2738. doi:10.4049/jimmunol.172.5.2731

55. Longley R, Smith C, Fortin A, Berghout J, McMorran B, Burgio G, et al. Host resistance to malaria: using mouse models to explore the host response. Mamm Genome. 2011;22: 32–42. doi:10.1007/s00335-010-9302-6

56. Caignard G, Eva MM, van Bruggen R, Eveleigh R, Bourque G, Malo D, et al. Mouse ENU Mutagenesis to Understand Immunity to Infection: Methods, Selected Examples, and Perspectives. Genes (Basel). 2014;5: 887–925. doi:10.3390/genes5040887

57. Langhorne J, Buffet P, Galinski M, Good M, Harty J, Leroy D, et al. The relevance of

non-human primate and rodent malaria models for humans. Malar J. 2011;10: 23. doi:10.1186/1475-2875-10-23

58. Hunt NH, Grau GE. Cytokines: accelerators and brakes in the pathogenesis of cerebral malaria. Trends in Immunology. 2003;24: 491–499. doi:10.1016/S1471-4906(03)00229-1

59. de Souza JB, Hafalla JCR, Riley EM, Couper KN. Cerebral malaria: why experimental murine models are required to understand the pathogenesis of disease. Parasitology. 2010;137: 755–772. doi:10.1017/S0031182009991715

60. Howland SW, Claser C, Poh CM, Gun SY, Rénia L. Pathogenic CD8+ T cells in experimental cerebral malaria. Semin Immunopathol. 2015;37: 221–231. doi:10.1007/s00281-015-0476-6

61. El-Assaad F, Combes V, Grau GE. Experimental Models of Microvascular Immunopathology: The Example of Cerebral Malaria. J Neuroinfect Dis. 2014;5.

62. Stevenson MM, Gros P, Olivier M, Fortin A, Serghides L. Cerebral malaria: human versis mouse studies. Trends in Parasitology. Elsevier Ltd; 2010;: 1–2. doi:10.1016/j.pt.2010.03.008

63. Craig AG, Grau GE, Janse C, Kazura JW, Milner D, Barnwell JW, et al. The Role of Animal Models for Research on Severe Malaria. PLoS Pathog. Public Library of Science; 2012;8: e1002401. doi:10.1371/journal.ppat.1002401

64. Newbold C, Warn P, Black G, Berendt A, Craig A, Snow B, et al. Receptor-specific adhesion and clinical disease in Plasmodium falciparum. Am J Trop Med Hyg. 1997;57: 389–398.

65. White NJ, Turner GDH, Medana IM, Dondorp AM, Day NPJ. The murine cerebral malaria phenomenon. Trends in Parasitology. 2010;26: 11–15. doi:10.1016/j.pt.2009.10.007

66. Riley EM, Couper KN, Helmby H, Hafalla JCR, de Souza JB, Langhorne J, et al. Neuropathogenesis of human and murine malaria. Trends in Parasitology. 2010;26: 277–278. doi:10.1016/j.pt.2010.03.002

67. de Souza JB, Riley EM. Cerebral malaria: the contribution of studies in animal models to our understanding of immunopathogenesis. Microbes Infect. 2002;4: 291–300.

68. Lou J, Lucas R, Grau GE. Pathogenesis of cerebral malaria: recent experimental data and possible applications for humans. Clin Microbiol Rev. 2001;14: 810–20, table of contents. doi:10.1128/CMR.14.4.810-820.2001

69. Rest JR. Cerebral malaria in inbred mice. I. A new model and its pathology. Trans R Soc Trop Med Hyg. 1982.

70. Hearn J, Rayment N, Landon DN, Katz DR, de Souza JB. Immunopathology of cerebral malaria: morphological evidence of parasite sequestration in murine brain microvasculature. Infection and Immunity. 2000;68: 5364–5376.

71. Engwerda CR, Mynott TL, Sawhney S, de Souza JB, Bickle QD, Kaye PM. Locally up-regulated lymphotoxin alpha, not systemic tumor necrosis factor alpha, is the principle mediator of murine cerebral malaria. J Exp Med. 2002;195: 1371–1377.

72. Amante FH, Haque A, Stanley AC, Rivera F de L, Randall LM, Wilson YA, et al. Immune-mediated mechanisms of parasite tissue sequestration during experimental cerebral malaria. The Journal of Immunology. 2010;185: 3632–3642. doi:10.4049/jimmunol.1000944

73. El-Assaad F, Wheway J, Mitchell AJ, Lou J, Hunt NH, Combes V, et al. Cytoadherence of Plasmodium berghei-infected red blood cells to murine brain and lung microvascular endothelial cells in vitro. Infection and Immunity. 2013;81: 3984–3991. doi:10.1128/IAI.00428-13

74. Liehl P, Zuzarte-Luís V, Chan J, Zillinger T, Baptista F, Carapau D, et al. Host-cell sensors for Plasmodium activate innate immunity against liver-stage infection. Nat Med. 2014;20: 47–53. doi:10.1038/nm.3424

75. Miller JL, Sack BK, Baldwin M, Vaughan AM, Kappe SHI. Interferon-mediated innate immune responses against malaria parasite liver stages. Cell Rep. 2014;7: 436–447. doi:10.1016/j.celrep.2014.03.018

76. Leitner WW, Bergmann-Leitner ES, Angov E. Comparison of Plasmodium berghei challenge models for the evaluation of pre-erythrocytic malaria vaccines and their effect on perceived vaccine efficacy. Malar J. 2010;9: 145. doi:10.1186/1475-2875-9-145

77. Medana IM, Chaudhri G, Chan-Ling T, Hunt NH. Central nervous system in cerebral malaria: “Innocent bystander” or active participant in the induction of immunopathology? Immunol Cell Biol. 2001;79: 101–120. doi:10.1046/j.1440-1711.2001.00995.x

78. Taylor-Robinson AW. Validity of modelling cerebral malaria in mice: argument and counter argument. J Neuroparasitol. 2010.

79. Wah ST, Hananantachai H, Kerdpin U, Plabplueng C, Prachayasittikul V, Nuchnoi P. Molecular basis of human cerebral malaria development. Trop Med Health. 2016;44: 33. doi:10.1186/s41182-016-0033-6

80. Hansen DS. Inflammatory responses associated with the induction of cerebral malaria: lessons from experimental murine models. PLoS Pathog. 2012;8: e1003045. doi:10.1371/journal.ppat.1003045

81. Hiller NL. A Host-Targeting Signal in Virulence Proteins Reveals a Secretome in Malarial Infection. Science. American Association for the Advancement of Science; 2004;306: 1934–1937. doi:10.1126/science.1102737

82. Belnoue E, Kayibanda M, Vigario AM, Deschemin J-C, van Rooijen N, Viguier M, et al. On the pathogenic role of brain-sequestered alphabeta CD8+ T cells in experimental cerebral malaria. J Immunol. 2002;169: 6369–6375.

83. Haque A, Best SE, Unosson K, Amante FH, de Labastida F, Anstey NM, et al. Granzyme B expression by CD8+ T cells is required for the development of

experimental cerebral malaria. The Journal of Immunology. 2011;186: 6148–6156. doi:10.4049/jimmunol.1003955

84. van der Heyde HC, Nolan J, Combes V, Gramaglia I, Grau GE. A unified hypothesis for the genesis of cerebral malaria: sequestration, inflammation and hemostasis leading to microcirculatory dysfunction. Trends in Parasitology. 2006;22: 503–508. doi:10.1016/j.pt.2006.09.002

85. Dondorp AM, Kager PA, Vreeken J, White NJ. Abnormal blood flow and red blood cell deformability in severe malaria. Parasitol Today. 2000;16: 228–232.

86. Campino S, Bagot S, Bergman M-L, Almeida P, Sepúlveda N, Pied S, et al. Genetic control of parasite clearance leads to resistance to Plasmodium berghei ANKA infection and confers immunity. Genes and Immunity. 2005;6: 416–421. doi:10.1038/sj.gene.6364219

87. Nagayasu E, Nagakura K, Akaki M, Tamiya G, Makino S, Nakano Y, et al. Association of a determinant on mouse chromosome 18 with experimental severe Plasmodium berghei malaria. Infection and Immunity. 2002;70: 512–516.

88. Ohno T, Nishimura M. Detection of a new cerebral malaria susceptibility locus, using CBA mice. Immunogenetics. 2004;56: 675–678. doi:10.1007/s00251-004-0739-1

89. Bagot S, Campino S, Penha-Gonçalves C, Pied S, Cazenave P-A, Holmberg D. Identification of two cerebral malaria resistance loci using an inbred wild-derived mouse strain. Proc Natl Acad Sci USA. 2002;99: 9919–9923. doi:10.1073/pnas.152215199

90. Berghout J, Min-Oo G, Tam M, Gauthier S, Stevenson MM, Gros P. Identification of a novel cerebral malaria susceptibility locus (Berr5) on mouse chromosome 19. Genes and Immunity. Nature Publishing Group; 2009;: 1–9. doi:10.1038/gene.2009.79

91. Bopp SER, Ramachandran V, Henson K, Luzader A, Lindstrom M, Spooner M, et al. Genome wide analysis of inbred mouse lines identifies a locus containing Ppar-gamma as contributing to enhanced malaria survival. PLoS ONE. 2010;5: e10903. doi:10.1371/journal.pone.0010903

92. Torre S, van Bruggen R, Kennedy JM, Berghout J, Bongfen SE, Langat P, et al. Susceptibility to lethal cerebral malaria is regulated by epistatic interaction between chromosome 4 (Berr6) and chromosome 1 (Berr7) loci in mice. Genes and Immunity. 2013;14: 249–257.

93. Bopp SER, Rodrigo E, González-Páez GE, Frazer M, Barnes SW, Valim C, et al. Identification of the Plasmodium berghei resistance locus 9 linked to survival on chromosome 9. Malar J. 2013;12: 316. doi:10.1186/1475-2875-12-316

94. Combes V, Coltel N, Alibert M, van Eck M, Raymond C, Juhan-Vague I, et al. ABCA1 gene deletion protects against cerebral malaria: potential pathogenic role of microparticles in neuropathology. AJPA. 2005;166: 295–302. doi:10.1016/S0002-9440(10)62253-5

95. Shryock N, McBerry C, Salazar Gonzalez RM, Janes S, Costa FTM, Aliberti J. Lipoxin

A_4 and 15-epi-lipoxin A_4 protect against experimental cerebral malaria by inhibiting IL-12/IFN-γ in the brain. PLoS ONE. 2013;8: e61882. doi:10.1371/journal.pone.0061882

96. Kassa FA, Van Den Ham K, Rainone A, Fournier S, Boilard E, Olivier M. Absence of apolipoprotein E protects mice from cerebral malaria. Sci Rep. 2016;6: 33615. doi:10.1038/srep33615

97. Yañez DM, Manning DD, Cooley AJ, Weidanz WP, van der Heyde HC. Participation of lymphocyte subpopulations in the pathogenesis of experimental murine cerebral malaria. J Immunol. 1996;157: 1620–1624.

98. Ramos TN, Darley MM, Weckbach S, Stahel PF, Tomlinson S, Barnum SR. The C5 convertase is not required for activation of the terminal complement pathway in murine experimental cerebral malaria. Journal of Biological Chemistry. 2012;287: 24734–24738. doi:10.1074/jbc.C112.378364

99. Patel SN, Berghout J, Lovegrove FE, Ayi K, Conroy A, Serghides L, et al. C5 deficiency and C5a or C5aR blockade protects against cerebral malaria. Journal of Experimental Medicine. 2008;205: 1133–1143. doi:10.1084/jem.20072248

100. Kim H, Erdman LK, Lu Z, Serghides L, Zhong K, Dhabangi A, et al. Functional roles for C5a and C5aR but not C5L2 in the pathogenesis of human and experimental cerebral malaria. Infect Immun. 2014;82: 371–379. doi:10.1128/IAI.01246-13

101. Ramos TN, Darley MM, Hu X, Billker O, Rayner JC, Ahras M, et al. Cutting edge: the membrane attack complex of complement is required for the development of murine experimental cerebral malaria. The Journal of Immunology. 2011;186: 6657–6660. doi:10.4049/jimmunol.1100603

102. Reimer T, Shaw MH, Franchi L, Coban C, Ishii KJ, Akira S, et al. Experimental cerebral malaria progresses independently of the Nlrp3 inflammasome. Eur J Immunol. WILEY-VCH Verlag; 2010;40: 764–769. doi:10.1002/eji.200939996

103. Kordes M, Matuschewski K, Hafalla JCR. Caspase-1 activation of interleukin-1β (IL-1β) and IL-18 is dispensable for induction of experimental cerebral malaria. Infection and Immunity. 2011;79: 3633–3641. doi:10.1128/IAI.05459-11

104. Labbé K, Miu J, Yeretssian G, Serghides L, Tam M, Finney CA, et al. Caspase-12 dampens the immune response to malaria independently of the inflammasome by targeting NF-kappaB signaling. The Journal of Immunology. 2010;185: 5495–5502. doi:10.4049/jimmunol.1002517

105. Kennedy JM, Fodil N, Torre S, Bongfen SE, Olivier J-F, Leung V, et al. CCDC88B is a novel regulator of maturation and effector functions of T cells during pathological inflammation. J Exp Med. 2014;211: 2519–2535.

106. Belnoue E, Costa FTM, Vigario AM, Voza T, Gonnet F, Landau I, et al. Chemokine receptor CCR2 is not essential for the development of experimental cerebral malaria. Infection and Immunity. 2003;71: 3648–3651.

107. Belnoue E, Kayibanda M, Deschemin J-C, Viguier M, Mack M, Kuziel WA, et al. CCR5

deficiency decreases susceptibility to experimental cerebral malaria. Blood. 2003;101: 4253–4259. doi:10.1182/blood-2002-05-1493

108. Hansen DS, Siomos M-A, Buckingham L, Scalzo AA, Schofield L. Regulation of murine cerebral malaria pathogenesis by CD1d-restricted NKT cells and the natural killer complex. Immunity. 2003;18: 391–402.

109. Bagot S, Nogueira F, Collette A, do Rosario V, Lemonier F, Cazenave P-A, et al. Comparative study of brain CD8+ T cells induced by sporozoites and those induced by blood-stage Plasmodium berghei ANKA involved in the development of cerebral malaria. Infection and Immunity. 2004;72: 2817–2826.

110. Oakley MS, Majam V, Mahajan B, Gerald N, Anantharaman V, Ward JM, et al. Pathogenic roles of CD14, galectin-3, and OX40 during experimental cerebral malaria in mice. PLoS ONE. 2009;4: e6793. doi:10.1371/journal.pone.0006793

111. Lovegrove FE, Gharib SA, Peña-Castillo L, Patel SN, Ruzinski JT, Hughes TR, et al. Parasite burden and CD36-mediated sequestration are determinants of acute lung injury in an experimental malaria model. PLoS Pathog. 2008;4: e1000068. doi:10.1371/journal.ppat.1000068

112. Franke-Fayard B, Janse CJ, Cunha-Rodrigues M, Ramesar J, Büscher P, Que I, et al. Murine malaria parasite sequestration: CD36 is the major receptor, but cerebral pathology is unlinked to sequestration. Proc Natl Acad Sci USA. 2005;102: 11468–11473. doi:10.1073/pnas.0503386102

113. Boubou MI, Collette A, Voegtlé D, Mazier D, Cazenave P-A, Pied S. T cell response in malaria pathogenesis: selective increase in T cells carrying the TCR V 8 during experimental cerebral malaria. Int Immunol. 1999;11: 1553–1562. doi:10.1093/intimm/11.9.1553

114. Piguet PF, Kan CD, Vesin C, Rochat A, Donati Y, Barazzone C. Role of CD40-CVD40L in mouse severe malaria. The American Journal of Pathology. 2001;159: 733–742.

115. Oakley MS, McCutchan TF, Anantharaman V, Ward JM, Faucette L, Erexson C, et al. Host Biomarkers and Biological Pathways That Are Associated with the Expression of Experimental Cerebral Malaria in Mice. Infection and Immunity. 2008;76: 4518–4529. doi:10.1128/IAI.00525-08

116. Maglinao M, Klopfleisch R, Seeberger PH, Lepenies B. The C-type lectin receptor DCIR is crucial for the development of experimental cerebral malaria. The Journal of Immunology. 2013;191: 2551–2559. doi:10.4049/jimmunol.1203451

117. Alferink J, Specht S, Arends H, Schumak B, Schmidt K, Ruland C, et al. Cannabinoid Receptor 2 Modulates Susceptibility to Experimental Cerebral Malaria through a CCL17-dependent Mechanism. Journal of Biological Chemistry. 2016;291: 19517–19531. doi:10.1074/jbc.M116.746594

118. Darley MM, Ramos TN, Wetsel RA, Barnum SR. Deletion of carboxypeptidase N delays onset of experimental cerebral malaria. Parasite Immunology. 2012;34: 444–447. doi:10.1111/j.1365-3024.2012.01376.x

119. Ramos TN, Bullard DC, Barnum SR. Deletion of the complement phagocytic receptors CR3 and CR4 does not alter susceptibility to experimental cerebral malaria. Parasite Immunology. 2012;34: 547–550. doi:10.1111/pim.12002

120. Szalai AJ, Barnum SR, Ramos TN. Deletion of C-reactive protein ameliorates experimental cerebral malaria? Trans R Soc Trop Med Hyg. 2014;108: 591–593. doi:10.1093/trstmh/tru098

121. Campanella GSV, Tager AM, Khoury El JK, Thomas SY, Abrazinski TA, Manice LA, et al. Chemokine receptor CXCR3 and its ligands CXCL9 and CXCL10 are required for the development of murine cerebral malaria. Proc Natl Acad Sci USA. 2008;105: 4814–4819. doi:10.1073/pnas.0801544105

122. Nie CQ, Bernard NJ, Norman MU, Amante FH, Lundie RJ, Crabb BS, et al. IP-10-mediated T cell homing promotes cerebral inflammation over splenic immunity to malaria infection. PLoS Pathog. 2009;5: e1000369. doi:10.1371/journal.ppat.1000369

123. Miu J, Mitchell AJ, Müller M, Carter SL, Manders PM, McQuillan JA, et al. Chemokine gene expression during fatal murine cerebral malaria and protection due to CXCR3 deficiency. J Immunol. 2008;180: 1217–1230.

124. Potter SM, Mitchell AJ, Cowden WB, Sanni LA, Dinauer M, de Haan JB, et al. Phagocyte-derived reactive oxygen species do not influence the progression of murine blood-stage malaria infections. Infection and Immunity. 2005;73: 4941–4947. doi:10.1128/IAI.73.8.4941-4947.2005

125. Potter S, Chaudhri G, Hansen A, Hunt NH. Fas and perforin contribute to the pathogenesis of murine cerebral malaria. Redox Rep. 1999;4: 333–335. doi:10.1179/135100099101535070

126. Nitcheu J, Bonduelle O, Combadiere C, Tefit M, Seilhean D, Mazier D, et al. Perforin-dependent brain-infiltrating cytotoxic CD8+ T lymphocytes mediate experimental cerebral malaria pathogenesis. J Immunol. 2003;170: 2221–2228.

127. Potter SM, Chan-Ling T, Rosinova E, Ball HJ, Mitchell AJ, Hunt NH. A role for Fas-Fas ligand interactions during the late-stage neuropathological processes of experimental cerebral malaria. J Neuroimmunol. 2006;173: 96–107. doi:10.1016/j.jneuroim.2005.12.004

128. Ohno T, Kobayashi F, Nishimura M. Fas has a role in cerebral malaria, but not in proliferation or exclusion of the murine parasite in mice. Immunogenetics. 2005;57: 293–296. doi:10.1007/s00251-005-0791-5

129. Porcherie A, Mathieu C, Peronet R, Schneider E, Claver J, Commere P-H, et al. Critical role of the neutrophil-associated high-affinity receptor for IgE in the pathogenesis of experimental cerebral malaria. J Exp Med. 2011;208: 2225–2236. doi:10.1084/jem.20110845

130. Waisberg M, Tarasenko T, Vickers BK, Scott BL, Willcocks LC, Molina-Cruz A, et al. Genetic susceptibility to systemic lupus erythematosus protects against cerebral malaria in mice. Proc Natl Acad Sci USA. 2011;108: 1122–1127.

doi:10.1073/pnas.1017996108

131. Beghdadi W, Porcherie A, Schneider BS, Dubayle D, Peronet R, Huerre M, et al. Inhibition of histamine-mediated signaling confers significant protection against severe malaria in mouse models of disease. Journal of Experimental Medicine. 2008;205: 395–408. doi:10.1084/jem.20071548

132. Beghdadi W, Porcherie A, Schneider BS, Morisset S, Dubayle D, Peronet R, et al. Histamine H3 Receptor-Mediated Signaling Protects Mice from Cerebral Malaria. Rodrigues MM, editor. PLoS ONE. 2009;4: e6004. doi:10.1371/journal.pone.0006004.g009

133. Hunt NH, Driussi C, Sai-Kiang L. Haptoglobin and malaria. Redox Rep. 2001;6: 389–392. doi:10.1179/135100001101536508

134. Favre N, Da Laperousaz C, Ryffel B, Weiss NA, Imhof BA, Rudin W, et al. Role of ICAM-1 (CD54) in the development of murine cerebral malaria. Microbes Infect. 1999;1: 961–968.

135. Li J, Chang W-L, Sun G, Chen H-L, Specian RD, Berney SM, et al. Intercellular adhesion molecule 1 is important for the development of severe experimental malaria but is not required for leukocyte adhesion in the brain. J Investig Med. 2003;51: 128–140.

136. Sun G, Chang W-L, Li J, Berney SM, Kimpel D, van der Heyde HC. Inhibition of platelet adherence to brain microvasculature protects against severe Plasmodium berghei malaria. Infection and Immunity. 2003;71: 6553–6561.

137. Ramos TN, Bullard DC, Darley MM, McDonald K, Crawford DF, Barnum SR. Experimental cerebral malaria develops independently of endothelial expression of intercellular adhesion molecule-1 (icam-1). Journal of Biological Chemistry. 2013;288: 10962–10966. doi:10.1074/jbc.C113.457028

138. Miu J, Ball HJ, Mellor AL, Hunt NH. Effect of indoleamine dioxygenase-1 deficiency and kynurenine pathway inhibition on murine cerebral malaria. International Journal for Parasitology. 2009;39: 363–370. doi:10.1016/j.ijpara.2008.10.005

139. Berghout J, Langlais D, Radovanovic I, Tam M, MacMicking JD, Stevenson MM, et al. Irf8-regulated genomic responses drive pathological inflammation during cerebral malaria. PLoS Pathog. 2013;9: e1003491. doi:10.1371/journal.ppat.1003491

140. Everitt AR, Clare S, McDonald JU, Kane L, Harcourt K, Ahras M, et al. Defining the range of pathogens susceptible to Ifitm3 restriction using a knockout mouse model. PLoS ONE. 2013;8: e80723. doi:10.1371/journal.pone.0080723

141. Ball EA, Sambo MR, Martins M, Trovoada MJ, Benchimol C, Costa J, et al. IFNAR1 controls progression to cerebral malaria in children and CD8+ T cell brain pathology in Plasmodium berghei-infected mice. J Immunol. 2013;190: 5118–5127. doi:10.4049/jimmunol.1300114

142. Palomo J, Fauconnier M, Coquard L, Gilles M, Meme S, Szeremeta F, et al. Type I

interferons contribute to experimental cerebral malaria development in response to sporozoite or blood-stage Plasmodium berghei ANKA. Eur J Immunol. 2013;43: 2683–2695. doi:10.1002/eji.201343327

143. Rudin W, Favre N, Bordmann G, Ryffel B. Interferon-gamma is essential for the development of cerebral malaria. Eur J Immunol. 1997;27: 810–815. doi:10.1002/eji.1830270403

144. Amani V, Vigário AM, Belnoue E, Marussig M, Fonseca L, Mazier D, et al. Involvement of IFN-gamma receptor-medicated signaling in pathology and anti-malarial immunity induced by Plasmodium berghei infection. Eur J Immunol. 2000;30: 1646–1655.

145. Belnoue E, Potter SM, Rosa DS, MAUDUIT M, Grüner AC, KAYIBANDA M, et al. Control of pathogenic CD8+ T cell migration to the brain by IFN-gamma during experimental cerebral malaria. Parasite Immunology. 2008;30: 544–553. doi:10.1111/j.1365-3024.2008.01053.x

146. Guo J, McQuillan JA, Yau B, Tullo GS, Long CA, Bertolino P, et al. IRGM3 contributes to immunopathology and is required for differentiation of antigen-specific effector CD8+ T cells in experimental cerebral malaria. Infection and Immunity. 2015;83: 1406–1417. doi:10.1128/IAI.02701-14

147. van der Heyde HC, Bauer P, Sun G, Chang WL, Yin L, Fuseler J, et al. Assessing vascular permeability during experimental cerebral malaria by a radiolabeled monoclonal antibody technique. Infection and Immunity. 2001;69: 3460–3465. doi:10.1128/IAI.69.5.3460-3465.2001

148. Fauconnier M, Palomo J, Bourigault M-L, Meme S, Szeremeta F, Beloeil J-C, et al. IL-12Rβ2 is essential for the development of experimental cerebral malaria. The Journal of Immunology. 2012;188: 1905–1914. doi:10.4049/jimmunol.1101978

149. Ishida H, Matsuzaki-Moriya C, Imai T, Yanagisawa K, Nojima Y, Suzue K, et al. Development of experimental cerebral malaria is independent of IL-23 and IL-17. Biochemical and Biophysical Research Communications. Elsevier Inc; 2010;: 1–6. doi:10.1016/j.bbrc.2010.10.114

150. Villegas-Mendez A, Greig R, Shaw TN, de Souza JB, Gwyer Findlay E, Stumhofer JS, et al. IFN-γ-producing CD4+ T cells promote experimental cerebral malaria by modulating CD8+ T cell accumulation within the brain. The Journal of Immunology. 2012;189: 968–979. doi:10.4049/jimmunol.1200688

151. Palomo J, Reverchon F, Piotet J, Besnard A-G, Couturier-Maillard A, Maillet I, et al. Critical role of IL-33 receptor ST2 in experimental cerebral malaria development. Eur J Immunol. 2015;45: 1354–1365. doi:10.1002/eji.201445206

152. Sellau J, Alvarado CF, Hoenow S, Mackroth MS, Kleinschmidt D, Huber S, et al. IL-22 dampens the T cell response in experimental malaria. Sci Rep. Nature Publishing Group; 2016;6: 28058. doi:10.1038/srep28058

153. Finney CAM, Lu Z, Hawkes M, Yeh WC, Liles WC, Kain KC. Divergent Roles of IRAK4-Mediated Innate Immune Responses in Two Experimental Models of Severe Malaria.

Am J Trop Med Hyg. 2010;83: 69–74. doi:10.4269/ajtmh.2010.09-0753

154. Senaldi G, Shaklee CL, Guo J, Martin L, Boone T, Mak TW, et al. Protection against the mortality associated with disease models mediated by TNF and IFN-gamma in mice lacking IFN regulatory factor-1. J Immunol. 1999;163: 6820–6826.

155. Torre S, Polyak MJ, Langlais D, Fodil N, Kennedy JM, Radovanovic I, et al. USP15 regulates type I interferon response and is required for pathogenesis of neuroinflammation. Nature Publishing Group. Nature Publishing Group, a division of Macmillan Publishers Limited. All Rights Reserved; advance online publication SP - EP . doi:10.1038/ni.3581

156. Edwards CL, Best SE, Gun SY, Claser C, James KR, de Oca MM, et al. Spatiotemporal requirements for IRF7 in mediating type I IFN-dependent susceptibility to blood-stage Plasmodium infection. Eur J Immunol. 2015;45: 130–141. doi:10.1002/eji.201444824

157. Bongfen SE, Rodrigue-Gervais I-G, Berghout J, Torre S, Cingolani P, Wiltshire SA, et al. An N-Ethyl-N-Nitrosourea (ENU)-Induced Dominant Negative Mutation in the JAK3 Kinase Protects against Cerebral Malaria. PLoS ONE. 2012;7: e31012. doi:10.1371/journal.pone.0031012

158. Torre S, Faucher SP, Fodil-Cornu N, Bongfen SE, Berghout J, Schwartzentruber JA, et al. THEMIS is Required for Pathogenesis of Cerebral Malaria and for Protection Against Pulmonary Tuberculosis. Infection and Immunity. 2014;83: 759–768.

159. Togbe D, Schofield L, Grau GE, Schnyder B, Boissay V, Charron S, et al. Murine cerebral malaria development is independent of toll-like receptor signaling. AJPA. 2007;170: 1640–1648. doi:10.2353/ajpath.2007.060889

160. Togbe D, de Sousa PL, Fauconnier M, Boissay V, Fick L, Scheu S, et al. Both functional LTbeta receptor and TNF receptor 2 are required for the development of experimental cerebral malaria. PLoS ONE. 2008;3: e2608. doi:10.1371/journal.pone.0002608

161. Lu Z, Serghides L, Patel SN, Degousee N, Rubin BB, Krishnegowda G, et al. Disruption of JNK2 decreases the cytokine response to Plasmodium falciparum glycosylphosphatidylinositol in vitro and confers protection in a cerebral malaria model. J Immunol. 2006;177: 6344–6352.

162. Van den Steen PE, Van Aelst I, Starckx S, Maskos K, Opdenakker G, Pagenstecher A. Matrix metalloproteinases, tissue inhibitors of MMPs and TACE in experimental cerebral malaria. Lab Invest. 2006;86: 873–888. doi:10.1038/labinvest.3700454

163. Cunha-Rodrigues M, Portugal S, Febbraio M, Mota MM. Infection by and protective immune responses against Plasmodium berghei ANKA are not affected in macrophage scavenger receptors A deficient mice. BMC Microbiol. 2006;6: 73. doi:10.1186/1471-2180-6-73

164. Griffith JW, O'Connor C, Bernard K, Town T, Goldstein DR, Bucala R. Toll-like receptor modulation of murine cerebral malaria is dependent on the genetic background of the host. J Infect Dis. 2007;196: 1553–1564. doi:10.1086/522865

165. Baccarella A, Huang BW, Fontana MF, Kim CC. Loss of Toll-like receptor 7 alters cytokine production and protects against experimental cerebral malaria. Malar J. 2014;13: 354. doi:10.1186/1475-2875-13-354

166. Dostert C, Guarda G, Romero JF, Menu P, Gross O, Tardivel A, et al. Malarial hemozoin is a Nalp3 inflammasome activating danger signal. Dostert C, Guarda G, Romero JF, Menu P, Gross O, Tardivel A, et al., editors. PLoS ONE. 2009;4: e6510. doi:10.1371/journal.pone.0006510.g007

167. Gramaglia I, Sobolewski P, Meays D, Contreras R. Low nitric oxide bioavailability contributes to the genesis of experimental cerebral malaria. Nat Med. 2006.

168. Srivastava K, Cockburn IA, Swaim A, Thompson LE, Tripathi A, Fletcher CA, et al. Platelet factor 4 mediates inflammation in experimental cerebral malaria. Cell Host Microbe. 2008;4: 179–187. doi:10.1016/j.chom.2008.07.003

169. Lacerda-Queiroz N, Brant F, Rodrigues DH, Vago JP, Rachid MA, Sousa LP, et al. Phosphatidylinositol 3-Kinase γ is required for the development of experimental cerebral malaria. PLoS ONE. 2015;10: e0119633. doi:10.1371/journal.pone.0119633

170. Piguet PF, Da Laperrousaz C, Vesin C, Tacchini-Cottier F, Senaldi G, Grau GE. Delayed mortality and attenuated thrombocytopenia associated with severe malaria in urokinase- and urokinase receptor-deficient mice. Infection and Immunity. 2000;68: 3822–3829.

171. Potter S, Chan-Ling T, Ball HJ, Mansour H, Mitchell A, Maluish L, et al. Perforin mediated apoptosis of cerebral microvascular endothelial cells during experimental cerebral malaria. International Journal for Parasitology. 2006;36: 485–496. doi:10.1016/j.ijpara.2005.12.005

172. Ohayon A, Golenser J, Sinay R, Tamir A, Altman A, Pollack Y, et al. Protein kinase C θ deficiency increases resistance of C57BL/6J mice to Plasmodium berghei infection-induced cerebral malaria. Infection and Immunity. 2010;78: 4195–4205. doi:10.1128/IAI.00465-10

173. Fauconnier M, Bourigault ML, Meme S, Szeremeta F, Palomo J, Danneels A, et al. Protein Kinase C-Theta Is Required for Development of Experimental Cerebral Malaria. AJPA. Elsevier Inc; 2011;178: 212–221. doi:10.1016/j.ajpath.2010.11.008

174. Combes V, Rosenkranz AR, Redard M, Pizzolato G, Lepidi H, Vestweber D, et al. Pathogenic role of P-selectin in experimental cerebral malaria: importance of the endothelial compartment. AJPA. 2004;164: 781–786. doi:10.1016/S0002-9440(10)63166-5

175. Bullen DVR, Hansen DS, Siomos M-AV, Schofield L, Alexander WS, Handman E. The lack of suppressor of cytokine signalling-1 (SOCS1) protects mice from the development of cerebral malaria caused by Plasmodium berghei ANKA. Parasite Immunology. 2003;25: 113–118.

176. Brant F, Miranda AS, Esper L, Gualdrón-López M, Cisalpino D, de Souza DDG, et al. Suppressor of cytokine signaling 2 modulates the immune response profile and

development of experimental cerebral malaria. Brain Behav Immun. 2016;54: 73–85. doi:10.1016/j.bbi.2016.01.002

177. Sharma S, DeOliveira RB, Kalantari P, Parroche P, Goutagny N, Jiang Z, et al. Innate immune recognition of an AT-rich stem-loop DNA motif in the Plasmodium falciparum genome. Immunity. 2011;35: 194–207. doi:10.1016/j.immuni.2011.05.016

178. Oakley MS, Sahu BR, Lotspeich-Cole L, Solanki NR, Majam V, Pham PT, et al. The transcription factor T-bet regulates parasitemia and promotes pathogenesis during Plasmodium berghei ANKA murine malaria. The Journal of Immunology. 2013;191: 4699–4708. doi:10.4049/jimmunol.1300396

179. Coban C, Ishii KJ, Uematsu S, Arisue N, Sato S, Yamamoto M, et al. Pathological role of Toll-like receptor signaling in cerebral malaria. Int Immunol. 2007;19: 67–79. doi:10.1093/intimm/dxl123

180. Lucas R, Juillard P, Decoster E, Redard M, Burger D, Donati Y, et al. Crucial role of tumor necrosis factor (TNF) receptor 2 and membrane-bound TNF in experimental cerebral malaria. Eur J Immunol. 1997;27: 1719–1725. doi:10.1002/eji.1830270719

181. Piguet PF, Kan CD, Vesin C. Role of the tumor necrosis factor receptor 2 (TNFR2) in cerebral malaria in mice. Lab Invest. 2002;82: 1155–1166.

182. Herbas MS, Okazaki M, Terao E, Xuan X, Arai H, Suzuki H. alpha-Tocopherol transfer protein inhibition is effective in the prevention of cerebral malaria in mice. Am J Clin Nutr. 2010;91: 200–207. doi:10.3945/ajcn.2009.28260

183. Appleby MW, Ramsdell F. A forward-genetic approach for analysis of the immune system. Nat Rev Immunol. 2003;3: 463–471. doi:10.1038/nri1109

184. Russell WL, Kelly EM, Hunsicker PR, Bangham JW, Maddux SC, Phipps EL. Specific-locus test shows ethylnitrosourea to be the most potent mutagen in the mouse. Proc Natl Acad Sci USA. 1979;76: 5818–5819.

185. Noveroske JK, Weber JS, Justice MJ. The mutagenic action of N-ethyl-N-nitrosourea in the mouse. Mamm Genome. 2000;11: 478–483.

186. Bull KR, Rimmer AJ, Siggs OM, Miosge LA, Roots CM, Enders A, et al. Unlocking the bottleneck in forward genetics using whole-genome sequencing and identity by descent to isolate causative mutations. PLoS Genet. 2013;9: e1003219. doi:10.1371/journal.pgen.1003219

187. Acevedo-Arozena A, Wells S, Potter P, Kelly M, Cox RD, Brown SDM. ENU Mutagenesis, a Way Forward to Understand Gene Function. Annu Rev Genom Human Genet. 2008;9: 49–69. doi:10.1146/annurev.genom.9.081307.164224

188. Justice MJ. Capitalizing on large-scale mouse mutagenesis screens. Nat Rev Genet. 2000;1: 109–115. doi:10.1038/35038549

189. Simon MM, Moresco EMY, Bull KR, Kumar S, Mallon A-M, Beutler B, et al. Current strategies for mutation detection in phenotype-driven screens utilising next generation

sequencing. Mammalian Genome. 2015;26: 486–500. doi:10.1007/s00335-015-9603-x

190. Oliver PL, Davies KE. New insights into behaviour using mouse ENU mutagenesis. Hum Mol Genet. 2012;21: R72–81. doi:10.1093/hmg/dds318

191. Loftus EV. Clinical epidemiology of inflammatory bowel disease: Incidence, prevalence, and environmental influences. Gastroenterology. 2004;126: 1504–1517. doi:10.1053/j.gastro.2004.01.063

192. Medzhitov R. Origin and physiological roles of inflammation. Nature. 2008;454: 428–435. doi:10.1038/nature07201

193. Jostins L, Ripke S, Weersma RK, Duerr RH, McGovern DP, Hui KY, et al. Host-microbe interactions have shaped the genetic architecture of inflammatory bowel disease. Nature. 2012;491: 119–124. doi:10.1038/nature11582

194. Raychaudhuri S, Remmers EF, Lee AT, Hackett R, Guiducci C, Burtt NP, et al. Common variants at CD40 and other loci confer risk of rheumatoid arthritis. Nat Genet. 2008;40: 1216–1223. doi:10.1038/ng.233

195. International Multiple Sclerosis Genetics Consortium (IMSGC), Beecham AH, Patsopoulos NA, Xifara DK, Davis MF, Kemppinen A, et al. Analysis of immune-related loci identifies 48 new susceptibility variants for multiple sclerosis. Nat Genet. 2013;45: 1353–1360. doi:10.1038/ng.2770

196. Brown H, Hien TT, Day N, Mai NT, Chuong LV, Chau TT, et al. Evidence of blood-brain barrier dysfunction in human cerebral malaria. Neuropathol Appl Neurobiol. 1999;25: 331–340.

197. Ochiel DO, Awandare GA, Keller CC, Hittner JB, Kremsner PG, Weinberg JB, et al. Differential regulation of beta-chemokines in children with Plasmodium falciparum malaria. Infect Immun. 2005;73: 4190–4197. doi:10.1128/IAI.73.7.4190-4197.2005

198. Armah HB, Wilson NO, Sarfo BY, Powell MD, Bond VC, Anderson W, et al. Cerebrospinal fluid and serum biomarkers of cerebral malaria mortality in Ghanaian children. Malar J. 2007;6: 147. doi:10.1186/1475-2875-6-147

199. Xia Y, Won S, Du X, Lin P, Ross C, La Vine D, et al. Bulk segregation mapping of mutations in closely related strains of mice. Genetics. 2010;186: 1139–1146. doi:10.1534/genetics.110.121160

200. Li H, Durbin R. Fast and accurate short read alignment with Burrows-Wheeler transform. Bioinformatics. 2009;25: 1754–1760. doi:10.1093/bioinformatics/btp324

201. Quinlan AR, Hall IM. BEDTools: a flexible suite of utilities for comparing genomic features. Bioinformatics. 2010;26: 841–842. doi:10.1093/bioinformatics/btq033

202. Wang K, Li M, Hakonarson H. ANNOVAR: functional annotation of genetic variants from high-throughput sequencing data. Nucleic Acids Res. 2010;38: e164. doi:10.1093/nar/gkq603

203. Pino PA, Cardona AE. Isolation of brain and spinal cord mononuclear cells using percoll gradients. J Vis Exp. 2011. doi:10.3791/2348

204. Lesourne R, Uehara S, Lee J, Song K-D, Li L, Pinkhasov J, et al. Themis, a T cell–specific protein important for late thymocyte development. Nature Publishing Group. 2009;10: 840–847. doi:10.1038/ni.1768

205. Johnson AL, Aravind L, Shulzhenko N, Morgun A, Choi S-Y, Crockford TL, et al. Themis is a member of a new metazoan gene family and is required for the completion of thymocyte positive selection. Nature Publishing Group. 2009;10: 831–839. doi:10.1038/ni.1769

206. Patrick MS, Oda H, Hayakawa K, Sato Y, Eshima K, Kirikae T, et al. Gasp, a Grb2-associating protein, is critical for positive selection of thymocytes. Proc Natl Acad Sci USA. 2009;106: 16345–16350. doi:10.1073/pnas.0908593106

207. Fu G, Vallée S, Rybakin V, McGuire MV, Ampudia J, Brockmeyer C, et al. Themis controls thymocyte selection through regulation of T cell antigen receptor–mediated signaling. Nature Publishing Group. Nature Publishing Group; 2009;10: 848–856. doi:10.1038/ni.1766

208. Kakugawa K, Yasuda T, Miura I, Kobayashi A, Fukiage H, Satoh R, et al. A Novel Gene Essential for the Development of Single Positive Thymocytes. Molecular and Cellular Biology. 2009;29: 5128–5135. doi:10.1128/MCB.00793-09

209. Lamb TJ, Brown DE, Potocnik AJ, Langhorne J. Insights into the immunopathogenesis of malaria using mouse models. Expert Rev Mol Med. 2006;8: 1–22. doi:10.1017/S1462399406010581

210. Molina TJ, Kishihara K, Siderovski DP, van Ewijk W, Narendran A, Timms E, et al. Profound block in thymocyte development in mice lacking p56lck. Nature. 1992;357: 161–164. doi:10.1038/357161a0

211. Brockmeyer C, Paster W, Pepper D, Tan CP, Trudgian DC, McGowan S, et al. T Cell Receptor (TCR)-induced Tyrosine Phosphorylation Dynamics Identifies THEMIS as a New TCR Signalosome Component. Journal of Biological Chemistry. 2011;286: 7535–7547. doi:10.1074/jbc.M110.201236

212. Paster W, Brockmeyer C, Fu G, Simister PC, de Wet B, Martinez-Riaño A, et al. GRB2-mediated recruitment of THEMIS to LAT is essential for thymocyte development. The Journal of Immunology. 2013;190: 3749–3756. doi:10.4049/jimmunol.1203389

213. Lesourne R, Zvezdova E, Song K-D, El-Khoury D, Uehara S, Barr VA, et al. Interchangeability of Themis1 and Themis2 in thymocyte development reveals two related proteins with conserved molecular function. The Journal of Immunology. 2012;189: 1154–1161. doi:10.4049/jimmunol.1200123

214. Grau GE, Piguet PF, Engers HD, Louis JA, Vassalli P, Lambert PH. L3T4+ T lymphocytes play a major role in the pathogenesis of murine cerebral malaria. J Immunol. 1986;137: 2348–2354.

215. Zhang W, Sommers CL, Burshtyn DN, Stebbins CC. Essential role of LAT in T cell development. Immunity. 1999.

216. Jang IK, Zhang J, Chiang YJ, Kole HK, Cronshaw DG, Zou Y, et al. Grb2 functions at the top of the T-cell antigen receptor-induced tyrosine kinase cascade to control thymic selection. Proc Natl Acad Sci USA. 2010;107: 10620–10625. doi:10.1073/pnas.0905039107

217. Wang D, Zheng M, Lei L, Ji J, Yao Y, Qiu Y, et al. Tespa1 is involved in late thymocyte development through the regulation of TCR-mediated signaling. Nature Publishing Group. 2012;13: 560–568. doi:10.1038/ni.2301

218. Liao XC, Littman DR. Altered T cell receptor signaling and disrupted T cell development in mice lacking Itk. Immunity. 1995;3: 757–769.

219. Edgar JDM. T cell immunodeficiency. J Clin Pathol. 2008;61: 988–993. doi:10.1136/jcp.2007.051144

220. Allen PM. Themis imposes new law and order on positive selection. Nature Publishing Group. Nature Publishing Group; 2009;10: 805–806. doi:10.1038/ni0809-805

221. Okada T, Nitta T, Kaji K, Takashima A, Oda H, Tamehiro N, et al. Differential Function of Themis CABIT Domains during T Cell Development. PLoS ONE. 2014;9: e89115. doi:10.1371/journal.pone.0089115

222. Dubois PCA, Trynka G, Franke L, Hunt KA, Romanos J, Curtotti A, et al. Multiple common variants for celiac disease influencing immune gene expression. Nat Genet. 2010;42: 295–302. doi:10.1038/ng.543

223. Trynka G, Hunt KA, Bockett NA, Romanos J, Mistry V, Szperl A, et al. Dense genotyping identifies and localizes multiple common and rare variant association signals in celiac disease. Nat Genet. 2011;43: 1193–1201. doi:10.1038/ng.998

224. van Heel DA, Franke L, Hunt KA, Gwilliam R. A genome-wide association study for celiac disease identifies risk variants in the region harboring IL2 and IL21. Nature. 2007.

225. Bondar C, Plaza-Izurieta L, Fernandez-Jimenez N, Irastorza I, Withoff S, CEGEC, et al. THEMIS and PTPRK in celiac intestinal mucosa: coexpression in disease and after in vitro gliadin challenge. Eur J Hum Genet. 2013. doi:10.1038/ejhg.2013.136

226. International Multiple Sclerosis Genetics Consortium, Wellcome Trust Case Control Consortium 2, Sawcer S, Hellenthal G, Pirinen M, Spencer CCA, et al. Genetic risk and a primary role for cell-mediated immune mechanisms in multiple sclerosis. Nature. 2011;476: 214–219. doi:10.1038/nature10251

227. Okada Y, Wu D, Trynka G, Raj T, Terao C, Ikari K, et al. Genetics of rheumatoid arthritis contributes to biology and drug discovery. Nature. 2014;506: 376–381. doi:10.1038/nature12873

228. Cunninghame Graham DS, Morris DL, Bhangale TR, Criswell LA, Syvänen A-C, Rönnblom L, et al. Association of NCF2, IKZF1, IRF8, IFIH1, and TYK2 with systemic

lupus erythematosus. PLoS Genet. 2011;7: e1002341. doi:10.1371/journal.pgen.1002341

229. Fodil N, Langlais D, Gros P. Primary Immunodeficiencies and Inflammatory Disease: A Growing Genetic Intersection. Trends in Immunology. 2016;37: 126–140. doi:10.1016/j.it.2015.12.006

230. Pauli E-K, Chan YK, Davis ME, Gableske S, Wang MK, Feister KF, et al. The ubiquitin-specific protease USP15 promotes RIG-I-mediated antiviral signaling by deubiquitylating TRIM25. Sci Signal. 2014;7: ra3. doi:10.1126/scisignal.2004577

231. Gack MU, Shin YC, Joo C-H, Urano T, Liang C, Sun L, et al. TRIM25 RING-finger E3 ubiquitin ligase is essential for RIG-I-mediated antiviral activity. Nature. 2007;446: 916–920. doi:10.1038/nature05732

232. Orimo A, Inoue S, Minowa O, Tominaga N, Tomioka Y, Sato M, et al. Underdeveloped uterus and reduced estrogen responsiveness in mice with disruption of the estrogen-responsive finger protein gene, which is a direct target of estrogen receptor alpha. Proc Natl Acad Sci USA. 1999;96: 12027–12032.

233. Urano T, Saito T, Tsukui T, Fujita M, Hosoi T, Muramatsu M, et al. Efp targets 14-3-3 sigma for proteolysis and promotes breast tumour growth. Nature. 2002;417: 871–875. doi:10.1038/nature00826

234. Tanaka K, Ichiyama K, Hashimoto M, Yoshida H, Takimoto T, Takaesu G, et al. Loss of suppressor of cytokine signaling 1 in helper T cells leads to defective Th17 differentiation by enhancing antagonistic effects of IFN-gamma on STAT3 and Smads. J Immunol. 2008;180: 3746–3756.

235. Gold R, Linington C, Lassmann H. Understanding pathogenesis and therapy of multiple sclerosis via animal models: 70 years of merits and culprits in experimental autoimmune encephalomyelitis research. Brain. 2006;129: 1953–1971. doi:10.1093/brain/awl075

236. Langmead B, Trapnell C, Pop M, Salzberg SL. Ultrafast and memory-efficient alignment of short DNA sequences to the human genome. Genome Biol. 2009;10: R25. doi:10.1186/gb-2009-10-3-r25

237. Kim D, Pertea G, Trapnell C, Pimentel H, Kelley R, Salzberg SL. TopHat2: accurate alignment of transcriptomes in the presence of insertions, deletions and gene fusions. Genome Biol. 2013;14: R36. doi:10.1186/gb-2013-14-4-r36

238. Liao Y, Smyth GK, Shi W. featureCounts: an efficient general purpose program for assigning sequence reads to genomic features. Bioinformatics. 2014;30: 923–930. doi:10.1093/bioinformatics/btt656

239. Robinson MD, Oshlack A. A scaling normalization method for differential expression analysis of RNA-seq data. Genome Biol. 2010;11: R25. doi:10.1186/gb-2010-11-3-r25

240. Thorvaldsdóttir H, Robinson JT, Mesirov JP. Integrative Genomics Viewer (IGV): high-performance genomics data visualization and exploration. Brief Bioinformatics. 2013;14:

178–192. doi:10.1093/bib/bbs017

241. Saeed AI, Sharov V, White J, Li J, Liang W, Bhagabati N, et al. TM4: a free, open-source system for microarray data management and analysis. BioTechniques. 2003;34: 374–378.

242. Huang DW, Sherman BT, Lempicki RA. Systematic and integrative analysis of large gene lists using DAVID bioinformatics resources. Nat Protoc. 2009;4: 44–57. doi:10.1038/nprot.2008.211

243. Subramanian A, Tamayo P, Mootha VK, Mukherjee S, Ebert BL, Gillette MA, et al. Gene set enrichment analysis: a knowledge-based approach for interpreting genome-wide expression profiles. Proc Natl Acad Sci USA. 2005;102: 15545–15550. doi:10.1073/pnas.0506580102

244. Saikali P, Antel JP, Newcombe J, Chen Z, Freedman M, Blain M, et al. NKG2D-mediated cytotoxicity toward oligodendrocytes suggests a mechanism for tissue injury in multiple sclerosis. J Neurosci. 2007;27: 1220–1228. doi:10.1523/JNEUROSCI.4402-06.2007

245. Durafourt BA, Moore CS, Zammit DA, Johnson TA, Zaguia F, Guiot M-C, et al. Comparison of polarization properties of human adult microglia and blood-derived macrophages. Glia. 2012;60: 717–727. doi:10.1002/glia.22298

246. de Jong RN, Ab E, Diercks T, Truffault V, Daniëls M, Kaptein R, et al. Solution structure of the human ubiquitin-specific protease 15 DUSP domain. J Biol Chem. 2006;281: 5026–5031. doi:10.1074/jbc.M510993200

247. Hetfeld B, Helfrich A, Kapelarl B, Scheel H, Hofmann K, Guterman A, et al. The zinc finger of the CSN-associated deubiquitinating enzyme USP15 is essential to rescue the E3 ligase Rbx1. Current Biology. 2005;15: 1217–1221. doi:10.1016/j.cub.2005.05.059

248. Man S, Ubogu EE, Ransohoff RM. Inflammatory cell migration into the central nervous system: a few new twists on an old tale. Brain Pathol. 2007;17: 243–250. doi:10.1111/j.1750-3639.2007.00067.x

249. Rusinova I, Forster S, Yu S, Kannan A, Masse M, Cumming H, et al. Interferome v2.0: an updated database of annotated interferon-regulated genes. Nucleic Acids Res. 2013;41: D1040–6. doi:10.1093/nar/gks1215

250. Schweitzer K, Bozko PM, Dubiel W, Naumann M. CSN controls NF-kappaB by deubiquitinylation of IkappaBalpha. EMBO J. 2007;26: 1532–1541. doi:10.1038/sj.emboj.7601600

251. Cornelissen T, Haddad D, Wauters F, Van Humbeeck C, Mandemakers W, Koentjoro B, et al. The deubiquitinase USP15 antagonizes Parkin-mediated mitochondrial ubiquitination and mitophagy. Hum Mol Genet. 2014;23: 5227–5242.

252. Hayes SD, Liu H, MacDonald E, Sanderson CM, Coulson JM, Clague MJ, et al. Direct and indirect control of mitogen-activated protein kinase pathway-associated components, BRAP/IMP E3 ubiquitin ligase and CRAF/RAF1 kinase, by the

deubiquitylating enzyme USP15. J Biol Chem. 2012;287: 43007–43018. doi:10.1074/jbc.M112.386938

253. Villeneuve NF, Tian W, Wu T, Sun Z, Lau A, Chapman E, et al. USP15 negatively regulates Nrf2 through deubiquitination of Keap1. Mol Cell. 2013;51: 68–79. doi:10.1016/j.molcel.2013.04.022

254. Long L, Thelen JP, Furgason M, Haj-Yahya M, Brik A, Cheng D, et al. The U4/U6 recycling factor SART3 has histone chaperone activity and associates with USP15 to regulate H2B deubiquitination. J Biol Chem. 2014;289: 8916–8930. doi:10.1074/jbc.M114.551754

255. Inui M, Manfrin A, Mamidi A, Martello G, Morsut L, Soligo S, et al. USP15 is a deubiquitylating enzyme for receptor-activated SMADs. Nat Cell Biol. 2011;13: 1368–1375. doi:10.1038/ncb2346

256. Eichhorn PJA, Rodón L, Gonzàlez-Juncà A, Dirac A, Gili M, Martínez-Sáez E, et al. USP15 stabilizes TGF-β receptor I and promotes oncogenesis through the activation of TGF-β signaling in glioblastoma. Nat Med. 2012;18: 429–435. doi:10.1038/nm.2619

257. Iyengar PV, Jaynes P, Rodón L, Lama D, Law KP, Lim YP, et al. USP15 regulates SMURF2 kinetics through C-lobe mediated deubiquitination. Sci Rep. 2015;5: 14733. doi:10.1038/srep14733

258. Zou Q, Jin J, Hu H, Li HS, Romano S, Xiao Y, et al. USP15 stabilizes MDM2 to mediate cancer-cell survival and inhibit antitumor T cell responses. Nat Immunol. 2014;15: 562–570. doi:10.1038/ni.2885

259. Zhang H, Wang D, Zhong H, Luo R, Shang M, Liu D, et al. Ubiquitin-specific Protease 15 Negatively Regulates Virus-induced Type I Interferon Signaling via Catalytically-dependent and -independent Mechanisms. Sci Rep. The Author(s) SN ; 2015;5: 11220 EP –. doi:10.1038/srep11220

260. Inn K-S, Gack MU, Tokunaga F, Shi M, Wong L-Y, Iwai K, et al. Linear ubiquitin assembly complex negatively regulates RIG-I- and TRIM25-mediated type I interferon induction. Mol Cell. 2011;41: 354–365. doi:10.1016/j.molcel.2010.12.029

261. Imboden M, Bouzigon E, Curjuric I, Ramasamy A, Kumar A, Hancock DB, et al. Genome-wide association study of lung function decline in adults with and without asthma. J Allergy Clin Immunol. 2012;129: 1218–1228. doi:10.1016/j.jaci.2012.01.074

262. Friedman MJ. Erythrocytic mechanism of sickle cell resistance to malaria. Proc Natl Acad Sci USA. 1978;75: 1994–1997.

263. Flint J, Hill AV, Bowden DK, Oppenheimer SJ, Sill PR, Serjeantson SW, et al. High frequencies of alpha-thalassaemia are the result of natural selection by malaria. Nature. 1986;321: 744–750. doi:10.1038/321744a0

264. Williams TN, Maitland K, Bennett S, Ganczakowski M, Peto TE, Newbold CI, et al. High incidence of malaria in alpha-thalassaemic children. Nature. 1996;383: 522–525. doi:10.1038/383522a0

265. Foo LC, Rekhraj V, Chiang GL, Mak JW. Ovalocytosis protects against severe malaria parasitemia in the Malayan aborigines. Am J Trop Med Hyg. 1992;47: 271–275.

266. Allen SJ, O'Donnell A, Alexander ND, Mgone CS, Peto TE, Clegg JB, et al. Prevention of cerebral malaria in children in Papua New Guinea by southeast Asian ovalocytosis band 3. Am J Trop Med Hyg. 1999;60: 1056–1060.

267. Ruwende C, Khoo SC, Snow RW, Yates SN, Kwiatkowski D, Gupta S, et al. Natural selection of hemi- and heterozygotes for G6PD deficiency in Africa by resistance to severe malaria. Nature. 1995;376: 246–249. doi:10.1038/376246a0

268. Tishkoff SA, Varkonyi R, Cahinhinan N, Abbes S, Argyropoulos G, Destro-Bisol G, et al. Haplotype diversity and linkage disequilibrium at human G6PD: recent origin of alleles that confer malarial resistance. Science. 2001;293: 455–462. doi:10.1126/science.1061573

269. Aitman TJ, Cooper LD, Norsworthy PJ, Wahid FN, Gray JK, Curtis BR, et al. Malaria susceptibility and CD36 mutation. Nature. 2000;405: 1015–1016. doi:10.1038/35016636

270. Omi K, Ohashi J, Patarapotikul J, Hananantachai H, Naka I, Looareesuwan S, et al. CD36 polymorphism is associated with protection from cerebral malaria. Am J Hum Genet. 2003;72: 364–374. doi:10.1086/346091

271. Hill AV, Allsopp CE, Kwiatkowski D, Anstey NM, Twumasi P, Rowe PA, et al. Common west African HLA antigens are associated with protection from severe malaria. Nature. 1991;352: 595–600. doi:10.1038/352595a0

272. McGuire W, Hill AV, Allsopp CE, Greenwood BM, Kwiatkowski D. Variation in the TNF-alpha promoter region associated with susceptibility to cerebral malaria. Nature. 1994;371: 508–510. doi:10.1038/371508a0

273. Fortin A, Stevenson MM, Gros P. Complex genetic control of susceptibility to malaria in mice. Genes and Immunity. 2002;3: 177–186. doi:10.1038/sj.gene.6363841

274. Tripathi AK, Sha W, Shulaev V, Stins MF, Sullivan DJ. Plasmodium falciparum-infected erythrocytes induce NF-kappaB regulated inflammatory pathways in human cerebral endothelium. Blood. 2009;114: 4243–4252. doi:10.1182/blood-2009-06-226415

275. Newton CR, Hien TT, White N. Cerebral malaria. J Neurol Neurosurg Psychiatr. 2000;69: 433–441.

276. Hafalla JCR, Claser C, Couper KN, Grau GE, Rénia L, de Souza JB, et al. The CTLA-4 and PD-1/PD-L1 inhibitory pathways independently regulate host resistance to Plasmodium-induced acute immune pathology. PLoS Pathog. 2012;8: e1002504. doi:10.1371/journal.ppat.1002504

277. Lacerda-Queiroz N, Rodrigues DH, Vilela MC, Rachid MA, Soriani FM, Sousa LP, et al. Platelet-activating factor receptor is essential for the development of experimental cerebral malaria. The American Journal of Pathology. 2012;180: 246–255. doi:10.1016/j.ajpath.2011.09.038

278. Senaldi G, Vesin C, Chang R, Grau GE, Piguet PF. Role of polymorphonuclear neutrophil leukocytes and their integrin CD11a (LFA-1) in the pathogenesis of severe murine malaria. Infection and Immunity. 1994;62: 1144–1149.

279. Lucas R, Juillard P, Decoster E. Crucial role of tumor necrosis factor (TNF) receptor 2 and membrane-bound TNF in experimental cerebral malaria. Eur J Immunol. 2005;27: 1719–1725.

280. Miyazaki T, Ono M, Qu W-M, Zhang M-C, Mori S, Nakatsuru S, et al. Implication of allelic polymorphism of osteopontin in the development of lupus nephritis in MRL/lpr mice. Eur J Immunol. 2005;35: 1510–1520. doi:10.1002/eji.200425672

281. Weis JJ, McCracken BA, Ma Y, Fairbairn D, Roper RJ, Morrison TB, et al. Identification of quantitative trait loci governing arthritis severity and humoral responses in the murine model of Lyme disease. J Immunol. 1999;162: 948–956.

282. Jackson AU, Galecki AT, Burke DT, Miller RA. Genetic polymorphisms in mouse genes regulating age-sensitive and age-stable T cell subsets. Genes and Immunity. 2003;4: 30–39. doi:10.1038/sj.gene.6363895

283. Morel L, Rudofsky UH, Longmate JA, Schiffenbauer J, Wakeland EK. Polygenic control of susceptibility to murine systemic lupus erythematosus. Immunity. 1994;1: 219–229.

284. Loh C, Pau E, Lajoie G, Li TT, Baglaenko Y, Cheung Y-H, et al. Epistatic suppression of fatal autoimmunity in New Zealand black bicongenic mice. The Journal of Immunology. 2011;186: 5845–5853. doi:10.4049/jimmunol.1003426

285. Arakura F, Hida S, Ichikawa E, Yajima C, Nakajima S, Saida T, et al. Genetic control directed toward spontaneous IFN-alpha/IFN-beta responses and downstream IFN-gamma expression influences the pathogenesis of a murine psoriasis-like skin disease. J Immunol. 2007;179: 3249–3257.

286. Bullard DC, Scharffetter-Kochanek K, McArthur MJ, Chosay JG, McBride ME, Montgomery CA, et al. A polygenic mouse model of psoriasiform skin disease in CD18-deficient mice. Proc Natl Acad Sci USA. 1996;93: 2116–2121.

287. Barlow SC, Collins RG, Ball NJ. Psoriasiform dermatitis susceptibility in Itgb2(tm1Bay) PL/J mice requires low-level CD18 expression and at least two additional loci for progression to severe …. The American journal …. 2003.

288. Alkhateeb A, Stetler GL, Old W, Talbert J, Uhlhorn C, Taylor M, et al. Mapping of an autoimmunity susceptibility locus (AIS1) to chromosome 1p31.3-p32.2. Hum Mol Genet. 2002;11: 661–667.

289. Fain PR, Gowan K, LaBerge GS, Alkhateeb A, Stetler GL, Talbert J, et al. A genomewide screen for generalized vitiligo: confirmation of AIS1 on chromosome 1p31 and evidence for additional susceptibility loci. Am J Hum Genet. 2003;72: 1560–1564. doi:10.1086/375451

290. Liu J, Cao X. Cellular and molecular regulation of innate inflammatory responses. Cell Mol Immunol. 2016;13: 711–721. doi:10.1038/cmi.2016.58

291. Cordes SP. N-ethyl-N-nitrosourea mutagenesis: boarding the mouse mutant express. Microbiol Mol Biol Rev. 2005;69: 426–439. doi:10.1128/MMBR.69.3.426-439.2005

292. Kennedy CL, O'Bryan MK. N-ethyl-N-nitrosourea (ENU) mutagenesis and male fertility research. Hum Reprod Update. 2006;12: 293–301. doi:10.1093/humupd/dmk004

293. Libert C, Dejager L, Pinheiro I. The X chromosome in immune functions: when a chromosome makes the difference. Nat Rev Immunol. 2010;10: 594–604. doi:10.1038/nri2815

294. Sigmund CD. Viewpoint: are studies in genetically altered mice out of control? Arterioscler Thromb Vasc Biol. 2000;20: 1425–1429.

295. Montagutelli X. Effect of the genetic background on the phenotype of mouse mutations. Journal of the American Society of Nephrology. 2000.

296. Sackton TB, Hartl DL. Genotypic Context and Epistasis in Individuals and Populations. Cell. 2016;166: 279–287. doi:10.1016/j.cell.2016.06.047

297. Warden CH, Yi N, Fisler J. Epistasis among genes is a universal phenomenon in obesity: evidence from rodent models. Nutrition. 2004;20: 74–77.

298. Moore JH. The ubiquitous nature of epistasis in determining susceptibility to common human diseases. Human heredity. 2003.

299. Yoshiki A, Moriwaki K. Mouse phenome research: implications of genetic background. Ilar Journal. 2006.

300. Phillips PC. Epistasis—the essential role of gene interactions in the structure and evolution of genetic systems. Nat Rev Genet. 2008.

301. Mackay T. Epistasis and quantitative traits: using model organisms to study gene-gene interactions. Nat Rev Genet. 2014.

302. Wu M, Jiang R. Detecting epistatic interactions in metagenome-wide association studies by metaBOOST. Biomed Res Int. 2014;2014: 398147. doi:10.1155/2014/398147

303. Phillips TJ, Belknap JK, Hitzemann RJ. Harnessing the mouse to unravel the genetics of human disease. Genes (Basel). 2002.

304. Pal A, Young MA, Donato NJ. Emerging potential of therapeutic targeting of ubiquitin-specific proteases in the treatment of cancer. Cancer Res. 2014;74: 4955–4966. doi:10.1158/0008-5472.CAN-14-1211

305. Fraile JM, Quesada V, Rodriguez D, Freije J. Deubiquitinases in cancer: new functions and therapeutic options. Oncogene. 2012.

306. Lopez-Castejon G, Edelmann MJ. Deubiquitinases: Novel Therapeutic Targets in Immune Surveillance? Mediators Inflamm. 2016;2016: 3481371. doi:10.1155/2016/3481371

307. Kemp M. Recent Advances in the Discovery of Deubiquitinating Enzyme Inhibitors. Prog Med Chem. 2016;55: 149–192. doi:10.1016/bs.pmch.2015.10.002

308. Pfoh R, Lacdao IK, Saridakis V. Deubiquitinases and the new therapeutic opportunities offered to cancer. Endocr Relat Cancer. 2015;22: T35–54. doi:10.1530/ERC-14-0516

309. Huang X, Langelotz C, Hetfeld-Pechoc BKJ, Schwenk W, Dubiel W. The COP9 signalosome mediates beta-catenin degradation by deneddylation and blocks adenomatous polyposis coli destruction via USP15. J Mol Biol. 2009;391: 691–702. doi:10.1016/j.jmb.2009.06.066

310. Kielian T. Neuroinflammation: good, bad, or indifferent? J Neurochem. 2014;130: 1–3. doi:10.1111/jnc.12755

311. Craft JM, Watterson DM, Van Eldik LJ. Neuroinflammation: a potential therapeutic target. Expert Opinion on Therapeutic Targets. 2005;9: 887–900. doi:10.1517/14728222.9.5.887

Appendix

Appendix Table 1: List of dysregulated genes in USP15 mutant mice undergoing ECM and EAE models neuroinflammatory diseases

* NE = No expression detected

Clustering order	Gene symbol	PbA d5 (USP15/B6)			EAE d7 (USP15/B6)			B6 PbA d5 / B6 NI			PbA - Normalized read counts per million reads (CPM)									EAE - Normalized read counts per million reads (CPM)			
		Fold change	Log2 FC	adj. *p* val.	Fold change	Log2 FC	adj. *p* val.	Fold change	Log2 FC	adj. *p* val.	B6-2_NI	B6-3_NI	B6-4_NI	B6-1_d5_PbA	B6-2_d5_PbA	B6-3_d5_PbA	USP15-1_d5_PbA	USP15-2_d5_PbA	USP15-3_d5_PbA	B6-7	B6-8	USP15-19	USP15-21
1	I830012O16Rik	0.42	-1.25	2.73E-07	0.62	-0.68	5.90E-05	14.22	3.83	3.99E-60	13.4	14.0	11.0	181.9	167.2	195.9	50.1	116.7	61.7	23.0	16.5	12.3	12.5
2	Irf9	0.48	-1.06	3.02E-11	0.66	-0.60	6.39E-05	7.19	2.85	3.07E-77	9.7	9.6	8.7	65.4	62.6	73.5	24.9	42.6	29.1	20.3	17.5	11.8	13.2
3	Parp12	0.63	-0.66	1.37E-04	0.80	-0.32	1.76E-01	3.85	1.95	2.25E-39	10.3	11.3	12.1	46.4	39.3	44.1	21.4	35.6	25.3	19.1	15.8	14.2	13.8
4	Samd9l	0.64	-0.65	2.98E-03	0.80	-0.32	5.74E-01	4.78	2.26	2.85E-35	6.3	6.3	4.8	29.4	25.8	27.9	14.4	24.3	14.2	10.0	6.7	6.3	7.1
5	Pglyrp1	0.64	-0.65	3.60E-03	0.79	-0.33	4.11E-01	5.40	2.43	4.84E-37	2.4	1.9	2.0	9.4	9.6	15.1	6.4	7.4	7.9	6.7	6.1	4.5	5.7
6	Tsc22d3	0.59	-0.76	1.54E-08	0.71	-0.50	1.76E-07	2.47	1.30	7.50E-27	103.8	124.7	128.7	250.7	303.9	325.8	148.5	207.1	164.7	221.2	235.3	155.4	168.4
7	Lgals3bp	0.59	-0.75	1.49E-09	0.71	-0.49	6.59E-03	6.68	2.74	7.14E-121	17.8	16.1	16.0	113.2	95.1	124.8	55.4	76.7	65.7	23.5	18.8	13.4	16.8
8	Sult1a1	0.48	-1.05	7.09E-05	0.62	-0.70	3.69E-04	3.80	1.93	9.59E-17	7.0	8.1	6.9	20.4	25.9	37.4	9.0	18.1	13.4	9.9	13.4	7.3	7.2
9	Mt1	0.61	-0.71	3.83E-08	0.72	-0.48	6.11E-05	2.22	1.15	6.99E-23	141.7	124.5	137.1	253.8	284.8	356.7	154.2	201.8	191.0	197.3	219.7	167.6	134.5
10	Smim3	0.62	-0.68	5.48E-04	0.75	-0.41	1.41E-01	2.69	1.43	1.69E-17	4.5	4.9	5.6	12.1	13.7	14.7	6.5	10.7	8.1	6.4	7.2	5.0	5.3
11	Cd274	0.63	-0.68	2.20E-05	0.76	-0.40	8.23E-03	7.16	2.84	5.15E-88	6.2	7.0	7.4	54.8	46.9	46.7	23.5	37.7	31.8	39.4	31.1	24.1	29.2
12	Stat1	0.57	-0.81	2.64E-08	0.72	-0.48	8.66E-04	6.80	2.77	1.18E-92	34.8	35.3	35.2	262.6	212.5	241.3	105.1	172.8	130.4	76.3	53.3	44.7	48.6
13	Ncf1	0.66	-0.59	3.54E-04	0.79	-0.35	2.40E-01	2.39	1.26	3.16E-19	8.5	8.0	7.4	19.6	17.0	20.5	10.5	15.5	12.0	11.8	10.4	7.9	9.5
14	Sgk3	0.63	-0.66	8.58E-04	0.75	-0.41	1.22E-03	1.90	0.92	1.04E-07	14.0	15.6	16.0	19.8	29.9	36.8	17.0	19.6	18.0	39.2	48.5	32.7	34.0
15	Ifih1	0.61	-0.72	1.12E-04	0.73	-0.46	7.96E-02	4.58	2.19	1.12E-41	6.4	6.6	6.5	29.2	26.2	33.6	14.9	24.0	15.0	11.2	8.2	6.9	7.2
16	Apol8	0.65	-0.63	1.19E-03	0.76	-0.40	1.34E-01	0.95	-0.08	7.67E-01	7.5	5.5	5.3	5.5	5.6	6.1	3.9	3.3	4.0	8.7	8.2	6.8	6.1
17	Mt2	0.50	-0.99	4.77E-07	0.60	-0.74	7.11E-15	3.56	1.83	5.61E-25	38.2	30.7	38.7	102.6	125.7	154.8	47.0	83.6	62.1	68.4	78.8	47.8	41.5
18	Lrrc33	0.67	-0.59	7.86E-03	0.73	-0.45	5.19E-02	2.61	1.38	5.99E-15	8.7	6.6	6.4	16.7	18.6	21.5	11.1	16.4	10.3	9.4	9.2	7.2	6.6
19	Ptprc	0.60	-0.74	2.90E-03	0.70	-0.52	2.05E-01	5.92	2.56	1.77E-34	4.2	4.0	3.0	25.1	20.3	20.6	12.1	18.2	9.3	11.0	5.6	5.7	5.9
20	Ifit3	0.43	-1.21	6.56E-07	0.55	-0.86	3.25E-05	15.32	3.94	4.25E-64	19.6	20.6	16.2	289.1	262.6	311.0	82.5	190.5	100.9	27.1	15.9	10.5	13.2
21	Parp9	0.61	-0.72	6.05E-04	0.70	-0.51	1.45E-01	7.21	2.85	2.73E-54	4.2	4.2	4.2	32.9	27.3	31.0	13.8	25.7	16.0	9.5	6.0	6.3	4.8
22	C4a	0.66	-0.60	3.29E-03	0.74	-0.44	4.84E-02	4.13	2.05	8.85E-35	8.7	9.5	9.1	45.6	30.5	36.9	18.9	31.4	24.3	49.2	29.6	30.1	28.2
23	Icosl	0.65	-0.62	4.32E-04	0.73	-0.45	7.37E-02	1.79	0.84	4.70E-08	5.7	5.8	6.4	10.7	9.0	12.4	5.9	7.8	7.2	6.8	7.4	5.1	5.4
24	Fkbp5	0.51	-0.97	4.19E-07	0.59	-0.77	8.35E-12	2.83	1.50	5.50E-18	26.2	25.9	24.3	49.3	72.8	94.0	33.4	43.5	33.3	27.4	31.0	17.5	17.1
25	Trim34a	0.55	-0.87	2.60E-05	0.61	-0.71	5.46E-04	5.43	2.44	3.82E-39	2.7	2.6	3.3	16.8	15.2	15.2	5.9	10.3	9.7	7.3	6.1	4.0	4.3
26	Slc25a37	0.62	-0.70	1.46E-05	0.68	-0.57	3.34E-06	1.15	0.20	2.88E-01	14.4	14.1	12.7	16.1	15.7	15.5	8.8	8.0	12.3	28.7	25.3	18.0	18.6
27	Plin4	0.24	-2.08	1.41E-05	0.26	-1.94	4.33E-51	19.60	4.29	3.43E-21	6.3	8.5	8.5	69.5	165.5	222.4	14.2	59.6	34.0	78.9	120.9	27.2	25.6
28	Fam107a	0.47	-1.08	1.23E-12	0.52	-0.95	8.84E-25	2.15	1.10	1.72E-14	353.3	337.9	371.9	808.5	703.6	772.7	251.0	430.3	400.7	209.1	203.2	116.8	99.5
29	Ldb3	0.42	-1.26	5.40E-10	0.45	-1.14	8.29E-16	1.11	0.15	5.89E-01	6.9	6.6	6.9	7.2	8.0	7.4	2.3	2.7	4.4	16.1	17.2	7.3	7.8
30	Dao	0.62	-0.69	1.34E-04	0.65	-0.62	1.60E-05	1.17	0.23	2.59E-01	18.3	17.4	19.0	19.0	17.9	27.3	11.1	13.5	15.2	31.8	34.1	25.4	18.0
31	Ifit1	0.49	-1.02	3.36E-04	0.50	-1.01	3.60E-08	18.71	4.23	4.08E-57	3.2	4.5	2.8	60.2	56.6	79.1	23.4	48.7	24.2	10.6	8.1	4.8	4.5
32	Rpph1	0.50	-1.01	1.20E-21	0.50	-0.99	9.59E-23	1.60	0.68	9.02E-11	8849.3	7967.2	7422.3	11597.8	13566.7	13611.4	5581.2	6203.0	7441.9	2127.0	2461.8	1076.8	1235.2
33	Esd	0.63	-0.67	2.16E-08	0.64	-0.65	1.40E-11	1.11	0.15	2.86E-01	56.5	58.0	58.7	63.7	67.9	61.2	33.6	38.6	49.2	55.6	49.8	32.5	35.2
34	Arrdc2	0.43	-1.21	1.13E-05	0.42	-1.25	1.19E-30	3.81	1.93	3.34E-15	11.2	12.5	12.2	26.0	49.9	60.8	14.9	25.7	18.7	34.5	42.8	16.4	16.3
35	4930452B06Rik	0.64	-0.63	1.07E-03	0.64	-0.64	1.09E-02	0.86	-0.21	3.16E-01	11.7	12.3	12.0	10.6	9.9	10.5	4.7	7.5	7.8	7.5	7.3	5.8	3.8
36	C4b	0.65	-0.62	1.90E-03	0.63	-0.67	5.67E-04	4.62	2.21	1.80E-40	39.7	37.3	37.5	208.2	133.8	186.9	86.0	145.3	112.3	190.0	114.6	79.5	110.5
37	Phyhd1	0.61	-0.72	2.16E-05	0.59	-0.76	8.47E-13	2.56	1.35	4.77E-20	10.9	11.2	11.8	27.0	27.2	32.6	12.8	19.8	20.2	37.0	38.5	24.5	20.7
38	Slc25a34	0.52	-0.93	6.79E-08	0.50	-0.99	1.00E-07	2.80	1.49	5.06E-21	12.7	12.2	12.0	27.9	32.7	42.7	13.9	20.8	19.4	9.5	7.2	4.3	4.1
39	Net1	0.67	-0.58	2.58E-06	0.65	-0.62	3.07E-07	1.26	0.34	7.51E-03	33.1	36.1	33.4	35.3	45.3	49.0	28.1	31.5	27.0	25.7	27.8	18.6	16.6
40	Fcgr3	0.66	-0.59	8.69E-07	0.55	-0.86	1.72E-02	3.32	1.73	4.04E-58	13.0	12.3	12.2	39.6	40.5	44.0	24.3	32.8	25.3	15.2	6.6	4.7	7.3
41	Samhd1	0.75	-0.41	5.27E-03	0.66	-0.59	2.38E-04	3.65	1.87	1.72E-57	10.4	10.1	10.2	37.0	36.1	39.0	24.5	34.7	25.4	37.4	25.4	21.1	20.8
42	Irgm1	0.61	-0.71	1.82E-05	0.51	-0.97	6.75E-08	16.07	4.01	5.22E-148	8.5	10.6	9.9	161.3	145.2	157.7	75.1	125.0	84.5	37.9	22.3	14.1	16.6
43	Lcn2	0.42	-1.27	6.87E-02	0.30	-1.74	8.10E-20	15.66	3.97	1.53E-12	1.6	0.3	0.8	4.5	13.8	24.7	4.7	8.3	4.9	9.1	11.4	3.7	2.5
44	Galnt15	0.45	-1.17	5.06E-07	0.32	-1.63	9.47E-15	1.56	0.64	7.17E-03	8.1	8.3	8.9	10.9	11.5	17.2	3.9	6.6	7.1	8.4	13.1	4.1	3.0
45	Txnip	0.70	-0.52	6.61E-03	0.61	-0.72	1.24E-07	2.11	1.08	3.40E-12	26.1	21.1	23.7	40.2	46.4	63.0	30.4	41.6	32.3	23.6	31.2	17.4	16.2
46	Agxt2l1	0.47	-1.08	3.14E-09	0.37	-1.45	4.53E-48	1.97	0.98	1.50E-08	38.3	37.7	46.6	55.4	85.8	100.5	32.6	40.6	41.2	42.1	43.0	17.0	14.5
47	Entpd4	0.64	-0.65	6.14E-07	0.55	-0.87	9.90E-25	1.90	0.93	3.47E-15	113.4	110.6	116.1	209.2	225.7	212.1	121.3	115.8	174.6	206.0	199.2	110.8	112.6
48	B2m	0.71	-0.50	4.90E-08	0.63	-0.67	2.02E-07	3.82	1.94	5.88E-121	42.4	42.3	44.0	175.9	159.4	157.3	101.0	128.6	119.0	69.4	48.3	36.0	37.9
49	Adipor2	0.70	-0.52	1.82E-04	0.63	-0.68	2.87E-13	1.62	0.69	1.95E-08	86.5	104.1	111.9	137.9	169.4	181.5	98.1	129.5	112.5	172.7	192.1	109.0	120.1
50	Trim30a	0.54	-0.89	1.62E-04	0.49	-1.04	1.26E-04	11.33	3.50	2.42E-58	1.6	2.7	2.1	25.8	21.9	23.2	9.6	17.7	11.0	11.0	5.4	3.8	4.2
51	Apobec3	0.61	-0.70	5.84E-04	0.57	-0.81	1.77E-04	5.47	2.45	8.89E-42	2.2	2.6	2.0	13.9	10.8	12.3	5.9	9.5	7.4	9.2	6.3	4.2	4.6
52	Mertk	0.69	-0.54	2.34E-06	0.65	-0.62	3.98E-08	1.89	0.92	6.10E-20	30.8	31.2	28.3	57.4	53.8	59.7	35.3	46.5	35.9	30.0	35.4	21.1	21.7
53	Oasl2	0.48	-1.07	2.89E-07	0.40	-1.33	2.88E-08	18.37	4.20	2.01E-91	3.5	3.5	3.1	64.3	50.8	71.3	20.6	40.7	27.6	10.4	5.6	3.4	3.0
54	Ucp2	0.65	-0.63	1.89E-03	0.59	-0.77	6.29E-11	2.03	1.02	2.09E-09	17.5	17.2	20.7	30.9	30.4	51.1	22.1	26.2	24.6	24.3	24.7	14.5	14.5
55	6720456H20Rik	0.62	-0.68	6.82E-07	0.55	-0.86	1.06E-19	1.01	0.01	9.53E-01	27.4	27.0	26.3	28.3	27.6	25.5	14.7	15.0	21.2	39.4	39.7	21.2	22.7
56	Slco4a1	0.70	-0.50	7.68E-02	0.64	-0.64	4.50E-03	1.56	0.64	5.75E-03	4.1	4.6	6.1	6.9	6.2	10.1	4.8	6.6	5.0	7.7	5.9	4.4	4.3
57	Map3k6	0.38	-1.39	2.97E-05	0.19	-2.36	4.84E-34	2.97	1.57	2.49E-07	5.9	5.8	4.8	12.4	14.7	21.6	3.3	9.6	5.7	8.6	12.0	1.7	2.3
58	Cebpd	0.59	-0.77	4.77E-07	0.40	-1.32	4.97E-14	5.18	2.37	6.77E-65	6.3	6.5	7.1	29.6	32.3	41.2	18.9	24.1	17.5	11.6	9.7	3.7	4.8
59	Socs3	0.62	-0.69	4.02E-03	0.43	-1.21	6.58E-05	4.92	2.30	8.36E-31	3.7	2.9	3.9	18.2	13.6	20.3	10.8	13.6	7.9	12.7	5.2	3.9	3.9
60	H2-K1	0.74	-0.44	2.60E-05	0.60	-0.73	1.67E-11	5.10	2.35	5.36E-145	40.7	45.9	40.5	234.7	203.7	209.7	136.5	171.5	169.5	69.7	53.0	36.7	37.3
61	Irf1	0.69	-0.54	7.57E-05	0.55	-0.87	9.31E-03	8.31	3.05	8.42E-141	8.6	7.3	8.1	72.1	59.6	67.6	39.1	55.2	43.2	18.4	7.7	7.4	7.0
62	Klf15	0.76	-0.40	5.27E-03	0.65	-0.63	5.39E-08	1.84	0.88	1.59E-14	27.8	32.7	30.4	46.2	55.9	65.7	38.7	45.3	43.3	33.7	42.5	25.0	24.7
63	Uba7	0.79	-0.33	1.33E-01	0.58	-0.78	5.73E-03	5.78	2.53	6.51E-57	2.8	2.7	3.0	17.2	15.4	16.0	10.1	16.1	12.5	10.2	5.4	4.5	4.6
64	Apold1	0.74	-0.44	1.40E-01	0.46	-1.13	9.40E-11	3.80	1.93	1.39E-20	4.1	5.9	7.3	15.7	21.4	28.7	15.4	15.9	17.1	7.8	9.0	3.5	4.2
65	Ddit4	0.73	-0.44	4.80E-02	0.47	-1.09	5.63E-18	1.69	0.76	1.87E-05	24.1	29.0	27.8	35.6	38.1	63.1	32.4	34.7	33.4	33.9	47.1	18.4	20.0
66	Tap1	0.65	-0.62	1.65E-03	0.40	-1.32	2.14E-06	14.13	3.82	3.31E-106	5.6	6.5	4.7	91.7	67.6	79.1	40.5	66.9	47.3	14.9	6.6	4.3	4.4
67	Gbp6	0.65	-0.62	1.67E-02	0.40	-1.33	3.40E-04	29.90	4.90	7.50E-108	6.1	5.6	4.5	203.3	144.4	136.3	75.7	145.4	94.7	20.4	6.4	4.8	5.8
68	Gbp3	0.65	-0.62	1.56E-03	0.41	-1.29	1.61E-04	17.51	4.13	2.21E-124	5.3	5.9	5.9	118.1	95.2	86.3	49.7	86.3	59.4	26.1	8.8	7.6	6.8
69	Gbp7	0.67	-0.58	1.08E-03	0.44	-1.19	9.79E-05	12.16	3.60	3.89E-119	6.9	6.5	6.3	84.3	79.0	75.8	44.4	71.8	44.1	32.2	12.1	9.3	10.2
70	Parp14	0.72	-0.48	2.93E-02	0.53	-0.91	2.90E-03	9.85	3.30	6.43E-78	3.8	4.1	5.0	45.1	39.7	42.7	24.1	41.4	25.9	24.8	10.5	8.9	9.9
71	Ly6c2	0.75	-0.42	4.66E-03	0.59	-0.77	2.82E-03	5.50	2.46	1.23E-84	4.4	4.2	4.0	24.1	23.3	22.0	14.8	20.4	16.6	12.4	9.2	8.1	4.8
72	Nfkbia	0.72	-0.47	3.73E-02	0.53	-0.92	8.10E-20	2.30	1.20	1.82E-12	19.2	29.1	25.5	43.7	53.1	72.7	36.6	44.3	41.7	35.5	40.1	19.4	20.8
73	Ccdc3	0.79	-0.34	4.75E-02	0.63	-0.67	2.66E-07	1.19	0.25	1.12E-01	17.7	15.6	16.4	17.6	18.3	23.4	14.4	17.9	14.4	36.6	39.3	28.0	20.4
74	Lrg1	0.69	-0.54	3.25E-02	0.35	-1.53	1.19E-07	5.72	2.52	1.48E-36	1.6	1.3	1.8	7.0	9.5	10.8	5.1	7.8	5.9	6.9	8.8	4.0	1.6
75	Il1r1	0.78	-0.36	1.04E-01	0.51	-0.96	2.18E-09	1.88	0.91	2.06E-08	3.4	4.1	4.2	6.5	7.0	8.4	5.9	6.4	4.8	12.8	13.8	7.6	6.2
76	Gm8979	0.66	-0.60	3.38E-03	0.28	-1.84	1.76E-13	9.36	3.23	2.40E-66	0.8	0.9	1.2	10.2	9.5	7.7	4.9	6.9	6.3	14.4	7.1	2.6	3.4
77	Zbtb16	0.80	-0.32	1.31E-02	0.51	-0.96	5.59E-08	1.73	0.79	5.07E-15	32.1	35.1	34.1	50.6	55.4	69.0	47.6	47.7	44.9	54.2	99.9	40.2	39.7
78	Tmem252	0.63	-0.67	1.17E-02	0.18	-2.47	1.68E-42	18.94	4.24	3.11E-72	1.1	0.6	1.6	18.1	21.6	24.9	10.2	16.2	14.2	8.6	8.8	1.8	1.4
79	Xdh	0.69	-0.54	9.25E-03	0.26	-1.93	2.15E-42	6.35	2.67	7.78E-58	5.9	7.4	7.3	35.0	45.7	49.9	23.7	38.1	28.2	30.4	22.4	6.6	7.3
80	Nlrc5	0.68	-0.56	1.07E-02	0.26	-1.92	1.69E-12	27.25	4.77	3.39E-120	1.1	1.3	0.9	33.0	26.4	29.7	15.3	26.6	18.4	17.3	7.3	3.3	3.2
81	Plekhf1	0.77	-0.38	2.02E-01	0.41	-1.30	3.61E-20	1.75	0.81	1.14E-04	7.7	9.9	12.9	13.2	19.1	21.2	12.0	15.6	13.5	16.8	18.1	6.7	7.5

82	Vwf	0.88	-0.19	4.62E-01	0.66	-0.61	1.36E-07	1.44	0.53	7.57E-04	24.9	22.7	28.5	31.3	32.1	46.4	33.6	28.2	34.5	76.8	72.2	56.8	42.4
83	Myo7a	0.86	-0.22	4.16E-01	0.61	-0.72	9.37E-13	0.83	-0.26	1.83E-01	37.3	34.8	37.7	31.8	28.9	30.8	17.8	31.4	29.2	35.7	40.1	22.8	23.5
84	Bub1b	0.69	-0.53	4.72E-02	0.30	-1.76	1.19E-08	2.46	1.30	3.38E-10	2.0	2.4	2.6	6.3	5.1	5.8	2.9	5.4	3.5	6.3	12.3	1.6	3.8
85	Ptgs2	0.75	-0.42	7.78E-03	0.38	-1.40	2.30E-06	2.88	1.53	1.08E-33	6.5	8.5	8.4	24.4	20.6	22.5	15.1	15.9	19.3	12.7	7.2	5.2	2.5
86	Htr3a	0.88	-0.18	4.86E-01	0.66	-0.60	2.23E-02	0.94	-0.09	6.74E-01	6.3	6.5	5.7	5.7	5.1	6.6	4.7	5.4	5.2	5.7	5.1	2.8	4.3
87	Sgk1	0.64	-0.64	8.07E-04	0.15	-2.78	2.04E-234	3.34	1.74	7.27E-28	59.5	82.6	83.5	207.8	267.3	277.7	122.3	192.7	168.8	248.7	261.1	37.7	37.1
88	Igtp	0.69	-0.55	1.20E-02	0.20	-2.35	7.16E-10	22.28	4.48	1.01E-127	6.6	8.1	6.4	192.0	140.8	136.3	82.1	140.4	98.9	34.7	8.5	4.1	4.4
89	Arl4d	0.76	-0.40	1.55E-01	0.31	-1.69	1.31E-23	1.85	0.88	1.42E-05	15.4	22.9	26.2	30.2	43.4	45.4	24.0	30.4	35.6	15.2	22.3	5.9	5.8
90	Mgp	0.81	-0.30	2.53E-01	0.44	-1.19	5.35E-12	1.47	0.55	2.96E-03	23.3	18.0	23.3	30.2	28.9	35.7	21.2	34.1	21.6	8.6	8.4	3.3	4.1
91	Arid5b	0.88	-0.18	1.79E-01	0.60	-0.74	8.13E-17	1.41	0.50	5.19E-08	22.8	27.2	25.0	32.9	36.9	35.9	29.7	32.5	31.2	52.8	53.7	30.8	33.1
92	Gbp9	0.86	-0.22	3.35E-01	0.48	-1.05	6.90E-03	7.87	2.98	6.16E-102	5.0	4.7	4.5	42.2	37.0	33.0	26.3	39.4	30.8	21.2	7.1	7.5	6.4
93	Tgm2	0.91	-0.14	4.90E-01	0.64	-0.65	2.68E-08	3.55	1.83	2.26E-64	19.0	18.1	17.1	70.9	59.4	62.1	49.3	68.3	57.2	33.7	31.1	22.6	19.1
94	Ly6a	0.83	-0.27	4.58E-02	0.42	-1.24	2.58E-18	6.29	2.65	6.11E-155	14.4	12.5	12.4	81.6	87.4	77.9	58.8	77.8	68.9	46.5	32.2	18.7	14.9
95	Acer2	0.88	-0.19	5.61E-01	0.55	-0.87	4.51E-08	3.64	1.86	2.00E-27	5.9	6.1	8.7	20.2	28.1	27.2	18.0	26.1	22.1	35.9	34.7	24.4	15.1
96	Cp	0.88	-0.18	5.17E-01	0.56	-0.83	1.31E-14	1.87	0.91	4.05E-09	20.4	18.9	22.2	37.5	37.0	41.0	27.4	45.2	29.2	33.6	33.8	20.6	17.7
97	Ly6c1	0.87	-0.19	8.64E-02	0.51	-0.97	2.92E-19	3.89	1.96	2.48E-135	21.6	21.5	21.6	77.9	90.2	83.9	66.3	76.5	77.8	59.0	46.0	25.9	27.7
98	Iigp1	0.68	-0.56	8.91E-03	0.14	-2.88	3.39E-12	47.70	5.58	2.43E-171	2.0	2.5	2.2	109.1	101.2	106.5	58.3	100.7	56.2	31.5	7.0	2.9	2.4
99	Tob2	0.92	-0.13	5.34E-01	0.63	-0.67	7.81E-11	1.15	0.20	1.38E-01	38.4	47.9	52.5	49.0	50.9	59.7	47.0	48.9	50.3	35.1	39.9	24.0	23.5
100	Gbp5	0.84	-0.26	9.95E-02	0.24	-2.04	7.13E-09	21.65	4.44	1.15E-251	1.8	1.7	1.6	37.8	35.0	37.5	25.6	34.5	32.1	31.9	8.9	5.0	4.9
101	Osmr	0.92	-0.12	8.15E-01	0.54	-0.88	1.43E-11	4.32	2.11	2.67E-22	2.9	3.0	2.5	14.2	10.1	12.1	9.4	15.7	8.3	19.7	20.5	11.1	10.9
102	Xlr3b	0.91	-0.13	9.00E-01	0.55	-0.86	1.50E-05	1.94	0.95	3.47E-02	4.1	5.6	2.2	5.5	10.1	7.4	3.1	10.0	7.9	20.1	12.7	9.6	8.5
103	Gbp2	0.73	-0.45	5.57E-03	0.17	-2.59	9.29E-10	41.41	5.37	5.29E-287	5.5	6.3	5.6	292.4	229.0	200.0	144.4	194.9	188.7	50.0	10.0	5.0	5.0
104	Klf2	0.88	-0.18	6.85E-01	0.50	-0.99	1.50E-07	2.02	1.01	2.65E-06	3.3	4.7	6.7	8.4	9.7	11.6	8.7	9.0	8.5	6.9	8.6	3.5	4.3
105	Per2	0.92	-0.12	4.68E-01	0.60	-0.73	2.69E-11	1.24	0.31	1.44E-03	18.4	21.6	19.1	24.3	24.7	24.4	22.2	22.3	23.2	29.8	34.3	19.1	19.6
106	Csmp1	0.93	-0.11	7.49E-01	0.63	-0.66	4.54E-04	1.35	0.43	1.26E-02	10.1	12.3	14.0	14.2	15.0	19.7	15.0	13.7	16.7	8.9	9.0	5.6	5.9
107	Grrp1	0.93	-0.10	7.56E-01	0.49	-1.02	1.49E-08	2.03	1.02	7.87E-12	4.4	3.4	3.8	8.2	8.1	7.4	6.2	8.4	7.4	9.9	8.2	4.8	4.2
108	Gbp4	0.85	-0.23	4.36E-01	0.16	-2.63	3.35E-10	30.25	4.92	3.12E-142	2.4	3.5	1.7	83.9	73.3	70.6	53.5	78.8	61.4	61.0	12.2	6.1	5.8
109	Tgtp2	0.81	-0.30	1.13E-01	0.08	-3.73	5.16E-26	24.51	4.62	1.15E-225	4.7	5.8	5.5	147.3	127.8	117.1	89.4	132.9	96.6	55.8	15.1	2.6	2.7
110	Extl1	0.97	-0.05	7.86E-01	0.65	-0.63	6.13E-08	1.04	0.05	6.60E-01	73.4	68.4	66.2	70.5	69.0	76.1	72.9	63.2	72.3	39.3	39.7	22.3	28.6
111	Ier3	1.01	0.01	9.80E-01	0.64	-0.64	6.89E-03	1.22	0.28	6.37E-02	8.4	8.6	10.0	9.9	10.6	12.4	10.9	10.7	11.4	13.0	9.6	8.5	6.2
112	S100a9	NE	NE	NE	0.26	-1.97	2.98E-04	NE	NE	NE	NE	NE	NE	NE	NE	NE	NE	NE	NE	20.8	7.5	6.2	1.3
113	Hif3a	NE	NE	NE	0.33	-1.60	4.04E-23	NE	NE	NE	NE	NE	NE	NE	NE	NE	NE	NE	NE	17.5	25.5	7.7	6.7
114	E030018B13Rik	NE	NE	NE	0.47	-1.09	2.83E-09	NE	NE	NE	NE	NE	NE	NE	NE	NE	NE	NE	NE	6.1	6.6	3.1	2.9
115	Gm13152	NE	NE	NE	0.57	-0.80	1.22E-04	NE	NE	NE	NE	NE	NE	NE	NE	NE	NE	NE	NE	6.9	9.3	4.1	5.2
116	Pla2g3	NE	NE	NE	0.57	-0.80	7.16E-10	NE	NE	NE	NE	NE	NE	NE	NE	NE	NE	NE	NE	19.8	22.6	12.6	12.0
117	Xlr3c	NE	NE	NE	0.61	-0.70	1.26E-02	NE	NE	NE	NE	NE	NE	NE	NE	NE	NE	NE	NE	10.5	6.7	6.4	4.4
118	Gm13275	NE	NE	NE	0.62	-0.69	1.30E-03	NE	NE	NE	NE	NE	NE	NE	NE	NE	NE	NE	NE	5.2	5.8	3.1	3.7
119	4930564K09Rik	NE	NE	NE	0.62	-0.69	1.58E-03	NE	NE	NE	NE	NE	NE	NE	NE	NE	NE	NE	NE	6.3	7.5	3.7	4.9
120	Znf41-ps	NE	NE	NE	0.62	-0.68	4.99E-04	NE	NE	NE	NE	NE	NE	NE	NE	NE	NE	NE	NE	7.0	8.1	4.5	5.0
121	Paqr5	NE	NE	NE	0.63	-0.66	1.67E-03	NE	NE	NE	NE	NE	NE	NE	NE	NE	NE	NE	NE	6.4	8.0	4.5	4.7
122	4931406H21Rik	NE	NE	NE	0.66	-0.59	1.43E-03	NE	NE	NE	NE	NE	NE	NE	NE	NE	NE	NE	NE	12.7	14.5	9.9	8.3
123	Xlr3a	1.06	0.09	9.38E-01	0.58	-0.78	1.01E-03	1.55	0.63	1.75E-01	3.8	4.4	2.5	4.6	7.5	4.4	2.3	7.8	7.4	14.3	9.0	7.7	6.0
124	Hspa1a	1.10	0.14	6.46E-01	0.56	-0.83	3.37E-10	0.92	-0.12	5.57E-01	32.9	34.6	50.0	38.6	33.5	36.1	38.7	34.8	45.2	23.4	29.3	14.0	15.7
125	Hspa1b	1.11	0.15	6.06E-01	0.55	-0.87	1.50E-10	0.94	-0.09	6.75E-01	31.6	31.9	48.2	37.4	32.5	34.8	36.7	35.3	44.1	21.3	26.3	12.1	13.9
126	Trib1	1.14	0.19	6.19E-01	0.54	-0.88	6.99E-07	1.05	0.07	8.37E-01	7.9	14.2	15.2	13.3	11.8	14.0	14.7	13.2	16.8	7.6	8.6	4.3	4.5
127	Per1	1.20	0.26	1.85E-01	0.55	-0.87	6.95E-20	0.93	-0.11	5.54E-01	43.0	50.6	54.1	37.9	42.1	56.7	56.3	51.1	56.1	42.4	48.0	25.1	24.7
128	Podxl	1.23	0.30	5.47E-02	0.51	-0.96	6.45E-21	1.39	0.47	1.09E-04	30.3	27.2	26.7	45.2	40.3	31.4	45.3	48.8	49.3	65.1	64.2	38.1	29.3
129	Pisd-ps2	1.32	0.40	2.25E-03	0.65	-0.62	8.23E-07	0.71	-0.49	2.15E-05	21.5	21.1	23.5	17.8	13.9	15.5	19.0	21.7	21.6	40.8	48.9	33.3	25.9
130	Hist1h1d	0.63	-0.67	6.56E-07	1.41	0.50	4.89E-03	2.04	1.03	2.43E-17	47.1	37.5	32.1	83.4	79.2	75.3	47.7	57.1	44.6	14.4	11.7	20.0	17.1
131	Hist1h2ae	0.66	-0.60	1.33E-10	1.32	0.40	7.12E-02	2.10	1.07	4.41E-36	38.8	38.1	39.8	88.5	77.0	79.5	49.6	61.4	51.0	17.1	14.5	24.8	17.5
132	Hist1h2ag	0.64	-0.63	4.05E-11	1.31	0.39	1.71E-01	2.19	1.13	2.66E-37	38.2	35.8	38.9	89.0	75.3	82.7	51.5	60.0	47.8	17.3	13.2	24.2	16.3
133	Hist1h2ab	0.66	-0.59	2.17E-09	1.28	0.36	1.36E-01	2.21	1.14	1.76E-37	38.8	36.8	39.5	91.5	79.0	84.0	51.5	64.9	52.8	18.7	14.2	24.2	18.6
134	Mki67	0.60	-0.73	2.77E-03	1.30	0.38	8.97E-01	2.76	1.47	6.77E-13	3.6	3.0	2.7	10.4	8.2	7.1	4.9	6.7	3.9	5.9	2.6	4.0	6.8
135	Hist1h2ai	0.67	-0.59	1.95E-08	1.24	0.31	1.88E-01	2.10	1.07	4.25E-30	43.6	41.4	45.2	99.4	83.5	90.4	54.7	70.3	57.1	20.5	16.1	24.8	21.1
136	Hist1h2ac	0.66	-0.59	1.51E-09	1.26	0.33	2.71E-01	1.97	0.98	5.00E-28	40.5	38.3	42.4	87.5	73.0	78.3	52.7	58.7	47.2	17.8	14.7	24.8	16.7
137	Hist1h2bh	0.66	-0.59	4.34E-08	1.54	0.62	2.16E-02	2.01	1.00	4.90E-25	21.2	18.1	21.8	43.3	39.3	40.2	24.2	30.1	27.3	12.1	8.8	20.8	11.9
138	Hist1h2an	0.68	-0.56	2.02E-06	1.50	0.59	1.28E-02	2.27	1.18	1.83E-29	30.0	26.5	29.7	69.6	61.2	64.5	37.7	52.1	42.2	13.2	10.0	21.7	13.7
139	Hist1h2bf	0.67	-0.59	4.58E-08	1.44	0.52	1.01E-01	1.93	0.95	2.15E-22	22.0	19.0	20.3	43.0	36.6	38.7	23.8	29.1	25.9	11.6	9.6	20.5	10.8
140	Hist1h3g	0.62	-0.69	4.27E-08	1.17	0.22	8.49E-01	2.16	1.11	1.20E-22	27.8	23.3	25.3	59.5	53.1	52.3	30.2	41.3	31.1	11.6	9.3	14.3	10.3
141	Hist1h2bb	0.63	-0.66	3.29E-08	1.14	0.20	7.55E-01	2.14	1.09	7.76E-24	38.3	33.9	35.3	83.0	73.6	73.0	44.7	58.5	41.7	17.6	14.9	20.4	17.2
142	Hist1h3c	0.53	-0.93	8.38E-16	1.08	0.11	1.00E+00	2.57	1.36	1.08E-35	28.9	25.4	25.5	77.3	61.4	67.0	33.2	42.3	32.6	12.1	9.7	13.1	10.6
143	Icam1	0.66	-0.61	4.13E-04	1.04	0.06	1.00E+00	7.57	2.92	4.13E-79	3.4	2.4	2.6	20.0	19.8	23.5	13.4	16.4	11.8	7.5	5.5	6.2	7.3
144	Hist1h3b	0.59	-0.75	2.18E-11	1.08	0.11	1.00E+00	2.40	1.26	2.68E-34	43.6	38.3	37.9	104.7	89.3	93.8	51.4	67.8	51.9	16.6	14.4	17.0	16.6
145	Hist2h3c2	0.66	-0.60	5.67E-08	1.06	0.09	1.00E+00	2.14	1.10	4.04E-28	21.6	17.6	18.4	43.9	39.3	40.0	26.2	30.3	24.9	11.1	9.6	11.7	10.5
146	Hist1h3a	0.56	-0.83	5.06E-12	1.02	0.02	1.00E+00	2.27	1.18	4.41E-26	31.7	25.8	25.7	71.3	58.7	58.8	34.5	40.3	31.5	13.1	10.4	13.4	10.8
147	Hist1h3d	0.64	-0.64	2.88E-08	1.01	0.01	1.00E+00	2.14	1.10	3.76E-26	41.3	34.6	35.7	86.3	75.1	77.5	46.8	60.3	46.4	15.5	13.3	15.5	13.8
148	Hist2h3c1	0.66	-0.59	4.90E-08	1.02	0.03	1.00E+00	2.12	1.08	1.53E-28	21.7	17.7	19.0	43.9	39.6	40.2	26.5	30.5	25.2	11.6	10.7	11.9	11.1
149	D7Ertd715e	0.63	-0.66	1.37E-04	1.02	0.03	1.00E+00	1.38	0.46	6.06E-03	7.3	7.7	10.2	11.7	12.6	10.5	7.3	8.1	6.6	48.7	52.8	51.5	52.7
150	Hist1h1a	0.65	-0.62	6.07E-07	0.99	-0.01	1.00E+00	1.59	0.67	5.23E-09	19.5	16.6	15.8	27.4	26.1	28.9	17.5	20.4	15.9	5.6	5.4	5.6	5.3
151	Ptac8	0.37	-1.45	1.86E-05	NE	NE	NE	73.20	6.19	2.62E-59	0.2	0.2	0.2	16.3	13.2	11.4	4.2	8.1	2.7	NE	NE	NE	NE
152	Gzma	0.37	-1.44	9.16E-09	NE	NE	NE	357.84	8.48	4.06E-98	0.0	0.0	0.0	7.8	8.9	8.7	2.0	4.5	2.8	NE	NE	NE	NE
153	Usp18	0.39	-1.35	4.80E-06	NE	NE	NE	23.25	4.54	8.85E-54	1.4	1.9	0.9	33.5	28.5	35.5	8.0	19.4	10.8	NE	NE	NE	NE
154	Ifi27l2a	0.41	-1.30	1.06E-08	NE	NE	NE	21.56	4.43	4.15E-80	1.9	1.6	1.2	34.3	28.0	37.3	9.1	18.5	12.8	NE	NE	NE	NE
155	Trim30d	0.43	-1.23	1.31E-07	NE	NE	NE	6.86	2.78	7.76E-36	1.9	1.8	1.8	13.7	11.7	12.5	3.2	7.0	5.9	NE	NE	NE	NE
156	Mx2	0.45	-1.16	7.06E-04	NE	NE	NE	11.30	3.50	3.61E-29	0.9	0.6	1.1	8.3	9.7	12.5	3.0	7.3	3.4	NE	NE	NE	NE
157	Gzmb	0.45	-1.14	2.09E-03	NE	NE	NE	1014.50	9.99	4.04E-86	0.0	0.0	0.0	25.1	22.6	24.1	7.5	18.6	6.5	NE	NE	NE	NE
158	Trim12a	0.46	-1.13	1.07E-07	NE	NE	NE	4.20	2.07	4.00E-25	1.5	1.8	2.2	8.8	7.3	7.2	2.5	3.6	4.5	NE	NE	NE	NE
159	Ddx60	0.47	-1.09	5.44E-07	NE	NE	NE	7.53	2.91	2.97E-42	1.0	0.9	1.0	6.9	6.6	8.2	2.4	4.7	3.1	NE	NE	NE	NE
160	Cdkn1a	0.47	-1.09	1.93E-03	NE	NE	NE	3.43	1.78	4.60E-09	2.3	3.6	2.1	5.3	8.0	14.3	4.0	4.6	4.4	NE	NE	NE	NE
161	Rsad2	0.48	-1.06	1.82E-04	NE	NE	NE	22.93	4.52	1.68E-61	1.5	1.7	1.3	28.1	31.5	45.0	11.9	25.1	13.1	NE	NE	NE	NE
162	Ifi204	0.49	-1.04	7.21E-04	NE	NE	NE	23.17	4.53	2.06E-52	0.8	0.6	0.6	16.7	15.1	15.3	4.9	12.2	5.7	NE	NE	NE	NE
163	Cd52	0.49	-1.04	1.86E-05	NE	NE	NE	11.33	3.50	1.21E-49	0.7	0.6	0.9	9.2	7.7	9.0	3.0	6.0	3.6	NE	NE	NE	NE
164	Mnda	0.50	-1.00	1.59E-02	NE	NE	NE	38.62	5.27	7.39E-42	0.2	0.1	0.5	11.4	8.8	11.8	3.5	8.6	3.9	NE	NE	NE	NE
165	Lilrb3	0.51	-0.98	4.05E-04	NE	NE	NE	8.21	3.04	3.15E-32	1.1	0.7	0.4	5.9	5.6	6.4	2.9	4.0	2.2	NE	NE	NE	NE
166	Oasl1	0.51	-0.97	1.23E-02	NE	NE	NE	22.27	4.48	9.69E-36	0.5	0.4	0.1	6.2	5.7	9.2	3.1	5.4	2.3	NE	NE	NE	NE
167	Ms4a6b	0.51	-0.97	3.67E-03	NE	NE	NE	12.06	3.59	2.08E-33	0.6	0.6	0.9	9.7	6.8	8.6	2.7	6.6	3.5	NE	NE	NE	NE
168	Rtp4	0.51	-0.96	2.36E-06	NE	NE	NE	14.72	3.88	1.44E-82	1.9	1.7	1.7	24.5	23.9	28.6	10.0	18.3	11.3	NE	NE	NE	NE

169	Mx1	0.51	-0.96	1.44E-02	NE	NE	NE	17.80	4.15	9.61E-33	0.4	0.5	0.6	8.7	8.3	10.8	3.1	8.0	3.1	NE	NE	NE	NE
170	Fcgr4	0.51	-0.96	1.43E-03	NE	NE	NE	60.14	5.91	2.51E-71	0.1	0.2	0.2	10.9	9.3	9.4	3.9	7.9	3.5	NE	NE	NE	NE
171	Angptl4	0.52	-0.95	1.31E-03	NE	NE	NE	3.75	1.91	4.61E-14	3.9	2.9	4.1	10.2	13.1	17.4	4.7	9.9	6.5	NE	NE	NE	NE
172	Top2a	0.52	-0.93	8.16E-04	NE	NE	NE	4.81	2.27	4.10E-21	2.9	2.2	3.0	18.0	10.4	10.9	5.0	9.0	6.6	NE	NE	NE	NE
173	2010002M12Rik	0.53	-0.93	2.03E-05	NE	NE	NE	4.88	2.29	3.23E-30	1.8	1.3	1.3	6.9	6.9	7.9	3.0	5.1	3.4	NE	NE	NE	NE
174	Ccl12	0.53	-0.93	2.76E-02	NE	NE	NE	117.00	6.87	7.52E-61	0.2	0.1	0.2	22.0	18.6	17.7	8.1	17.2	5.4	NE	NE	NE	NE
175	Cxcl10	0.53	-0.92	3.84E-03	NE	NE	NE	125.62	6.97	3.13E-96	0.2	0.4	0.3	42.2	34.0	43.0	17.4	33.0	12.7	NE	NE	NE	NE
176	Slfn8	0.54	-0.89	2.05E-03	NE	NE	NE	11.99	3.58	4.79E-43	1.4	1.1	1.2	16.9	12.7	14.2	5.7	12.0	5.9	NE	NE	NE	NE
177	Phf11b	0.54	-0.89	6.40E-04	NE	NE	NE	19.80	4.31	7.32E-59	0.3	0.4	0.3	8.0	5.8	6.5	2.9	5.2	2.9	NE	NE	NE	NE
178	Plekha4	0.54	-0.88	4.00E-03	NE	NE	NE	2.60	1.38	1.15E-07	2.3	2.5	2.4	5.4	5.4	7.7	2.4	5.1	2.5	NE	NE	NE	NE
179	Kirrel2	0.55	-0.87	1.54E-04	NE	NE	NE	2.29	1.19	3.73E-09	4.8	6.5	6.1	10.2	11.4	18.1	6.6	7.8	7.4	NE	NE	NE	NE
180	Epsti1	0.55	-0.86	6.53E-06	NE	NE	NE	8.49	3.09	1.26E-61	1.2	1.2	0.9	9.5	9.7	8.8	4.4	6.6	4.5	NE	NE	NE	NE
181	Ch25h	0.55	-0.86	5.67E-05	NE	NE	NE	22.17	4.47	2.27E-83	0.2	0.4	0.4	8.4	7.6	7.9	3.3	5.7	4.3	NE	NE	NE	NE
182	Spn	0.56	-0.84	1.25E-05	NE	NE	NE	14.11	3.82	1.61E-76	0.5	0.4	0.4	6.4	6.7	6.1	3.0	4.6	3.1	NE	NE	NE	NE
183	Cybb	0.56	-0.83	8.69E-07	NE	NE	NE	4.75	2.25	2.44E-43	1.4	1.2	1.5	7.0	6.3	6.1	3.6	4.3	3.1	NE	NE	NE	NE
184	Ifi205	0.56	-0.82	3.57E-02	NE	NE	NE	85.39	6.42	8.05E-53	0.1	0.0	0.1	6.2	4.5	6.1	2.4	5.2	2.0	NE	NE	NE	NE
185	Gm8989	0.57	-0.81	4.19E-05	NE	NE	NE	10.96	3.45	6.04E-66	0.6	0.6	0.7	7.8	7.4	5.6	3.1	4.4	4.3	NE	NE	NE	NE
186	Oas1a	0.57	-0.81	2.73E-02	NE	NE	NE	19.88	4.31	5.77E-44	1.6	1.1	0.8	26.5	19.8	20.9	8.8	20.0	9.7	NE	NE	NE	NE
187	Hist1h1b	0.57	-0.80	1.00E-03	NE	NE	NE	2.47	1.31	3.92E-10	9.5	7.5	7.7	23.6	13.9	23.4	11.2	14.7	9.1	NE	NE	NE	NE
188	Zfp36	0.58	-0.78	2.98E-03	NE	NE	NE	2.97	1.57	1.35E-12	2.1	2.6	2.5	5.8	5.7	9.8	4.1	4.9	3.4	NE	NE	NE	NE
189	Phf11d	0.59	-0.77	6.94E-03	NE	NE	NE	11.96	3.58	1.07E-44	0.8	0.6	0.7	9.0	6.9	8.5	3.6	7.0	3.7	NE	NE	NE	NE
190	Itgb7	0.60	-0.75	1.55E-05	NE	NE	NE	2.78	1.47	4.85E-21	2.2	2.1	2.2	6.8	5.3	6.1	3.4	4.2	3.3	NE	NE	NE	NE
191	Bst2	0.60	-0.74	4.99E-04	NE	NE	NE	12.18	3.61	5.91E-79	4.5	4.2	3.4	58.0	39.7	48.5	21.8	38.2	27.7	NE	NE	NE	NE
192	Isg15	0.60	-0.73	3.96E-02	NE	NE	NE	17.35	4.12	5.48E-44	1.2	1.0	1.1	20.1	13.8	23.8	8.4	17.9	8.4	NE	NE	NE	NE
193	Maff	0.61	-0.72	3.18E-03	NE	NE	NE	5.09	2.35	1.68E-28	0.9	1.1	1.6	5.4	6.2	7.2	2.8	4.5	4.1	NE	NE	NE	NE
194	Cyp1b1	0.61	-0.71	1.38E-02	NE	NE	NE	4.10	2.03	2.56E-18	2.8	2.6	2.7	9.0	11.6	12.3	5.5	9.9	4.7	NE	NE	NE	NE
195	Crybb1	0.61	-0.71	5.63E-03	NE	NE	NE	3.21	1.68	3.29E-15	2.3	3.0	2.4	9.4	6.9	8.3	4.1	4.0	6.9	NE	NE	NE	NE
196	Ms4a6d	0.62	-0.70	1.14E-02	NE	NE	NE	8.13	3.02	4.65E-36	0.7	0.8	0.6	5.1	6.0	6.2	2.4	5.0	3.2	NE	NE	NE	NE
197	Hck	0.62	-0.69	1.61E-04	NE	NE	NE	4.91	2.29	3.56E-45	2.8	3.3	3.0	17.1	13.6	13.6	8.0	11.4	8.1	NE	NE	NE	NE
198	Slfn2	0.62	-0.68	7.68E-06	NE	NE	NE	10.32	3.37	8.99E-112	2.0	1.7	1.9	20.1	18.3	19.8	10.6	14.7	10.9	NE	NE	NE	NE
199	Irf7	0.63	-0.68	2.75E-04	NE	NE	NE	19.78	4.31	6.83E-130	2.6	2.9	2.6	49.7	48.5	60.1	26.4	44.1	28.5	NE	NE	NE	NE
200	Serpina3f	0.63	-0.67	2.31E-02	NE	NE	NE	152.24	7.25	2.72E-104	0.1	0.1	0.1	10.7	13.8	18.4	6.1	10.9	9.9	NE	NE	NE	NE
201	Parp10	0.63	-0.66	1.91E-03	NE	NE	NE	5.52	2.46	3.87E-42	4.8	4.2	3.9	24.6	19.6	26.9	12.5	19.9	12.6	NE	NE	NE	NE
202	Hist1h3l	0.64	-0.65	1.24E-08	1.00	0.00	1.00E+00	2.23	1.16	1.67E-29	42.1	36.9	39.6	96.4	83.5	84.6	51.5	67.0	50.6	18.6	14.4	17.3	15.9
203	Dhx58	0.64	-0.64	1.31E-02	NE	NE	NE	4.31	2.11	4.37E-24	2.1	2.2	3.3	10.2	9.7	13.2	5.5	9.1	6.7	NE	NE	NE	NE
204	Itgb2	0.64	-0.64	5.96E-05	NE	NE	NE	3.29	1.72	5.61E-35	6.4	5.8	5.3	20.7	18.3	18.4	11.1	15.1	10.7	NE	NE	NE	NE
205	Nmi	0.64	-0.64	6.83E-04	NE	NE	NE	3.05	1.61	1.43E-23	3.6	3.3	3.8	11.9	10.3	10.5	5.7	8.8	6.5	NE	NE	NE	NE
206	Gm12250	0.64	-0.63	3.80E-03	NE	NE	NE	76.11	6.25	2.38E-157	0.5	0.4	0.3	31.8	28.4	30.8	13.9	26.1	18.6	NE	NE	NE	NE
207	Psmb8	0.65	-0.62	1.89E-03	NE	NE	NE	12.96	3.70	2.29E-95	4.2	4.5	3.8	65.3	47.6	49.9	26.3	45.2	34.1	NE	NE	NE	NE
208	Srgn	0.65	-0.62	1.49E-03	NE	NE	NE	2.98	1.58	5.15E-22	3.9	3.0	4.0	11.5	9.8	11.4	6.7	8.8	5.9	NE	NE	NE	NE
209	Serpina3g	0.65	-0.61	2.63E-02	NE	NE	NE	13.88	3.79	4.78E-60	1.2	1.3	1.2	11.6	17.5	22.2	8.5	12.9	12.2	NE	NE	NE	NE
210	AW112010	0.66	-0.60	1.31E-02	NE	NE	NE	8.58	3.10	1.77E-47	0.6	1.2	0.7	7.9	6.9	6.3	3.8	5.7	4.4	NE	NE	NE	NE
211	Hmgb2	0.66	-0.60	9.75E-04	NE	NE	NE	2.35	1.23	9.30E-16	6.6	5.2	5.0	14.3	12.6	12.8	7.7	10.6	7.9	NE	NE	NE	NE
212	Plaur	0.66	-0.59	4.96E-03	NE	NE	NE	8.15	3.03	1.86E-55	1.0	0.8	0.6	6.0	6.6	7.3	3.5	5.1	4.7	NE	NE	NE	NE
213	Gm7030	0.66	-0.59	9.76E-04	NE	NE	NE	3.97	1.99	4.69E-38	3.8	4.0	3.3	15.8	14.1	14.0	7.5	10.7	11.0	NE	NE	NE	NE
214	Irf8	0.67	-0.59	9.23E-04	NE	NE	NE	4.11	2.04	2.37E-42	6.6	4.9	4.6	24.6	20.1	21.5	13.4	17.5	13.3	NE	NE	NE	NE
215	AF251705	0.67	-0.58	4.75E-04	NE	NE	NE	1.63	0.71	2.55E-06	3.7	2.9	3.6	5.4	5.7	5.5	3.4	3.7	4.0	NE	NE	NE	NE
216	Ltbp2	0.54	-0.89	1.13E-05	NE	NE	NE	1.09	0.13	6.39E-01	5.4	6.4	5.7	7.3	4.5	7.2	3.7	3.3	3.3	NE	NE	NE	NE
217	Il20rb	0.57	-0.81	3.14E-05	NE	NE	NE	1.12	0.16	5.08E-01	5.3	5.4	5.7	6.2	5.2	6.9	2.9	4.4	3.1	NE	NE	NE	NE
218	Crtam	0.57	-0.81	1.80E-10	NE	NE	NE	1.18	0.24	9.97E-02	13.4	12.9	14.1	16.2	14.6	16.8	7.9	10.4	9.0	NE	NE	NE	NE
219	Ror1	0.57	-0.80	5.44E-07	NE	NE	NE	1.12	0.16	4.26E-01	5.6	6.2	5.7	6.6	6.0	7.0	3.5	4.4	3.3	NE	NE	NE	NE
220	Mybpc3	0.65	-0.63	3.22E-05	NE	NE	NE	0.68	-0.56	5.93E-05	13.9	14.4	14.9	9.3	8.7	11.4	5.9	7.0	6.1	NE	NE	NE	NE
221	Fermt3	0.66	-0.60	2.91E-03	0.92	-0.13	1.00E+00	2.53	1.34	1.13E-15	5.8	5.4	5.6	17.2	11.3	14.1	7.5	10.8	9.8	6.1	5.2	5.0	5.4
222	Tor3a	0.57	-0.80	7.13E-07	0.87	-0.20	8.75E-01	3.14	1.65	5.76E-30	8.1	7.0	7.1	24.4	21.2	24.3	11.0	17.0	12.1	10.0	9.0	8.5	8.2
223	Rac2	0.62	-0.68	6.01E-04	0.89	-0.17	7.92E-01	2.89	1.53	2.80E-19	3.3	4.0	3.7	12.5	9.8	9.6	5.5	8.3	6.1	18.5	17.3	15.2	16.5
224	Cmpk2	0.65	-0.61	4.90E-08	0.91	-0.14	8.28E-01	2.21	1.14	1.43E-29	32.9	32.0	34.4	74.2	69.5	75.8	42.4	57.8	43.4	37.9	33.2	32.7	32.3
225	Oas1b	0.61	-0.72	3.19E-04	0.89	-0.17	6.37E-01	2.51	1.33	1.96E-14	3.0	3.8	3.4	8.1	7.7	9.8	4.0	6.2	5.4	30.0	32.5	26.8	29.2
226	Pyhin1	0.50	-1.00	8.49E-04	0.85	-0.24	8.25E-01	14.10	3.82	4.07E-40	0.6	0.4	0.4	7.1	6.2	7.1	3.0	5.2	2.0	6.2	5.4	4.4	5.5
227	Rorc	0.58	-0.78	5.91E-06	0.88	-0.19	9.35E-01	1.23	0.30	1.14E-01	6.2	6.5	7.7	7.2	7.9	10.0	4.4	5.3	4.9	6.1	6.6	5.0	6.2
228	Ms4a6c	0.62	-0.70	5.10E-05	0.82	-0.29	1.66E-01	2.39	1.26	1.74E-16	3.6	4.0	4.3	9.0	8.6	10.6	5.0	6.9	5.6	70.3	71.0	46.5	68.8
229	Rhoj	0.67	-0.59	1.16E-02	0.85	-0.24	7.65E-01	2.55	1.35	5.70E-13	4.9	3.5	3.7	8.6	10.2	12.0	6.2	8.6	5.8	7.2	7.8	6.0	6.8
230	Trim21	0.60	-0.73	5.90E-04	0.83	-0.28	7.17E-01	5.49	2.46	1.85E-40	3.0	3.5	4.0	19.9	18.1	19.8	8.8	15.7	10.5	6.5	5.2	5.0	4.7
231	Pdk4	0.52	-0.93	5.05E-06	0.79	-0.33	1.44E-01	2.03	1.02	4.94E-08	6.8	6.6	7.2	9.8	18.4	13.5	7.2	7.7	7.0	16.2	18.2	12.6	14.8
232	Herc6	0.60	-0.74	7.32E-06	0.83	-0.27	6.61E-01	2.94	1.55	1.70E-26	12.4	12.9	12.8	42.8	34.5	34.5	17.1	28.1	21.6	12.2	8.8	8.3	9.2
233	Rbm3	0.58	-0.78	3.09E-02	0.82	-0.29	1.03E-02	1.06	0.09	8.45E-01	80.1	87.3	81.6	48.9	84.4	131.6	58.6	62.8	33.3	63.6	67.5	56.8	51.2
234	Zc3hav1	0.61	-0.72	7.32E-06	0.85	-0.24	6.88E-01	2.85	1.51	1.67E-26	8.8	8.4	7.8	26.3	20.0	25.0	12.2	17.6	13.5	10.4	10.2	8.6	9.0
235	Ddx58	0.60	-0.73	3.04E-05	0.87	-0.21	8.83E-01	5.09	2.35	1.07E-51	6.3	6.9	6.6	34.4	31.4	34.9	16.2	27.0	17.5	13.8	10.4	9.4	11.5
236	Gm4951	0.61	-0.72	3.48E-04	0.86	-0.21	5.77E-01	7.81	2.97	1.24E-59	2.7	2.6	2.4	22.9	18.6	18.1	9.8	16.0	10.3	18.2	18.0	15.1	16.3
237	Hist1h3f	0.66	-0.60	4.90E-08	0.89	-0.17	8.44E-01	1.73	0.79	3.01E-15	68.5	60.2	63.4	112.6	107.5	111.6	68.8	87.4	63.3	24.8	20.2	18.1	21.8
238	Crlf2	0.63	-0.67	2.89E-04	0.87	-0.20	8.75E-01	1.35	0.43	1.85E-02	13.0	11.6	10.8	17.3	14.9	15.5	7.2	11.1	11.7	8.6	8.9	7.6	7.7
239	Hist1h3h	0.63	-0.67	4.90E-08	0.97	-0.05	1.00E+00	2.27	1.18	7.42E-27	47.0	39.9	42.4	108.1	91.6	94.0	55.6	74.4	55.0	20.6	15.7	18.2	17.1
240	Naip2	0.62	-0.70	1.25E-05	0.93	-0.11	1.00E+00	2.42	1.28	4.68E-19	2.4	2.6	3.2	7.1	6.7	6.5	4.1	4.5	3.9	10.0	9.3	8.8	9.2
241	Hspb8	0.66	-0.61	1.70E-04	0.95	-0.08	1.00E+00	1.45	0.54	3.61E-04	29.1	29.0	30.8	43.0	41.1	45.2	20.2	32.9	31.8	44.5	41.9	38.7	43.5
242	Eif2ak2	0.60	-0.73	7.47E-05	0.93	-0.10	9.10E-01	3.47	1.79	2.04E-29	9.8	11.8	11.3	40.3	32.4	41.3	18.3	30.2	20.3	58.9	57.0	54.2	54.7
243	Car8	0.66	-0.59	2.24E-08	0.94	-0.08	1.00E+00	1.05	0.07	6.38E-01	270.9	258.4	284.1	290.0	241.2	322.0	171.1	205.5	189.2	9.0	11.1	9.5	9.7
244	Gdf10	0.66	-0.59	1.68E-03	2.52	1.33	1.74E-11	1.35	0.43	1.70E-02	23.1	21.8	27.0	29.0	25.7	42.2	21.4	23.5	19.5	3.4	5.5	12.5	10.3
245	Atp1a4	1.13	0.18	4.19E-01	1.91	0.93	1.37E-02	0.87	-0.20	2.24E-01	8.0	7.9	9.3	7.5	6.6	7.8	7.9	8.0	8.9	19.3	18.1	57.1	17.1
246	Aldoart1	1.15	0.20	2.86E-01	2.24	1.16	1.05E-03	0.87	-0.21	1.47E-01	9.4	9.2	10.0	8.6	8.1	8.1	10.0	9.1	9.2	5.6	5.4	19.4	6.3
247	Gm10012	0.91	-0.13	4.74E-01	1.84	0.88	8.81E-05	1.16	0.22	6.52E-02	13.1	12.7	14.6	15.9	16.1	15.2	14.6	14.8	13.7	11.1	12.2	29.0	14.8
248	Gm6548	0.88	-0.18	1.69E-01	2.00	1.00	3.50E-03	1.39	0.47	2.51E-07	36.0	36.6	41.8	55.2	52.7	51.3	44.4	52.2	43.6	36.4	31.7	107.5	33.7
249	Hmgcs2	0.92	-0.11	7.53E-01	1.56	0.64	6.15E-03	1.52	0.60	6.25E-04	12.7	10.2	11.3	14.4	15.1	22.2	15.4	18.0	14.5	3.7	4.1	5.4	6.7
250	Igfbp4	0.93	-0.10	5.67E-01	1.53	0.61	4.73E-03	1.23	0.30	3.41E-03	62.8	57.5	64.0	87.7	70.9	68.2	72.2	68.2	71.0	9.1	11.6	13.2	18.4
251	Gm6402	0.93	-0.10	7.26E-01	1.78	0.84	9.30E-03	1.15	0.20	2.35E-01	6.1	6.1	7.1	7.6	7.7	7.0	7.5	7.2	6.2	7.0	6.2	17.2	7.2
252	Gm12504	0.95	-0.08	7.96E-01	1.99	0.99	4.03E-03	1.21	0.27	8.69E-02	7.5	6.7	8.0	10.1	9.0	7.8	8.6	8.6	8.2	7.8	8.5	24.8	8.7
253	Mid1	0.95	-0.08	9.43E-01	1.81	0.86	2.23E-02	2.73	1.45	2.40E-04	6.8	5.7	1.8	13.3	11.9	13.9	12.2	16.9	8.0	8.9	24.2	24.5	35.7
254	Smarca5-ps	0.95	-0.07	8.32E-01	1.61	0.69	3.21E-02	1.12	0.17	3.19E-01	8.4	9.2	11.0	11.5	10.7	10.0	10.0	10.9	9.9	13.2	11.9	29.3	12.3
255	Gm6251	0.99	-0.02	9.67E-01	1.84	0.88	1.13E-02	1.07	0.10	6.09E-01	4.5	5.2	5.0	5.0	5.5	5.3	5.0	5.2	5.3	6.2	6.4	17.4	6.6

256	Acta1	0.99	-0.01	9.71E-01	2.56	1.36	7.95E-04	0.93	-0.10	5.56E-01	16.3	15.2	16.5	16.9	14.5	13.4	15.9	15.1	13.4	8.1	7.2	32.7	8.2
257	Haus4	NE	NE	NE	1.53	0.61	5.03E-03	NE	NE	NE	NE	NE	NE	NE	NE	NE	NE	NE	NE	4.0	4.2	6.9	5.8
258	Gm6194	NE	NE	NE	1.80	0.85	1.86E-03	NE	NE	NE	NE	NE	NE	NE	NE	NE	NE	NE	NE	5.0	4.5	11.6	5.9
259	Calca	NE	NE	NE	1.87	0.90	8.78E-13	NE	NE	NE	NE	NE	NE	NE	NE	NE	NE	NE	NE	11.5	12.0	20.8	23.2
260	Calcb	NE	NE	NE	1.93	0.95	1.26E-04	NE	NE	NE	NE	NE	NE	NE	NE	NE	NE	NE	NE	4.1	2.6	5.4	7.4
261	Gm10413	NE	NE	NE	2.19	1.13	2.66E-07	NE	NE	NE	NE	NE	NE	NE	NE	NE	NE	NE	NE	3.3	2.3	5.1	7.2
262	4930555G01Rik	NE	NE	NE	2.65	1.40	4.57E-30	NE	NE	NE	NE	NE	NE	NE	NE	NE	NE	NE	NE	9.4	10.1	24.2	27.6
263	Gdpd3	NE	NE	NE	2.85	1.51	4.79E-16	NE	NE	NE	NE	NE	NE	NE	NE	NE	NE	NE	NE	1.8	2.1	5.2	6.0
264	Gm5795	NE	NE	NE	3.15	1.66	3.95E-15	NE	NE	NE	NE	NE	NE	NE	NE	NE	NE	NE	NE	5.6	4.4	11.7	19.8
265	Eps8l1	NE	NE	NE	3.56	1.83	3.55E-13	NE	NE	NE	NE	NE	NE	NE	NE	NE	NE	NE	NE	2.3	1.0	5.2	6.7
266	Mmm2	1.64	0.71	4.56E-06	1.62	0.70	2.48E-05	1.61	0.69	4.22E-06	6.3	6.2	6.0	11.8	10.0	8.0	17.4	15.7	15.6	8.3	7.6	13.0	13.0
267	Gm5796	2.76	1.47	1.25E-14	2.81	1.49	3.69E-36	1.28	0.35	1.27E-01	11.8	10.7	13.9	12.5	16.5	17.3	57.9	35.2	35.2	38.9	39.3	89.5	129.3
268	Beta-s	2.73	1.45	1.17E-08	2.57	1.36	9.44E-03	0.19	-2.37	4.09E-24	46.4	73.7	31.8	9.7	8.6	11.0	33.3	22.6	24.3	83.5	29.2	64.5	217.3
269	Gm3500	3.21	1.68	2.35E-18	3.02	1.59	3.13E-31	1.21	0.27	2.70E-01	23.2	21.5	26.2	21.0	31.3	33.1	123.1	75.9	75.6	75.9	74.9	176.9	275.4
270	Gm10409	2.59	1.37	2.97E-11	2.30	1.20	1.93E-18	1.11	0.15	6.02E-01	24.8	22.4	31.3	21.9	32.8	32.4	101.2	58.7	65.8	85.4	89.3	157.2	241.9
271	Gm3383	3.11	1.64	8.32E-19	2.70	1.43	1.45E-25	1.22	0.29	2.08E-01	15.3	13.6	16.0	14.0	20.1	20.9	76.1	46.0	48.8	52.1	50.6	105.3	170.1
272	Nlrp5-ps	1.72	0.78	8.14E-03	1.59	0.67	1.07E-07	0.80	-0.31	3.19E-01	29.6	24.9	34.7	29.3	27.3	15.2	32.7	57.0	33.9	25.8	20.6	40.7	33.6
273	Gm10406	3.20	1.68	1.11E-17	2.70	1.43	1.14E-20	1.12	0.17	5.44E-01	12.2	9.5	12.2	9.3	13.6	15.3	53.3	34.8	34.4	33.4	34.2	67.0	114.3
274	LOC100861615	3.12	1.64	3.66E-14	2.77	1.47	3.86E-21	1.21	0.27	3.32E-01	7.4	7.2	8.9	7.5	9.3	11.5	41.3	23.6	23.5	19.5	20.0	40.7	68.2
275	Bche	1.55	0.64	8.08E-04	1.49	0.57	1.70E-04	0.62	-0.69	6.31E-05	8.9	8.7	10.6	5.7	6.2	5.6	8.0	11.5	7.8	11.3	11.2	16.5	17.2
276	Serpinb1a	1.72	0.78	1.28E-06	1.52	0.61	2.44E-08	0.44	-1.20	5.81E-17	21.3	22.7	23.4	11.1	11.1	7.3	18.7	15.4	16.3	24.6	24.4	34.4	40.3
277	Sh3bp5	2.03	1.02	7.51E-15	1.77	0.82	1.03E-19	0.90	-0.16	3.58E-01	30.9	31.8	31.3	27.4	24.6	32.1	62.9	63.4	44.7	28.4	28.9	49.2	52.5
278	Gm3264	3.37	1.75	5.48E-25	2.64	1.40	4.86E-17	1.23	0.30	1.54E-01	10.6	9.9	11.2	11.2	13.9	14.1	58.8	34.2	38.9	32.1	34.5	62.3	112.1
279	Gm3558	2.73	1.45	3.28E-14	2.26	1.18	3.80E-17	1.19	0.25	3.19E-01	11.5	10.7	14.5	11.3	15.3	16.8	51.8	32.2	34.8	36.7	37.6	64.8	102.5
280	Gjc2	1.57	0.65	1.02E-09	1.45	0.53	2.08E-09	0.57	-0.82	6.00E-17	38.3	35.5	37.2	22.5	21.4	18.9	33.2	28.9	36.6	59.7	58.9	81.5	90.7
281	Rprl3	1632.08	10.67	0.00E+00	3550.60	11.79	0.00E+00	0.95	-0.07	8.52E-01	0.7	1.2	0.6	0.6	0.7	0.9	1321.3	1482.1	888.8	0.1	0.2	469.9	382.7
282	Opalin	1.44	0.53	6.52E-04	1.55	0.64	7.34E-11	0.47	-1.08	3.63E-17	38.2	35.8	39.3	17.7	21.6	14.3	28.8	25.6	22.8	26.1	27.8	40.5	43.7
283	Rprl2	452.46	8.82	5.47E-146	3446.78	11.75	5.98E-148	0.88	-0.18	9.31E-01	0.0	0.2	0.1	0.1	0.1	0.0	39.8	44.1	22.7	0.0	0.0	70.8	28.2
284	BC002163	1.33	0.42	1.13E-02	1.52	0.61	4.72E-09	1.16	0.22	1.96E-01	53.5	51.4	50.7	59.3	59.3	62.0	99.7	81.1	60.2	36.3	34.0	59.9	48.3
285	Hmcn1	1.24	0.31	2.71E-01	1.63	0.71	7.50E-14	0.46	-1.13	2.16E-11	6.3	8.6	6.9	3.2	3.2	3.6	4.8	4.1	3.3	29.4	30.4	46.5	51.6
286	Scd4	1.20	0.26	3.42E-01	1.51	0.59	2.52E-02	0.67	-0.57	1.81E-03	9.5	11.2	12.6	7.1	6.0	9.2	10.0	7.9	9.0	30.0	27.2	60.0	28.4
287	Olfml1	1.19	0.25	2.47E-01	1.61	0.69	2.83E-09	0.95	-0.08	6.97E-01	17.9	17.4	19.7	15.6	18.9	17.5	22.6	23.2	16.0	19.1	16.9	28.1	30.1
288	Rps15a-ps6	1.25	0.33	2.48E-01	1.83	0.87	2.65E-05	1.14	0.19	4.38E-01	11.8	12.3	13.5	13.5	16.2	13.3	19.9	22.1	12.1	11.8	11.0	27.7	15.2
289	Kdr	1.30	0.38	3.33E-02	1.98	0.99	5.68E-14	0.67	-0.57	6.83E-05	15.4	12.8	12.1	9.7	8.3	9.0	13.1	10.2	11.9	12.9	11.4	22.1	26.1
290	Padi2	1.27	0.35	2.28E-02	1.60	0.68	2.08E-14	0.78	-0.36	5.87E-03	44.3	47.3	46.5	35.2	38.2	33.9	56.2	39.5	40.6	122.4	129.6	197.9	207.3
291	Igf2	1.33	0.41	3.54E-02	1.65	0.73	4.81E-04	0.81	-0.30	8.93E-02	53.4	48.5	52.0	32.9	39.8	51.9	56.9	63.4	45.0	5.4	5.4	10.6	7.5
292	Rgcc	1.33	0.42	9.36E-04	1.65	0.72	1.42E-05	1.48	0.57	3.74E-07	16.2	16.9	14.7	21.8	24.4	24.5	32.9	34.4	27.0	8.3	9.2	13.4	15.6
293	Tnc	1.59	0.67	1.24E-05	1.28	0.35	1.20E-01	0.44	-1.20	1.64E-19	17.7	18.0	16.2	8.6	7.0	7.1	13.4	12.9	9.9	13.7	18.9	21.6	20.5
294	Gm20594	1.71	0.77	2.02E-02	1.32	0.40	1.38E-03	0.59	-0.76	9.56E-03	14.1	19.6	18.5	12.6	5.5	12.7	17.2	21.8	13.7	43.4	57.3	67.9	66.3
295	Hddc3	2.90	1.54	1.06E-20	2.18	1.13	7.75E-16	1.06	0.09	7.25E-01	12.3	11.2	11.5	12.7	13.0	11.5	29.2	48.3	30.3	7.6	7.9	16.6	17.4
296	Gm3002	2.66	1.41	8.38E-16	1.96	0.97	5.64E-09	1.13	0.17	4.78E-01	23.0	22.8	27.5	21.1	30.1	31.2	95.1	60.8	63.5	163.9	171.0	242.6	409.7
297	Ide	1.54	0.63	2.60E-05	1.34	0.42	9.93E-06	1.24	0.31	5.07E-02	49.0	49.4	54.7	45.8	73.7	70.0	98.1	99.6	95.1	104.4	96.7	135.5	135.5
298	Fabp7	2.65	1.41	9.83E-18	1.81	0.86	1.81E-11	0.34	-1.55	5.65E-23	25.1	24.7	24.6	10.1	9.2	6.2	25.6	23.7	18.2	16.3	18.8	36.7	27.8
299	Galnra2	2.78	1.48	1.56E-19	1.95	0.96	2.84E-33	0.33	-1.58	4.86E-24	62.9	60.1	54.6	22.8	21.6	15.0	63.7	41.9	59.7	39.7	41.6	81.2	78.4
300	Col3a1	1.73	0.79	1.50E-05	1.41	0.50	6.24E-03	0.79	-0.34	8.54E-02	18.7	15.9	15.3	13.9	12.9	12.6	20.8	29.8	17.5	9.5	9.2	13.3	13.3
301	Ndn	1.79	0.84	2.78E-18	1.24	0.31	6.22E-03	0.61	-0.71	2.80E-14	378.5	368.1	365.1	201.6	208.2	269.2	418.6	383.2	413.8	179.0	194.0	238.0	229.4
302	Srsf4	1.65	0.72	1.16E-03	1.16	0.21	1.95E-01	0.68	-0.57	7.59E-03	42.8	42.5	42.6	32.2	17.7	36.5	53.8	42.6	46.1	36.3	38.6	45.2	42.3
303	Txn2	1.56	0.64	6.94E-03	1.12	0.16	5.75E-01	0.66	-0.59	5.95E-03	50.8	54.4	55.5	39.4	21.2	46.1	58.6	52.8	54.8	33.4	35.8	39.3	38.7
304	Arc	1.84	0.88	3.60E-02	1.15	0.21	6.11E-01	0.63	-0.67	8.35E-02	85.2	158.2	250.6	124.6	97.3	89.4	192.0	115.6	264.7	22.2	23.1	23.4	28.9
305	Nr4a1	2.46	1.30	1.26E-04	0.57	-0.82	6.51E-06	0.54	-0.88	7.58E-03	25.0	44.9	67.9	24.8	22.5	27.4	66.1	37.4	80.2	8.1	9.0	4.6	5.1
306	Mir5109	1.78	0.83	1.07E-02	0.83	-0.26	8.24E-01	0.22	-2.20	1.09E-17	10.9	16.5	18.4	3.1	4.7	2.2	4.7	6.1	6.9	17.3	11.0	9.4	14.0
307	Egr1	2.12	1.08	1.22E-05	0.85	-0.24	7.14E-01	0.62	-0.69	5.23E-03	26.4	39.9	49.6	25.6	25.6	20.8	53.3	34.5	64.5	9.8	11.2	8.8	9.1
308	Rasl11b	2.06	1.04	1.72E-14	1.07	0.09	1.00E+00	0.76	-0.40	8.72E-03	16.8	19.5	18.1	13.5	14.5	13.3	30.8	22.0	32.3	4.4	5.2	4.6	5.7
309	Atp10d	2.74	1.46	9.97E-17	1.07	0.10	1.00E+00	1.34	0.43	4.93E-02	2.4	2.7	2.9	3.2	3.9	3.6	10.3	7.5	11.6	8.2	7.6	8.8	8.3
310	Lars2	1.74	0.80	4.32E-03	0.98	-0.03	1.00E+00	0.22	-2.18	1.64E-21	696.6	1109.8	1246.8	193.9	318.7	160.5	329.0	431.5	409.6	927.2	556.9	969.3	520.5
311	Bdnf	1.51	0.59	2.21E-05	0.99	-0.02	1.00E+00	0.87	-0.21	1.96E-01	16.8	15.6	15.5	16.5	12.6	12.4	22.4	18.6	21.6	7.6	8.2	7.9	7.8
312	Efnb2	1.52	0.60	4.64E-05	0.99	-0.02	1.00E+00	0.67	-0.58	3.02E-05	37.9	37.6	35.8	27.2	18.5	29.0	39.7	35.2	38.4	10.2	12.3	10.7	11.7
313	Egr2	3.48	1.80	3.60E-03	NE	NE	NE	0.38	-1.40	1.51E-02	2.2	8.3	16.1	3.9	2.6	3.6	11.2	5.7	18.1	NE	NE	NE	NE
314	Egr4	1.95	0.96	9.62E-05	NE	NE	NE	0.59	-0.76	1.28E-03	10.8	15.9	20.9	9.9	9.1	9.1	18.9	13.2	22.5	NE	NE	NE	NE
315	Fosb	1.67	0.74	2.83E-02	NE	NE	NE	0.88	-0.19	6.31E-01	3.1	4.7	7.0	4.7	4.0	4.3	6.7	5.3	9.7	NE	NE	NE	NE
316	Cdhr1	4.23	2.08	3.70E-11	NE	NE	NE	0.80	-0.33	4.14E-01	6.8	6.4	4.8	3.4	5.8	5.1	25.8	24.5	10.1	NE	NE	NE	NE

Appendix Table 2. Detailed matrix of leading edge analysis clustering performed on ECM and EAE depleted gene signatures in *Usp15*^{L749R} mutant mice

Due to sizing constraints, Appendix Table 2 can be found as a .xls file named Supplementary Table 2, available for download online by the publisher, Nature Immunology.

Torre, S.,et al. (2016). USP15 regulates type I interferon response and is required for pathogenesis of neuroinflammation. *Nature Publishing Group*, http://doi.org/10.1038/ni.3581